AN ABSTRACT OF THE THESIS OF

John W. Jenson for the degree of Doctor of Philosophy in Geology presented on September 27, 1993.

Title: A Nonlinear Numerical Model of the Lake Michigan Lobe, Laurentide Ice Sheet

Abstract approved: Redacted for Privacy

Peter U. Clark

A finite difference flowband model of the Late Wisconsin (ca. 20,000 years BP) Lake Michigan Lobe (LML) of the Laurentide Ice Sheet has been constructed to investigate how saturated, fine-grained sediment beneath the ice might have influenced lobe behavior. The flow line of the model extends from an ice divide near the southern end of Hudson Bay to the terminus of the lobe in northern Illinois. Geologic data from the area provide constraints on ice sheet surface morphology, ice velocity, and sediment flux during the last glacial maximum. The model incorporates hard-bed dynamics over the Canadian Shield and coupled ice-sediment dynamics over the unlithified sediments in the James Bay Lowland and Lake Michigan Basin. Geotechnical tests of clay-rich till deposited by the LML delimit rheological parameters (yield strength, residual strength, rate-dependent strain behavior) for the model. Sediment rheology is based on a general constitutive law that can treat a wide range of possible sediment behavior. Input to the model includes parameters for sediment and ice rheology, climate forcing, and topographic data. Mass flux values calculated from the stress-strain laws for the ice and sediment are inserted into the one-dimensional mass continuity equation to calculate the ice thickness as it varies over time. From the calculated ice thickness, the model determines surface elevation, shear stress, and velocity profiles for ice and sediment. The model also incorporates isostatic adjustment and elevation effects on climate forcing, and a first-order thermodynamic system. Results indicate that although the steady-state terminus of the ice is not affected by changes in sediment parameters, abrupt changes in climate forcing or sediment viscosity can induce significant transient changes in

ice margin location. While either of the two processes can produce responses consistent with observations from the geologic record, results suggest that it may be possible to find empirical clues in the geologic record that would enable workers to distinguish between lobe behavior induced by changes in climate forcing and that induced by changes in subglacial conditions.

A Nonlinear Numerical Model of the Lake Michigan Lobe, Laurentide Ice Sheet

by
John W. Jenson

A thesis
submitted to
Oregon State University

in partial fulfillment of
the requirements for
the degree of

Doctor of Philosophy

Completed September 27, 1993

Commencement June 1994

APPROVED:

Redacted for Privacy

Peter U. Clark, Associate Prof. of Geology, co-advisor in charge of major

Redacted for Privacy

Douglas R. MacAyeal, Prof. of Geophysical Sciences, co-advisor in charge of major

Redacted for Privacy

Head of department of Geosciences

Redacted for Privacy

Dean of Graduate School

Date thesis presented September 27, 1993.

Typed by John Jenson

Acknowledgments

I am indebted to many people who helped to make possible the timely completion of this project:

I wish to first thank my friend and colleague, Hailing Wang, whom I was most fortunate to have as "fellow traveler" through the last long winter of coding and verification. We labored together for several months through the inception and development of the thermal code. The successful implementation and verification of the thermodynamic subroutines, however, are due to Hailing's skill and tenacity.

I also wish to thank my good buddy, Todd K. (T.K.) Dupont, who endured midwestern thunderstorms, blistered hands, stinging and blood-sucking insects, and numerous other forms of physical abuse in the cause of helping me collect the sediment samples. His skill and tenacity with the pick and shovel were crucial to the success of the field portion of the project.

T.K.'s assistance also proved decisive to the success of the modeling project when he alerted his father, Todd F. Dupont, to my eleventh-hour discovery of a problem in the numerics. Todd F. generously took time to study my notes, diagnose the problem, and prescribe the right medicine! My debt to the "TD^2 team" is exceeded only by my gratitude!

Spencer Zitka, Doug Gerner, and Ken Olson of the Wedron Silica Company were most generous in allowing T.K. and me access to the exposures at Wedron and took a genuine interest in the success of our work. T.K.'s labor would have been even more arduous had Ken not arranged twice for the assistance of the back-hoe operator, Jim, who worked the back hoe with the skill of a surgeon to patiently scrape out just the right section for us. Fellow geologist Michael Regan, also of Wedron Silica, generously provided us with a shower and place to crash that made our evenings in the "field" most pleasant. Thanks, Mike!

Maureen Dungy, at the University of Chicago, Department of Geophysical Sciences was most helpful with logistical and administrative support that was no less essential to the success of the summer's field work. Maureen always came up a clever solution to every little (but potentially "show-stopping") problem from sharpening tools and repairing shipping crates to bundling up samples to survive the trip from Wedron to Hyde Park.

Carl Ho and Julio Vela in the Civil Engineering Department at Washington State University conducted the geotechnical tests and provided continual expert advice on geotechnical questions. Carl also took time to review and critique the geotechnical sections of this thesis.

J.R. Bell, Department of Civil Engineering at OSU took an active interest in my project from the beginning, and besides teaching me most of what

I know about soil mechanics was an invaluable unofficial advisor throughout the project.

Ardith Hansel and Hilt Johnson spent many hours educating me on the stratigraphy of northeastern Illinois and the exposures at Wedron.

Dean Lindstrom took me in as a house guest on several trips to Chicago and sat up many evenings sharing his experiences from his previous trip down this same road. Thanks, Dean.

I also wish to thank Mark Abbot and the College of Oceanographic and Atmospheric Sciences at Oregon State University for use of the CM-200 system. In particular, Paul Oppenheimer of Thinking Machines Corporation and Curt Vandetta, system adminstrator of the CM-200 system, were most generous in assisting me as an initiate to CMFORTRAN, UNIX, and the art of parallel computing.

Dick Iverson, who's constitutive model for mass movement was the inspiration for this project, graciously consented to sit on my committee and took time to explain the details, help interpret results, and troubleshoot things that "didn't look right." He also reviewed and helped to improve several of the grant proposals that made the project possible.

The model constructed in this study has undergone enough evolution that its connection to its progenitors is now indistinct, but it owes a large part of its initial inspiration to Richard Alley and those who collaborated with him in the construction of the Ice Stream B model (Alley and others, 1987) that served as a prototype and which provided a means of verifying the initial algorithm and code.

My thesis advisor, Peter Clark, patiently listened to my complaining, but kept me hacking away (at both computer as well as geology) even during my moments of doubt about the outcome. I was most fortunate to have the opportunity to work under someone with his capacity for recognizing the "nuggets" among mounds of disparate data and seemingly unrelated information. I would have never made it through the whole "sluice pile" without his confidence (always vindicated) there was "pay dirt" in there somewhere!

Through it all Doug MacAyeal was mentor, sponsor, banker, coach, counselor, cheer leader, co-conspirator, and friend. I would never have pulled this off (...or gotten into it in the first place!!!) without Doug's confidence, patience, and support.

The National Science Foundation provided support for the final year of my thesis research. Grants from the Geological Society of America, Sigma Xi, Chevron, ARCO, and Royal Dutch Shell got me started and kept me going.

My friend, Randy Milstein, did me the huge favor of taking on the task of pushing the final edit of this thesis through the graduate school so that I could blast out across the Pacific to start work. Thanks, Randy!

Finally, my wife, Cheri, and daughters Lynda Marie and Aubri Anne endured my many absences--both physical and mental--and never wavered in their confidence and support. Thanks for hanging in there with me! I couldn't have done it without you!

Contents

Contents, continued

List of Figures

List of Figures, continued

List of Figures, continued

List of Figures, continued

Tables

List of Notations

Note: Standard (kms) units are used for all quantities in the numerical model. Some English units are used in the geotechnical test data.

A	subdiagonal coefficient in tridagonal matrix mass continuity equation	
$A_{(T)}$	Temperature-dependent stiffness constant, ice flow law	$s^{-1}kPa^{-3}$
$\dot{A}$	ice accumulation rate	m/s
$\dot{A}_{present}$	modern precipitation rate	m/s
B	main diagonal coefficient in tridagonal matrix, mass continuity equation	
$\dot{B}$	basal melting rate	m/s
b	viscoplastic parameter from CDSR test	Pa
C	superdiagonal coefficient in tridagonal matrix, mass continuity equation	
c	sediment cohesion	Pa
C_c	Compression index for consolidation	dimensionless
c'_y	cohesion (normally consolidated sediment)	Pa
c'_y	cohesion (preconsolidated sediment)	Pa
D_0	Newtonian reference deformation rate	s^{-1}
e	sediment void ratio	unitless
e_0	initial sediment void ratio	unitless
F	flow law coefficient for sediment rheologic equation	$(Pa\text{-}s)^{-1}$
g	gravitational constant	m/s^2
G	geothermal heat flux at base of ice	W/m

List of Notations, continued

h	ice thickness	m
$\bar{h}$	cell-centered ice thickness	m
II_e	second invariant of excess stress tensor	Pa^2
II_D	second invariant of rate of deformation tensor	s^{-2}
i	numerical index for horizontal coordinate	
j	numerical index for vertical coordinate, till equations	
K	thermal conductivity of ice	$WC^{-1}m^{-1}$
k	grid-point index for vertical coordinate, ice equations	
ka	thousands of years	
L	ice sheet length scale	m
LapseRate	adiabatic atmospheric lapse rate	Kelvin/m
LHF_{ice}	latent heat of fusion of ice	J/kg
m	viscoplastic parameter from CDSR test	dimensionless
n	power law exponent for sediment flow law when associated with sediment constituve law	dimensionless
n	index indicating current timestep when associated with discretized numerical equations	
o.m.	"order of magnitude"	
p'	effective confining stress	Pa
p'_0	initial effective stress	Pa
psi	pounds per square inch (used in geotechnical tests)	
Q	arbitrarily-defined quantity for till rheology computations	m/s

List of Notations, continued

RHS	"right-hand-side" of discretized mass continuity equations.	
$Sensitivity_{CO_2}$	coefficient of sensitivity between temp and CO_2	Kelvin/ppm
S_0	strength constant in sediment rheologic equation	Pa
$S_{(z)}$	depth-dependent strength term in sediment constitutive eqn.	Pa
T	internal ice temperature	Kelvin
t	time	s
t*	exponential decay constant for isostasy	s
u	horizontal velocity of ice or sediment	m/s
u_{ice}	depth-averaged ice velocity	m/s
u_0	depth-averaged total velocity	m/s
u_{z_b}	basal ice velocity	m/s
w	vertical ice velocity	m/s
x	horizontal direction	m
$x_{\max \dot{A}}$	distance from ice divide where accumulation is maximum	m
z	vertical direction	m
z_b	basal elevation	m
z_d	depth to dilatant horizon, or thickness of shear zone	m
$z_{initial}$	initial topographic elevation (before ice loading)	m
z_S	ice surface elevation	m
ΔCO_2	difference between LGM and modern CO_2	ppm

List of Notations, continued

$\Delta\theta_{CO_{2effect}}$	temperature difference due to CO_2 effects	Kelvin
$\Delta\theta_{ElevationEffect}$	temperature difference due to elevation effects	Kelvin
Δt	timestep increment	s
Δx	horizontal distance increment for finite difference grid	m
ε_{till}	basal heat production	W/m
ϕ	sediment angle of internal friction	
ϕ'_y	angle of internal friction (preconsolidated)	Kelvin
η	mantle viscosity	Pa-s
μ_0	Newtonian reference viscosity	Pa-s
θ	mean annual air temperature/ice surface temperature	Kelvin
ρ_{ice}	density of ice	kg/m^3
ρ_{mantle}	density of upper mantle	kg/m^3
σ_1	maximum principal stress	Pa
σ_3	minimum principal stress	Pa
τ_{basal}	basal shear stress	Pa
ζ	vertical direction in normalized, "flexible" coordinate system	dimensionless

A Nonlinear Numerical Model of the Lake Michigan Lobe, Laurentide Ice Sheet

Chapter 1

Introduction

Significance and Motivation for the study

The Laurentide Ice Sheet (LIS) was the largest of the Northern Hemisphere ice sheets during the Last Glacial Maximum (LGM, ca. 18-21 ka). Accurate reconstruction of it is crucial for understanding Quaternary climate history, ocean circulation, global sea-level history, and the dynamics of modern ice sheets. A significant debate has focused on the degrees to which different mechanisms of ice movement might dominate ice sheet dynamics at given places and times. Mechanisms that have received attention from glaciologists and glacial geologists include internal deformation of the ice over a non-yielding base, basal sliding with deposition from active ice with high basal water pressure (e.g., Budd and others, 1979; Binschadler, 1983; Clayton et al., 1985, 1989), and transport of the ice by coupled flow over deforming subglacial sediment (e.g., Boulton and others, 1985; Fischer, 1985; Boulton and Hindmarsh, 1987; Alley, 1991). A compelling question is the degree to which pervasive deformation of saturated subglacial sediment might influence the dynamics of continental ice sheets. By lubricating the base of the ice, a deforming sediment layer could significantly influence the rate and timing of ice-sheet growth and collapse. Deforming subglacial sediment could therefore play an important role in determining ice sheet response to climatic forcing.

Until recently, the growth and disappearance of the Pleistocene mid-latitude ice sheets have generally been regarded as responses to changes in climate forcing. The possibility of deforming saturated sediment layers beneath large regions of the ice sheets, however, suggests that subglacial processes could influence the behavior of continental ice sheets largely independent of climate change. Given that the Pleistocene continental ice sheets exerted profound influence on global climate (cf., Manabe and Broccoli, 1985), the

possibility of a non-climatic mechanism operating because of conditions at the base of the ice sheets implies that ice sheet growth and collapse may not necessarily be direct responses to climate change, and that the ice sheets themselves could have exerted autonomous influence on climate once they were in place.

Paleoclimate research has increasingly manifest the need for integrated studies of solar forcing, atmospheric circulation, oceanic circulation, and ice sheet behavior to accurately reconstruct and predict the behavior of the global climate system. Orbital radiation changes appear to have triggered growth and retreat of the Pleistocene ice sheets, but the changes in orbital radiation themselves are too small to *cause* large changes in climate unless they are tied to amplifying feedback effects such as ice and snow-induced albedo changes, precipitation changes, atmospheric gas and aerosol changes, glacial isostatic rebound, sea level changes, or oceanic circulation changes (cf. Hays and others, 1976; Imbrie and Imbrie, 1980; Imbrie, 1982; Oerlemans, 1980; Pollard and others, 1980; Budd and Smith, 1981; Birchfield and others, 1981; Denton and Hughs, 1983; Hyde and Peltier, 1985; Lamb and Woodruffe, 1970; Johnson and Andrews, 1979; Rudiman and MacIntyre, 1979, 1981; Manabe and Broccoli, 1985; Broecker and Denton, 1989 ; Rind and others, 1989; Peteet and others, 1992). While orbital cycles appear to play a central role in modulating the pace of climate oscillations, major climatic events that are not synchronous with orbital forcing, such as the 1,000-year-long Younger Dryas cooling event about 11,000 BP or the Dansgaard-Oeschaer events of oxygen isotope stage 3, indicate that mechanisms other than orbital forcing must also exert profound effects on the global climate system. Large, episodic discharges of glacial ice and fresh water into the North Atlantic via Hudson Straight (Heinrich, 1988, Broecker and others, 1992), possibly activated by saturated subglacial sediment, are now thought to have played a pivotal role in altering oceanic circulation and climate during the Pleistocene (MacAyeal, in press).

To gain insight into how deforming substrate might influence ice sheet dynamics, I selected the Lake Michigan Lobe (LML) of the LIS for a focused study. The active behavior of the southern lobes of the LIS has long been

recognized as one of the striking features of the LIS (Prest, 1970; Dreimanis and Goldthwait, 1973; Wright, 1973; Clayton and others, 1985). Common characteristics of the southern lobes include soft sediments at the base and evidence of episodic oscillation during their retreat (Clark, in press). Because of their soft-bedded nature and evident activity, the southern lobes are promising subjects for studying the potential role of subglacial sediment in influencing ice sheet behavior not only at the margins but perhaps well into the interior.

A second reason for examining the sediments deposited by the southern lobes, and by the LML in particular, is that the sediment record is accessible, well documented, and well-constrained in time. Glacial deposits in Illinois have been studied for over 100 years and the regional stratigraphy of the glacial sediment is well-constrained (Willman and Frye, 1970; Johnson and Hansel, 1987, 1990). Detailed sedimentological investigations of till genesis have been initiated (e.g., Johnson et al., 1985; Hansel et al., 1985; Clark and Hansel, 1989; Johnson and Hansel, 1989, 1990; Clark and Rudloff, 1990), and several hypotheses have been presented to explain their characteristics (Clayton et al., 1989; Johnson and Hansel, 1990; Clark, 1991; Alley, 1991). The surface geometry of the LML has been reconstructed from moraines deposited by the lobe (Clark, 1992), and numerous radiocarbon ages constrain the temporal framework of deposits from the last glaciation, from which rates of ice margin advance and retreat, as well as till deposition, can be estimated (Hansel and Johnson, 1992).

Objectives of the study

The objective of this study is to develop a numerical model of ice lobe behavior that relates sediment properties to the behavior and morphology of the Lake Michigan Lobe. To meet this objective, the study had two complementary components: (1) a comprehensive one-dimensional (flowband) model, the centerpiece of which is a non-linear, rate-dependent, constitutive model for the sediment, and (2) sample collection and experimental evaluation of rheologic parameters which describe the sediment. The model recreates a cross-section of unit width along an inferred flowline of the LML. It provides a means for quantitatively evaluating sedimentologic, geomorphic, and till flux observations

against current theoretical understanding of the physical processes (e.g., ice and sediment rheology, heat flow, climate and mass balance, basal hydrology, etc.) that govern the dynamics of continental ice sheets. Experimental evaluation of sediment physical properties from Pleistocene deposits provides a means of constraining model parameters, especially since basal materials and processes beneath modern ice sheets are difficult and expensive to observe.

Preview of results

Ice surface profiles and sediment flux calculated from the measured sediment parameters were in general agreement with previous independent reconstructions and estimates from geological data. Initial results suggest that plausible changes in either climate or sediment parameters are capable of generating the magnitude of fluctuations in the lobe margin observed in the geologic record. Although more comprehensive and intensive experimentation will be needed to fully characterize the differences between ice lobe behavior induced by climate change and behavior induced by changes in sediment conditions, the results of the numerical experiments in this study suggest that the character and rates of the responses to the respective types of forcing are probably fundamentally different. While either of the two processes could produce responses consistent with various observations in the geologic record, it may be possible to find empirical clues in the geologic record that would enable glacial geologists to distinguish between lobe oscillations induced by changes in climate forcing and those induced by changes in subglacial conditions.

Chapter 2

Composition of the Model

The conceptual model: physiography of the modeled area

Interpretations of the geologic record regarding the growth of the Laurentide Ice Sheet are still highly conjectural. Dyke and Prest's (1987) reconstruction for 18ka (Fig. 2.1) shows ice domes centered over the Labrador peninsula and Keewatin sector with a northwest-trending ridge between. Accepting this inferred morphology, I have taken the flow line for the model directly from Dyke and Prest's map of the LGM ice sheet, using one of their inferred flowlines, which departs perpendicular to the ice divide over James, crosses the Lake Michigan Basin approximately through the center, and terminates perpendicular to the line of moraines that mark the southern limit of Wisconsin glaciation (Fig. 2.1).

There is evidence that ice sheet growth began during oxygen isotope stage 5, and that a substantial volume of ice was present during stage 4. The geologic record, however, reflects either the absence or substantial retreat of ice at many places along the margin, and possibly even the collapse of the central part of the ice sheet occupying Hudson Bay during the Early and Middle Wisconsinan (Andrews and others 1983; Thorleifson and others, 1992; Clark and others, 1993). In any case, advance of the southern margin into the Midwestern United States at 18ka must have followed the inception of the ice centers by several thousands of years (Vincent and Prest, 1987). Taken together, the above arguments suggest that the extreme limit for the lifetime of the LML must have been no more than 50 ka, and that its actual lifetime during successive ice advances could have been as short as 10-20 ka. A realistic model should therefore reproduce lobe dynamics and morphology on time scales of 10 to 50 ka.

The James Bay Lowland, where the flow line originates (Fig 2.2), is an area of low-relief carbonate bedrock overlain by a thick mantle of unlithified silty carbonate till . Hicock and others (1989) concluded that the fine-grained carbonate till could have promoted high subglacial water pressure and would

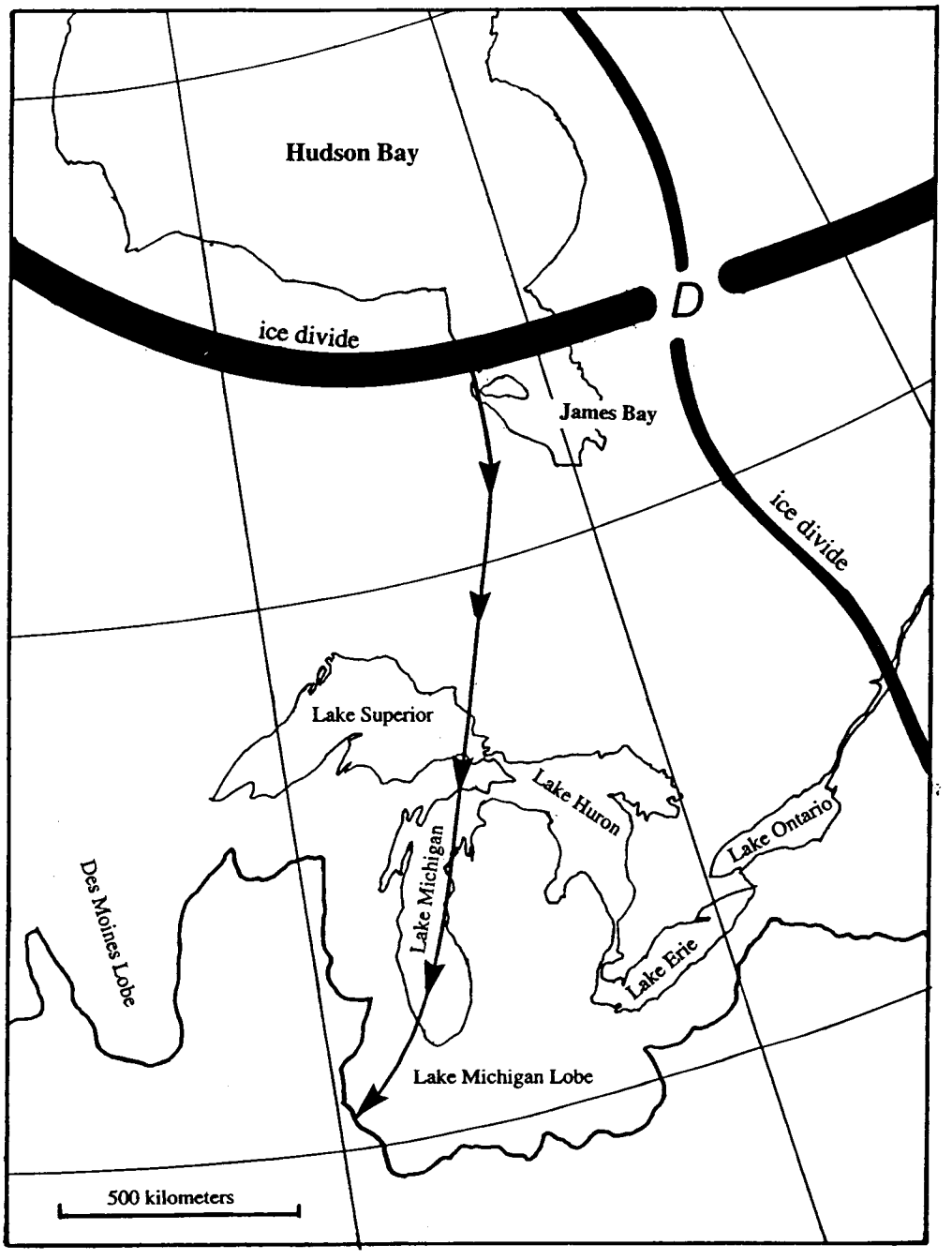

Fig. 2.1. Central flowband of Lake Michigan Lobe (after Dyke and Prest, 1987). "D" indicates presumed location of ice dome.

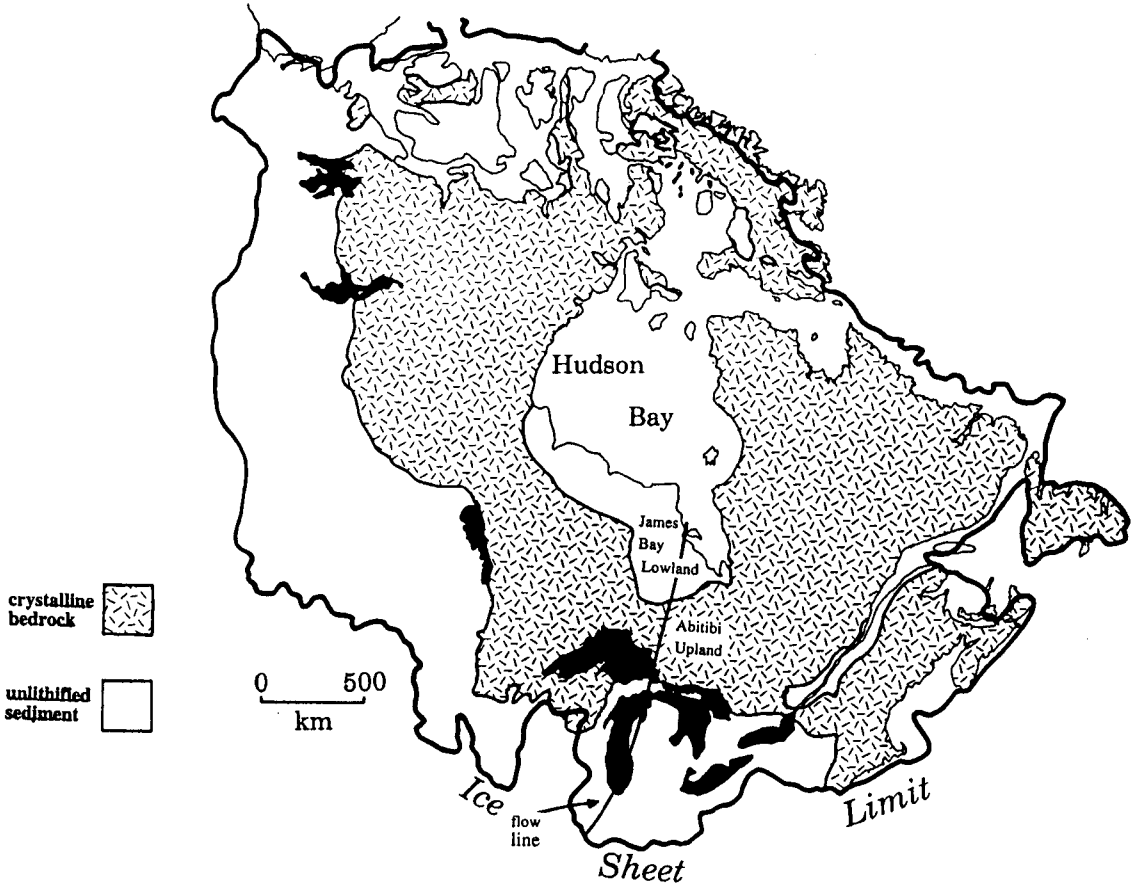

Fig. 2.2. Central flowband of Lake Michigan Lobe superimposed on regional surface lithology (after Clark, 1993).

have possessed low yield strength, thereby promoting either soft bed deformation, sliding, or both. In the LML simulation in this study I have followed their conclusion that models of the Laurentide Ice Sheet should treat the region as a soft bed.

South of the James Bay Lowland the flowline crosses the Abitibi Upland, which forms the height of land between the Lake Superior and Hudson Bay drainages (Fig. 2.3). Topography here is low and rolling with local relief exceeding 60 to 90 m only in deeply incised canyons. Elevations rise from near sea level to 500-600 m . The upland surface is exposed Precambrian crystalline bedrock sparsely overlain by patches of sandy till. The arc of crystalline bedrock across the northern edge of Lake Superior would have thus constituted a hard bed barrier for the ice flowing southward off of the soft sediments in the James Bay Lowland.

Previous workers (Ambrose, 1964) have concluded that much of the present day topography of the Laurentian Shield is pre-Paleozoic and that overall erosion of the shield area by Pleistocene glaciers was relatively modest, perhaps only a few meters (Dredge and Cowan, 1989). I have therefore adopted the modern topography, with the elevations under James Bay set to sea level, as a reasonable approximation for the initial topography (Fig. 2.3).

South of the Abitibi Upland the transect crosses the Lake Superior Basin before entering the Lake Michigan Basin. The Lake Superior Basin occupies a structural basin that may have originated as a result of Precambrian crustal rifting and plate separation (Drege and Cowan, 1989), but it has been modified by fluvial and glacial erosion. During the Pleistocene, the lake bed was most likely composed of crystalline rock, the present sediments being entirely Holocene age (Farrand and others, 1984). The Lake Michigan Basin is a structurally controlled topographic basin with its long axis associated with the more easily eroded units of the Michigan Structural Basin. Extensive deposits of Late Wisconsin clayey and silty till on the lakebed and surrounding regions (Lineback and others, 1983) indicate that it was most likely occupied with fine-grained sediment during the LGM.

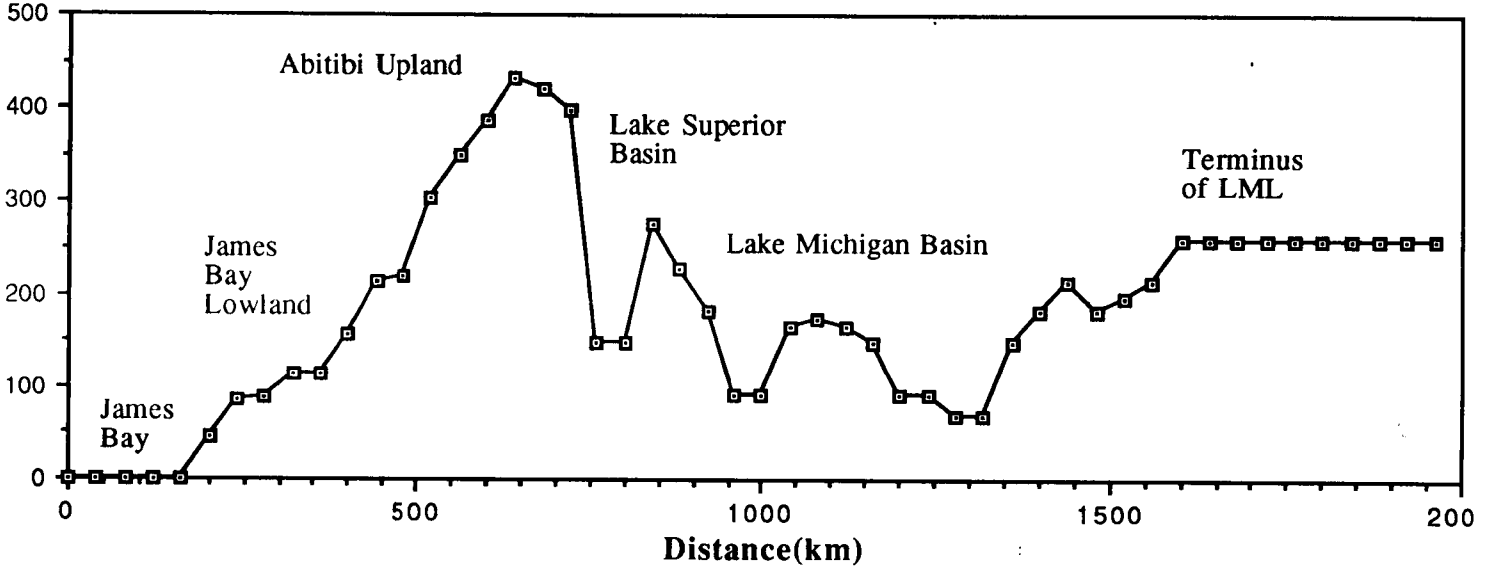

Fig. 2.3. Modern topographic profile of the traverse of the modeled flowline of the Lake Michigan Lobe. Elevation of James Bay area is set to zero. Elevation beyond historic LML terminus is assumed to be uniform.

Numerical implementation

Physical processes included in the model: Fig. 2.4 is a schematic cross section of a generalized ice lobe originating on crystalline, or hard bedrock and flowing onto an unlithified, or soft sediment cover atop sedimentary rock. Processes incorporated in the model, as depicted in Fig. 2.4 include climatic forcing, vertical advection and conduction of heat through the ice, temperature effects on ice stiffness, basal shear stress generated by ice flow, flow of ice and sediment to basal shear stress, basal heat production in the till, geothermal heat flow, basal melting, isostatic adjustment, and topographic effects.

Throughout the rest of this text the term "soft bed" refers to subglacial conditions in which the base of the ice is underlain by water-saturated unlithified sediment that is capable of deforming under the stresses imposed by the ice. In the soft-bedded regions, I have assumed full coupling of the ice and sediment at the ice-sediment interface and zero flow at the base of the shear zone. The term "hard bed" refers to subglacial conditions in which the base of the ice rests on crystalline rock. For simplicity, I have chosen to treat regions of crystalline rock as non-slip surfaces, therefore assuming that ice movement over hard-bedded regions was driven exclusively by internal deformation of the ice.

Grid geometry: For numerical implementation, the conceptual model is rendered into a finite-difference model employing a one-dimensional, cell-centered, 51-node (50-increment) grid superimposed on the central flow line (Fig. 2.5) beginning at the inferred ice divide over James Bay and terminating about 400 km south of the historical terminus of the LML (at node 41). Node-spacing is 40 km, giving a total span of 2000 km. Details of the numerical implementation and grid geometry are described in Appendix A. Source code for the model is in Appendix B.

Program algorithm: The algorithm of the numerical model is shown schematically in Fig. 2.6. Discretization of the governing equations in the main algorithm is described in Appendix A. At the start of program execution, the program initializes the ice thickness and surface elevation with nominal

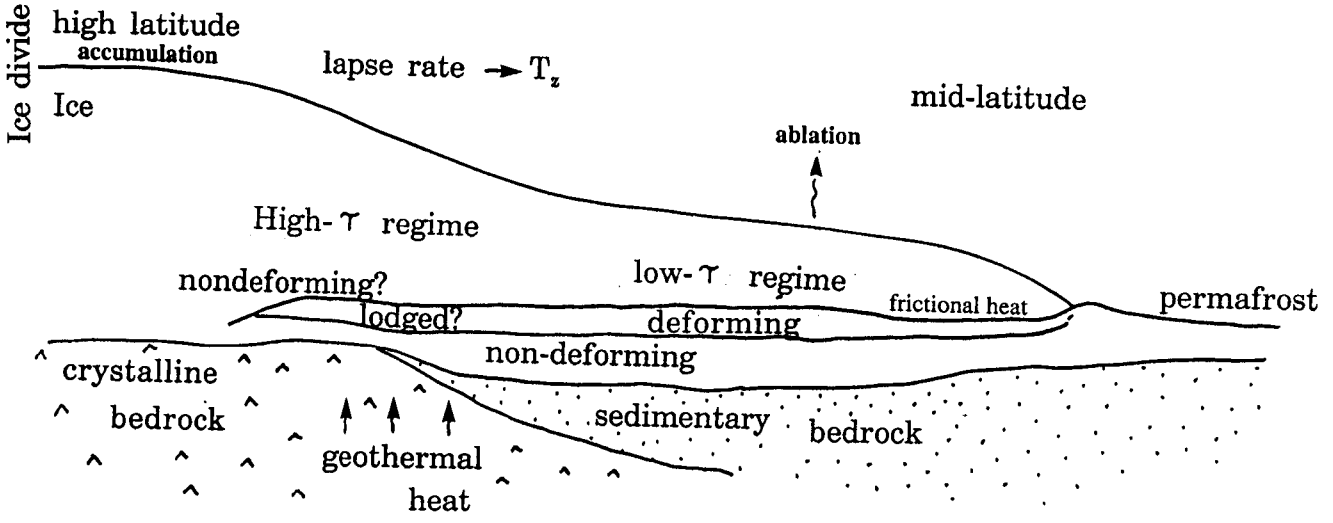

Fig. 2.4. Schematic conceptual model of generalized ice lobe flowing from a non-deforming (and non-slip) surface onto deforming sediment.

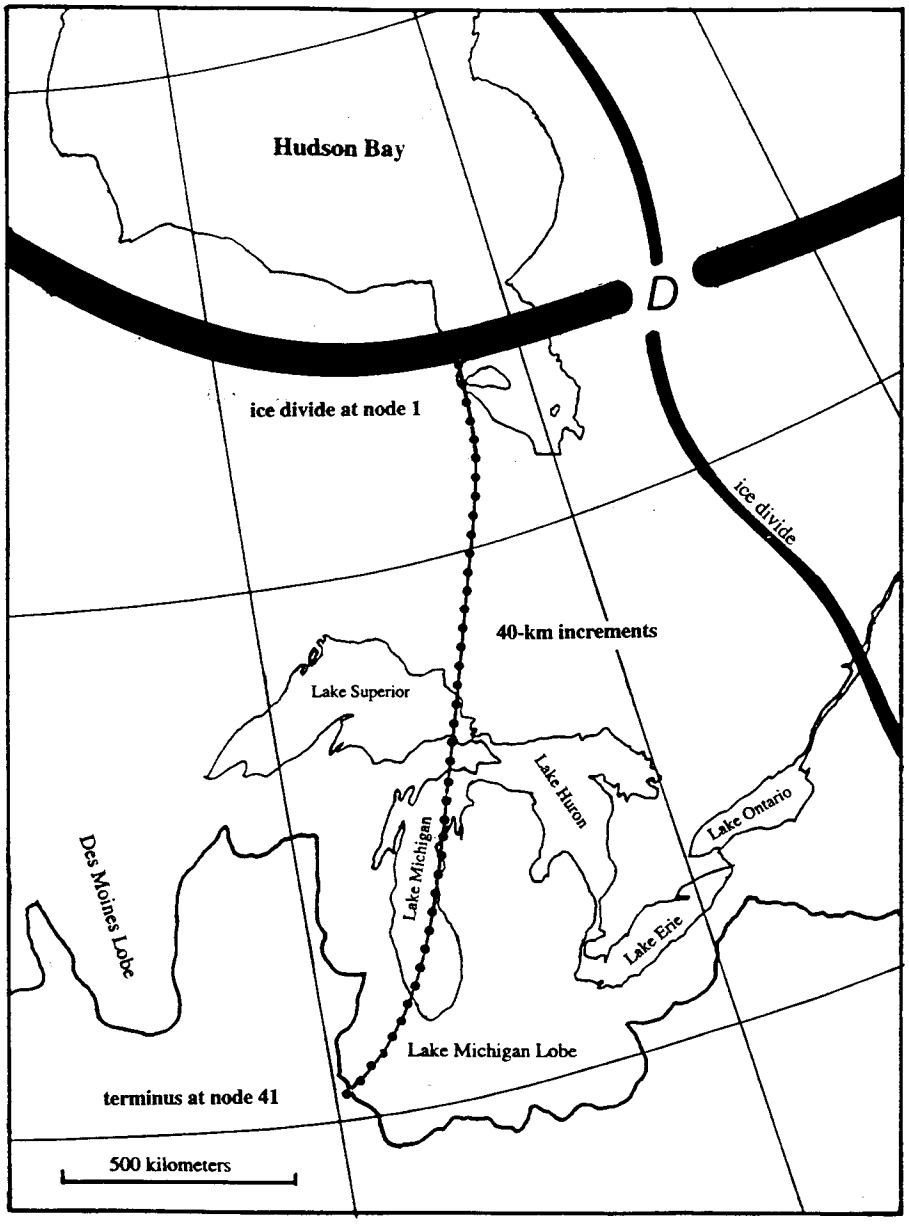

Fig. 2.5. Finite difference grid for the LML model.

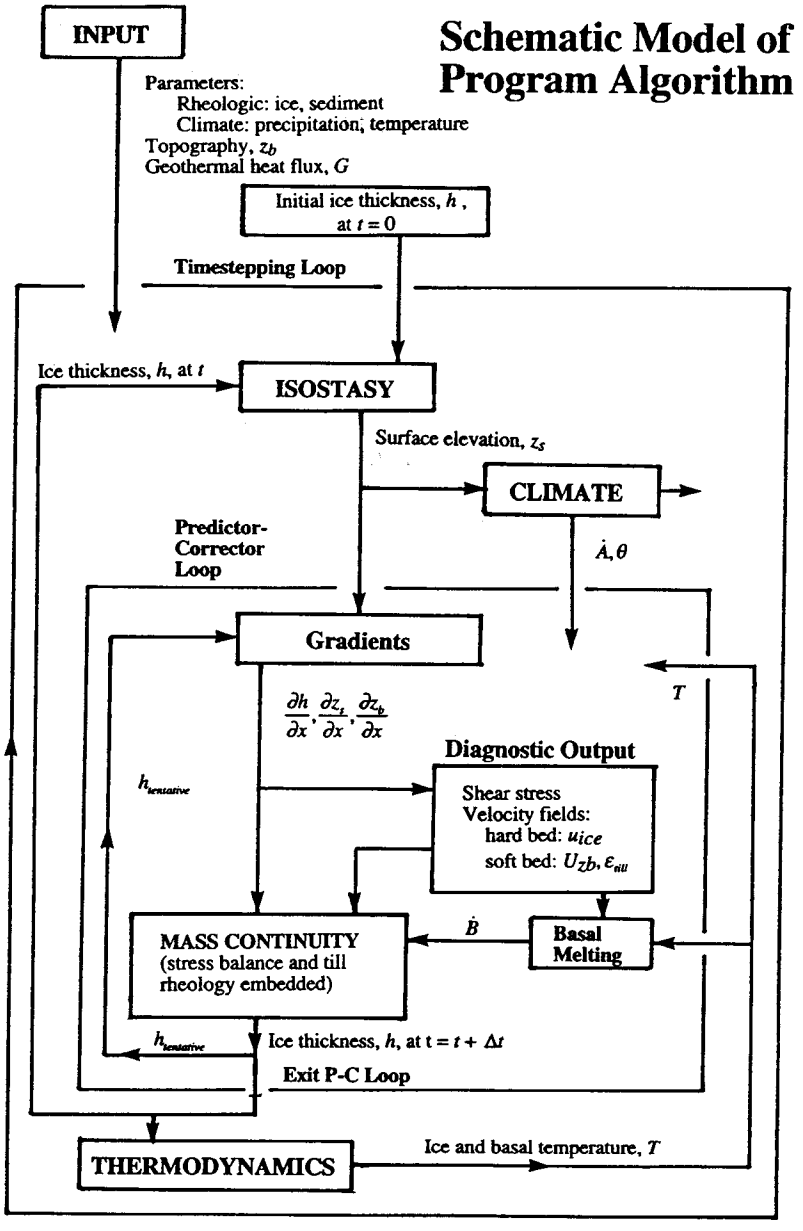

Fig. 2.6. Schematic model of the program algorithm.

values (to prevent computational aberrations such a divide-by-zero error) and reads the geotechnical and climatic parameters, topographic data, and geothermal heat flux from input data files (Appendix B).

At the beginning of each timestep the algorithm adjusts the basal topography and ice surface elevation for isostatic response to the ice thickness computed at the previous timestep, then computes the ice surface temperature and net surface accumulation rate across the ice sheet. To improve accuracy and help stabilize the numerics, the algorithm then enters a predictor-corrector (PC) loop, which essentially "retakes" the dynamic computations at each timestep until the values of ice thickness at each point on the grid are no longer changing. (This is necessary because ice velocity is a strong function of h and z_s, which change during each time step.) More specifically, the PC loop is repeated until the maximum difference between the newly calculated values of ice thickness and those of the previous trip through the loop have converged to within a specified percent deviation (about 0.0001%). When the convergence criterion has been satisfied, the algorithm exits the PC loop and assigns the tentative values of all variables to their "permanent" counterparts for the current timestep. (As shown in Appendix B, variables whose values change inside the PC loop are designated with the abbreviation "TNT" for "tentative", e.g., "tauTNT" is the tentative identifier of the "permanent" variable, "TauBas," for the basal shear stress.)

Inside the PC loop, the first quantities computed are the gradients of the ice surface, ice thickness, and basal surface, and the cell-centered ice thickness (See Appendix A.). From these quantities, the algorithm computes basal shear stress, sediment shear-zone thickness and sediment velocity profiles (where the base is soft-bedded), internal ice deformation velocity profiles, and the basal melting rate at each of the grid nodes. The final step inside the predictor-corrector loop is the solution of a tridiagonal matrix equation to simultaneously (or "directly") determine the ice thickness at each grid node.

The solution is also made as implicit as possible by embedding the constitutive laws for the ice and sediment directly into the flux terms of the mass

continuity equation before rendering it into numerical form. (This is a standard numerical technique for achieving maximum numerical stability. See any basic text in applied numerical analysis (e.g., Maron, 1987).) Experience dictated that as many terms of the constitutive equations as possible be dealt with implicitly.

At the end of each timestep, the algorithm invokes thermodynamic subroutines to calculate vertical advection rates and temperature profiles in the ice (See Appendix B). Thermodynamic computations are saved for use at the next timestep. Timestepping continues until a specified number of timesteps is completed. Output data are collected at selected intervals.

The numerical model: governing equations

The physical processes are represented by the governing equations, which are described in detail below in the order in which they are implemented in the algorithm as described above (Fig. 2.6). The numerical discretization of the equations is described in Appendix A.

Isostatic adjustment: To adjust the basal and surface elevations for isostatic adjustment at each timestep, I adopted a simple model (after Oerlemans, 1982) for isostatic adjustment:

$$\frac{\partial z_b}{\partial t} = \frac{1}{t^*}\left(z_{initial} - \frac{\rho_{ice}}{\rho_{mantle}} h - z_b \right) \qquad (2.1a)$$

where z_b is the current elevation of the base, t is time, t^* the exponential decay constant, $z_{initial}$ is the initial (load-free) elevation of the land surface before isostatic loading, ρ_{ice} and ρ_{mantle} are the ice and mantle densities, respectively, and h is ice thickness. The term

$$z_{initial} - \frac{\rho_{ice}}{\rho_{mantle}} h$$

is the equilibrium value of z_b load imposed by ice thickness, h.

In this equation the amount of bed depression is directly proportional to the ice thickness and inversely proportional to the upper mantle density (as implied by Archimedes' Principle). The rate of adjustment is controlled by the time scale, t^*. The value of t^* is different for different-sized loads. Here I simplify by taking a single value of t^* associated with an ice sheet of diameter L, where

$$t^* = \frac{2\eta\pi}{\rho_{mantle} g L} \qquad (2.1b)$$

and η is the mantle viscosity (Lindstrom, 1989). Based on Dyke and Prest's (1987) reconstruction, I have used an ice sheet (one-dimensional) length scale of 3,000 km. (Values of all parameters used in the model are listed in Appendix B.)

Climate forcing: There are no modern analogs for mid-latitude continental ice sheets with terrestrial margins, and there is little indirect evidence for regional or local paleoclimatic conditions. Previous paleoclimate modeling results (e.g., Budd and Smith, 1981; Manabe and Broccoli, 1985) have too coarse a grid size for direct application to this study or are applicable to only higher latitudes. Given these difficulties, it is beyond the scope of this study to attempt to reconstruct the actual evolution of the ice sheet under extant climate conditions. My sole objective with regard to paleoclimate simulation is therefore simply to produce an ice sheet/lobe that reasonably approximates known or inferred characteristics of the LIS and LML at the LGM. Such a model provides a suitable surrogate on which to perform experiments regarding lobe responses to till rheology and mass balance changes. I have therefore employed a first-order model for paleoclimate forcing using modern temperature and precipitation data, which are adjusted to LGM conditions based on empirical data, experience with the model, and paleoclimatic evidence.

The simplified equation for mean annual ice surface temperature, θ, is

$$\theta = \theta_{present} + \Delta\theta_{CO_2 effect} + \Delta\theta_{ElevationEffect} \qquad (2.2a)$$

where $\theta_{present}$ is the modern mean annual temperature and $\Delta\theta_{CO_2effect}$ is the depression in atmospheric temperature at the LGM, presumed to be primarily due to the difference in CO_2 concentration between LGM and now. The LGM temperature depression is computed from

$$\Delta\theta_{CO_2effect} = \Delta CO_2 \times Sensitivity_{CO_2} \qquad (2.2b)$$

where ΔCO_2 is the difference between LGM and modern (preindustrial) mean global atmospheric carbon dioxide concentrations and $Sensitivity_{CO_2}$ is a coefficient that relates temperature change to changes in atmospheric CO_2 concentration. $\Delta\theta_{ElevationEffect}$ reflects the depression in temperature due to increases in elevation and is therefore computed from

$$\Delta\theta_{ElevationEffect} = LapseRate \times z_s \qquad (2.2c)$$

where *LapseRate* is the global average adiabatic lapse rate and z_s is surface elevation.

Eqn. (2.2b) provides a means for eventually including a more sophisticated climate model of CO_2 and other effects. I had originally hoped to incorporate models of temperature and net accumulation sensitivity to changes in CO_2 concentration, but I could find no suitable theoretical model for the latitudes spanned by the LML. To simplify the current study, I have thus adopted a purely empirical approach, and have estimated the temperature drop across the LML from the constraint that permafrost is known to have existed in northern Illinois around the LGM.

Johnson (1989) documented the existence of widespread permafrost in northern and central Illinois at the LGM from observations of patterned ground and frost wedging. The existence of permafrost implies a maximum mean annual temperature of -6°C (Washburn, 1980, Johnson, 1989). I have thus uniformly lowered modern mean annual temperatures across the entire flow band by adjusting the CO_2 sensitivity coefficient by the amount necessary to

bring the mean annual LGM temperature at the margin from its modern value of 11°C to the inferred LGM value of -6°C. This approach has the twin virtues of being simple and empirically based. In the absence of other paleoclimatic data for the area and suitable theory for incorporating other temperature-altering phenomena, it is perhaps the most reasonable way to incorporate the effects of lower atmospheric CO_2 concentration as well as ice sheet-induced albedo changes and other regional effects. The surface temperatures thus obtained (see Fig. 5.12) are consistent with observations for modern ice sheets in Antarctica and Greenland. The model does not account for dynamic effects such as katabatic winds, large-scale atmospheric circulation changes, or changes to the surface boundary layer of the atmosphere.

Sensitivity studies by Budd and Smith (1981) indicated that large changes in LGM and modern precipitation were not necessary to account for the growth or decay of Pleistocene ice sheets in the time available, although the "elevation desert effect" (whereby the accumulation decreases with increasing surface elevation as the ice sheet grows) could not be disregarded. Apart from the elevation desert effect, Budd and Smith's sensitivity studies showed that it was not necessary to vary the basic precipitation rates from the present values, except perhaps to the extent that GCM studies (e.g., Manabe and Hahn, 1977) suggested higher precipitation along the southern margins. Net accumulation and ablation rates, however, are another matter. There is no geologic evidence from which to infer the mass budget of the system, nor are there any suitable modern analogs from which to infer the net amount or distribution of mass input and loss or seasonal variations for the LML. As Oelermans (1991) points out with reference to modern glaciers, there are simply no "typical" profiles for the accumulation and ablation gradients.

I have therefore imposed a reasonable but purely inferential first-order mass forcing system based on modern precipitation values to generate the ice sheet. I have proceeded from Oerleman's (1991) observations that maximum accumulation typically occurs a short proportion of the distance downstream from the ice divide. Modern mean annual precipitation values increase southward from James Bay (Walter and Lieth, 1967; Korzoun, 1977), so I took

advantage of the modern gradient, allowing the precipitation values in the model to follow the modern values up to about 10% of the distance downstream of the ice divide. In the absence of a sophisticated theoretical basis for determining the paleo-accumulation and ablation rates I simply imposed a linear negative gradient (invoking Occam's Razor) on net accumulation beginning from the point of maximum accumulation and adjusting the magnitude of the gradient so as to place the steady-state margin of the ice at the historical terminus when the sediment rheology in the model was set to the experimental values described in Chapter 4 (See Fig. 5.13). Net accumulation is thus calculated from the following

$$x < x_{\dot{A}_{\max}} \Rightarrow \dot{A} = \dot{A}_{present} - \frac{\partial \dot{A}}{\partial z_s} \cdot z_s$$

$$x \geq x_{\dot{A}_{\max}} \Rightarrow \dot{A} = \left[\dot{A}_{\max} - \frac{\partial \dot{A}}{\partial x} \cdot \left(x - x_{\dot{A}_{\max}} \right) \right] - \frac{\partial \dot{A}}{\partial z_s} \cdot z_s \qquad (2.3)$$

where $\dot{A}$ is the hypothetical LGM net accumulation rate, $\dot{A}_{present}$ is the modern precipitation rate, x is the distance from the ice divide, $x_{\dot{A}_{\max}}$ is the distance from the ice divide at which the maximum net accumulation rate occurs, $d\dot{A}/dx$ is the hypothetical horizontal gradient in net accumulation, and $\partial\dot{A}/\partial z_s$ is the coefficient that accounts for the "elevation desert effect." The value of $\partial\dot{A}/\partial z_s$ in this study is based on modern data from Antarctica (Lindstrom and MacAyeal, 1989).

This is admittedly neither a rigorous nor objective approach, but since paleoclimate is merely a means to another end in this study, it suffices to have a simple but physically reasonable climate model that produces ice sheet conditions consistent with what we know about ice sheet extent, morphology, and behavior from the geologic record. In spite of the simplicity of the climate system, the calculated steady-state elevations of the ice dome, and required times to reach steady state (20,000 to 60,000 years), are plausible (See Figs. 5.1, 5.5, 5.9), and the resulting mass budget curves (b_n vs. elevation, Fig 5.35) is comparable to those of modern Antarctica and Greenland (Boulton and others,

1984). It thus appears to be suitably realistic to serve as a basis for experimentation to determine the relative effects of parameter changes.

Shear stress equation: Basal shear stress is the first quantity calculated inside the PC loop (Fig. 2.6). From glaciological theory, the shear stress at the base of the ice is determined by the ice thickness and surface elevation (Paterson, 1981)

$$\tau_{basal} = -\rho_{ice} g h \frac{dz_s}{dx} \qquad (2.4)$$

where τ_{basal} is the shear stress, ρ_{ice} is the density of ice, g is the gravitational constant, h is ice thickness, and dz_s/dx is the surface slope. The longitudinal stresses in the ice sheet are disregarded because their effect on basal shear stress is small. This equation is evaluated at the beginning of the algorithm to obtain diagnostic values of shear stress, till velocity, and viscous heat production in the deforming till. These diagnostic values are not used in the mass continuity equation, but are used to determine the thickness of the deforming layer (shear zone), ice and sediment velocity fields, and basal melting rate.

Sediment constitutive equation: Over the soft-bedded regions, the basal velocity of the ice, u_{zb}, is calculated from a sediment stress-strain law derived from Iverson's (1985,1986) general model of mass-movement. Although developed for application to the study of creeping landslides, his equation is appropriate for application to coupled ice sheet movement over deforming sediments because such a system is merely a special case of mass movement. In the case of deforming subglacial sediment, the shear stress experienced by the sediment is applied at the surface of the sediment layer by the base of the ice. It is therefore constant with depth, in contrast to the more general case of landslides, in which the shear stress is a depth-dependent function of the hillside slope and the weight of the overlying sediment.

In one dimension, Iverson's equation takes the form

$$\tau_{till} = \left(\frac{1}{2D_0}\right)^{\frac{1-n}{n}} \mu_0 \left(\frac{du}{dz}\right)^{\frac{1}{n}} + c + p' \tan\phi \qquad (2.5a)$$

subject to the boundary condition

$$u_{(z=z_d)} = 0$$

where τ_{till} is the shear stress in the sediment (assumed to be positive in this expression), u is the horizontal velocity, z is the distance below the surface (z = 0 at the sediment surface) and z_d is the thickness of the deforming layer or "shear zone"), D_0 is the Newtonian reference deformation rate, μ_0 is the Newtonian reference viscosity, n is the power law exponent (which determines the sensitivity of non-linear viscosity to the deformation rate), c is sediment cohesion, p' is effective normal (confining) stress, ϕ is the sediment angle of internal friction (Fig. 2.7).

D_0 is required to maintain dimensional consistency between the terms carrying the exponent, n, and the rest of the terms of the equation. It also provides a means of computing the Newtonian reference viscosity, μ_0, which can be thought of as the viscosity of a hypothetical Newtonian material that would produce the same maximum velocity (i.e., velocity at the top of the velocity profile) as the non-linear material responding to the same shear stress. Derivation and interpretation of the Newtonian reference parameters is covered in detail in Chapter 4 and Appendix E.

The last two terms on the right-hand side of eqn. (2.5a) constitute the yield criterion, and it is apparent that in one dimension the yield criterion is the Mohr-Coulomb criterion. The cohesion, c, can be thought of as the inherent strength (resistance to shear) of the material, independent of confining stress. The tangent of the angle of internal friction, $\tan\phi$, determines the sensitivity of the strength of the material to changes in the confining stress. One can see by inspection of the equation that the fundamental constitutive hypothesis is that the deformation rate is non-linearly proportional to the excess of the shear stress

over the extant yield strength (the so-called "excess stress"). When the excess shear stress is zero, the sediment does not deform.

To achieve numerical stability, eqn. (2.5a) had to be solved for the maximum velocity (i.e., velocity at the ice-sediment interface) and rendered into an expression containing the ice thickness, h, so that it could be substituted directly into the mass balance equation. This proved to be a challenging but pivotal step in the success of the project. Details of the implicit implementation

STRESS-STRAIN LAW FOR SEDIMENT DEFORMATION

$$\tau = \left(\frac{1}{2D_0}\right)^{(1-n/n)} \cdot \mu_0 \left(\frac{du}{dz}\right)^{(1/n)} + c + p' \tan\phi$$

u = horizontal velocity
z = vertical coordinate

τ_{till} = basal shear stress
p' = effective normal (confining) stress
D_0 = reference deformation rate
μ_0 = Newtonian reference viscosity
c = sediment cohesion
ϕ = sediment angle of internal friction
n = power law exponent

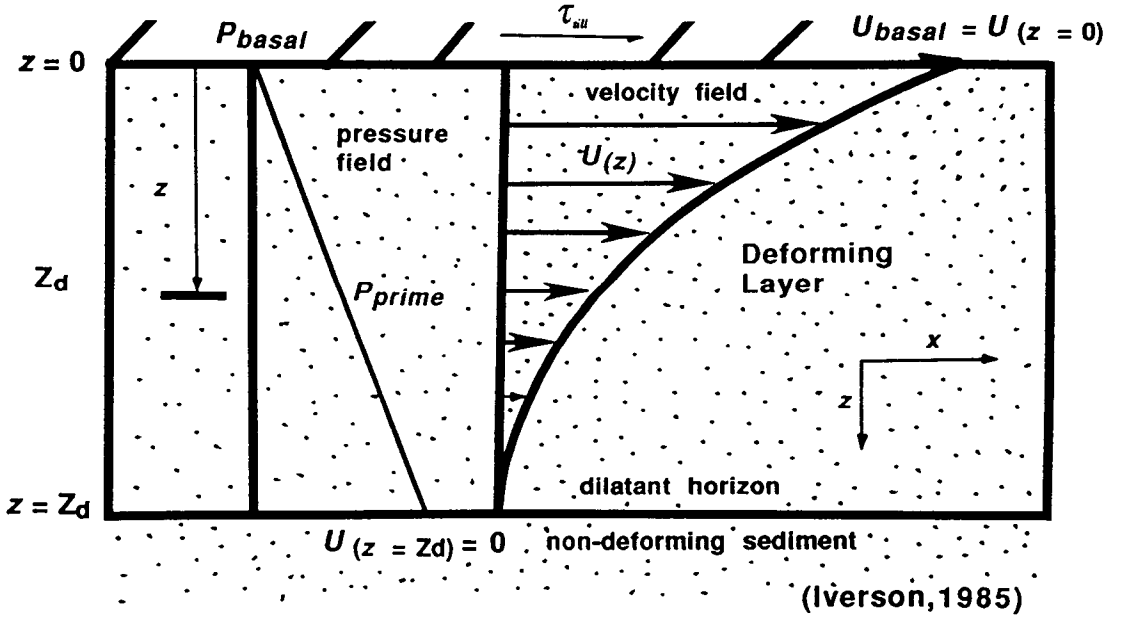

Fig. 2.7. Constitutive model for till rheology and schematic model of typical sediment velocity profile for the case of vertically uniform stress.

of eqn. (2.5a) in the mass continuity equation are described in Chapter 3. Numerical implementation is detailed in Appendix A.

For computing diagnostic sediment velocity profiles, however, the analytical solution of the one-dimensional equation (Iverson, 1986) suffices. For the special case of constant shear stress the solution is

$$u_z = \left| \left(\frac{2D_0^{1-n}}{\mu_0^n (n+1) A_1} \right) \left[(A_2 + A_1 z)^{n+1} - (A_2 + A_1 z_d)^{n+1} \right] \right| \quad (2.6a)$$

$$A_1 = -\rho' g \tan \phi \quad (2.6b)$$

$$A_2 = |\tau| - (c + P'_{basal} \tan \phi) \quad (2.6c)$$

where u_z is the horizontal velocity at depth z, ρ' is the buoyant density of the sediment, g is the gravitational constant, and the rest of the variables are as defined for equation (2.5a). The velocity at the ice-sediment interface, which is assigned to the basal velocity of the ice under the assumption of full coupling (i.e., no slip at the interface), is the sediment velocity at the top of the velocity profile

$$u_{z_b} = u_{(z=0)} \quad (2.6e)$$

A notable feature of the sediment velocity profile (Fig. 2.7) for the case of vertically uniform shear stress is that it is characteristically concave downward in contrast to the familiar concave upward profile exhibited by landslides, in which shear stress increases with depth. The downward concavity implies that strain rates (slope of the velocity profile) below the reference depth are less than the Newtonian reference rate while strain rates at depths above the reference depth are higher than the Newtonian rate. (See Appendix E for derivation and interpretation of the reference parameters used in this study.)

In the coupled ice-sediment flow model, the sediment is assumed to be an incompressible continuum (consistent with Iverson's model), and the deforming layer is assumed to develop atop an infinite half-space (i.e., the thickness of the deforming layer is not limited by the thickness of available sediment). Some additional assumptions inherent in Iverson's constitutive equation also warrant mention since they determine some of the fundamental limitations of the coupled model (Iverson, 1985). The most important is that sediment deformation and water percolation are only weakly coupled, i.e., that pore water pressures are insignificantly affected by deformation. This implies either that water movement is rapid relative to sediment deformation, or that sediment deformation is at steady state. The first of these conditions may not strictly hold at the highest strain rates calculated in the coupled model, but the second condition--that sediment deformation is at steady state--can be confidently assumed given the relatively long time frame (tens of thousands of years) in which the coupled model is applied. Second, the use of the one-dimensional model implies that sediment strength is isotropic. Since unlithified materials cannot support large deviatoric stresses, this assumption has long been applied in geotechnical engineering research with little apparent compromise in validity of the results. Third, stress history is assumed to be irrelevant. This is consistent with the assumption of the large strain and long time frame for deformation; soil deformation properties would eventually become equilibrated to the ambient style of deformation, just as in the case of slowly-moving landslides. Finally, the sediment layer beneath the ice is assumed to be an infinite half-space; there is no physical limit to the depth of the shear zone other than that determined by the effective stress and strength of the material.

Viscous heat production: Following computation of the diagnostic shear stress and sediment velocity, the heat production rate per unit length of flowline in the sediment is computed from

$$\varepsilon_{till} = \left| \tau_{basal} \cdot u_{z_b} \right| \qquad (2.7)$$

where ε_{till} is the unit rate of heat production, u_{z_b} is the maximum sediment velocity, and τ_{basal} is the applied shear stress.

Ice dynamics: To calculate ice deformation velocity, I adopted the ice deformation equation as employed by Huybrechts (1992), which in one dimension is

$$u_z - u_{z_b} = -2(\rho_{ice} g)^3 \left(\frac{\partial z_s}{\partial x}\right)^3 \int_{z_b}^{z} A_{(T^*)} (z_s - z)^3 dz \qquad (2.8)$$

where u_z is the horizontal velocity at position z, u_{z_b} is the basal velocity, z_s is the elevation of the ice surface, z_b is the elevation at the base, T^* is temperature, and A is the temperature-dependent rheologic parameter for ice (Thomas and others, 1980; Barnes and others, 1971).

To achieve numerical stability, the ice velocity, like the till velocity, was rendered in terms of ice thickness, h, and substituted directly into the mass balance equation. The required manipulation of (2.8), substitution into the mass balance equation, and numerical implementation are detailed in Appendix A. The explicit solution of (2.8) is used in the model only for diagnostic computation of the ice velocity fields.

Depth-averaged ice velocity is also calculated for diagnostic purposes by integrating the ice velocity equation over the thickness of the ice and dividing by the ice thickness

$$u_{ice} = -\frac{2(\rho g)^3}{h} \left(\frac{\partial z_s}{\partial x}\right)^3 \int_{z_b}^{z_s} \int_{z_b}^{z} A_{(T(x,z))} (z_s - z)^3 dz dz \qquad (2.9)$$

Mass continuity: The central component of the algorithm is the mass continuity equation. Conservation of mass is enforced by solving the one-dimensional form

$$\frac{\partial h}{\partial t} = \dot{A} + \dot{B} - \frac{\partial (u_0 h)}{\partial x} \qquad (2.10a)$$

where h is ice thickness, t is time, $\dot{A}$ is the accumulation rate, $\dot{B}$ is the basal melting rate. u_0 is the depth-averaged *total* velocity:

$$u_0 = u_{ice} + u_{z_b} \qquad (2.10b)$$

where u_{ice} is the depth-averaged ice velocity, and u_{zb} is the basal ice velocity. Expanding the equation to reflect the separate contributions of ice and sediment rheology to the ice flux gives

$$\frac{\partial h}{\partial t} = \dot{A} + \dot{B} - \frac{\partial}{\partial x}\left(u_{ice} h\right) - \frac{\partial}{\partial x}\left(u_{z_b} h\right) \qquad (2.10c)$$

The value of h at each timestep is computed by substituting the constitutive laws for ice and sediment deformation into eqn. (2.10c), writing the resulting equation in terms of finite differences, then solving the system of equations for h to obtain an implicit solution for each point on the grid at each timestep. At the upstream boundary, where I have assumed an ice divide, I have imposed a boundary condition requiring the mass flux to be equal in opposite directions, thus dictating either an ice dome or saddle point. The terminus requires no boundary condition. Discretization and implementation of eqn (2.10c) and the boundary condition are described in detail in Appendix A.

Thermodynamics: At the completion of each timestep the program invokes the thermodynamic subroutines (Appendix B) to compute the temperature distribution in the ice. The temperature values are retained and used in the subsequent timestep to compute the ice stiffness term, A, in the ice deformation law (eqn.s 2.8, 2.9). Details of the numerical implementation and encoding of the heat equation are found in Wang (1993).

The heat equation for the model includes vertical diffusion and vertical advection. Horizontal diffusion can be neglected because of the high aspect ratio of the ice sheet. Horizontal advection cannot be so readily dismissed, especially for the high velocities observed in this model. Including it, however, extracts a price of much greater computational complexity for a fairly modest gain in physical accuracy. Since the effect of neglecting this term is predictable

(downstream temperatures will be erroneously warmer than they should be by a few percent), and since the objective of this study (the influence of till rheology on ice sheet dynamics) can be met without it, I elected to exclude it in the interest of economy. The heat equation is thus

$$\frac{\partial T}{\partial t} + w\frac{\partial T}{\partial z} = K\frac{\partial^2 T}{\partial z^2} \qquad (2.11)$$

where T is temperature, t is time, w is the vertical velocity of the ice, and K is the thermal conductivity of ice. For the surface boundary condition the temperature is set to the mean annual air temperature at the glacier surface, as determined by equation (2.2a)

$$T_{(z=z_s)} = \theta \qquad (2.12)$$

To compute the vertical advection term, w, the two-dimensional incompressible mass continuity law,

$$\frac{\partial w}{\partial z} + \frac{\partial u}{\partial x} = 0 \qquad (2.13)$$

is integrated to give

$$w_{(z)} = -\int_{z_b}^{z} \frac{\partial u}{\partial x} dz + \left(u_{z_b} \frac{\partial z_b}{\partial x} - \dot{B} \right) \qquad (2.14)$$

where the last term on the right hand side is from the basal boundary condition (in which the derivative term incorporates the effect of flow over the topographic surface and $\dot{B}$ is the basal melting rate). Advection due to englacial water is excluded since the ice is assumed to have been "non-temperate" and therefore devoid of englacial channels.

If the ice is melting at the base, the basal boundary temperature is fixed at the pressure melting point. If the ice remains frozen at the base, then the heat flux into the ice at the boundary is set equal to the geothermal heat flux. Heat flow in the bedrock is calculated from 1500 meters below the surface by arbitrarily

assigning a constant flux boundary at the -1500 m level. Over the time spans employed by the model the heat distribution below this level will not be significantly affected. The basal melting rate of the ice, $\dot{B}$, is determined from the basal heat budget

$$\dot{B} = \left(G + H + \varepsilon_{till}\right) / \left(\rho_{ice} LHF_{ice}\right) \qquad (2.15)$$

where G is the basal heat flux due to the geothermal gradient, H is the heat flux due to the internal ice temperature gradient, and ε_{till} is the heat of viscous dissipation from the deforming sediment layer (where present), ρ_{ice} is the density of ice, and LHF_{ice} is the latent heat of fusion for ice.

Chapter 3

Sediment rheology: Implementation of the Iverson equation

Implementation of the sediment rheologic equation

Before the sediment constitutive law can be embedded in the mass continuity equation it must first be converted to an expression for the basal ice velocity, u_{zb}, in terms of the ice thickness, h,. To make this transformation, one starts with the fundamental form

$$\frac{du}{dz} = F \cdot \left(|\tau| - S_0 - S_{(z)} \right)^n \qquad (3.1a)$$

where

$$F = \left(\frac{1}{2D_0} \right)^{n-1} \mu_0^{-n} \qquad (3.1b)$$

$$S_0 = \left(c + P_b' \tan \phi \right) \qquad (3.1c)$$

$$S_{(z)} = \rho' g \tan \phi \cdot z \qquad (3.1d)$$

and the rest of the parameters are as defined for equation (2.5). Once this is rendered into an equivalent form (see Appendix F)

$$\frac{du}{dz} = F \left[\left(\frac{z_d - z}{z_d} \right) \left(|\tau| - S_0 \right) \right]^n \qquad (3.2)$$

one can solve analytically for the velocity at the interface by separating variables and integrating

$$\int_0^{z_d} du = F \left(|\tau| - S_0 \right)^n \int_0^{z_d} \left(\frac{z_d - z}{z_d} \right)^n dz \qquad (3.3)$$

Note that the term containing the shear stress can be taken outside the integral since shear stress is in this case constant with depth. The above is therefore a solution to only this special case of Iverson's equation. Equation (3.3) can be solved to yield an analytical expression for the basal velocity, u_{zb}:

$$u_{z_b} = F(|\tau| - S_0)^n \frac{z_d}{(n+1)} \qquad (3.4)$$

Although we now have an expression for the magnitude of basal velocity of the ice, the exponent can take on *any real value* greater than zero, so the expression cannot indicate the direction of the ice flow by simply carrying an algebraic sign. Since ice flow is in the direction of shear stress, however, one can work around this limitation by multiplying eqn. (3.4) by the shear stress divided by its absolute value. The final term, equal to unity, carries the directional sign for the velocity.

$$u_{z_b} = F(|\tau| - S_0)^n \frac{z_d}{(n+1)} \frac{\tau}{|\tau|} \qquad (3.5)$$

We can express the shear stress in the denominator of the final term in (3.5) in terms of ice thickness and surface slope by substituting in equation (2.4) to obtain

$$u_{z_b} = -F \frac{z_d}{(n+1)|\tau|} (|\tau| - S_0)^n \rho g h \frac{dz_s}{dx} \qquad (3.6a)$$

where

$$\frac{dz_s}{dx} = \frac{dh}{dx} + \frac{dz_b}{dx} \qquad (3.6b)$$

so that equation (3.6a) becomes

$$u_{z_b} = -F \frac{z_d}{(n+1)|\tau|} (|\tau| - S_0)^n \rho g h \left(\frac{dh}{dx} + \frac{dz_b}{dx} \right) \qquad (3.7)$$

Note that the shear stress terms inside the absolute value signs must be computed explicitly using ice thickness and surface gradient quantities from the previous time step.

For convenience we define the quantity $Q_{(x)}$, where

$$Q_{(x)} = -F\frac{z_{d(x)}}{(n+1)\left|\tau_{(x)}\right|}\left(\left|\tau_{(x)}\right| - S_{0(x)}\right)^n \rho g h_{(x)} \qquad (3.8)$$

We can now express eqn. (3.7) as

$$u_{z_b} = Q_{(x)}\left(\frac{dh}{dx} + \frac{dz_b}{dx}\right) \qquad (3.9)$$

Eqn. (3.9) expresses the basal velocity in terms of the independent variable, h, so we now have the type of expression we have been seeking to substitute into eqn. (2.10c)

$$\frac{\partial h}{\partial t} = \dot{A} + \dot{B} - \frac{\partial}{\partial x}\left(u_{ice}h\right) - \frac{\partial}{\partial x}\left(u_{z_b}h\right) \qquad (2.10c)$$

thus expanding it to

$$\frac{\partial h}{\partial t} = \dot{A} + \dot{B} - \frac{\partial}{\partial x}\left(u_{ice}h\right) - \frac{\partial}{\partial x}\left[Q_{(x)}h\left(\frac{\partial h}{\partial x} + \frac{\partial z_b}{\partial x}\right)\right] \qquad (3.12)$$

(The ice velocity term is manipulated in an analogous fashion. Its implementation is described in Appendix A.)

Note that the value of $Q_{(x)}$, the ice thickness, h, and the basal topographic slope, $\partial z_b/\partial x$, in (3.12) must be taken from the calculations of the previous timestep. The ice thickness derivative, $\partial h/\partial x$, however, can be rendered implicit in the mass balance equation--this is key to numerical stability. Details of the numerical discretization and encoding are in Appendices A and B.

The quantity $Q_{(x)}$ requires an explicit value for z_d, the thickness of the shear zone (See eqn. 3.8). The "instantaneous" value of z_d is determined from the Mohr-Coulomb failure criterion

$$z_{dinst} = \left\{\left[(|\tau| - c)/\tan\phi\right] - P_{basal}\right\}/(\rho' g) \qquad (3.13)$$

The current value of z_d, however, (the one that is inserted into $Q_{(x)}$) is computed from the following "relaxation" condition

$$\frac{dz_d}{dt} = -\frac{1}{t^*}(z_d - z_{dinst}) \qquad (3.14)$$

which restrains the rate at which the value of z_d can change at any given point on the grid. (Details of the implementation of eqn (3.14) are given in Appendix A.) Treating z_d in this manner is a numerical smoothing technique that reduces the magnitude of the "jump" in z_d at each iteration of the PC loop (Fig. 2.6). The relaxation constant, t*, is set to within an order of magnitude of the timestep, however, so that the relaxation is relatively rapid. Full relaxation is probably complete by the time the PC loop achieves convergence at the end of each timestep, so end results are unlikely to be significantly altered. Moreover, the imposition of the relaxation condition, though lacking an empirical basis for its parameters, is consistent with what one might infer happens in reality--the development of the dilatant horizon is probably not instantaneous.

With the mass balance equation rendered implicit as described above, the model is capable of running at a timestep of 3 years or less for values of n less than about 1.5. For values of n above 1.5, the timestep must be reduced to less than one year to keep the algorithm stable. I was able to accomplish most of the experiments for this study on a Macintosh Quadra 950 using 3-year timesteps. Steady-state runs to 30,000 years at 3-year timesteps require about 5 hours of computing time when the thermodynamic modules were active. Grid-centered differencing drastically improves the stability of the code, but the transition across the physical boundary between hard- and soft-bedded ice necessitates cell-centered differencing. Further application of the model to problems involving higher values of n or incorporating additional physical phenomena

will require optimization of the code and porting it to a work station or supercomputer to keep the run times practicable.

Chapter 4

Sample collection and sediment parameter evaluation

Sample collection: glacigenic sediments at Wedron, Illinois

To provide appropriate parameters for sediment properties in the model, I collected samples of selected till and proglacial sediments deposited by the LML in northern Illinois. These have been subjected to geotechnical tests to evaluate the confining stress, shear strength, and flow behavior of the material under conditions inferred to have been likely during deposition.

Sediment samples for this study came from the Wedron Silica Company quarries at Wedron, Illinois, about 70 km inside the terminus of the LML (Fig.s 4.1 and 4.3b). The exposures here are among the best constrained in time, most stratigraphically continuous, and most easily accessible in the area. The glacial deposits overlie the Ordovician St. Peter Sandstone, which has been mined locally for commercial silica for over one hundred years. Ongoing mining facilitates continuous stratigraphic study and collection of fresh sediment samples for geotechnical analysis. Fig 4.1b shows the composite lithofacies and facies associations at Wedron, along with the processes, sequences, glacial environments, and ice sheet status inferred by Johnson and Hansel (1990).

Johnson and Hansel (1990) interpreted the deposits at Wedron, Illinois, as the result of three glacial events. Their interpretation is a revision of the previous stratigraphic interpretation (Willman and Frye, 1973). Their revision will eventually include a proposal to upgrade the status of the Tiskilwa Till to formation rank, and reclassify the Malden Till Member as the Batestown Formation (Johnson and Hansel, personal comm., 1992). In this discussion I have adopted their forthcoming revision. During the summer, 1992, I collected undisturbed block samples of the lacustrine clays deposited beneath glacial sequences I and II (A1, A2, Fig. 4.1), and disturbed but undesiccated samples of the lodgment till (D1 and D3) in each sequence. Certain strata in each sequence

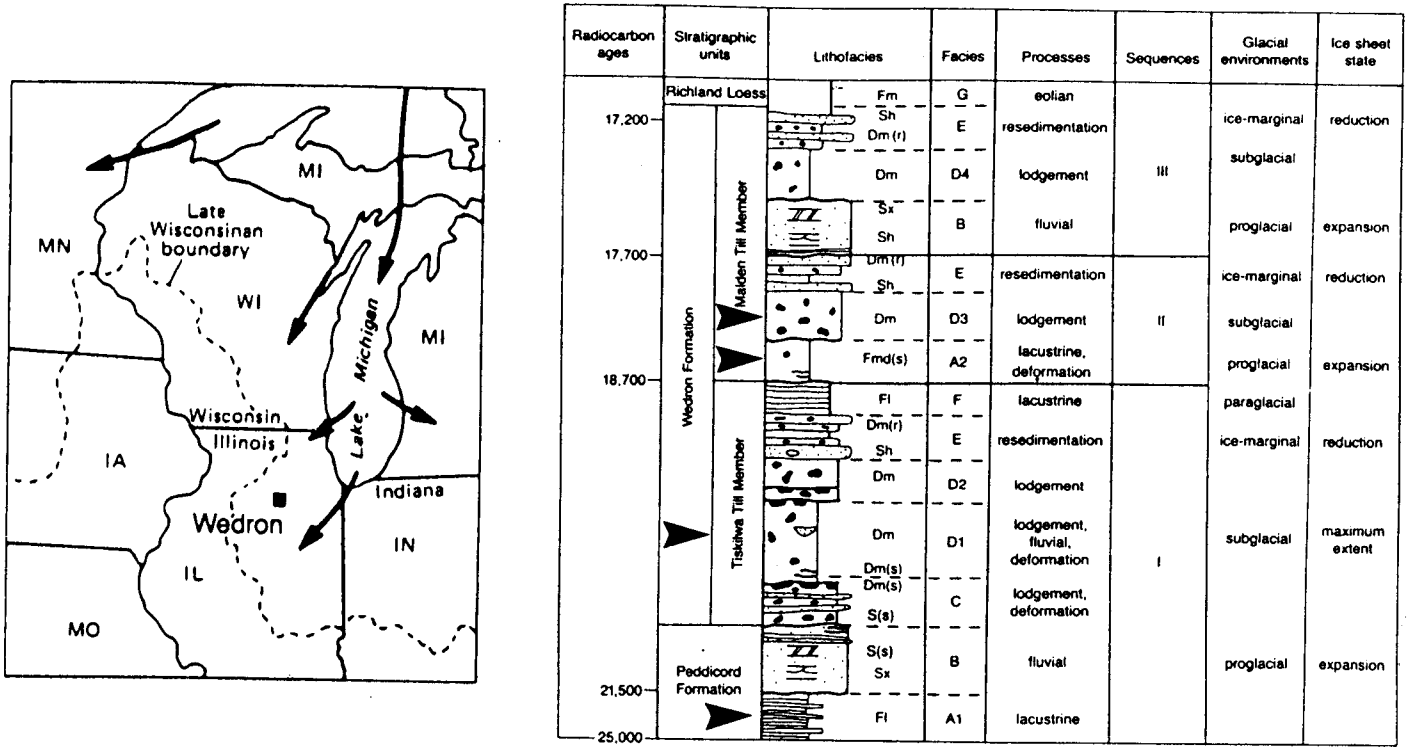

Fig. 4.1a. Location map, Wedron, Illinois, site of geotechnical sample collection, relative to late Wisconsin glacial boundary and Lake Michigan b. Composite stratigraphy at Wedron, Illinois, with inferred processes, sequences, glacial environments, and ice sheet state. Arrows mark sampled members. (From Johnson and Hansel, 1990, Figs. 1 and 16).

display evidence of deformation, including faults and shear planes, folds and boudinage, and deformed channel structures.

Sequence I, dated at 25-18.7 ka, includes the Peddicord Formation and the overlying Tiskilwa Till. The Peddicord Formation includes a slackwater glaciolacustrine facies (A1) overlain by a proglacial fluvial facies (B). These were deposited ahead of the advancing glacier that deposited the Tiskilwa Till. The Tiskilwa Till contains three facies/subfacies: C, D1, and D2. Johnson and Hansel report that although facies C shows evidence of deformation during and following deposition, subfacies D1 and D2 contain undeformed channel features which suggest that even if these layers were deforming during deposition, deformation eventually ceased and was followed by a period of subglacial fluvial action. Johnson and Hansel conclude that extensive subglacial deformation was discontinuous and probably limited to the early stages of the glacial event.

Sequence II, dated at 18.7-17.7 ka, is similar to sequence I. Facies A2 at the base of the sequence is interpreted by Johnson and Hansel as an ice-contact lacustrine facies influenced by deposition of outwash ahead of the readvancing ice. Facies A2 contains deformation features. Facies D3 is homogeneous and does not contain the channel features observed in D1 and D2. The presence of deformation features in the lacustrine clays probably reflects shearing and/or dewatering under the overriding ice: the erosional contact is abrupt, and the abrupt change in grain size and increase in illite in A2 indicate a sudden significant change in the lacustrine environment. The absence of deformation features in D1 and D2 does not necessarily preclude deformation. Some workers (e.g., Boulton, 1987; Alley, 1991) have suggested that homogeneous textures might simply reflect thorough, pervasive deformation that completely destroyed initial structures in the sediment. The preservation of deformational features in the underlying lacustrine sediments could reflect initial response to the shear stress from the overriding ice. The features may have been spared subsequent obliteration either because the shear stress was relieved by straining of the overlying sediments deposited once the glacier arrived, or because sediment strength was increased by dewatering until it became resistant to the stress, or a combination of the two effects (Alley, 1991).

Selection of strata for geotechnical investigation

Although I collected samples of till and underlying lacustrine clays from both sequences, I restricted the experimental work for this study to sequence II for two reasons. Laboratory equipment was sufficient for testing only one suite of samples in a single year. Second, because sequence II was the most accessible I was able to obtain a larger number of samples from it than from sequence I. Since we anticipated that preparation and testing under the high effective stresses required would be challenging, we thought it prudent to work from the largest set of samples.

From a geologic point of view, sequence II is especially interesting. Because it was deposited within a one thousand-year interval during one of the readvances that followed the glacial maximum, the sequence is a good candidate for exhibiting characteristics associated with active coupled ice-sediment movement. Finally, sequence II is also somewhat more well-constrained in time and less complex stratigraphically than sequence I.

Because the subglacial sediments appear to have been covered immediately following deposition, it is reasonable to assume that their geotechnical properties have not been substantially altered since deposition, at least not by desiccation or other subaerial processes. In both sequences, proglacial lacustrine sediments show no evidence of desiccation and appear to be in conformable contact with the overlying proglacial sediment. The lodgment till is conformably overlain by meltout till, which in the Batestown sequence is in turn overlain by a thick blanket of proglacial sediment and loess. There is no evidence of disturbance by root penetration, bioturbation, or wetting-drying cycles, nor any evidence of pedogenic alteration or cementation. Moreover, since the clay component of these sediments is predominantly illite, and there is no apparent reason to suspect significant change in groundwater chemistry since deposition, the geotechnical properties of the clay and till layers are unlikely to have been altered by cation exchange.

Geotechnical testing

Two types of geotechnical tests were conducted to obtain experimental parameters for the model. Undisturbed block samples of the lacustrine clay from the Batestown sequence were used to obtain preconsolidation values. Remolded and reconsolidated samples of the till were used to obtain shear strength and viscosity parameters. Details regarding the execution of the geotechnical experiments and data analysis for the Batestown sequence samples are reported separately (Vela, Ho, and Jenson, in prep.). Results are summarized below.

Preconsolidation: Following deposition, sediments may be consolidated exclusively under their own weight or may be consolidated under an additional, externally applied vertical stress. Sediments that have consolidated exclusively under the stress imposed by their own weight are said to be *normally* consolidated. (Test specimens that have been remolded and subsequently tested without being consolidated beyond the vertical stress applied during the test are also said to be normally consolidated.) Sediments that have previously been consolidated beyond their current vertical confining stress are said to be *overconsolidated.* Disturbed or dilated materials that have not consolidated to equilibrate with their current stress state are said to be *underconsolidated.*

So long as drainage from the system is uninhibited (the "well-drained" case in engineering terms) consolidation proceeds at a logarithmically decaying rate that is a function of the effective confining stress (Holtz and Kovacs, 1981):

$$e = e_0 - C_c \log \frac{p'}{p'_0} \qquad (4.1)$$

where e is the void ratio, p' is the applied vertical stress, e_0 is the void ratio at the designated pressure p'_0 and C_C is the compression index, an experimentally determined parameter that defines the relationship between applied pressure and void ratio.

Since unlithified sediments are only slightly elastic, the sediment skeleton will not return to its original void ratio when stress is removed; instead, it expands to a void ratio considerably smaller than the value before stress was applied. If stress is reapplied, the void ratio will again decrease, but at a much smaller rate until the stress exceeds the maximum value previously applied. The consolidation rate then suddenly increases, producing a "knee" in the curve that marks the maximum effective confining stress to which the material previously equilibrated (Fig. 4.2). The preconsolidation stress in this study is determined using the method of Casagrande to locate the point that marks the preconsolidation stress (See any elementary text in soil mechanics, e.g., Holtz and Kovacs, 1981).

Preconsolidation tests for this study were conducted on 3 samples, yielding preconsolidation values of about 1500 kPa (Fig. 4.2 and Appendix C). The clay was well-positioned stratigraphically to meet the objectives for this study. Both its upper and lower boundaries are in conformable contact with permeable proglacial sediment . It should thus have been sufficiently well drained to have equilibrated with the superposed load, with the drainage rate (hence consolidation rate) restricted only by the consolidation coefficient of the clay itself; it is therefore ideally suited for obtaining reliable measurements of the actual maximum effective stress.

The site from which the samples were removed was overlain by 9-10 meters of overburden, and there may have been up to about 10 additional meters removed by post-glacial erosion (Johnson, personal communication). Using an estimated value of 15-16 kPa/m for the soil column overlying the sample site, the stress imposed by the overburden would be about 300 kPa. Thus the overconsolidation stress for the samples is about 1200 kPa.

Clark's (1992) reconstruction of the LML based on moraine heights (Fig. 4.3) suggests an LGM thickness of the lobe in the Wedron area of about 140-150 meters. A meter-square column of ice imposes a load of 8.9 kPa per meter height. A 140-150 m column of ice would therefore impose about a 1300

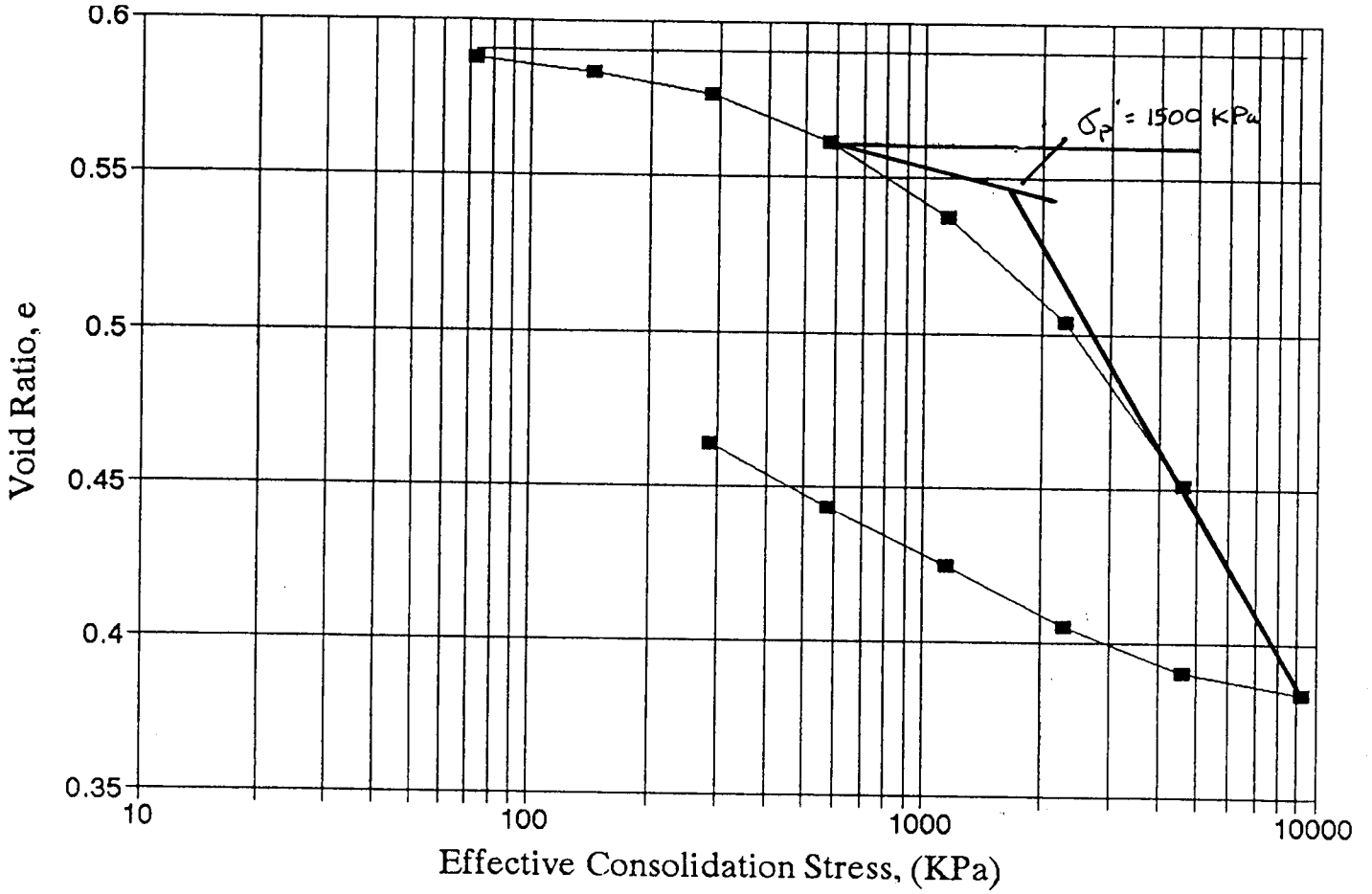

Fig. 4.2. Preconsolidation curve for one of the samples (block #1, Sample #2) of Batestown clay, showing preconsolidation stress as determined by Casagrande method. (See Appendix C for complete test data.)

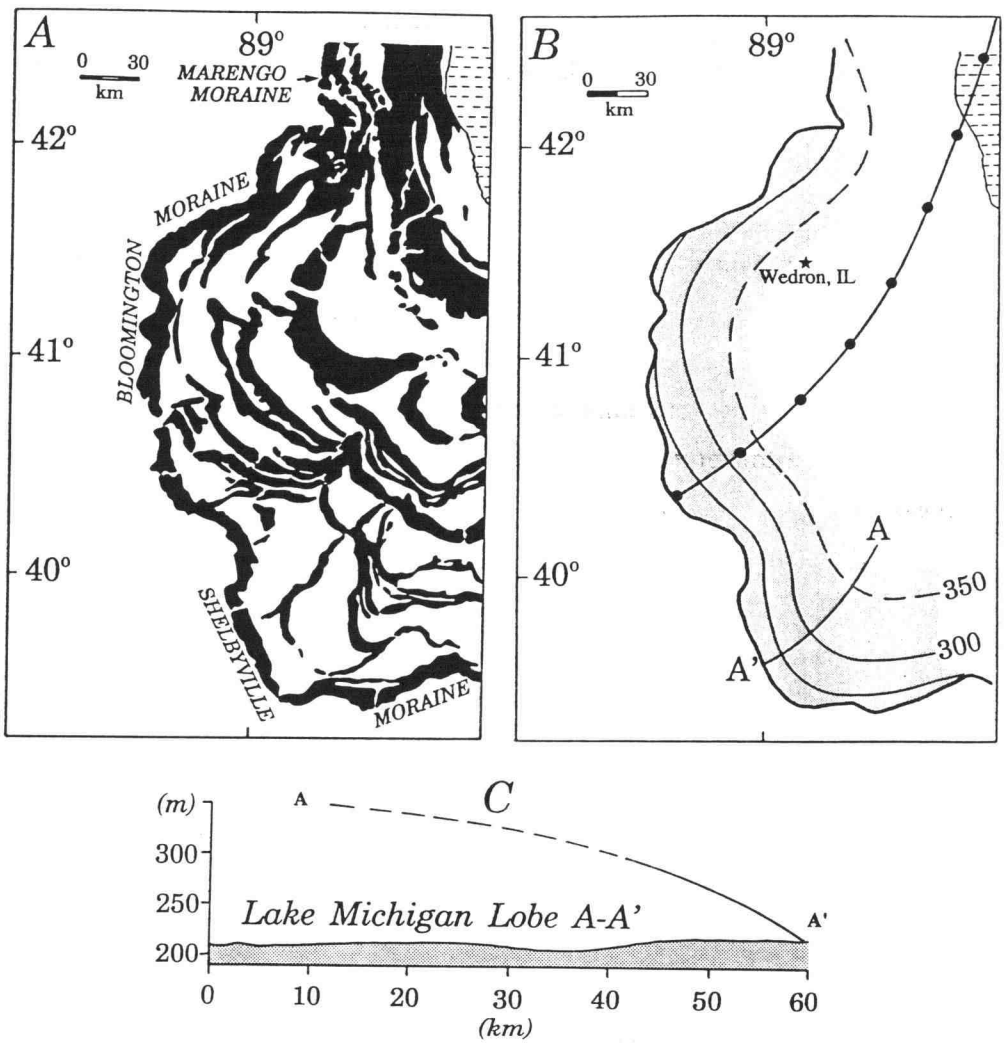

Fig. 4.3. Reconstruction of LML ice surface profile based on moraine height data (From Clark, 1992). A. Major moraines deposited by LML. (Lake Michigan is shown by dashed line pattern.) B. Clark's reconstructed morphology of the LGM LML. Contour interval is 50 m. Flowband of model with finite difference grid locations superimposed is shown for comparison. Location of sample collection site at Wedron, Illinois, is also shown. C. Clark's reconstruction of LML profile for the first 60 km.

kPa load at the base. The measured overconsolidation stress of approximately 1200 kPa in the Batestown clay at Wedron closely matches Clark's estimate of the ice load. Because the preconsolidation stress represents the applied load minus the pore water pressure, however, the thickness of the ice cannot be directly inferred from preconsolidation stress unless pore water pressure can be accurately determined.

Preconsolidation measurements have been used by others to infer basal confining stresses beneath glacial ice (cf. Mickelson and others, 1979; Sauer, 1974; Christiansen, 1987; Sauer and Christiansen, 1991). Although conclusions are generally equivocal, some insights have been gained. Boulton and Dobbie (1993) recently used preconsolidation data from the Netherlands and England to infer basal melting rates, subglacial groundwater flow patterns, ice overburden, basal shear stress, ice surface profile, and sediment volume removed by erosion. From preconsolidation tests on clay underlying the till in the Puget Lowland and calculations of maximum ice load from moraine elevations, Brown et al. (1987) concluded that subglacial water pressure had been sustained at about 90% of the ice overburden. van Gelder et al. (1990) recently demonstrated the application of preconsolidation tests on glacial till to reconstruct the thickness of former valley glaciers. Early attempts to reconstruct Pleistocene ice thickness south of the Great Lakes using the same technique (Harrison, 1958: Smith, 1961) obtained values ranging from 200 to 500 m (650 to 1,690 ft). The use of preconsolidation stress for ice sheet reconstruction in this region has since been largely neglected. Presumably, these earlier results were regarded as suspect because of the prevailing view that the ice had been much thicker (e.g., over 1000 meters). The values obtained by Harrison and Smith, however, are consistent with more recent reconstructions by independent methods that suggest thin ice (on the order of only a few hundred meters or less) (Mathews, 1974; Clark and Bruxvoort, 1989; Clark, 1992).

In the absence of data on the actual pore water pressure in the LML, it is difficult to say exactly what the measured preconsolidation stress from the Wedron samples tells us about the stress state of the sediment during and after deformation. If Clark's estimate of the LML thickness is accurate, and if the

measured excess overconsolidation at Wedron reflects full equilibration to the ice load, then the excess pore water pressure in the sediment would have had to be near zero during consolidation. Given the measured sediment angles of internal friction of 20-25° (reported in the following section), however, an applied shear stress on the order of 500 kPa would be required to induce sediment deformation given a confining stress on the order of 1500 kPa. Since 500 kPa shear stress is well beyond what can be generated even by hard-bedded, non-sliding ice (typically about 100kPa), deformation therefore implies very high basal pore-water pressures. Consolidation to the measured preconsolidation stress of 1500kPa would had to have taken place subsequent to deformation but prior to ice withdrawal if the excess overconsolidation stress does indeed reflect the ice load of the LML.

In this study, the main application of the measured preconsolidation stress from the Wedron samples is simply to determine an appropriate upper limit for the range of confining stresses at which to conduct the geotechnical tests for sediment yield strength. The rationale for selecting measured preconsolidation as the upper bound for testing is that it is likely to represent the actual initial consolidation state of the sediment when overridden by the lobe: If the preceding advance and retreat of the lobe took place under conditions similar to those which produced the Wedron sample values, then it is likely that the measured preconsolidation value is representative of the initial consolidation state as well as the final one.

On the other hand, if the sediment had been deforming during the previous lobe emplacement but had not been overconsolidated before or during the retreat of the lobe, it would have either been normally consolidated or returning from its dilated state to a normally consolidated state upon the final advance of the lobe. We therefore elected to conduct a second suite of tests on remolded material that was not previously reconsolidated to a higher confining stress than that at which it was to be tested--presumably reflecting as closely as possible the state of sediment overridden and sheared by the basal shear stress of the glacier before the sediment had the opportunity to equilibrate to any higher confining stress. It should be noted that in its dilated state the sediment would

be underconsolidated or normally consolidated. The normally consolidated strength is probably a reasonable approximation of its strength when dilated. Previous work has shown that critical-state strength (i.e., strength of sediment that has dilated to an equilibrium density under prolonged deformation at constant load) generally lies within a few percent of the normally consolidated strength (Skempton, 1964).

Since there is no empirical or theoretical basis for inferring extant pore water pressures beneath the LML, there is no basis for inferring extant basal confining stress from measured preconsolidation values for the LML. Numerical experiments in this study were therefore conducted using assumed values of zero effective stress at the ice-sediment interface. Since the effect of higher basal confining stress is predictable (higher confining stress implies a thinner shear zone and commensurately lower basal ice velocity) this approach provides a suitable baseline for experimental control. This assumption is also supported by Antarctic ice stream data. Englehardt and others (1991) measured basal water pressures beneath Ice Stream B equal or nearly equal to the weight of the overlying ice. Coupling of the sediment and ice under such circumstances is assumed to be due to adhesive effects at the interface.

Yield strength and viscoplastic flow parameters: The yield strength and viscoplastic parameters were determined from standard consolidated drained triaxial (CDTX) tests and consolidated drained controlled strain-rate (CDSR) tests conducted at the Civil Engineering Laboratory, Washington State University, using methods developed by Wong (1992). Wong's methodology for deriving viscoplastic parameters from laboratory test data has been tested for slow-moving landslides by comparing laboratory test results with field inclinometer measurements (Wong and others, in review).

The Mohr-Coulomb yield strength parameters, c_y, ϕ_y, c'_y and ϕ'_y (the prime mark indicates parameters from overconsolidated material),were obtained from two suites of CDTX tests conducted at 7, 15, 25, 40, and 50 psi confining stress (Appendix D). The first suite of tests was conducted on remolded samples of Batestown till that were reconsolidated to the same density as the *in*

situ sample (2.39 gm/cm^3), thus reflecting the overconsolidated state (1500 kPa) of the field sample (hereafter referred to as the "overconsolidated tests"). The second suite of tests was conducted on remolded samples that were consolidated only up to the confining stresses for each test (hereafter referred to as the "normally consolidated tests"). Both sets of tests were conducted drained to allow the sediment to equilibrate to the confining stress, as it would likely have done in the subglacial setting, given the 1,000 to 10,000 year lifetime of the system. The overconsolidated tests provides a "high-end" estimate for the sediment yield strength, τ_y. The normally consolidated tests provide a reasonable "low-end" yield strength estimate (Fig. 4.4).

The yield strength in both tests is defined as the stress below which the material behaves near-elastically. In materials testing, the yield point is typically defined as the point on the stress-strain curve where the stress-strain behavior deviates from linear elastic behavior by an arbitrary amount (typically 0.2%). For viscoplastic analysis, the yield stress is defined by identifying a theoretically determined range of stresses on the stress-strain curve where near-linear elastic behavior occurs (Fig. 4.4). (The tests in this study employed the "secant modulus method," Hovind (1990), Wong (1992), and Wong and others (in review), to identify the yield strength.) The stress at which the behavior shifts from near-elastic to viscoplastic is specified as the yield stress. Because the material undergoing viscoplastic deformation eventually reaches residual strength (Fig. 4.4), the cohesion, c, is theoretically zero (Skempton, 1964, 1985; Skempton and Peltley, 1967; Lupinini, 1981). The CDTX tests in this study angles of internal friction of 24.1° for the overconsolidated and 21.8° for the normally consolidated case (Tables 4.1,2 and Appendix D).

In addition to determining the yield strength (stress at which the material begins deforming viscoplastically) the CDTX tests also provide the failure strength, τ_f, which is defined as the peak strength of the overconsolidated material (Fig. 4.4). τ_f is required in order to set up the CDSR tests, from which the remaining sediment parameters, u_0, D_0, and n, are derived. The CDSR tests for this study (Appendix D) was conducted on remolded, overconsolidated specimens. Since the viscoplastic parameters of the sediment

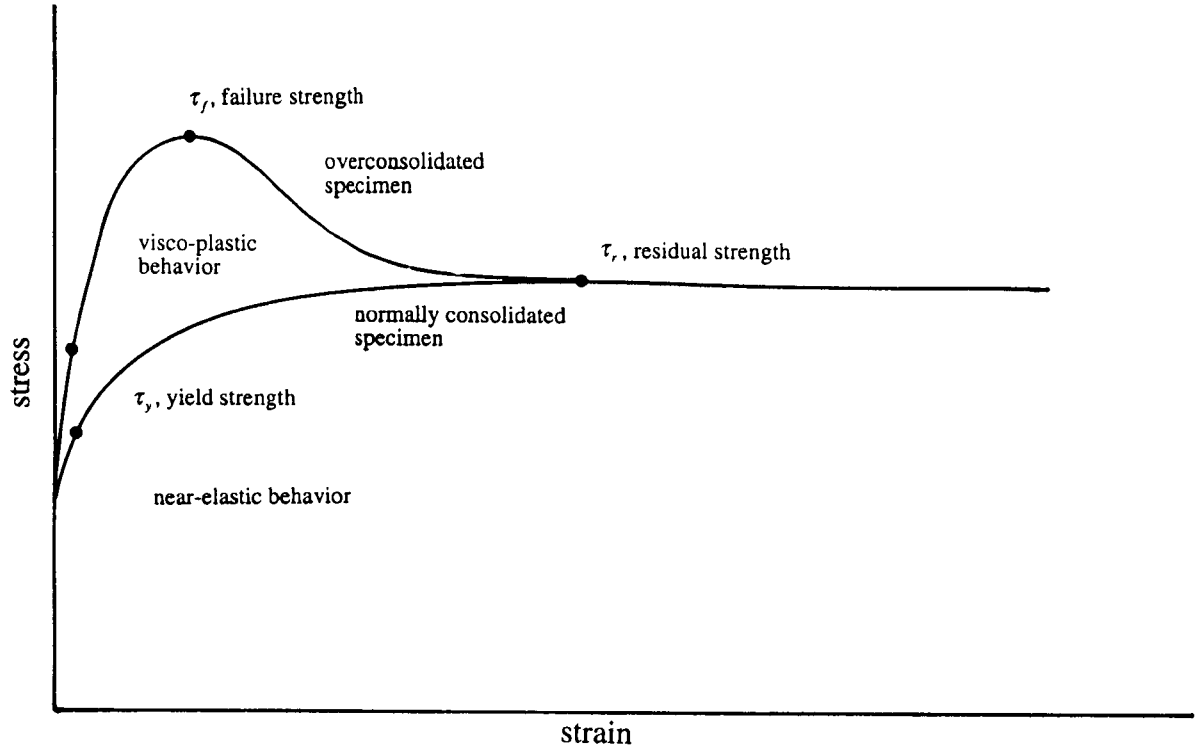

Fig. 4.4. Idealized stress-strain curves for overconsolidated and normally consolidated sediment showing the various regimes of strain and failure.

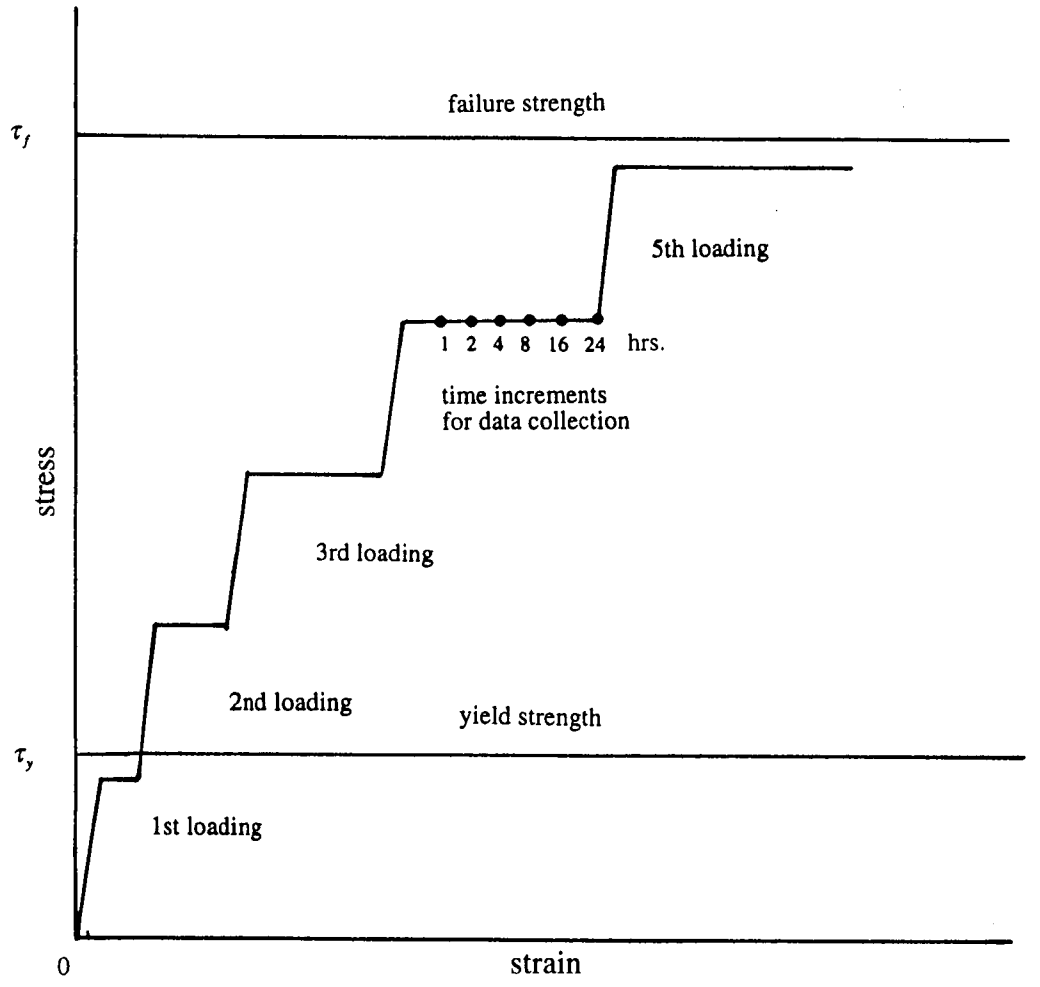

Fig. 4.5. Idealized diagram of CDSR stress-strain plots.

are independent of the initial consolidation state, the data are theoretically valid for normally consolidated or critical-state conditions as well (Skempton, 1964; Ho, personal communication, 1993).

For the CDSR tests (Fig. 4.5), the test specimens are each placed in a standard triaxial test cell, brought to 100% saturation at a nominal confining stress (typically 4-5 psi), then consolidated to the same confining stresses as for the CDTX tests described above (7, 15, 25 40, and 50 psi, respectively.). For each test, the respective specimen is then subjected to a series of loads that are increased incrementally. The first loading is calibrated to bring the specimen to about 90% of the yield stress. The final load brings it to near the failure stress. Several intermediate loads are imposed to produce uniform increments in stress between the first and final loadings . At each loading, a stress-strain curve is plotted at geometrically-spaced time increments (1, 2,4, 8, 16, 24 hrs) spanning a 24 hr period.

The excess stress intensity, $II_e^{1/2}$ (square root of the second invariant of the excess stress tensor), and the corresponding strain-rate intensity, $II_D^{1/2}$ (square root of the second invariant of the rate-of -deformation tensor) are then calculated from the stress-strain data. (Excess stress is defined as the difference between the applied stress and the extant yield strength.) A regression analysis is then made from a plot of a log linearized form of the stress-strain relation

$$II_e^{1/2} = b\left(II_D^{1/2}\right)^m \qquad (4.2)$$

at each time increment (Appendix D). b is determined from the vertical intercept of the regression line and m from the slope.

Finally, the viscoplastic parameters for Iverson's equation are derived from the test data through the following identities (Wong and others, in review):

$$b \equiv 2\mu_0 D_0^{(n-1/n)} \qquad (4.3a)$$

$$n \equiv 1/m \qquad (4.3b)$$

Application of this methodology reveals that although Iverson's equation includes five separate parameters, they actually represent only four independent fundamental material properties. The reference deformation rate, D_0 , and reference viscosity, μ_0, are not independent; they are derived from a single parameter, b, which fully characterizes the nonlinear-viscosity of the material for a given value of n. That b rather than D_0 and μ_0 is the fundamental parameter for nonlinear flow behavior can be seen by examining the relationship between b and the viscosity term, F, defined in Chapter 3 for the differential form of the Iverson equation

$$\frac{du}{dz} = F\left(|\tau| - S_0 - S_{(z)}\right)^n \qquad (3.1a)$$

where

$$F = \left(\frac{1}{2D_0}\right)^{n-1} \mu_0^{-n} \qquad (3.1b)$$

From equations (4.3a) and (3.1b) above it can be shown that

$$F = 2b^{-n} \qquad (4.4)$$

Note that for a given value of n the viscous behavior of the constitutive equation (3.1a) is fully determined by F, which in turn is uniquely determined by b. Thus, even if the *Newtonian reference* parameters are not available, the rheological behavior of the material can be fully characterized so long as b and n are known. The only limitation of not knowing the Newtonian reference parameters is that in their absence there is no basis for direct comparison of the nonlinear parameters to those of an analogous Newtonian material.

In the case of observable mass movement phenomena such as landslides, D_0 can be inferred from field data (Iverson, 1984; Wong and others, in press). When strain cannot be directly observed, however, as in this study, the

Newtonian reference parameters can be determined by calculating the velocity profile using the test parameters b and m, then deriving the Newtonian reference parameters from a graphical analysis of the calculated velocity profile (Appendix E).

Conclusions regarding the geotechnical tests

The parameters derived from the test data (Table 4.1) and employed in the numerical expériments are summarized in Table 4.2. Although the precision of the paramters is limited by the small number of samples, the results are consistent with other other experiments on similar materials and therefore appear to be suitable for application in this study. (See Appendices C and D for description of the tests and discussion of the precision of the laboratoty mesurements.) As can be seen in Table 4.1, values of b were consistent across the suite of tests. The b-value in table 4.2 is therefore based on an average of the values from each time increment. The values of m, on the other hand, varied significantly across the time intervals of the CDSR test (Table 4.1). The value of m, hence n, is therefore less precisely known. Values of the Newtonian reference parameters in Table 4.2 therefore reflect the averaged b value of 6.21×10^8 but span the range of n-values from 1.25 to 1.75. (See Appendix E for the derivation of the parameters.) The angles of internal friction for the overconsolidated and normally consolidated tests varied only from 24.1° to 21.8°. The strength of the material thus does not appear to be strongly affected by the consolidation state.

The numerical modeling experiments described in Chapter 5 were conducted across the range of n-values in Table 4.1 to evaluate the implications of the imprecision in the in the value of m. Most of the experiments were conducted at the low end of the range, however, since the reference viscosity values associated with the lower value of n were more consistent with other estimates of viscosity in the literature for silty-clay soils (Vyalov, 1986).

I also elected, for purposes of experimental control, to conduct most of the numerical experiments using the overconsolidated yield strength parameters. Since the difference between the angles of internal friction for the overconsolidated and normally consolidated was not great, the selection of

Table 4.1 Summary of results from geotechnical tests

Preconsolidation tests:

Undisturbed glaciolacustrine clay from beneath sequence II:

1500 kPa ± 100 kPa (2 test specimens from single sample)

CDTX tests:

Remolded Batestown till reconsolidated to 2.39 gm/cm^3 ("overconsolidated"):

$c'_y = 0.0$ $\phi'_y = 24.0°$ (5 specimens, 5 tests, from single sample, $R^2 = .942$)

Remolded Batestown till reconsolidated to 2.28 gm/cm^3 ("normally consolidated"):

$c_y = 0.0$ $\phi_y = 21.8°$ (5 specimens, 5 tests, from single sample, $R^2 = .997$)

CDSR tests:

Remolded Batestown till reconsolidated to 1500 kPa:

Time interval (hrs)	log b	m	R^2
24	8.35	.56	.99
16	8.33	.58	.99
08	6.56	.24	.74
04	6.71	.28	.66
02	8.52	.72	.91
01	9.06	.88	.82

mean values:

all data	7.92	.54
01, 02 hrs	8.79	.80
01, 02, 16, 24	8.57	.69

For test data and discussion of precision limitations see Appendices B and C. Full details of testing are contained in Vela and others (in prep.)

Table 4.2. Summary of the parameters derived from the geotechnical tests and applied in the numerical modeling experiments. See Appendix E for derivation of the reference paramters.

Consolidation State	c (Pascals)	ϕ' (degrees)	b (Pa)	m	n	D_0 (sec^{-1})	μ_0 (Pa-sec)
Normal consol.	0.0	21.8	no data	no data	no data	no data	no data
Overconsolidated	0.0	24.1	6.21×10^8	0.57-0.80	1.25-1.75	7.9×10^{-7}	5.2×10^9-1.3×10^{11}

which yield strength to use for the control purposes is unlikely to fundamentally alter the results of any given experiment for the investigations made in this study.

Chapter 5

Numerical Experiments: Observations and Conclusions

Objectives of the numerical experiments:

The numerical experiments reported below had four immediate objectives: (1) to test the model by checking whether results are consistent with known physical properties and behavior of ice sheets, (2) to estimate the general lobe morphology and behavior implied for the Lake Michigan Lobe by the experimentally determined parameters for till rheology, and (3) to identify the sensitivities of steady-state lobe morphology and dynamics to changes in the till parameters and briefly compare the relative role of till rheology versus mass forcing and ablation rates in determining steady-state morphology, and (4) make a preliminary exploration of transient responses of the lobe to changes in sediment viscosity. Table 5.1 lists the set of experiments.

Although most of the experiments reported in this study reflect steady-state results, it is important to note that there is no reason to conclude *a priori* that the LIS ever reached steady state, especially given the substantial fluctuations in climate during the last glaciation (oxygen isotope substage 5d-stage 2). Previous modeling has demonstrated, (e.g., Budd and Smith, 1981, 1987) that a North American ice sheet could never be in equilibrium because of the continually varying radiation forcing and the feedback between the ice sheet and climate. The delayed isostatic response of the bedrock accentuates the departures from equilibrium. Budd and Smith concluded that for many applications in ice-sheet modeling it is probably more important to focus modeling studies on dynamic non-equilibrium time-dependent interactions of climate and ice sheets rather than to assume or investigate steady-state behavior.

Steady-state experiments nevertheless are essential to obtain the experimental control by which one can characterize the ultimate direction and relative influence of the various physical processes that govern ice sheet behavior. Steady-state experiments also provide a perspective from which to evaluate transient behavior. The results of the steady state expeiments in this

Table 5.1. Summary of modeling experiments described in text.

Steady state experiments:

Control experiments: "Baseline" configurations against which to compare sensitivity tests in subsequent experiments

Experiment #1: Entirely hard-bedded ice sheet
Experiment #2: Entirely soft-bedded ice sheet (using till parameters determined from geotechnical tests)
Experiment #3: LML simulation: actual bed lithology (actual geographic distribution of soft and hard bed conditions)

Investigation of suitability of simplified configurations for till rheology experiments:

Experiment #4: Simplified bed lithology (hard bed conditions assumed from ice divide to Lake Michigan Basin)
Experiment #5: Simplified bed lithology + isothermal ice (uniform ice temp of -5 ° C assumed)
Experiment #6: Linear vs. nonlinear till rheology (comparison of nonlinear till and linear analog)

Sensitivity tests of till parameters: implications for steady state ice sheet behavior

Till viscosity tests: Model configured as for Expt. #5, but till viscosity varied for each run

Experiment #7: Viscosity 5.2×10^{11} Pa-s
Experiment #8: Viscosity 5.2×10^{10} Pa-s
Experiment #9: Viscosity 5.2×10^{9} Pa-s
Experiment #10: Viscosity 5.2×10^{8} Pa-s
Experiment #11: Viscosity 5.2×10^{7} Pa-s
Experiment #12: Viscosity 5.2×10^{6} Pa-s
Experiment #13: Viscosity 5.2×10^{5} Pa-s
Experiment #14: Viscosity 5.2×10^{4} Pa-s

Till yield strength tests: Model configured as for Expt. #5, but till yield strength varied for each run

Experiment #15: $\phi' = 24.1$ degrees
Experiment #16: $\phi' = 20.0$ degrees

Table 5.1, continued

Experiment #17: $\phi' = 15.0$ degrees
Experiment #18: $\phi' = 10.0$ degrees
Experiment #19: $\phi' = 5.0$ degrees

Mass forcing experiments: Model configured as for Expt. #5, but climate parameters varied for each run

Experiment #20: 90% accumulation rate
Experiment #21: 80% accumulation rate
Experiment #22: 110% ablation
Experiment #23: 120% ablation

Till parameter precision: Comparison of effects for varied values of *n*

Experiment #24: Implication of imprecision in experimentally determined *n* values

Transient experiments:

Climate parameter changes: Model configured as for Expt. #5, but climate parameters varied after reaching steady state

Experimentt #25: Near-steady state response to shift from control climate to "wet-warm" climate
Experiment #26a: Transient effects of forced 3000-year oscillations between control and "wet-warm" cliimate
Experiment #26b: Transient effects of forced 3000-year oscillations between control and "wet-warm" cliimate, all hard be
Experiment #26c: Transient effects of forced 3000-year oscillations between control and "wet-warm" cliimate, all soft bed

Till parameter changes: Model configured as for Expt. #5, but till parameters varied after reaching steady state

Experiment #27a: Transient effects of forced 3000-year oscillations in sediment viscosity (o.m. 9 to o.m. 8 Pa-sec).
Experiment #27b: Transient effects of forced 3000-year oscillations in sediment viscosity (o.m. 10 to o.m. 9 Pa-sec).

study are thus meant to provide an essential "jumping-off point" for more intensive studies of transient responses to changes in sediment parameters and environmental conditions.

The transient experiments in this study are meant only to provide an initial assessment as to how ice lobes such as the LML might have responded to changes in sediment or climate conditions. They are not to be interpreted as simulations of the actual evolution of the LML. Reconstruction of the actual historical evolution ice lobe demands reliable data on the initial conditions and evolution of the LIS itself. At present, such data are extremely sparse or speculative for paleo-ice sheets. The transient experiments in this study can, however, help to ascertain the relative magnitudes, directions, and rate of responses to various changes in conditions.

Control experiments:

Experiment #1: the "all hard-bedded" case: To verify the consistency of the model with known characteristics of ice sheet behavior and to establish suitable control configurations against which to evaluate the role of till rheology in lobe behavior, I ran the model to steady state assuming no sediment deformation at the base. I arbitrarily adjusted the mass forcing parameters (location of the maximum accumulation rate with respect to the ice divide and the horizontal gradient for the net accumulation/ablation) until the steady state margin of the lobe coincided approximately with the historic terminus of the lobe. (In Fig. 5.1, the margin lies two grid increments, or 80 km, behind the actual terminus of the LML.)

Fig. 5.1 shows the profile of the hard-bedded ice surface, the initial topography, and the basal topography at steady state. All of the change in basal elevation is due to isostatic adjustment. Fig. 5.2 shows the flux curves for the hard-bedded ice. Since till is absent from the system, the curve reflecting the ice flux due to till deformation coincides with the abscissa. Note that the maximum flux lies at the point where net accumulation changes from positive to negative, as can be seen by comparison with the net accumulation/ablation curve shown in Fig. 5.3.

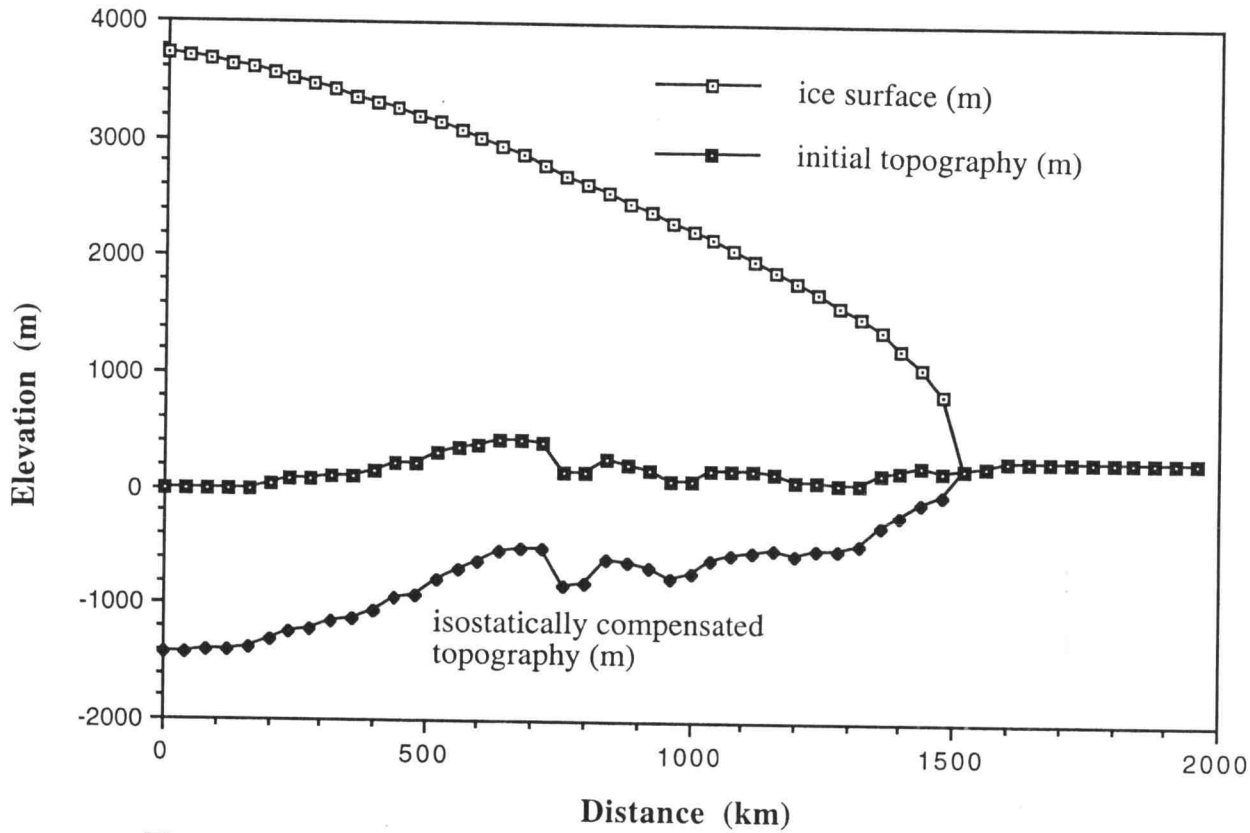

Fig. 5.1 Steady state (54,000 yr) surface profile for hard-bedded ice sheet.

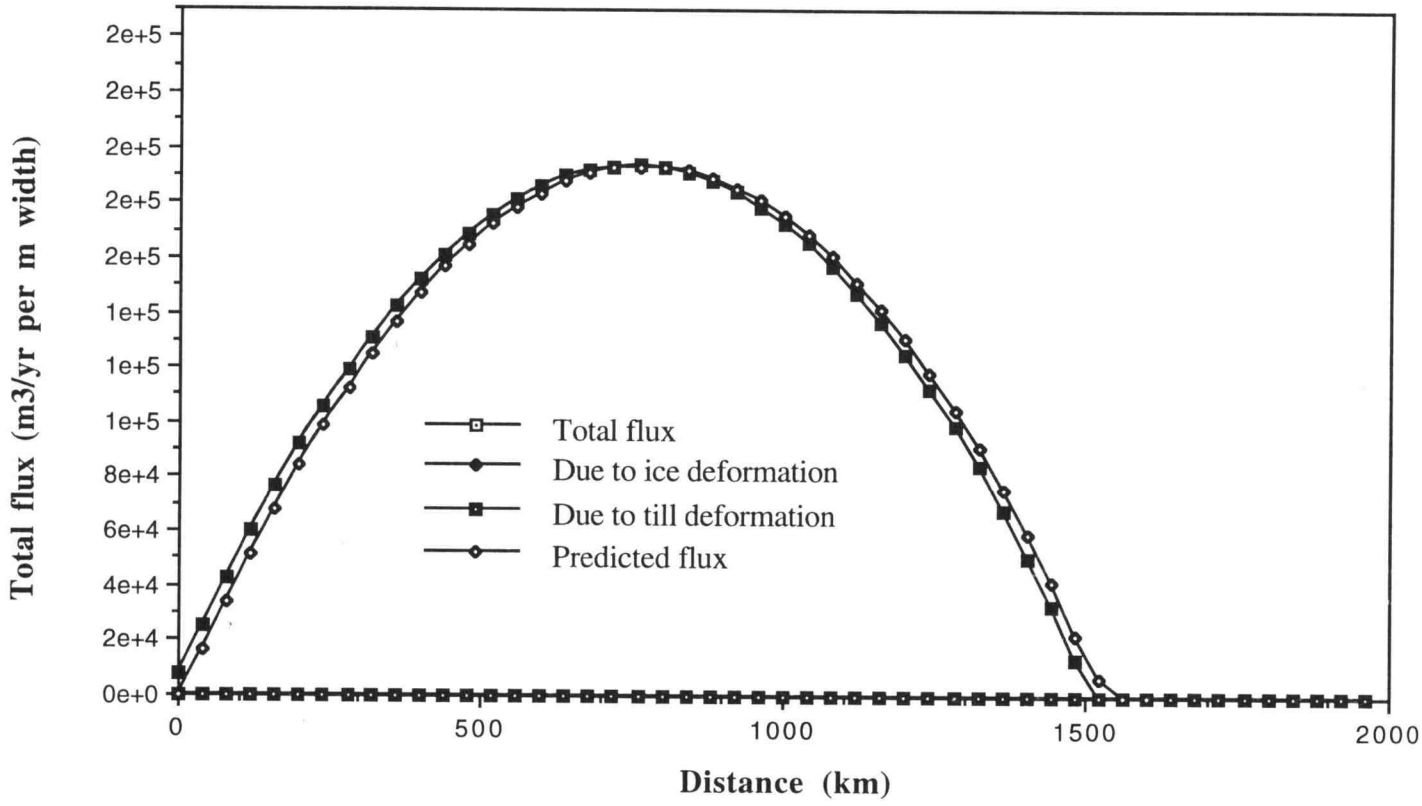

Fig. 5.2. Ice flux curves for hard-bedded ice at 54,000 years

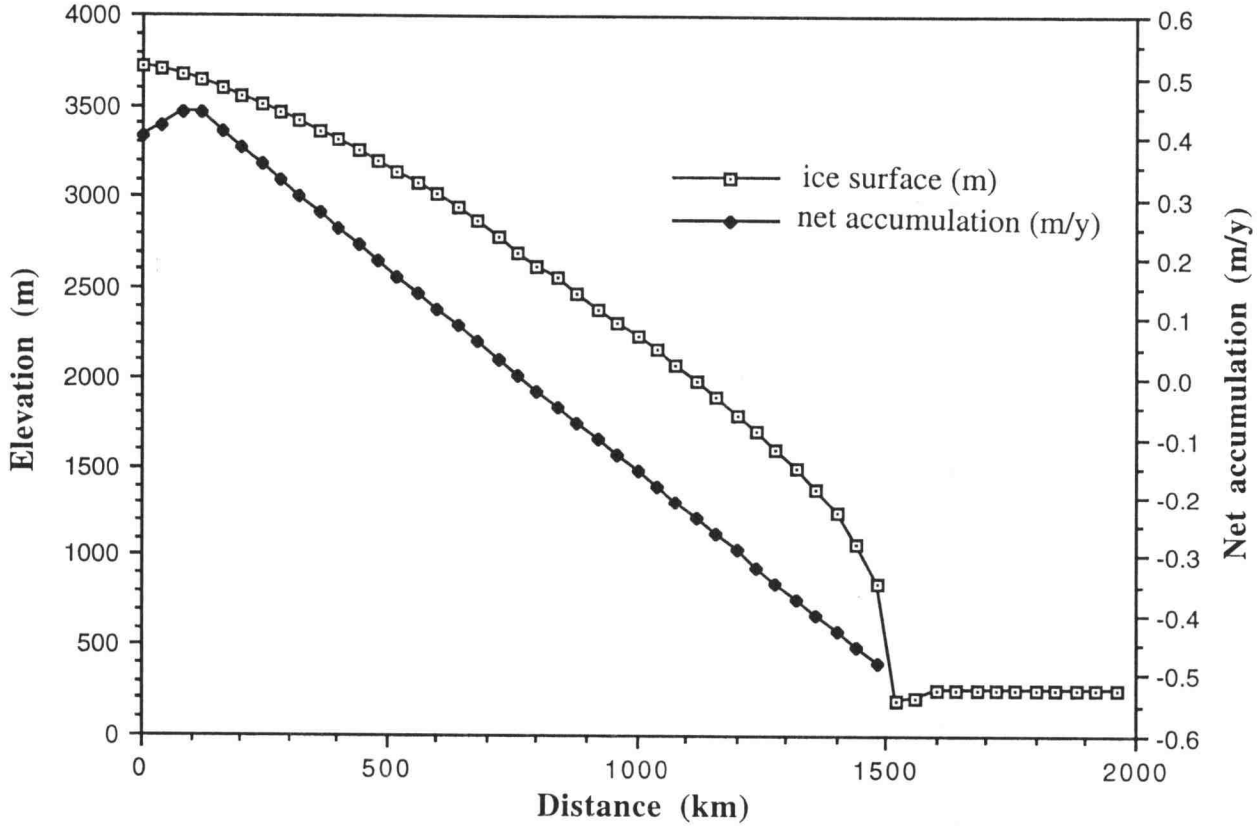

Fig. 5.3. Net accumulation/ablation for hard-bedded ice at 54,000 years

The steady state temperature profiles are shown in Fig. 5.4. These are consistent with the known physical characteristics of ice sheets; downward vertical convection of cold ice in the accumulation zone depresses the temperature profile downward, while in the ablation zone relative upward movement of the warmer ice toward the surface produces the opposite curvature in the temperature profile (Hooke, 1976). The most noteworthy observation from the hard-bedded experiment, besides its consistency with known ice sheet behavior, is that the hard-bedded ice sheet required 50,000 to 60,000 years to reach steady state, compared with 30,000 or less for configurations containing a soft-bedded portion using the same climate and mass forcing parameters.

Experiment #2: the "all soft-bedded case:" The opposite end member case for experimental control purposes is shown in Fig. 5.5. Here, the entire base is assumed to be soft-bedded, using as "baseline" sediment parameters the viscoplastic parameters derived from the geotechnical experiments (D_0=7.9x10^{-5}, μ_0=5.2x10^9, n=1.25, c_y'=0.0, $\phi_y' = 24.1°$). Note that the thickness at the ice divide is only about 60% of that for the hard-bedded case and the steady-state margin is two grid increments beyond the historic terminus (where the hard-bedded margin terminated two increments short of it). Fluxes for the soft- and hard-bedded cases are similar, with the soft-bedded case showing a slightly higher maximum (Fig. 5.6). Note that for the reference viscosity of 5.16 x 10^9 Pa-s, the soft-bedded flux curves indicate a minuscule but measurable amount of flux due to ice deformation (Fig. 5.6).

Experiment #3: Lake Michigan Lobe simulation: Experiment #3 is the "fully-configured" baseline experiment, in which all the physical systems included in the model are active, and the experimentally determined sediment parameters reported in Chapter 4 are used. To simulate the Lake Michigan Lobe as realistically as possible within the limitations of the model, I configured the base for soft-bedded conditions in the upstream portion coinciding with the James Bay Lowland, as well as the downstream portion coinciding with the Lake Michigan Basin. In the absence of data for the James Bay Lowland sediments, I used the same parameters as for the Lake Michigan Basin

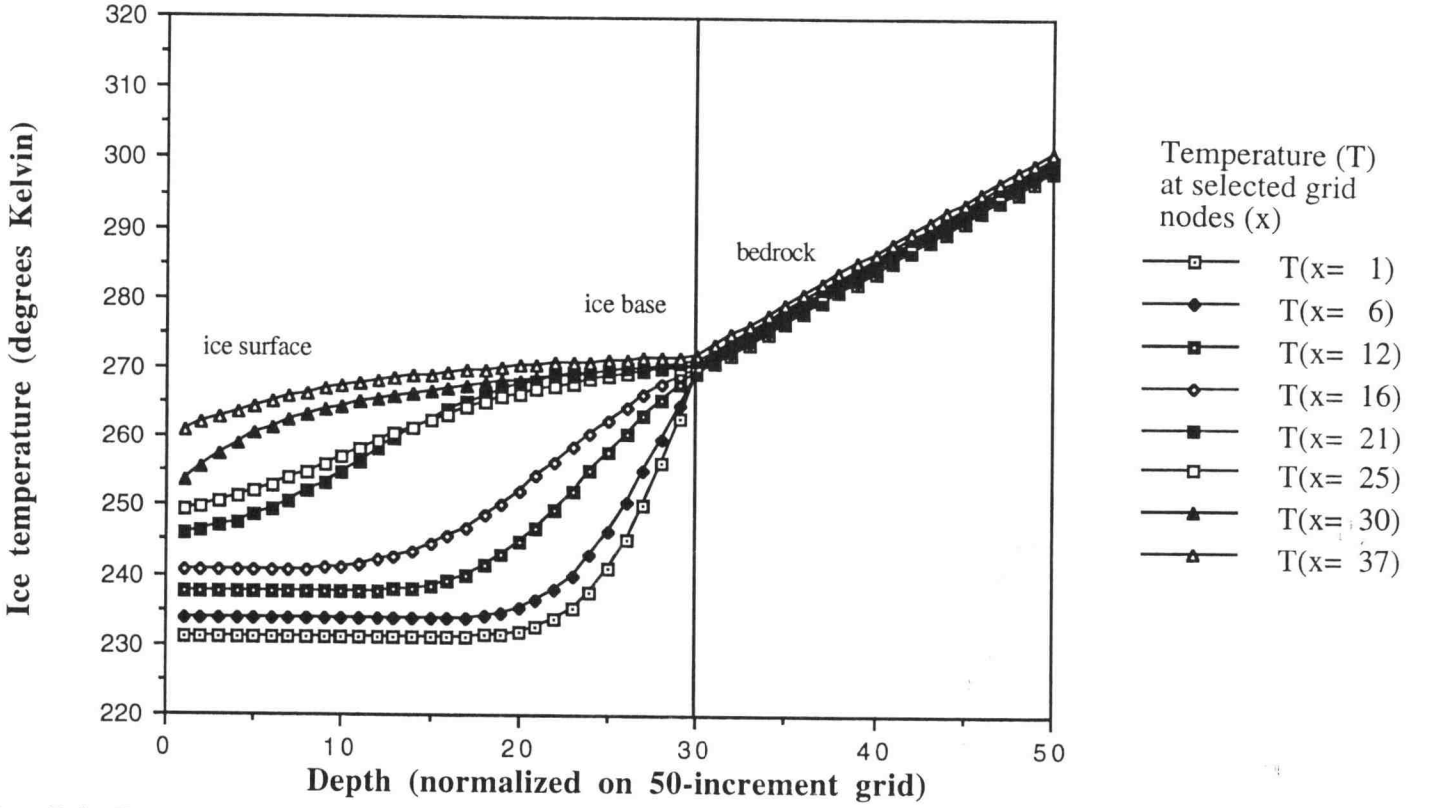

Fig. 5.4. Steady state (60 ka) temperature profiles at selected points for hard-bedded ice. x-position in legend indicates node number on finite difference grid. Node 1 is at ice divide. Node spacing is 40 km.

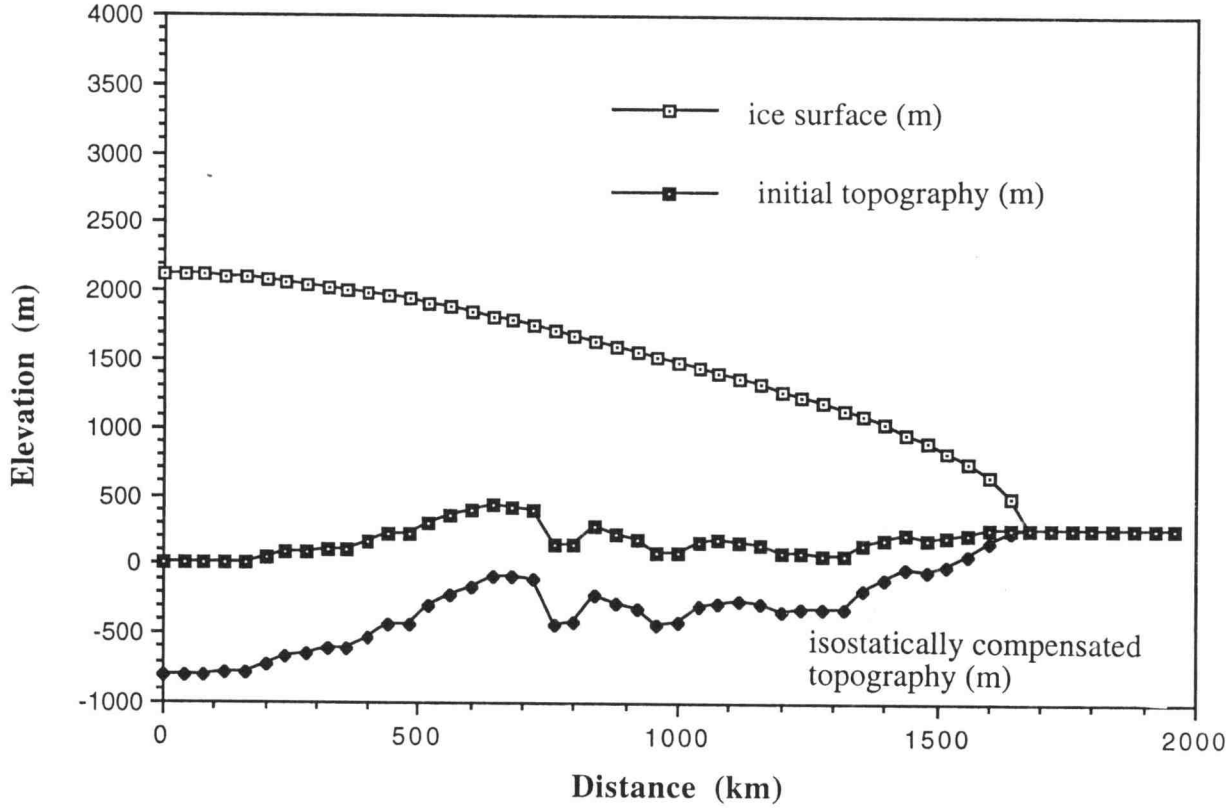

Fig. 5.5. Steady state (30,000) surface profile for soft-bedded ice sheet

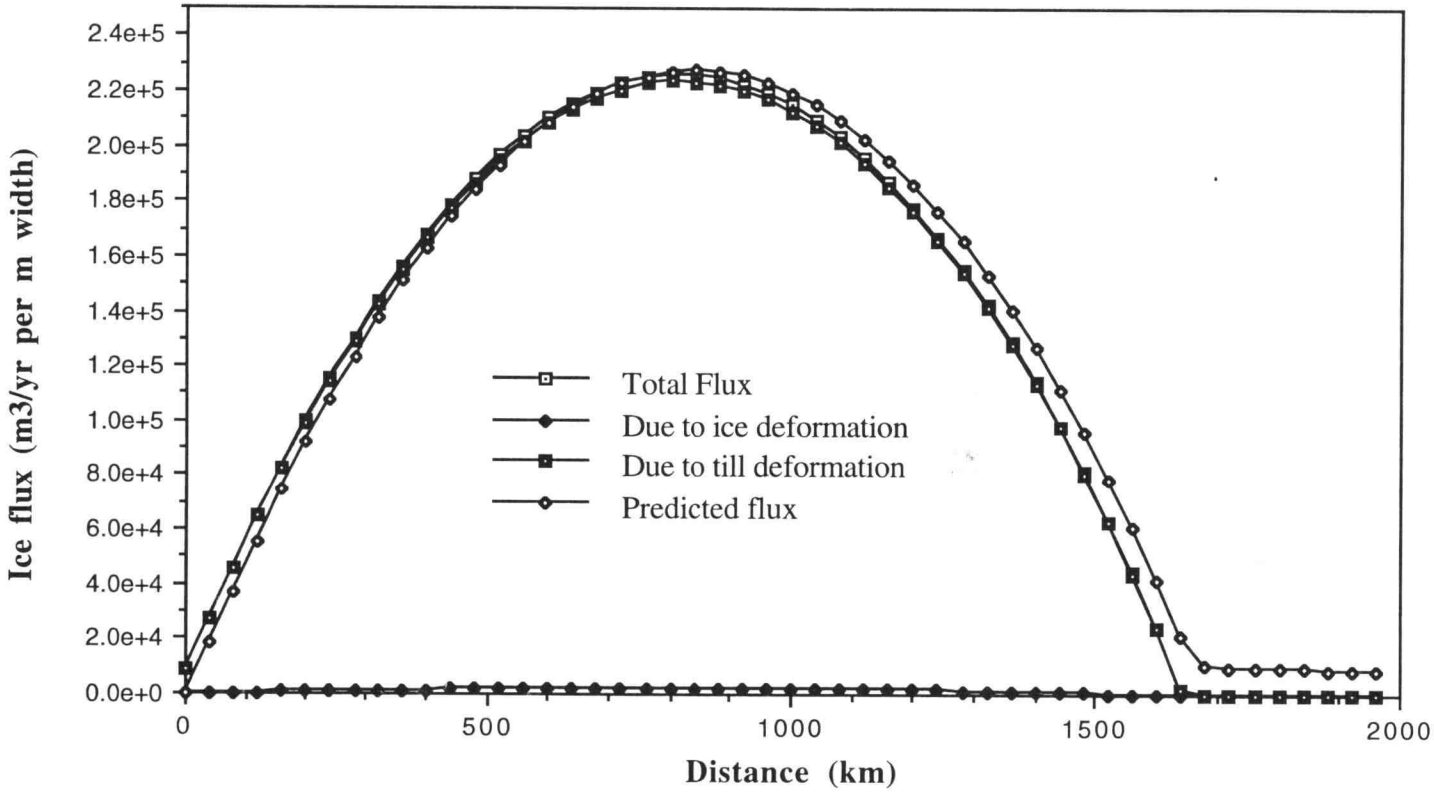

Fig. 5.6. Ice flux curves for soft-bedded ice at 30,000 years

sediments. Fig. 5.7 shows the simulated time-dependent advance of the lobe over the regional topography under the mass forcing conditions assumed for the model. By 30,000 years the model is very near steady state (see Fig. 5.10), with the margin coinciding with the historic terminus. The upstream soft-bedded portion is notably flat due to the limitation on basal shear stress imposed by the upstream sediment (Fig. 5.8). Where the ice crosses the contact to the crystalline bedrock (and is assumed to be non-sliding), the surface steepens as the ice deforms under the higher shear stress. At the contact with the Lake Michigan Basin sediments (which is placed here at the mid point across the Upper Peninsula of Michigan), the slope suddenly decreases. Fig. 5.9 shows the relationship between the simulated lobe geometry and the initial and steady-state basal topographic profiles. Fig. 5.10 shows the flux curves for the system. Note that the maximum flux is close to that of the all soft-bedded case, and that over the soft-bedded regions the ice flux is borne almost entirely by till deformation.

The temperature profiles for the LML simulation (Fig. 5.11) are significantly affected by the different morphology and gross dynamics of the lobe system. Profiles in the accumulation zone show the expected concavity with respect to the surface, but the concavity is more pronounced in the hard-bedded region, presumably because the higher differential horizontal ice velocity, due to the much higher internal strain rate in the ice, induces a higher rate of downward advection. In the ablation zone, the profiles are virtually linear, probably because the ice is sufficiently thin here and the surface still sufficiently cold relative to the base (Fig. 5.12) to permit conduction effects to overcome advection effects. Since actual boundary conditions are poorly known, there is no basis for inferring that the temperature profiles calculated here represent those of the actual system, particularly for the soft-bedded lobe. Nonetheless, the profiles for the upstream ice are consistent with what is known from modern ice sheet studies and is probably a reasonable approximation for the portion of the ice that "fed" the lobe. It thus provides a reasonable estimate of the upstream conditions from which the lobe propagated and permits some experimental examination of the role of upstream thermal conditions on lobe behavior. Actual thermal conditions in the lobe itself, while less certain, are also

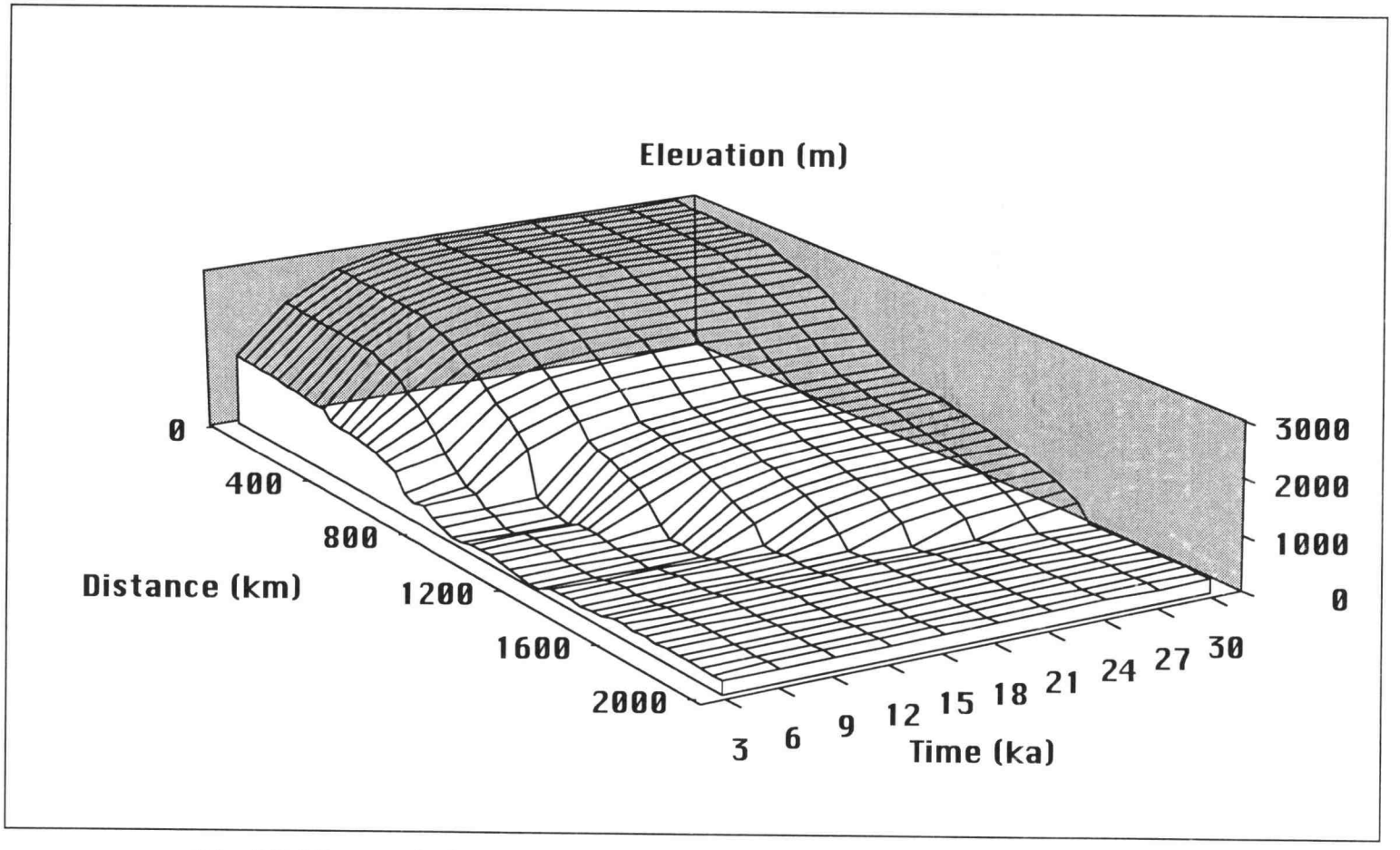

Fig. 5.7. Time evolution of the ice surface, Lake Michigan Lobe simulation

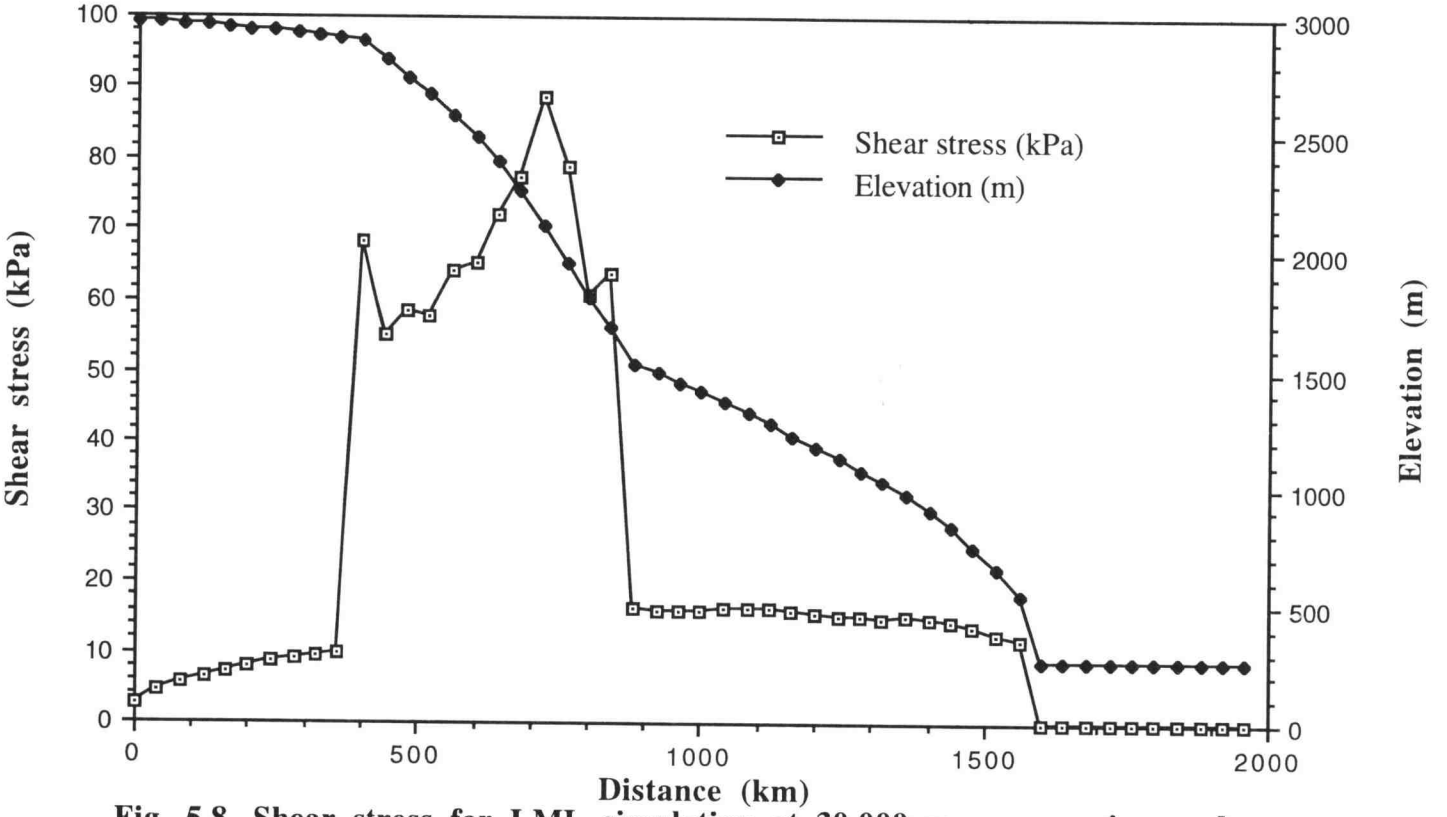

Fig. 5.8. Shear stress for LML simulation at 30,000 years, superimposed on plot of ice-surface elevation.

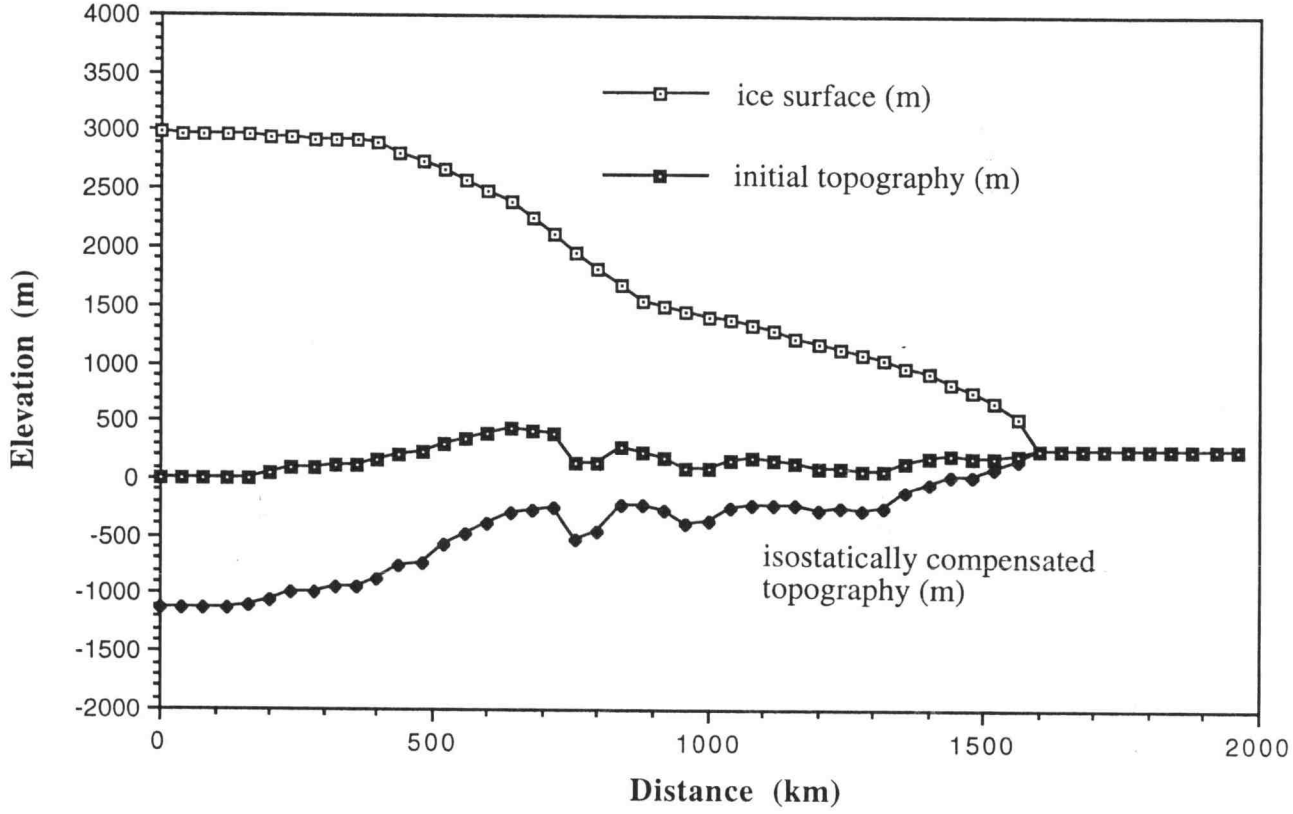

Fig. 5.9. Steady state (30,000yr) surface profile for LML simulation

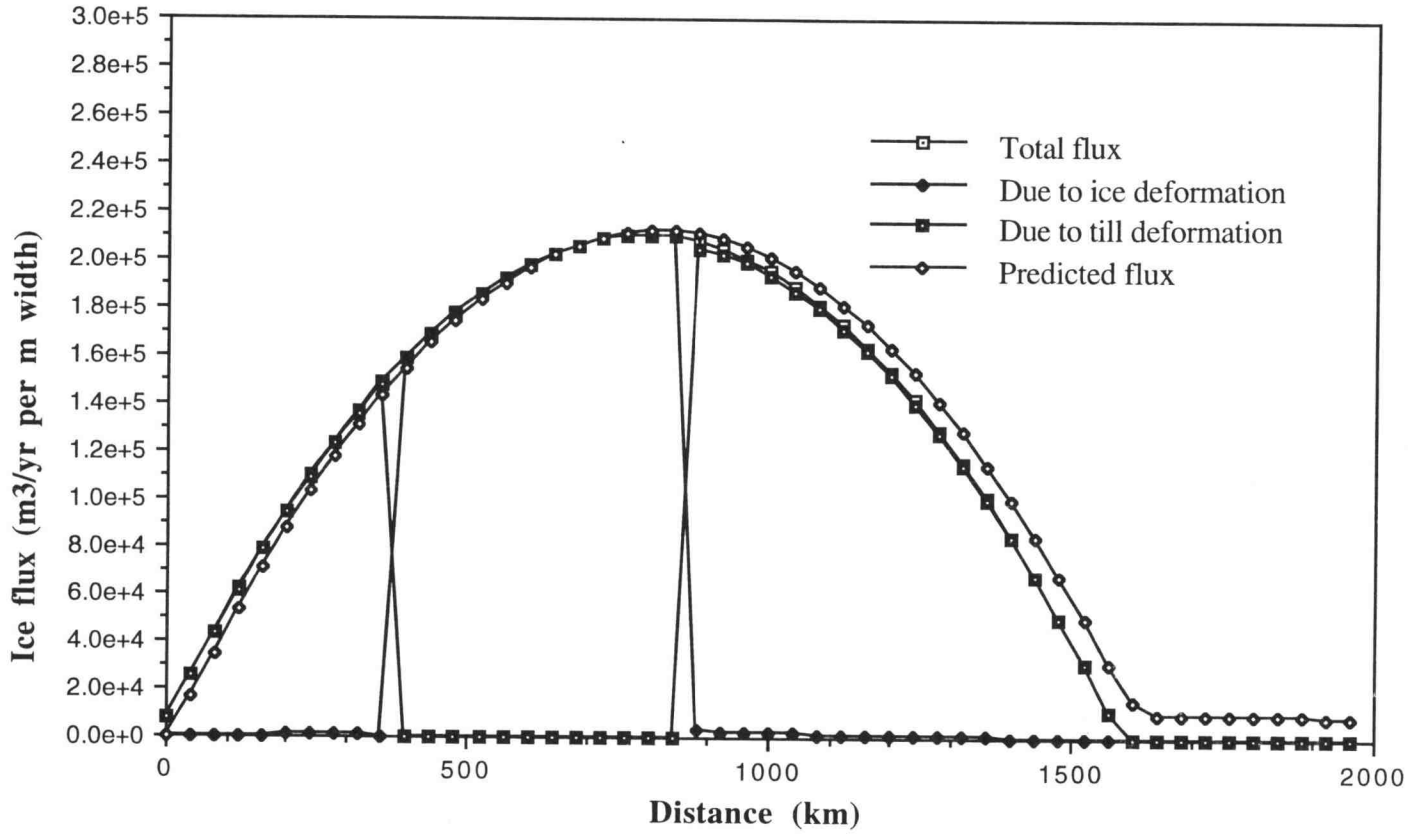

Fig. 5.10 Ice flux curves for LML simulation at 30,000 years

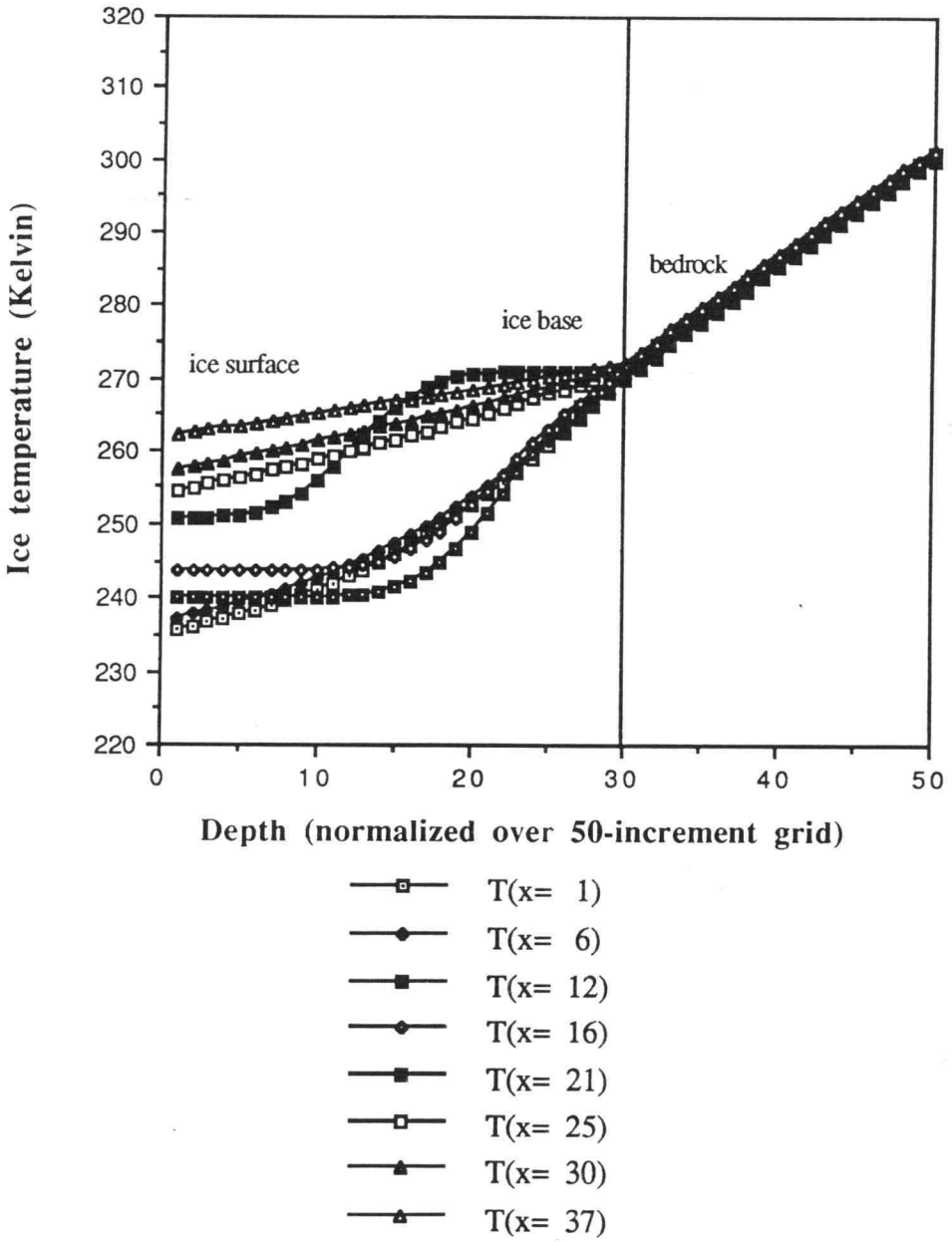

Fig. 5.11. Steady state (30 ka) temperature profiles at selected points for LML simulation. x-position in legend indicates node number on finite difference grid. Node 1 is at ice divide. Horizontal node spacing is 40 km.

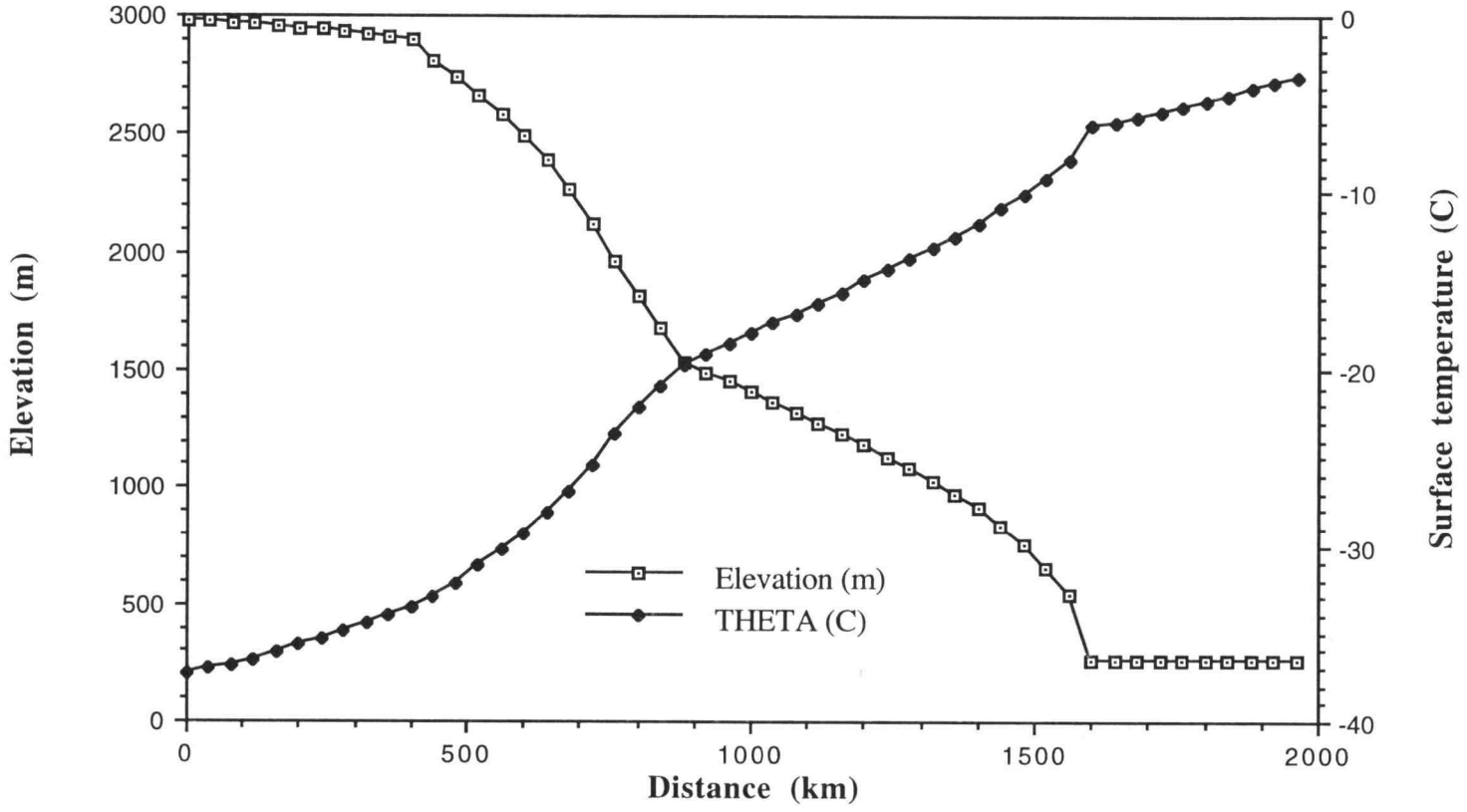

Fig. 5.12. Surface temperature (THETA) boundary condition for LML simulation at 30,000 yrs, superimposed on plot of ice surface elevation.

less relevant to the lobe dynamics since the ice in the lobe is virtually undeforming for the given sediment viscosity. Thermal conditions within the lobe are relevant only to the extent that they influence such conditions as the melting rates and water flux at the base. The implications of the latter two aspects, while ultimately important, are outside the scope of this study.

Additional diagnostic features of the simulated LML are shown in Figs. 5.13-17. Net accumulation rates near the ice divide are somewhat less than modern annual precipitation rates because of the elevation desert effect. The ablation rate near the margin seems reasonable, given that there are no modern analogs against which to evaluate it. It was obtained by adjusting the gradient of the net accumulation curve (Fig. 5.13) so that the steady-state ice margin coincided with the historic terminus. Depth-averaged ice velocities are shown in Fig. 5.14. Till velocity profiles for selected sampling points are shown in Fig. 5.15. These are based on the geotechnical parameters from the tests on the overconsolidated, remolded till (Table 4.). The two distinct groupings of the profiles reflect the different shear stress conditions between the two soft-bedded regions on either side of the hard-bedded region. Calculated thickness of the shear zone in each of the two regions is depicted in Fig. 5.16. The undulations in the thickness of the downstream portion reflect the influence of basal topography on the ice thickness, hence shear stress and thickness of the shear zone. A diagnostic computation of the maximum potential mass flux of the till at each point was made by multiplying depth-averaged till velocities times the thickness of the shear zone at each point (Fig. 5.17). This is a first order calculation that does not account for possible constraints imposed by abrasion rates, water production, drainage effects, or source material availability. The curve merely reflects the flux that would obtain at each point were the till simply being removed from or added to an infinite reservoir of till. It does show, however, the maximum rates that one might expect for the measured rheological properties of the till. Thus the calculations provide an "end member" system against which one might conduct a more rigorous and exhaustive examination of the potential redistribution of sediment mass at the base of the ice sheet.

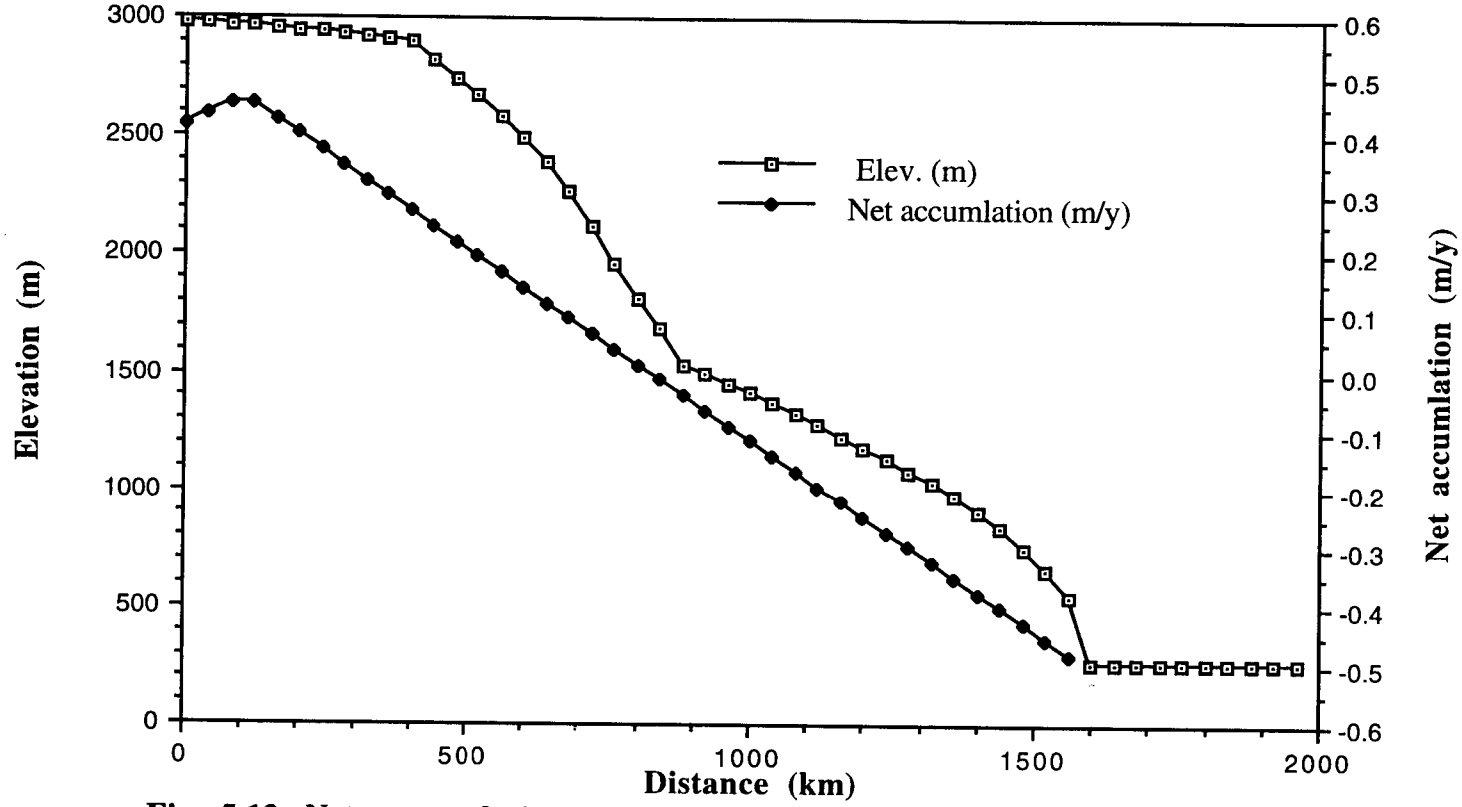

Fig. 5.13. Net accumulation for LML simulation at 30,000 years, superimposed on plot of ice surface elevation.

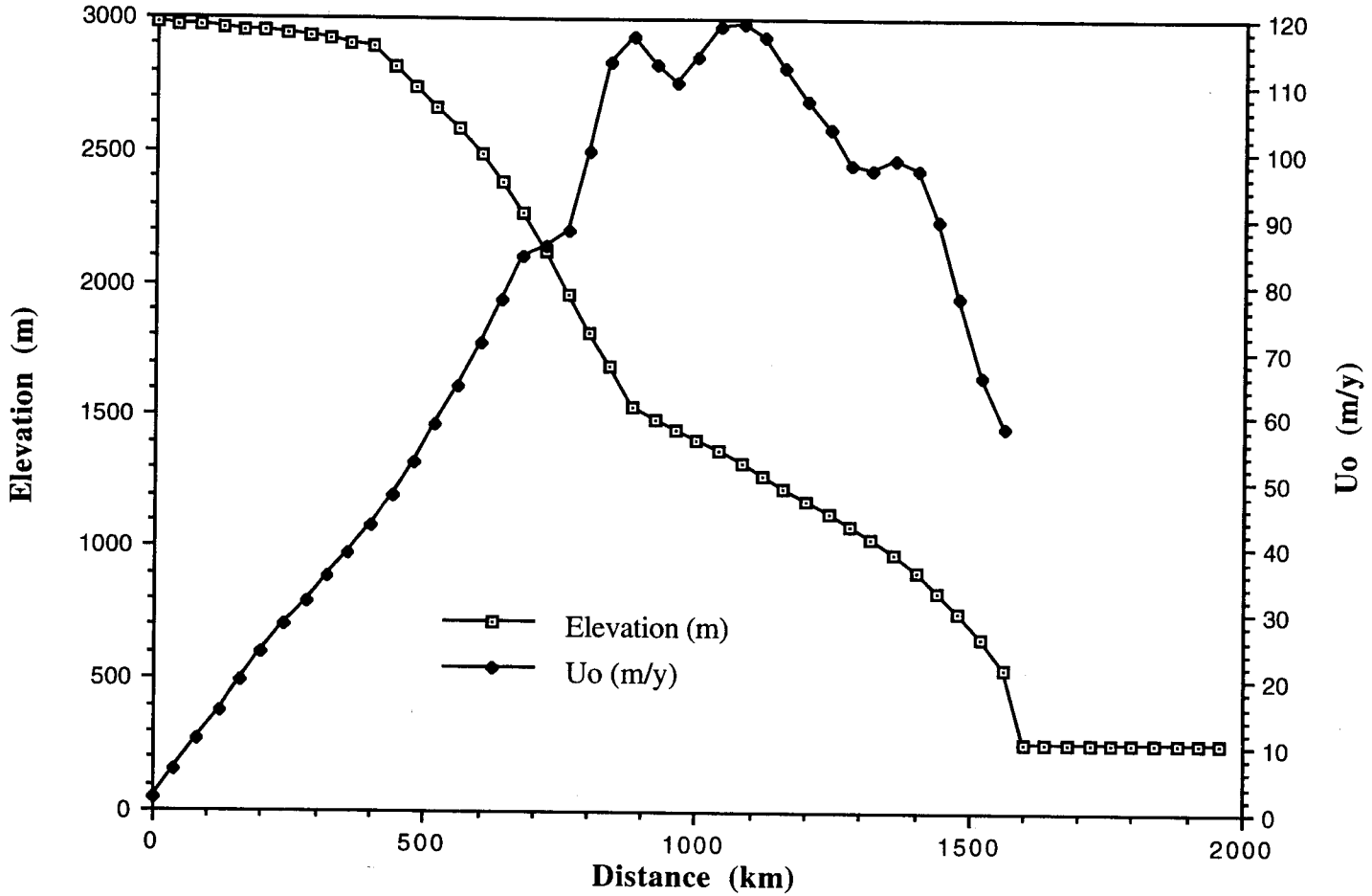

Fig. 5.14. Depth-averaged ice velocity (Uo) for LML simulation at 30,000 years, superimposed on ice surface elevation.

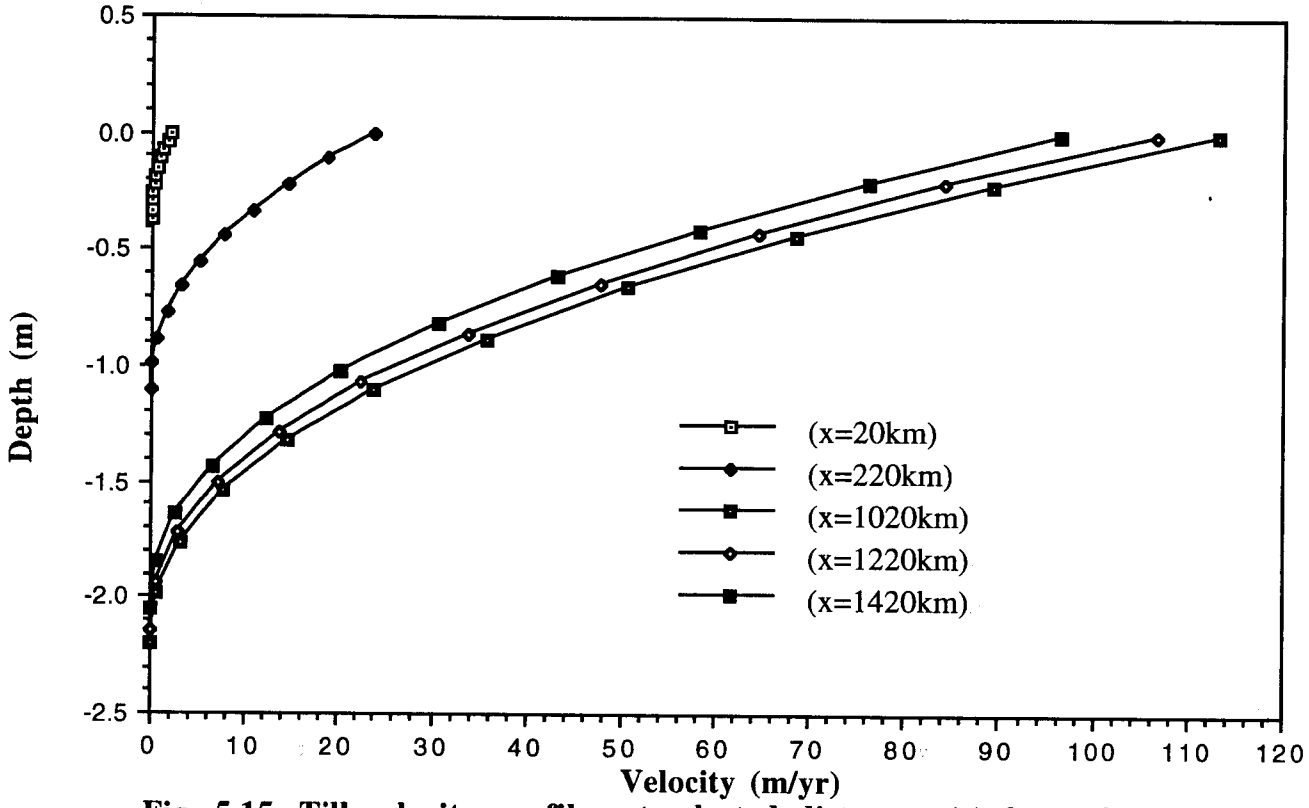

Fig. 5.15. Till velocity profiles at selected distances (x) from the ice divide for LML simulation at 30,000 years.

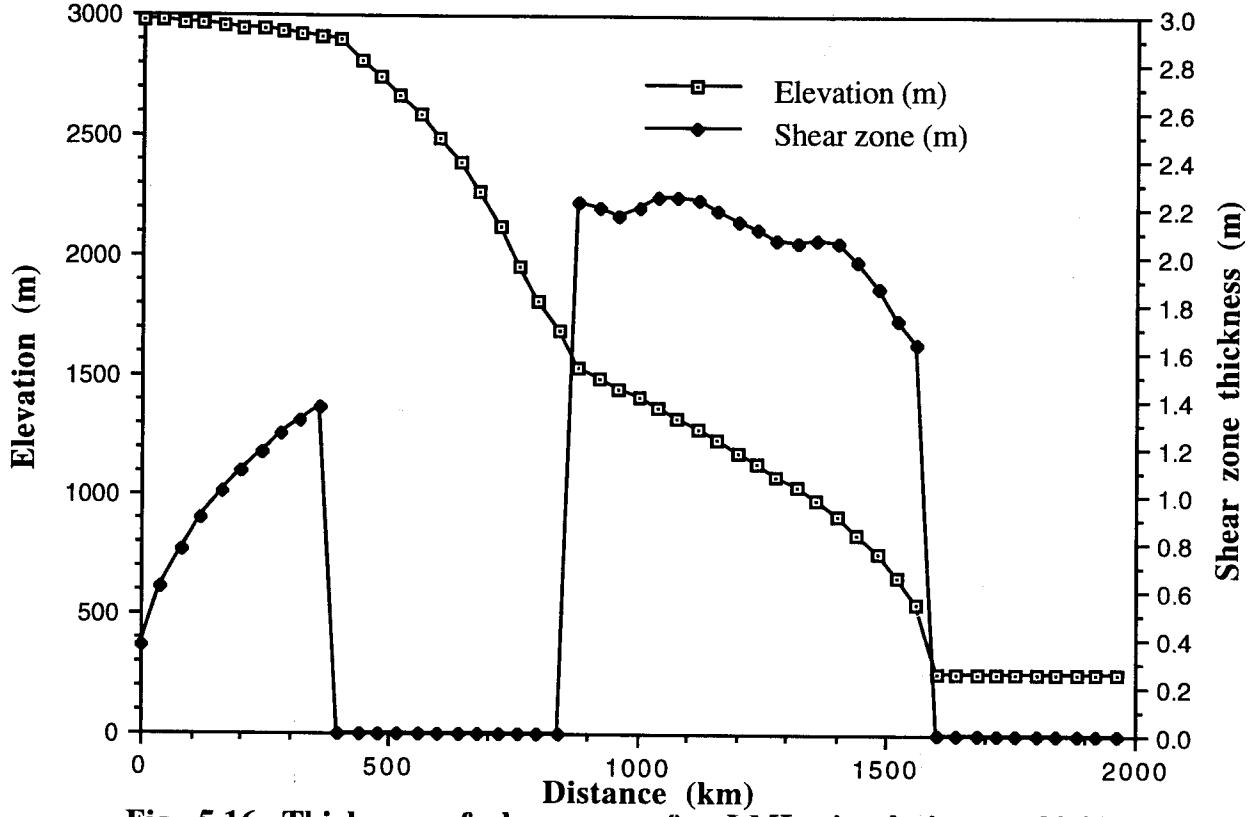

Fig. 5.16. Thickness of shear zone for LML simulation at 30,000 years, superimposed on ice surface elevation.

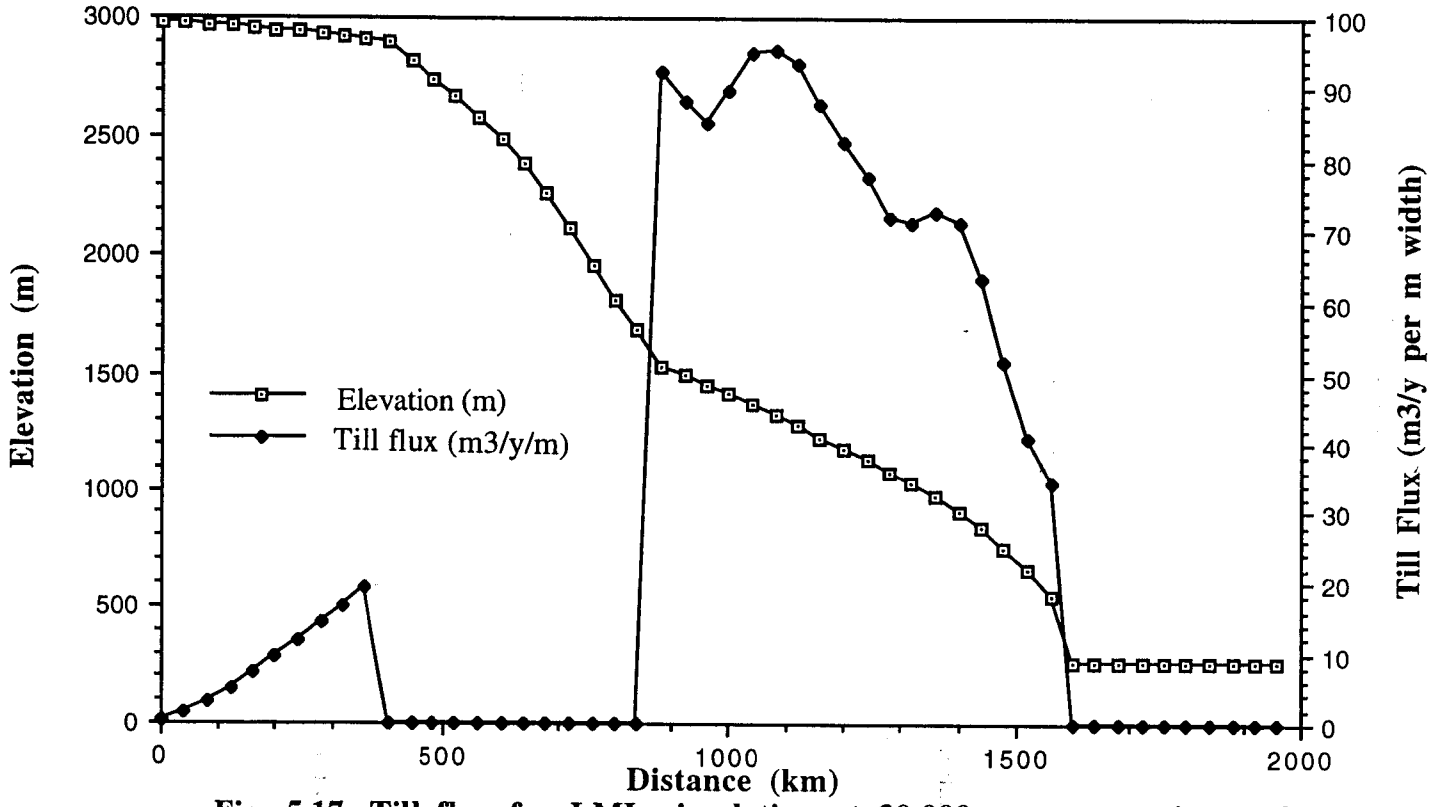

Fig. 5.17. Till flux for LML simulation at 30,000 years, superimposed on ice surface elevation.

Simplified configurations: Suitability for till rheology experiments

Experiments #4 and 5: Bed lithology and isothermal ice: To evaluate the significance of the upstream (James Bay Lowland) basal sediment and upstream thermal regime for the behavior of the downstream (Lake Michigan Basin) ice behavior, I ran two experiments: one experiment with a hard-bedded base from the ice divide to the Lake Michigan Basin (Experiment #4) and a second with the same bed configuration and the ice assumed to be everywhere isothermal (at -5°C) as well (Experiment #5). Comparative profiles are shown in Fig. 5.18. The all-hard-bedded, all-soft-bedded, and LML simulation are included for reference. In all cases the steady-state lobe morphology is similar to that of the LML simulation. When the upstream soft-bedded region was changed to hard-bedded, the entire ice surface upstream of the Lake Michigan Basin contact took on the high surface slope associated with nonsliding ice. The noteworthy observation here is that the two curves are virtually coincident where they are hard-bedded--relaxation of the soft-bedded configuration in the James Bay Lowland regions does not significantly affect the morphology of downstream hard-bedded ice. It does, however, result in a somewhat steeper downstream lobe profile with the terminus one grid increment short of that for the LML simulation. Interestingly, when the thermal regime is relaxed as well (Experiment #5) so that the ice is everywhere isothermal, the steady-state profile of the lobe is virtually coincident with the LML simulation (Experiment #3). Apparently the effects are opposite and compensating. In any case, it appears that if the crystalline bedrock north of the Lake Michigan Basin did, in fact, constitute a non-slip surface for the ice, the characteristics of the James Bay sediments had no appreciable influence on the behavior of the LML. Because of the close similarity between the downstream LML profiles for Experiments #3 and #5, I elected to conduct most subsequent experiments in the latter configuration since it required less than half of the computational time for a comparable run.

Experiment #6: Linear till rheology: To test the fidelity of the algorithm for consistency with Iverson's theoretical model, I ran the model (Experiment #6) with the nonlinear till parameters replaced by their analogous

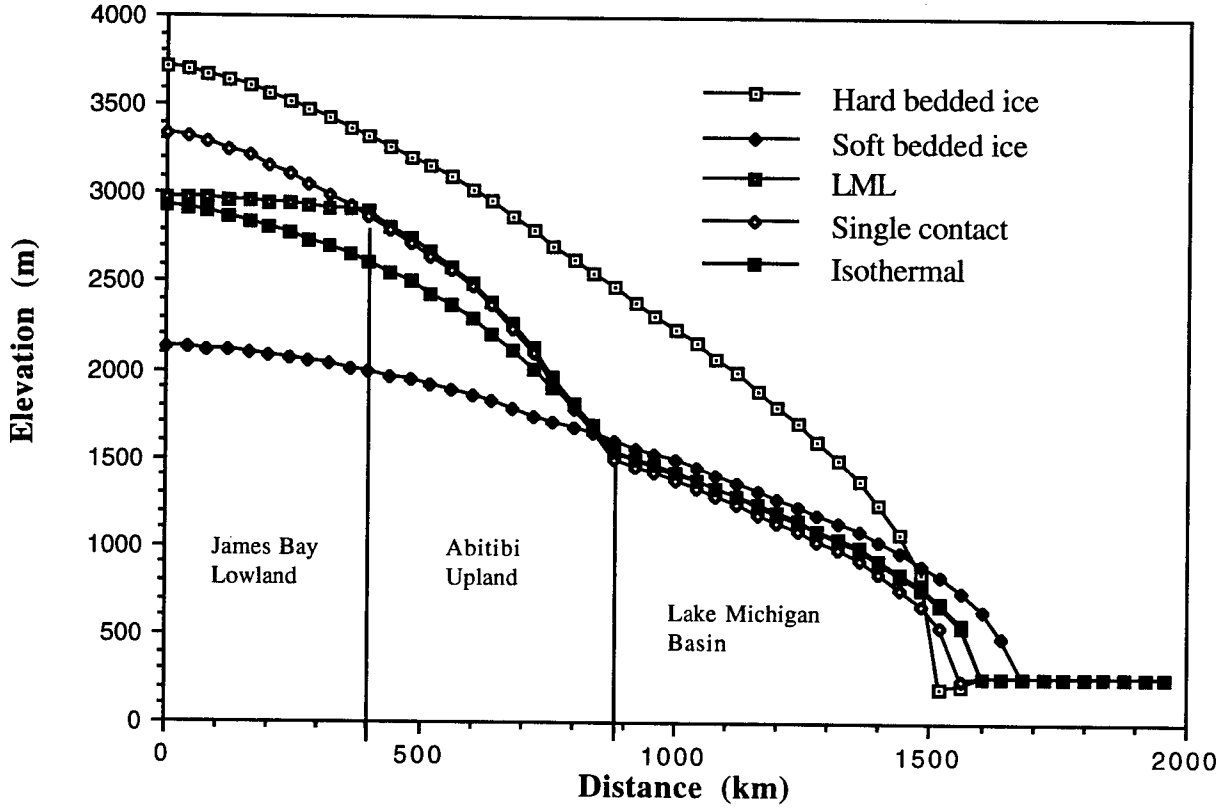

Fig. 5.18. Surface profile of LML simulation compared with hard-bedded ice, soft-bedded ice, LML with upstream soft bed removed (single contact), and the latter configuration with isothermal ice at -5 degrees C.

linear parameters, i.e., the viscosity set to the Newtonian reference viscosity, D_0 set to 1.0 s^{-1}, and n set to 1.0. Although the two cases result in different velocity profiles (Fig. 5.19) the uppermost velocity vectors of each profile are identical, as the theory predicts. Fig. 5.20 shows the ice surface profiles for the nonlinear and linear cases with the linear viscosity set to the reference viscosity of the nonlinear model. The profiles are identical.

The implications of this observation are that for reconstructing gross ice sheet behavior in which only the velocity of the till at the interface is of significance, linear till rheological models adjusted to the appropriate viscosity are sufficient. Accurate assessment of the appropriate viscosity, however, may require nonlinear testing; nearly all sediments are in fact nonlinear and standard viscometer tests, based on assumptions of linear behavior are likely to result in erroneous estimates of the actual viscosity (Ho, personal communication, 1993). If, on the other hand, the focus of interest is the dynamics of the till, till flux, till mass continuity, or the prospect of non-linear response to varying levels of water content, shear stress, or other variables, then a nonlinear model is required.

Steady-state lobe sensitivity to till parameters

Experiments #7-14: Till viscosity: Since linear viscosity suffices for experiments directed solely at the response of the ice sheet to the velocity at the sediment-ice interface, I employed linear parameters in a set of experiments to test the response of the lobe to changes in till viscosity. Fig. 5.21 shows the effect of varying the viscosity from 2 orders of magnitude higher to 5 orders of magnitude lower than the control case (for which the viscosity was the experimentally-determined value of 5.2×10^9 Pa-s). In all cases the profile was lower and less steep than for the hard-bedded ice, as expected since the viscosity of ice is about 2 to 3 orders of magnitude higher than the highest till viscosity in this set of experiments. A noteworthy observation is that at till viscosities greater than 10^9 Pa-s, no distinct lobe is present. There is only a hint of lobe development in the 5.2×10^{10} Pa-s curve. The measured viscosity of 5.2×10^9 Pa-s therefore appears to be very near a "threshold" at which higher viscosities do not allow a significant slope break to develope, but below which the slope

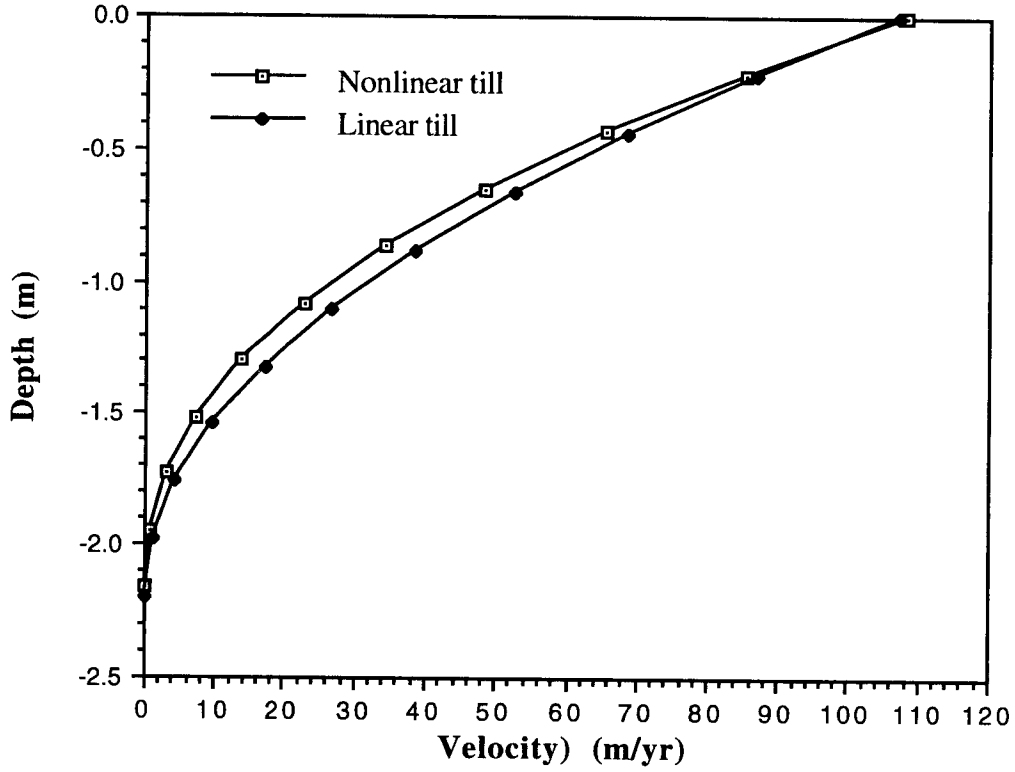

Fig. 5.19. Velocity profiles compared at grid node 31 for nonlinear (n=1.25) vs. linear (n=1.0) till rheologies.

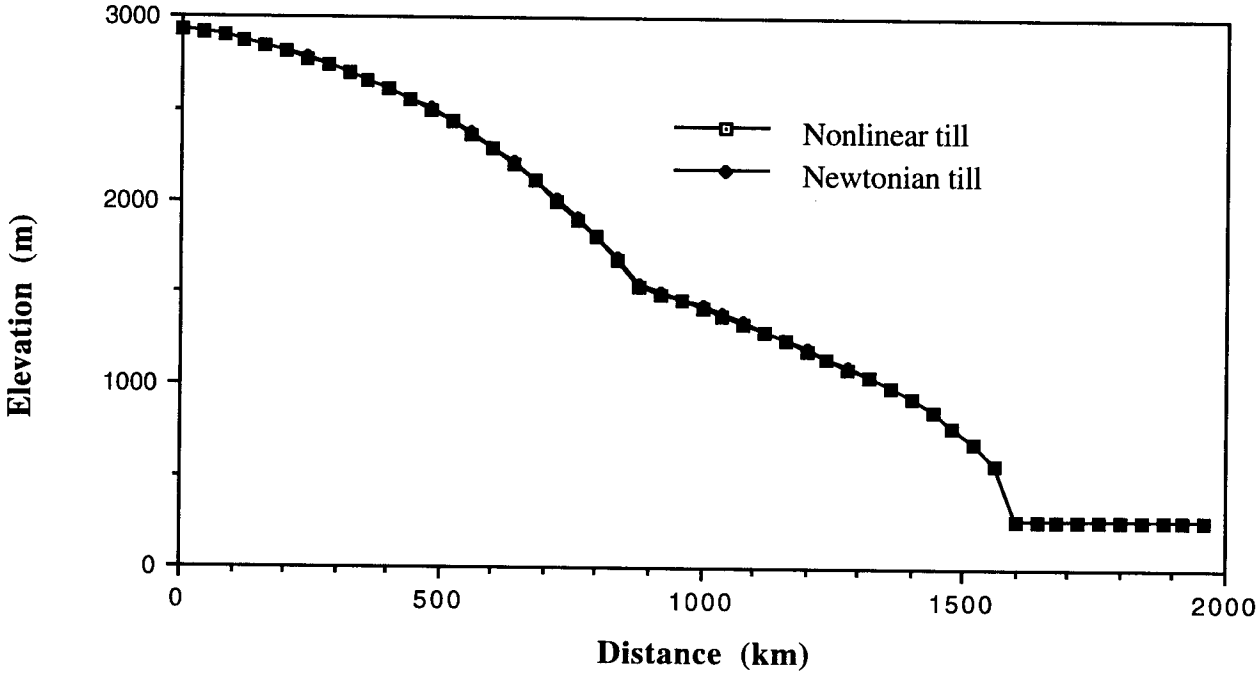

Fig. 5.20. Comparison of surface profiles computed using nonlinear rheology and analogous linear parameters.

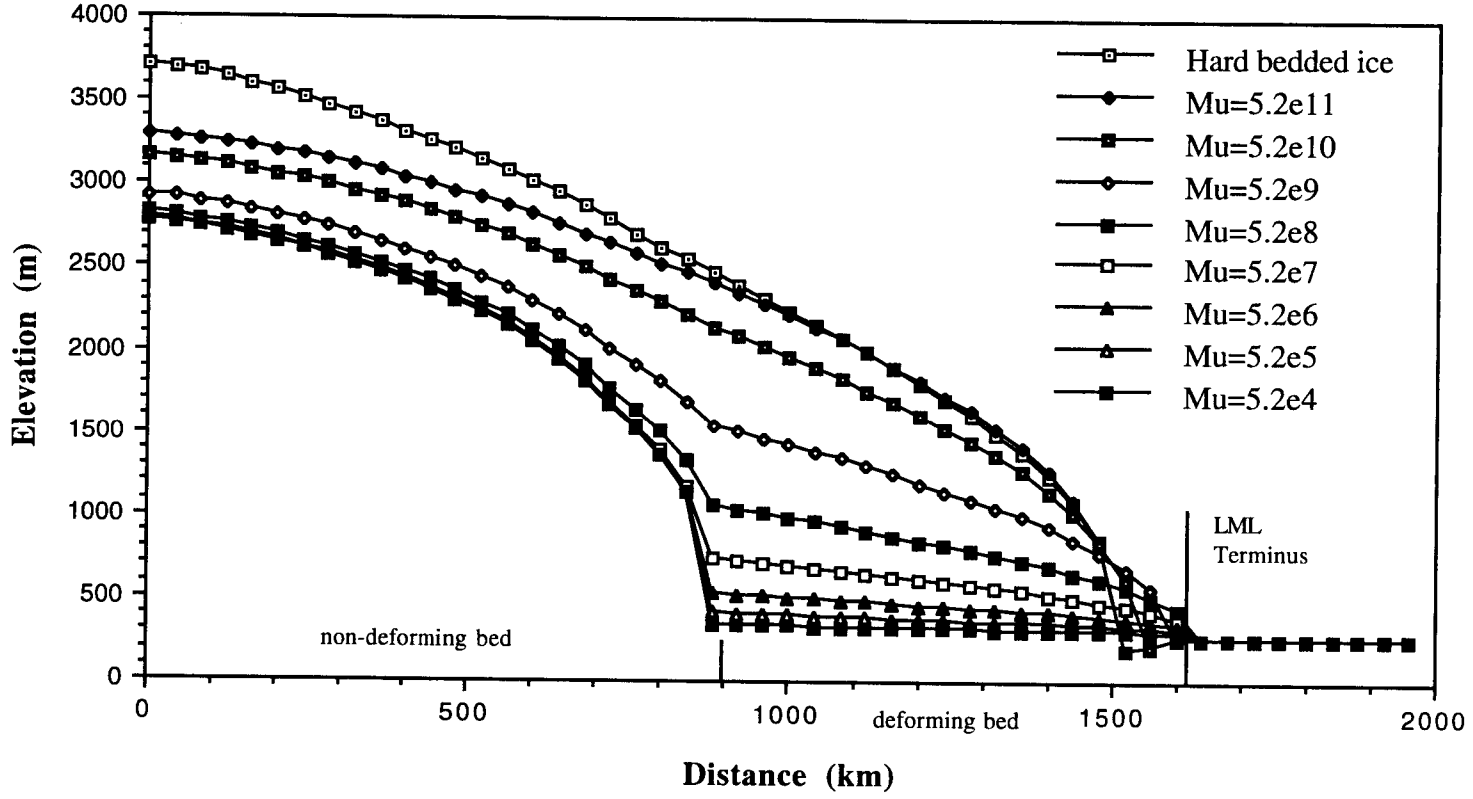

Fig. 5.21. Comparative profiles resulting from various till viscosities

break is distinct and is associated with fundamentally different downstream behavior.

The nature of this threshold is explained by Fig.s 5.22-24, which show the relative proportions of mass flux attributable to till deformation versus ice deformation at till viscosities of 5.2×10^9 Pa-s and higher . At the lowest of the three viscosities (Fig. 5.22) the ice flux over the soft-bedded ice is borne almost entirely by the till. At viscosity 5.2×10^{10} Pa-s (Fig. 5.23 the till is sufficiently stiff that ice deformation over the till becomes significant, accounting for about a third of the ice flux. At an order of magnitude higher viscosity (Fig. 5.24) ice deformation accounts for about 90% of the flux. The implication of this observation is that at the high end of the range of till viscosities a fundamental shift in lobe dynamics takes place. But as noted above, this change is manifest only in terms of changes in the morphology of the lobe, not in the steady-state location of the terminus.

The insensitivity of the steady-state terminus location to the till viscosity makes sense intuitively--to maintain mass balance for a given forcing the mass of ice that is delivered to a given point must remain constant. In the lobe, velocities are higher but the ice is also thinner. The terminus will be located where the cumulative amount of energy available for ablation is sufficient to ablate the entire mass. Since the flux distribution is relatively constant regardless of the till rheology, the terminus must remain in about the same location. Fig. 5.25 illustrates what is taking place. The flux curves are very similar over the entire range of viscosities. The slight differences (a few percent) in maxima of the curves for very high- versus very low-viscosity till are due to the relative distribution of mass between the accumulation and ablation zones as the steeper slope develops on the hard-bedded portion of the ice for systems with lower-viscosity till beneath the lobe. Except for that effect, which is proportionate to the few percent difference in the terminus of the highest-viscosity profiles versus the low-viscosity profiles, the curves are the same. Note that for the five lowest viscosity curves, which exhibit very similar hard-bedded ice profiles upstream of the slope break (and therefore have very similar mass distributions with respect to the accumulation and ablation zones) the

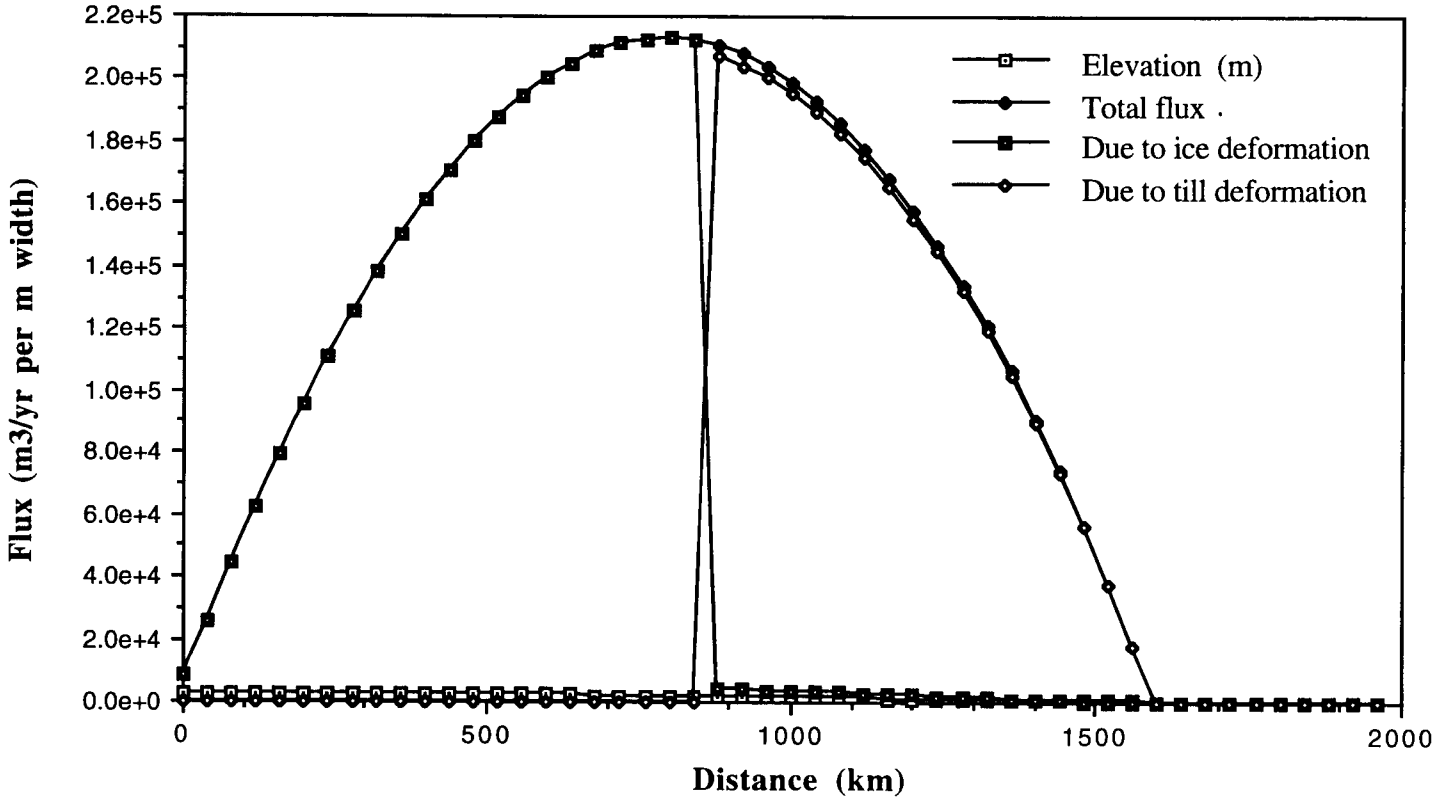

Fig. 5.22. Flux curves for linear till, Mu=5.2e9

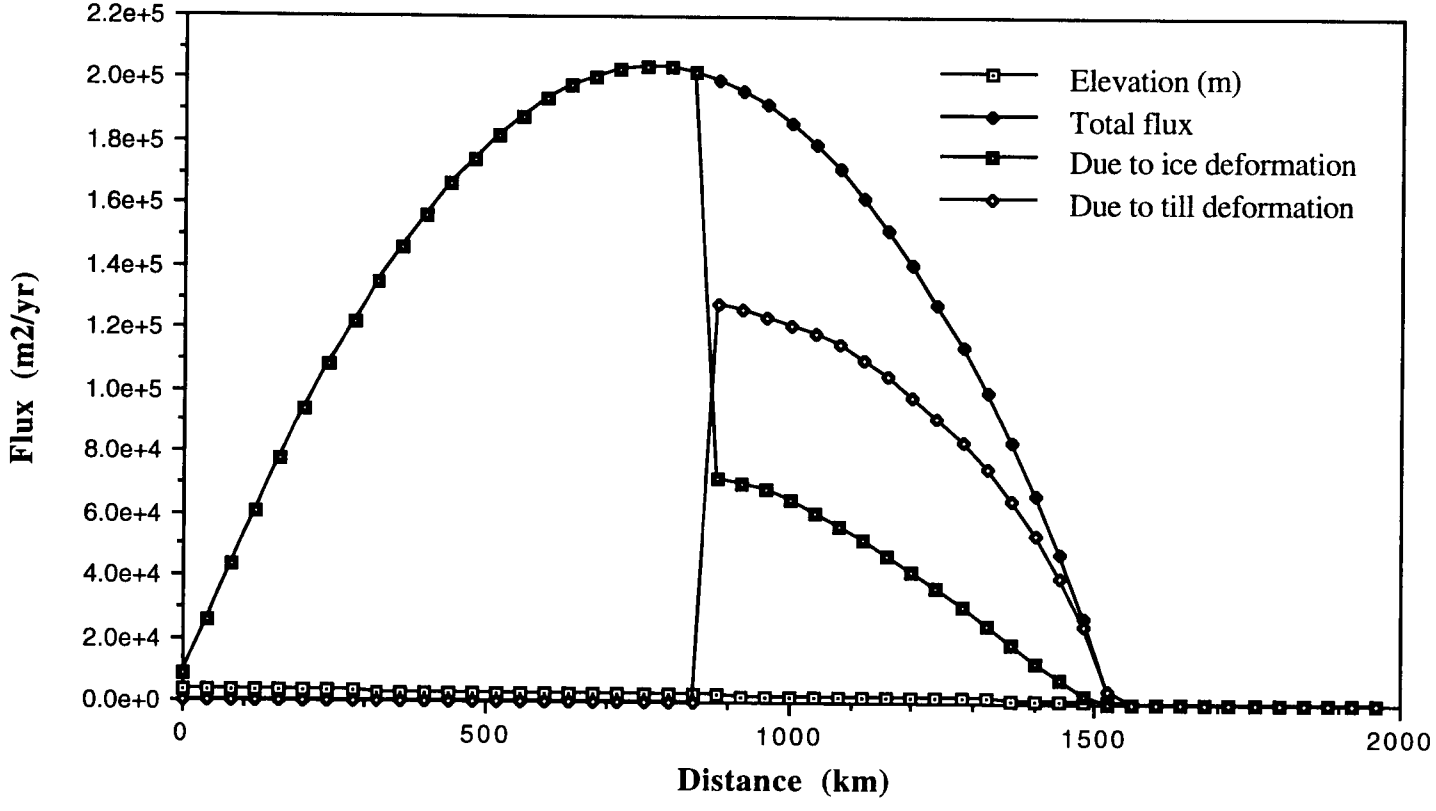

Fig 5.23. Flux curves for linear till, Mu=5.2e10

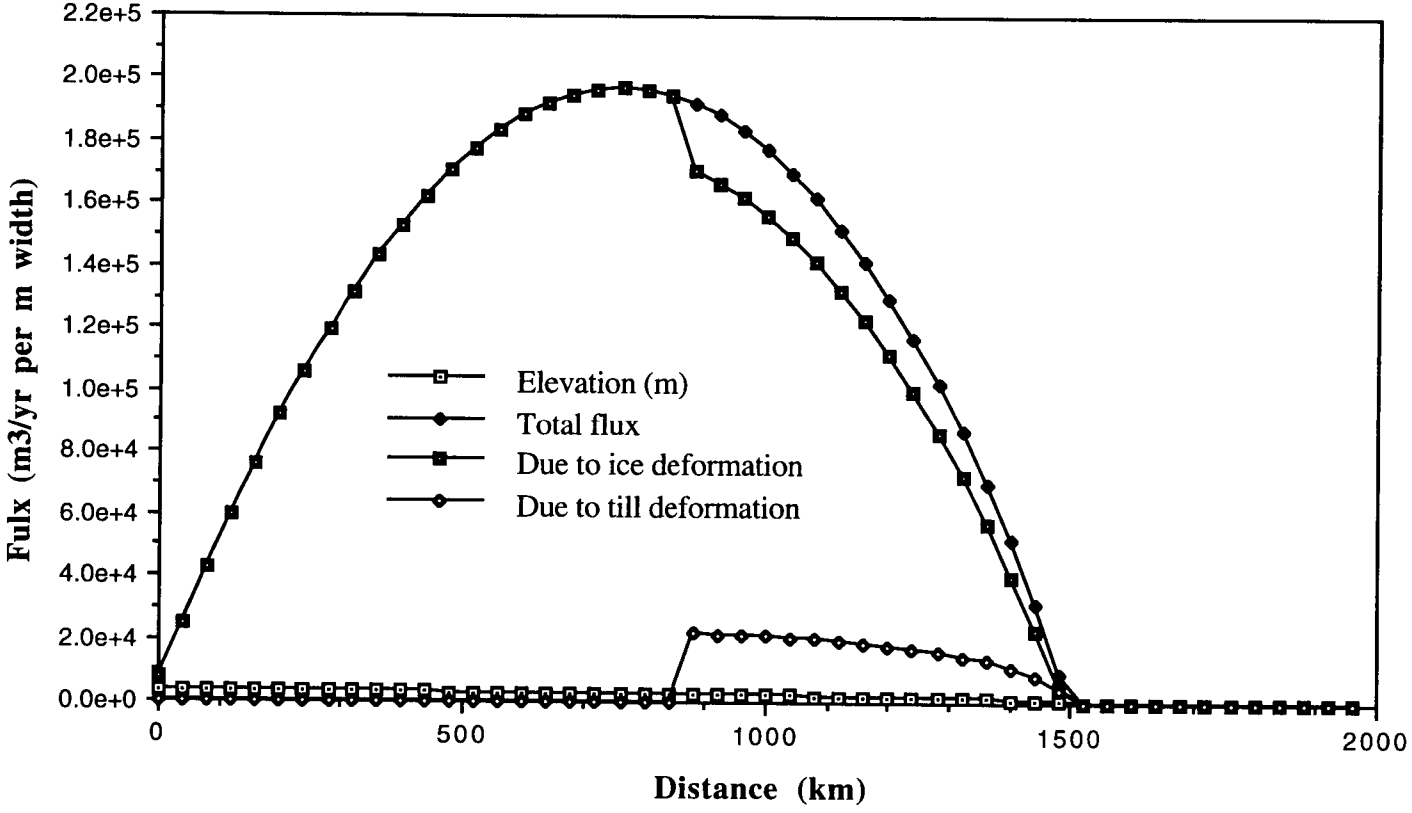

Fig 5.24. Flux curves for linear till, Mu=5.2e11

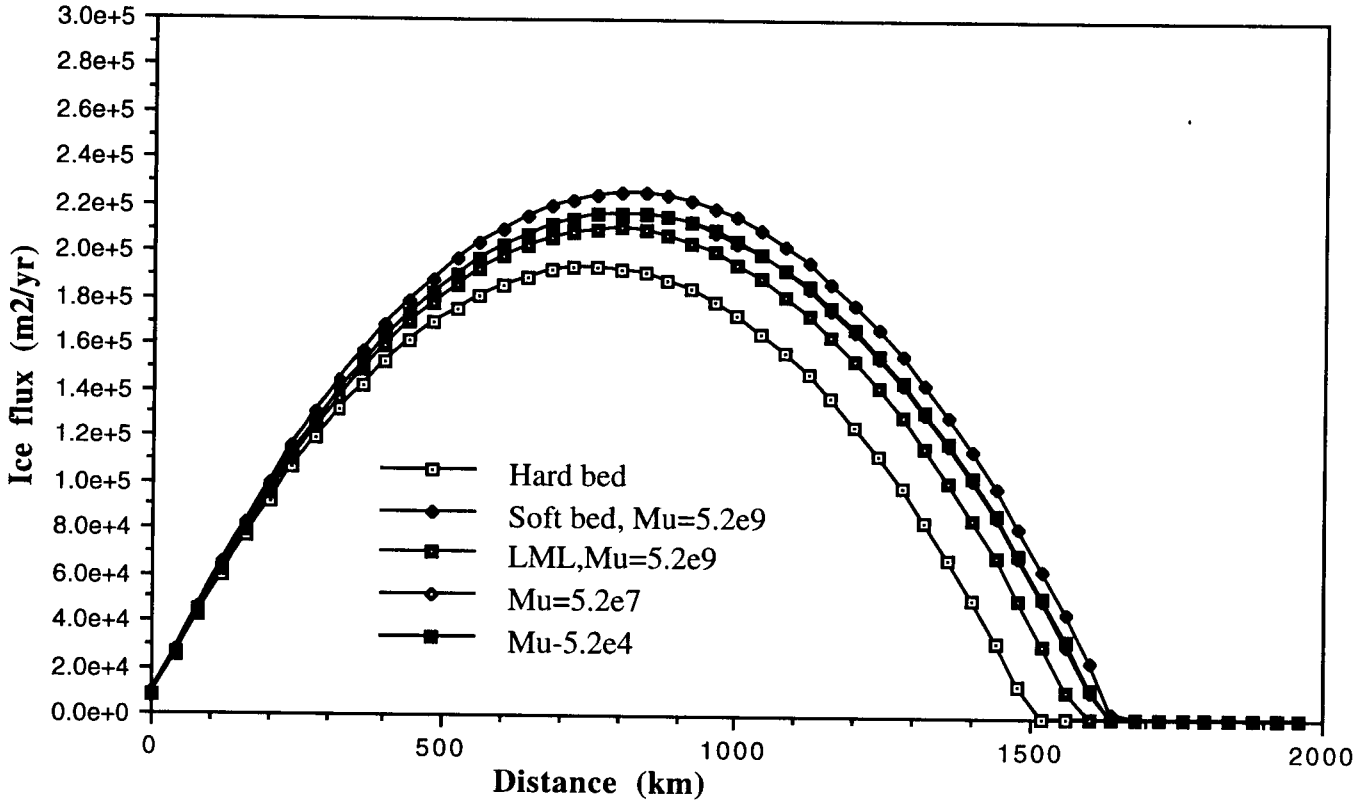

Fig. 5.25. Ice flux compared for various conditions

margin locations and the mass flux curves are virtually identical. These results suggest that if surging of the lobe is influenced by changes in sediment viscosity, the process must be strictly transient.

Experiments #15-19: Till yield strength: Fig. 5.26 shows the sensitivity of the steady state ice surface profiles to linear changes in the sediment yield strength. Except at very low yield strengths (angles of internal friction less than 5°) lobe morphology is not strongly affected by changes in yield strength. Over the range of experimentally-determined yield strengths in this study (ϕ =21.8-24.0°) the results are not significantly different.

Sensitivity to mass forcing changes

Experiments #20-23: Accumulation and ablation: As a first order test of the sensitivity of simulated LML to changes in mass forcing I conducted two sets of numerical experiments using the measured till rheologic parameters but altering the climate forcing parameters. Because of the first-order nature of the climate model employed in the LML model no direct inference can be made to the types of actual climate changes that might be represented by the parametric changes made in these experiments. But they do provide a useful first approximation for examining the relative magnitudes between climate forcing and steady state response of the lobe. Fig. 5.27 shows the changes in steady state profiles associated with 10% and 20% decreases, respectively, in the net accumulation. Fig. 5.28 shows the profiles associated 10% and 20% increases in the (negative) gradient of the net accumulation-ablation curve. The former is analogous to a uniform percentage decrease in precipitation. The latter is analogous to a uniform percentage increase in the rate of southward "warming," or more precisely, ablation. In both cases the steady state response appears to be consistent and roughly proportionate to the change in the "climate" parameters.

Sensitivity to nonlinearity parameter

Experiments #24-25: n-values: To evaluate the implications of the precision in the geotechnical data for the results of the numerical tests I ran the model with n set to 1.5 and 1.75, spanning the range of values from the tests.

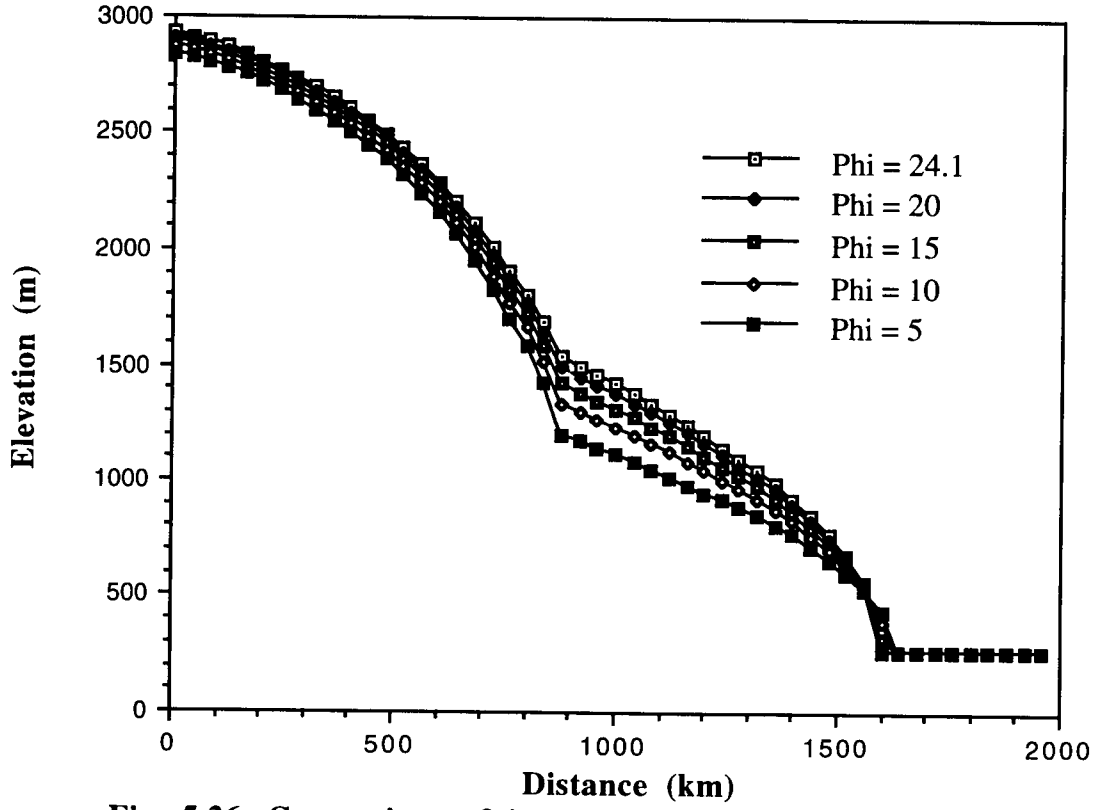

Fig. 5.26. Comparison of ice surface profiles associated with various sediment angles of internal friction (phi).

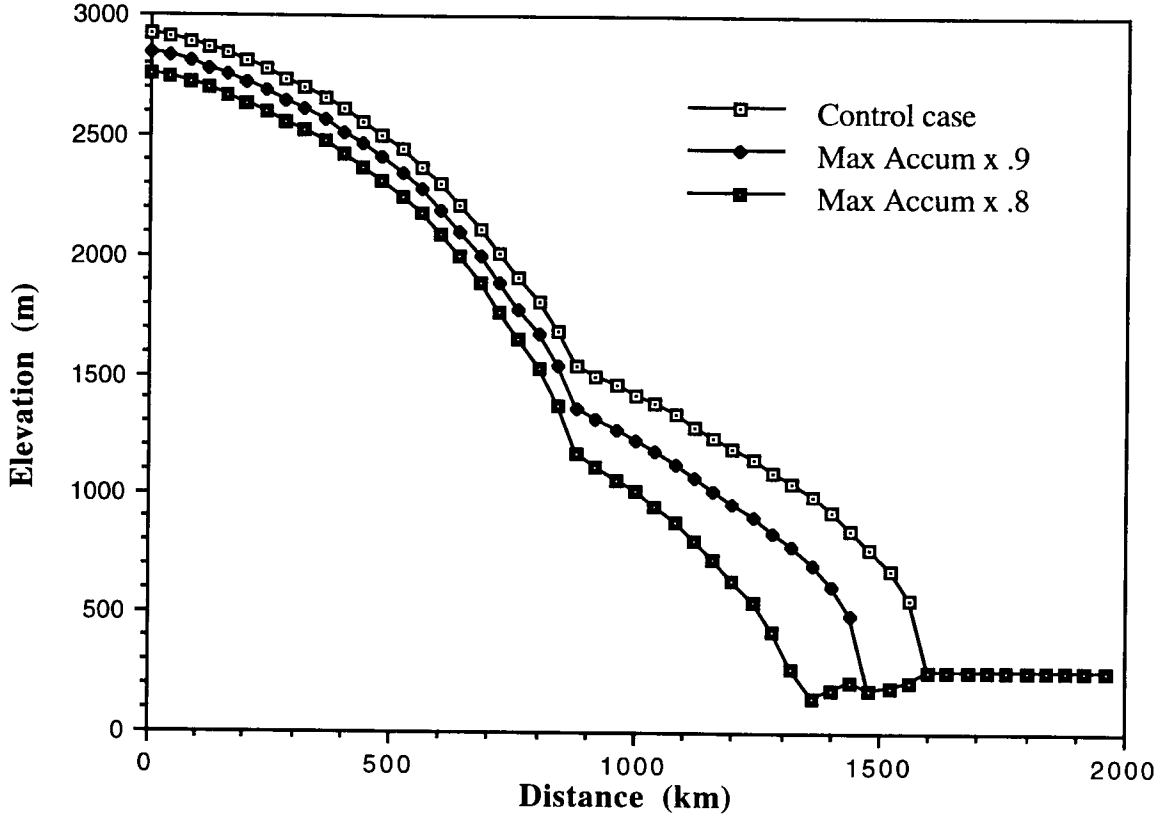

Fig. 5.27. Surface profiles associated withb10% decrease (max. accum. x .9) and 20% decrease (max. accum. x .8) in net accumulation.

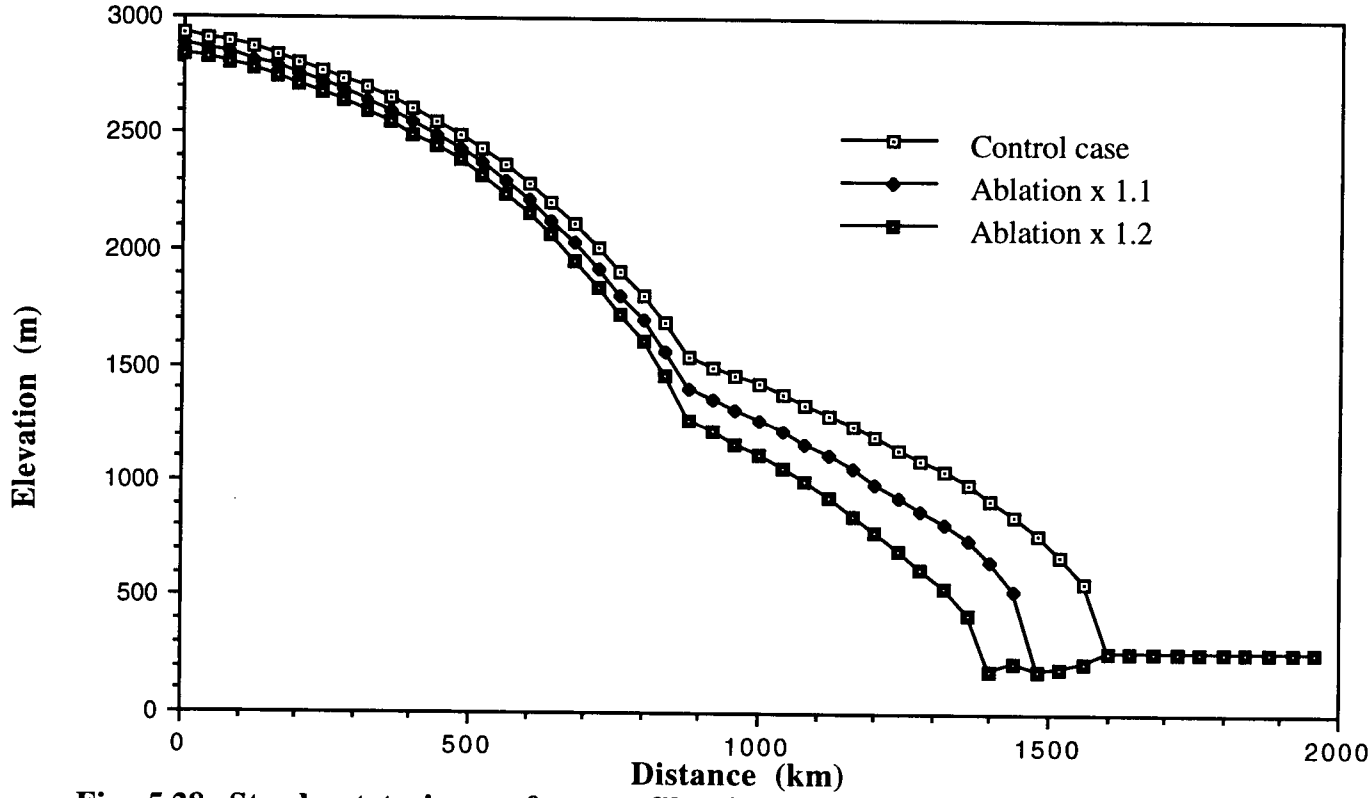

Fig. 5.28. Steady state ice surface profiles for 10 % increase in ablation (ablation x 1.1) and 20% increase in ablation (ablation x 1.2).

Fig. 5.29 shows the computed velocity profiles at grid node 31 for each of these cases. The results are profoundly different in terms of maximum velocity, thickness of the shear zone, and the implied mass flux of the till. Higher values of n imply higher effective viscosities, which imply lower maximum velocities. The lower basal velocity of the ice results in a more steeply sloping ice surface (Fig. 5.30) with attendantly higher shear stress. Thus the thickness of the shear zone is greater for the high viscosity till, in spite of the fact that the strength parameters are identical.

These results have significant implications for modeling studies. First, high precision in the geotechnical experiments is of premier interest in order for the data to be used with confidence in numerical predictions or reconstructions of ice sheet behavior. Since the numerical results are profoundly affected by differences in n for a given value of b, it is crucial to identify with some precision the actual rheology of the material in order to accurately characterize lobe dynamics, the nature of till deformation or predict magnitudes of till flux. Second, these results suggest that natural variations in the viscoplastic nonlinearity parameter, if possible, could have profound consequences for the evolution and behavior of soft-bedded ice sheets. Worthwhile lines of inquiry for future study would be the degree of variation in n as a function of sediment composition and texture, and whether these might have changed over time in deforming subglacial sediments.

Comparison of selected geological data with modeling results

Till flux. Based on sediment volumes and known age constraints, Johnson and others (1991) estimated sediment transport rates from the LML of about 400 m^3/y per meter width of the ice lobe, and inferred ice velocities on the order of 200 to 500 m/y. They noted that for the required sediment flux to have been achieved solely by intra-ice and basal debris transport, debris concentrations would have had to have been much higher than observed in modern glaciers. They concluded, therefore, that some additional mechanism, such as sediment deformation, must be invoked.

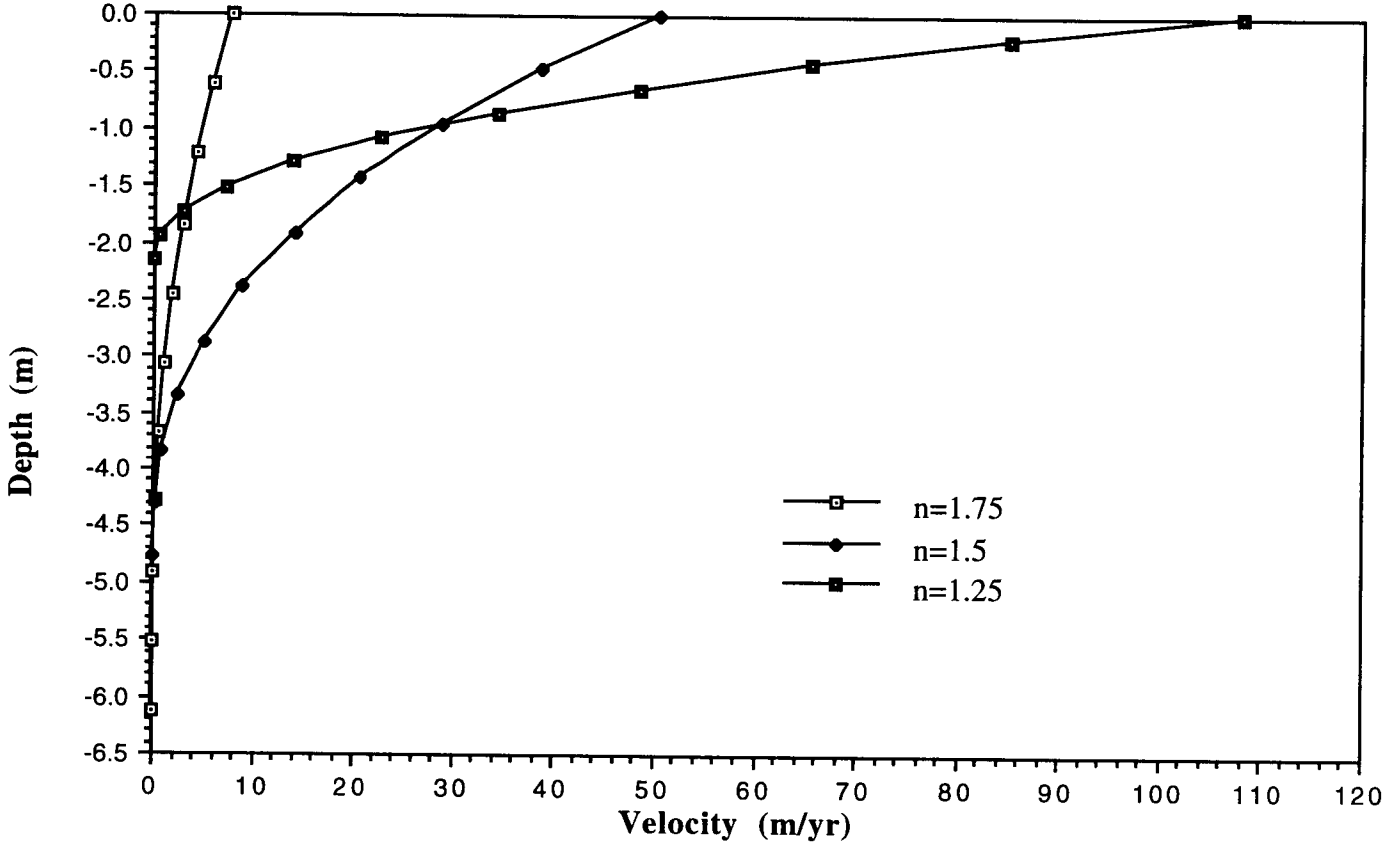

Fig. 5.29. Comparitive profiles for sediments with identical values of b but different values of n at node 31

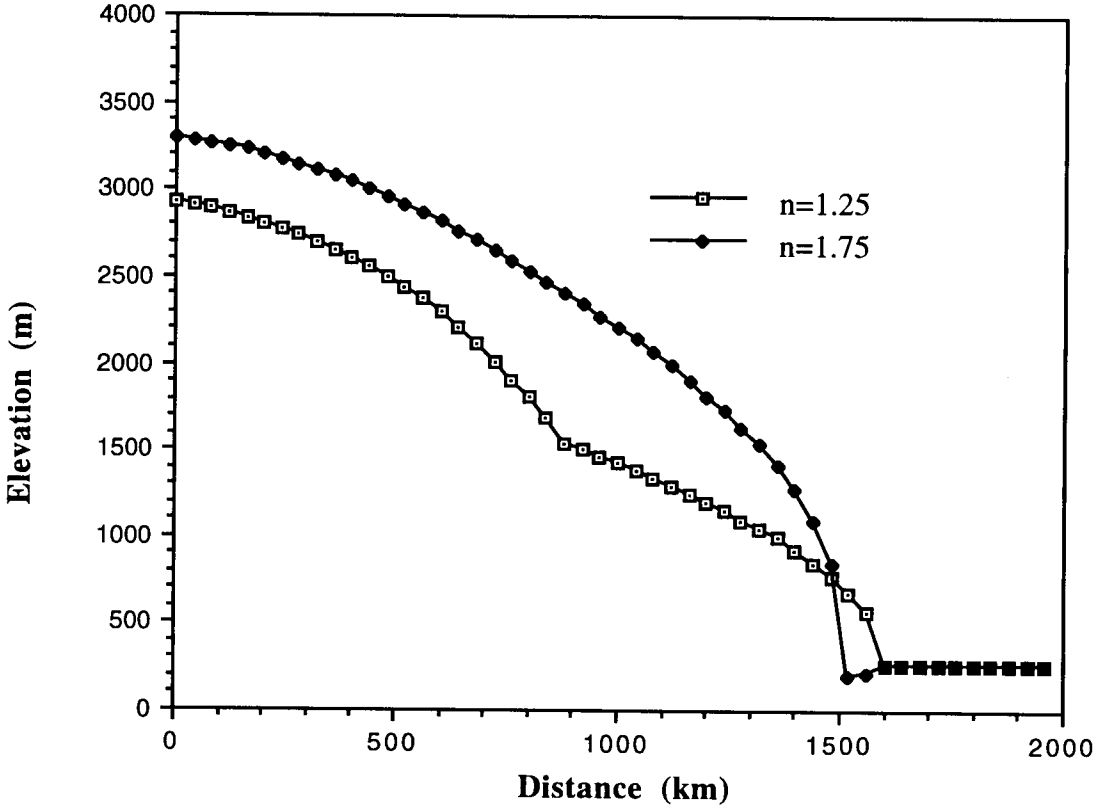

Fig 5.30. Profiles for identical till parameters, except for values of n.

Fig. 5.31 plots of the calculated sediment velocity profiles over the range of sediment viscosities examined in the numerical experiments of this study. The striking feature is that although the very low viscosities (o.m. 10^7-10^4 Pa-sec) induced very high velocities (300 to 600 m/y, respectively) at the ice-sediment interface, the shear zone for the low viscosity till was extremely thin, on the order of only a few centimeters. Since each curve was calculated using identical sediment yield strengths, the thinness of the shear zones for the low viscosity cases is due solely to the very low applied shear stress associated with the very low ice surface gradient of the low-viscosity lobes. On the other hand, the very highest viscosities exhibit very thick shear zones, on the order of several meters. The associated maximum velocities, however, are on the order of only tens of meters. Since the high velocities imply extremely thin shear zones, while on the other hand, thick shear zones imply very low velocities, one would expect that the maximum flux should be associated with an intermediate viscosity.

Fig. 5.32 compares the flux curves for the same set of viscosities examined in Fig. 5.31. The notable features are (1) a dramatic *increase* in the flux as the viscosity increases from 5.2×10^7 to 5.2×10^9 Pa-sec, and (2) a dramatic *drop* in the flux as the viscosity increases from 5.2×10^{10} to 5.2×10^{11} Pa-sec. Viscosity on the order of 5.2×10^{10} Pa-sec appears to produce the optimum combination of sediment velocity and shear-zone thickness to produce the maximum flux. Interestingly, this is also the viscosity which appears to be the "threshold" for the development of the lobate ice surface profile (Fig. 5.21), and at which the basal shear stress for "soft-bedded" ice is at a maximum.

The maximum flux from the numerical experiments, on the order of 100 m3/y per meter width, is roughly consistent with Johnson's and others (1991) estimate of 400 m3/y per meter width: Johnson's and others estimate includes sediment deposited from intra-ice and basal transport as well as sediment produced from ongoing erosion, and perhaps some unidentified processes. Calculations from the numerical model reflect only the transport of material that could have been mobilized from within a hypothetical infinite half-space of material. A more sophisticated model of sediment mass transport, incorporating

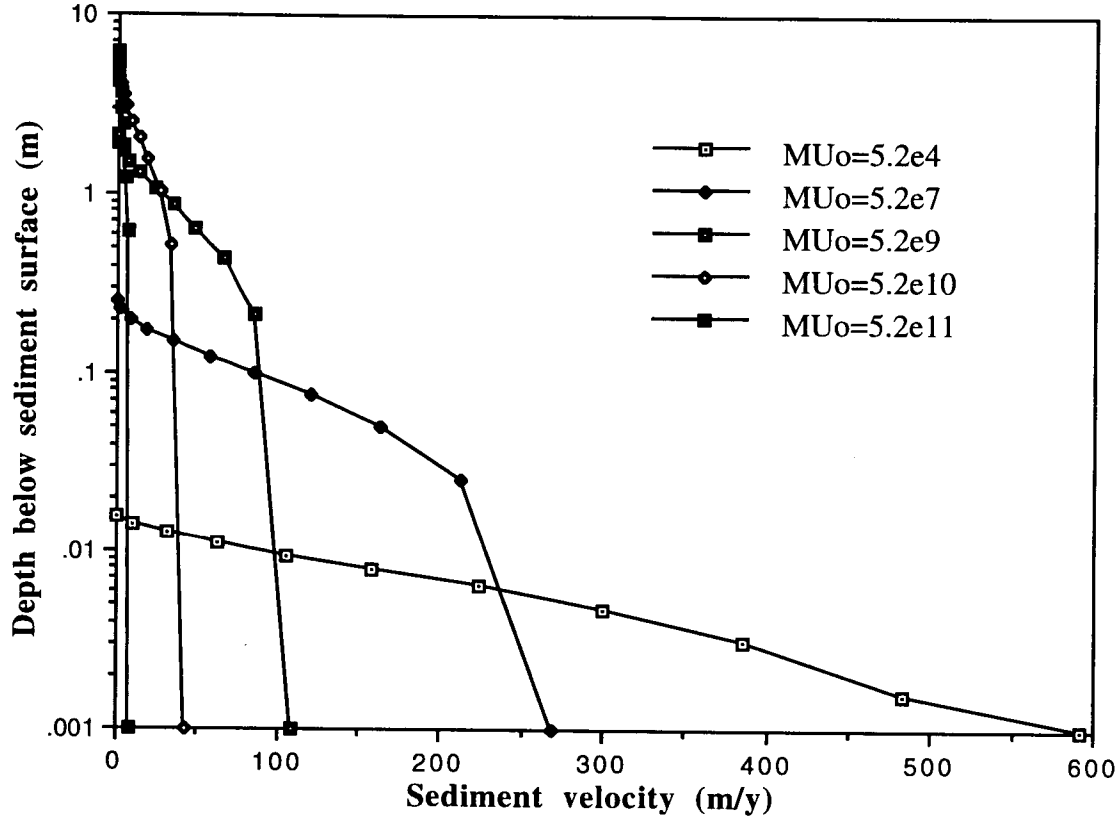

Fig. 5.31 Sediment velocity profiles at node 31 for various sediment viscosities.

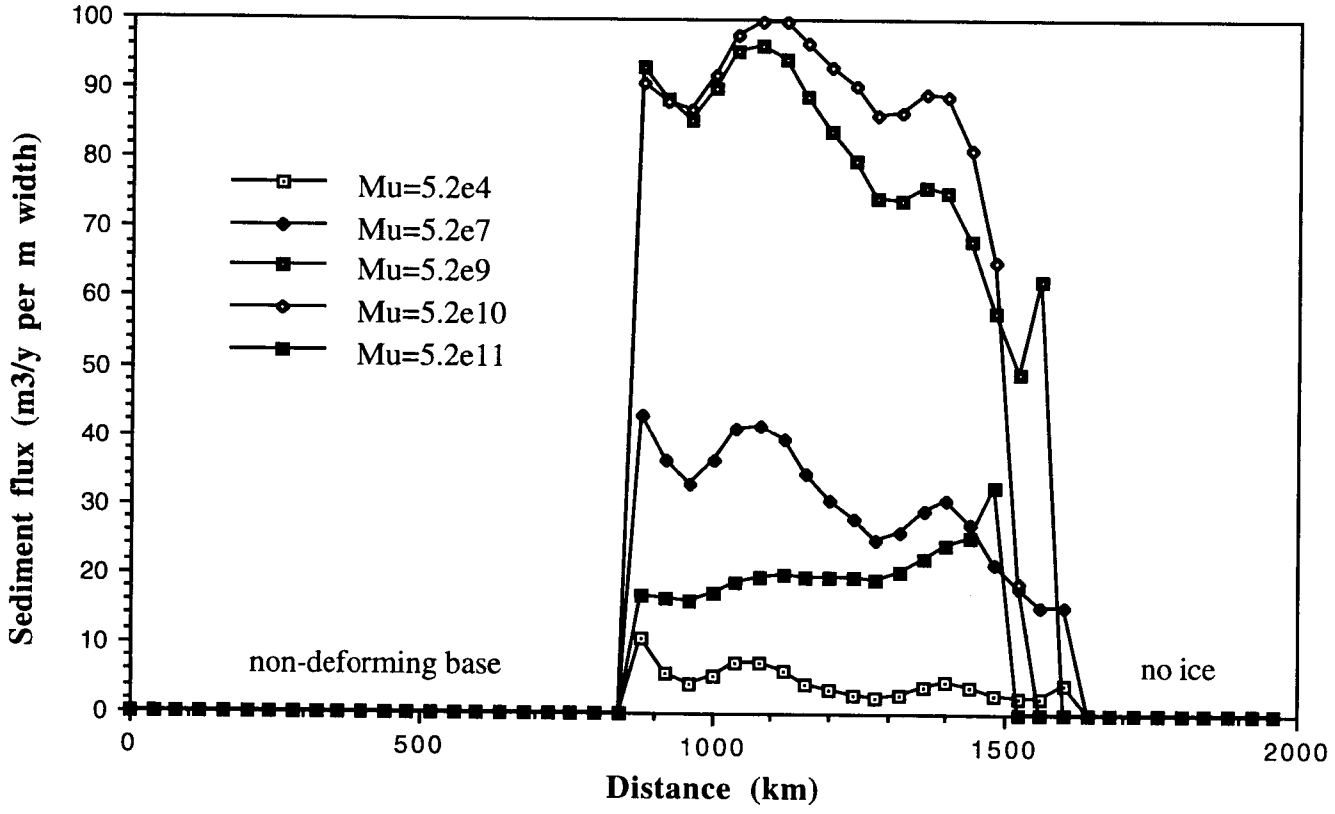

Fig. 5.32 Sediment flux curves for various sediment viscosities (Pa-sec).

mass conservation and mechanisms for production and loss (net mass forcing) will be required to make more accurate estimates of the actual mass transport rates. The preliminary experiments reported here, however, do provide some insights on kinds of conditions, specifically sediment viscosity, that might be consistent with empirically estimated flux rates. In general, the the ice-sediment interface, the shear zone for the low viscosity till was extremely thin, on the order of only a few centimeters. Since each curve was calculated using identical sediment yield strengths, the thinness of the shear zones for the low viscosity cases is due solely to the very low applied shear stress associated with the very low ice surface gradient of the low-viscosity lobes. On the other hand, the very highest viscosities exhibit very thick shear zones, on the order of several meters. The associated maximum velocities, however, are on the order of only tens of meters. Since the high velocities imply extremely thin shear zones, while on the other hand, thick shear zones imply very low velocities, one would expect that the maximum flux should be associated with an intermediate viscosity.

Fig. 5.32 compares the flux curves for the same set of viscosities examined in Fig. 5.31. The notable features are (1) a dramatic *increase* in the flux as the viscosity increases from 5.2×10^7 to 5.2×10^9 Pa-sec, and (2) a dramatic *drop* in the flux as the viscosity increases from 5.2×10^{10} to 5.2×10^{11} Pa-sec. Viscosity on the order of 5.2×10^{10} Pa-sec appears to produce the optimum combination of sediment velocity and shear-zone thickness to produce the maximum flux. Interestingly, this is also the viscosity which appears to be the "threshold" for the development of the lobate ice surface profile (Fig. 5.21), and at which the basal shear stress for "soft-bedded" ice is at a maximum.

The maximum flux from the numerical experiments, on the order of 100 m3/y per meter width, is roughly consistent with Johnson's and others (1991) estimate of 400 m3/y per meter width: Johnson's and others estimate includes sediment deposited from intra-ice and basal transport as well as sediment produced from ongoing erosion, and perhaps some unidentified processes. Calculations from the numerical model reflect only the transport of material that could have been mobilized from within a hypothetical infinite half-space of material. A more sophisticated model of sediment mass transport, incorporating

viscosities most consistent with Johnson's and others estimates are also consistent with the measured till viscosity (o.m. 10^9 Pa-sec) from the geotechnical tests in this study.

Surface profile. Fig. 5.33 shows calculated marginal profiles compared with the profile constructed by Clark (1992) (Fig. 4.2) from moraine height data. In this case, the geologic data appear to be more consistent with the lower-viscosity profiles. The comparison, however, is necessarily very tentative, since the geologic data are limited, and the calculated profiles are for only the first 80 km behind the margin. Precision and accuracy of the comparison are thus limited by the 40-km grid resolution as well as by the fact that the accuracy of the shear stress equation (eqn. (2.4)) diminishes significantly near the ice margin (Paterson, 1981). The shear stresses calculated over the range of viscosities from o.m. 10^8 down to about o.m. 10^6 Pa-sec, however, are consistent with the range inferred by Clark (1992), suggesting that o.m. 10^9 may be near the upper limit.

Evidence consistent with low-viscosity sediment, such as the profiles examined above (and possibly the associated preconsolidation stress reported in Chapter 4), does not necessarily contradict evidence for a high-viscosity regime. The low ice surface profiles recorded by the moraine-height data, and possibly by the preconsolidation data described in Chapter 4, may represent low-viscosity conditions that prevailed only during the final moraine-building period just before the ice withdrew. What physical process might have been responsible for viscosities orders of magnitude lower than that measured in this study, however, is an open question. The o.m. 10^9 Pa-sec reported here was based on sediment at 100% saturation. To achieve lower viscosities that sediment would had to have been in an "oversaturated, "slurrified ," and, therefore transient--and most likely unstable--state. While is difficult to imagine that such a state could have prevailed over the several thousands of years of lobe activity, it does not seem unreasonable to hypothesize that there could have been transient episodes of low viscosity conditions, particularly during the retreat of the lobe.

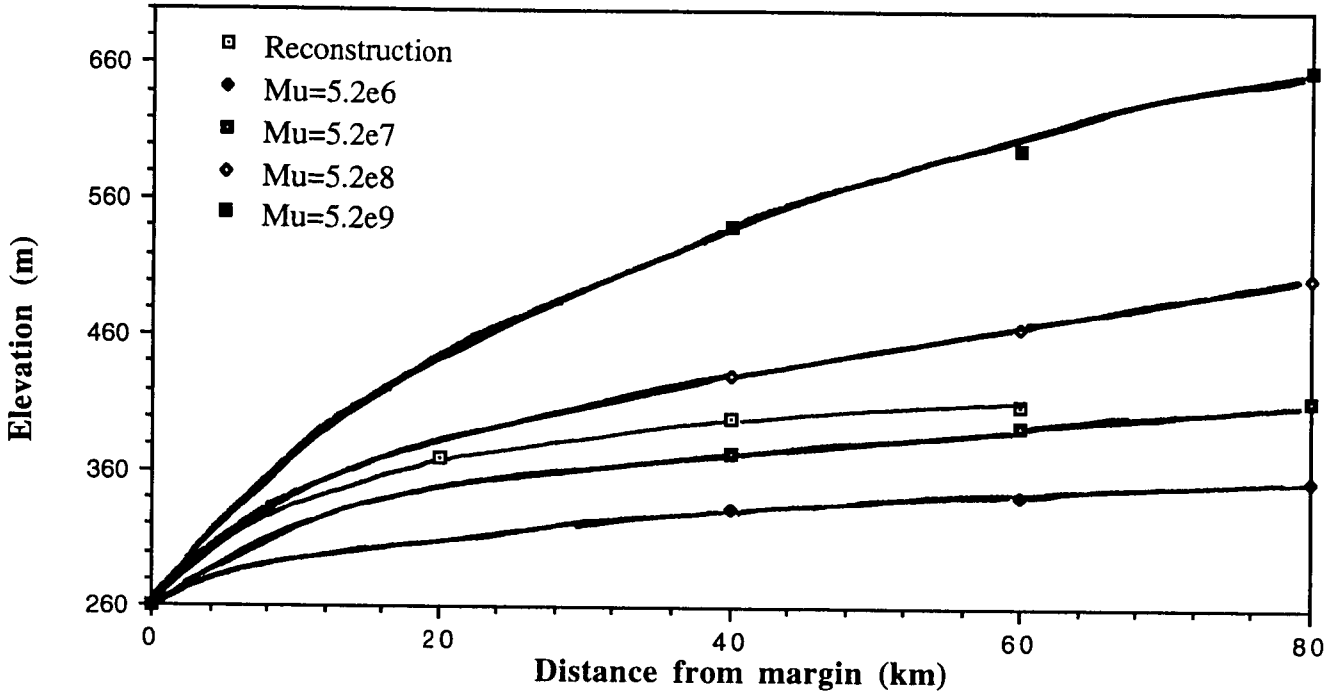

Fig. 5.33. Comparison of Clark's (1992) reconstruction with calculated ice surface profiles for various sediment viscosities (Pa-sec).

Transient responses to changes in external parameters. Identifying and quantifying the possible transient responses of the LIS to changes in climate and sediment conditions is crucial to reconstructing the history of the LIS and understanding its interaction with atmosphere and oceans. To investigate possible responses of the LML to paleoclimate change, I ran some preliminary numerical experiments in which climate parameters were altered to reflect the types of changes in accumulation and ablation rates suggested by geologic evidence. Alley and others (1993) reported that snow accumulation in Greenland ice cores apparently doubled rapidly from the Younger Dryas event (ca. 11.5 ka BP) to the subsequent Preboreal interval, possibly in less then 3 years. The change in accumulation rate from the Oldest Dryas to the Bolling/Allerod warm period was similarly large and abrupt. Greenland ice core data reported by Johnsen and others (1992) indicate that irregular interstadial episodes lasting only a few hundred years or less were associated with abrupt temperature changes in which the milder glacial stages were about 7°C warmer than the cold ones.

Fig. 5.34 shows the response of the steady state control configuration (Experiment #5) to an abrupt doubling of the maximum accumulation rate ($\dot{A}_{max}$ in eqn. (2.3)) and a simultaneous quadrupling of the southward decrease in net accumulation ($\partial\dot{A}/\partial x$ in eqn. (2.3)). This combination of climate parameters is meant to emulate the wetter, warmer interstadial climate suggested by the ice core data. It is hereafter referred to as the "wet-warm" experimental climate (in contrast to the "cold-dry" or "glacial" control climate). The striking effect is the retreat of the lobe margin to within about 80 km of the contact (at 920 km) between the crystalline bedrock and soft-sediment substrate. A small lobe is retained by the ice sheet after the climate shift, but the ice sheet adjusts to the new climate primarily by withdrawing most of the lobe from the "harsher" ablation area of the new climate.

Though strictly arbitrary, both the control and "wet-warm" climates appear to be sufficiently realistic to provide reasonable surrogate climates for sensitivity experiments on ice sheet response to dynamic changes. Both climate configurations produce glacier mass-balance curves (Fig. 5.35) for the simulated

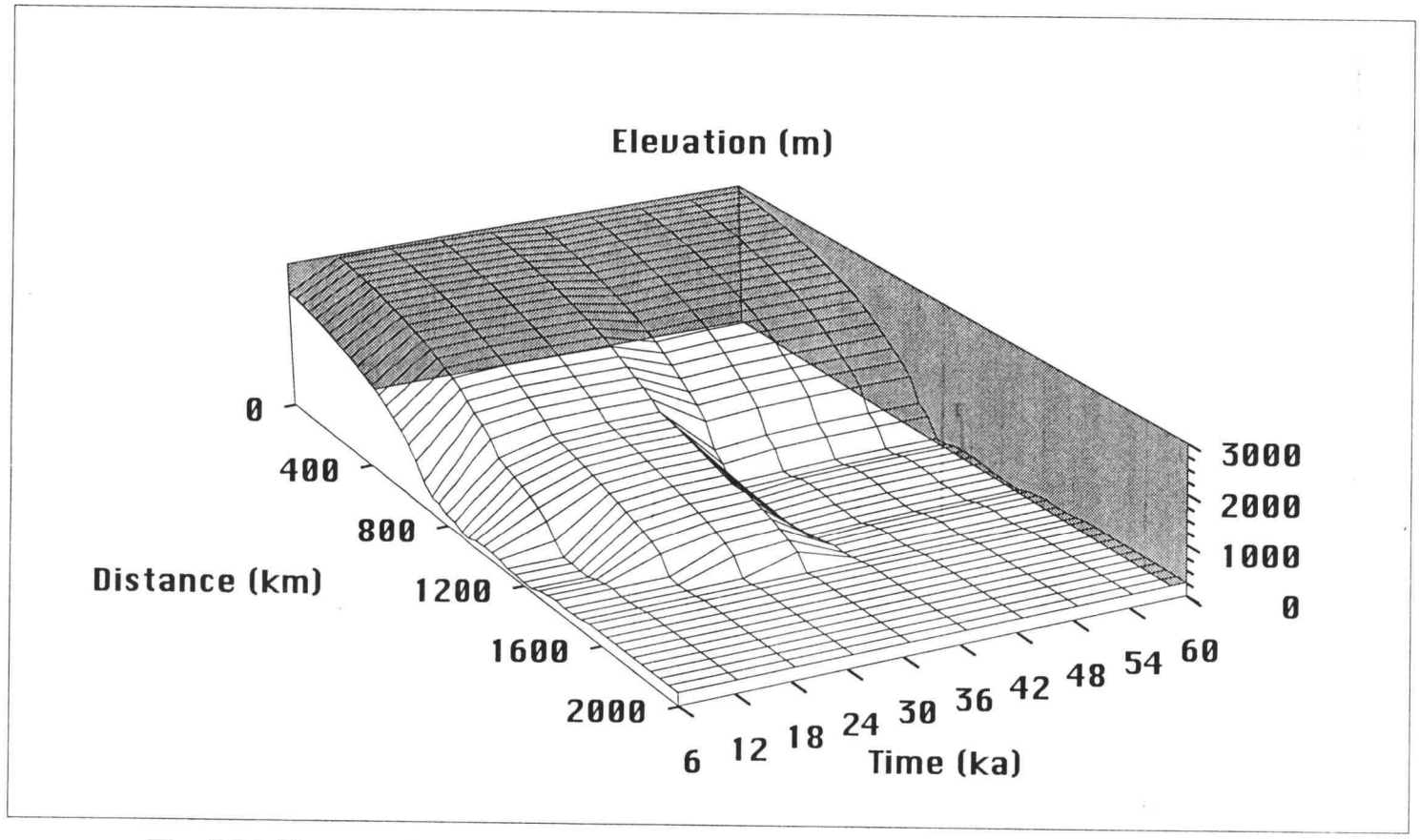

Fig. 5.34. Near-steady-state response of ice surface to shift from control ("cold-dry") to "wet-warm" climate at 30 ka.

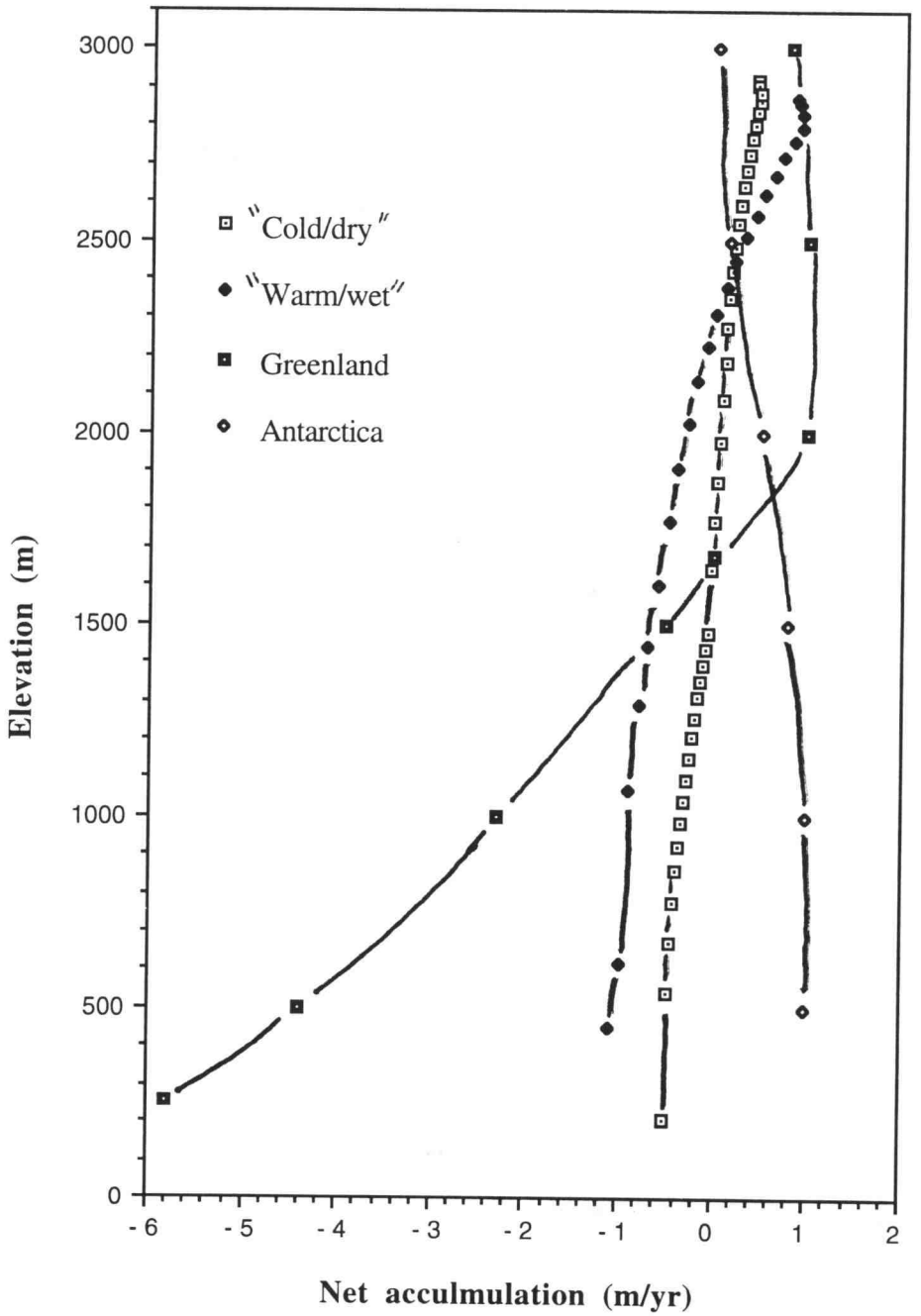

Fig. 5.35. Comparison of mass balance curves for "cold-dry" (control) climate and "wet-warm" climate with generalized modern curves for Greenland and Antarctica (After Boulton and others, 1984).

LML that fall roughly within an "envelope" defined by generalized curves for the Greenland and Antarctic Ice Sheets (Boulton and others, 1984). Perhaps the most striking attribute of the two experimental curves is their relative *similarity* compared to the drastic contrast between the modern Greenland and Antarctic curves. In spite of their relative similarity, however, the two mass balance curves are associated with substantially different "climates" and profoundly different steady-state lobe profiles.

Fig. 5.36 shows the response of the ice margin to a forced 3,000-year oscillation between the control and "wet-warm" climates, beginning at 30 ka, by which time the lobe was at steady state (i.e., beginning from the configuration of Experiment #5). Within 3,000 years from the onset of the "wet-warm" conditions the margin has withdrawn almost all the way to the near-steady-state "wet-warm" position shown in Fig. 5.34. When the control or "cold-dry climate" is reinstated, the lobe is unable to return to the original terminus within the 3,000-year period of the oscillation--readvance of the lobe is slower than the retreat, even in response to the same magnitude change in the climate forcing. In the first 500 years after the onset of the "wet-warm" climate the margin retreats 200 km, whereas in the first 500 years after reinitiation of the control climate, it advances only 80 km. Upon reinitiation of the "wet-warm" climate, the retreat is virtually parallel to the corresponding portion of the previous retreat. Subsequent readvances are very similar in magnitude and rate of response. The magnitude of the oscillations is fairly consistent, at about 350-400 km.

Fig. 5.37 shows the response of the lobe to the same climate forcing regime as shown in Fig. 5.36, but with the ice resting entirely on a non-deforming bed. The graph from Fig. 5.36 is superimposed for comparison. Note that although the timing of the responses is identical in the two cases, the magnitude and rate of the response in the all-hard-bed case are greatly reduced compared to the first experiment, in which ice beyond 920 km is soft-bedded. The magnitude of the response for the non-deforming-bed system over the 3,000-year period is only about half that of the hard/soft-bedded system if Fig. 5.36. In 500-600 years (the amount of time required for the viscosity experiments to show a 250 km advance) the ice advances no more than 40 km.

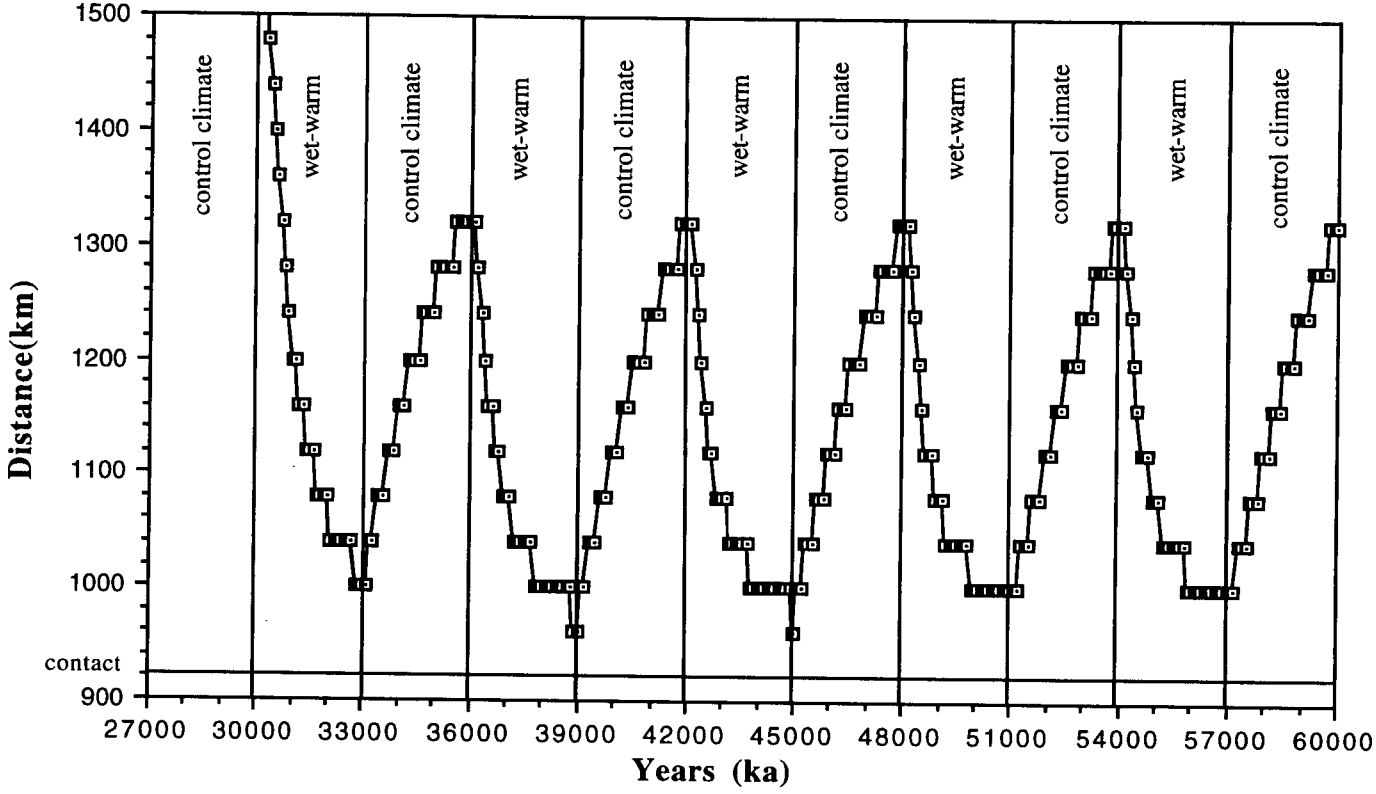

Fig. 5.36. Oscillations from steady-state terminus induced by 3000-year fluctuations between "dry-cold" and "wet-warm" climate forcing. Data points are 100 years apart. Contact between hard and soft bed at 920 km is marked on graph.

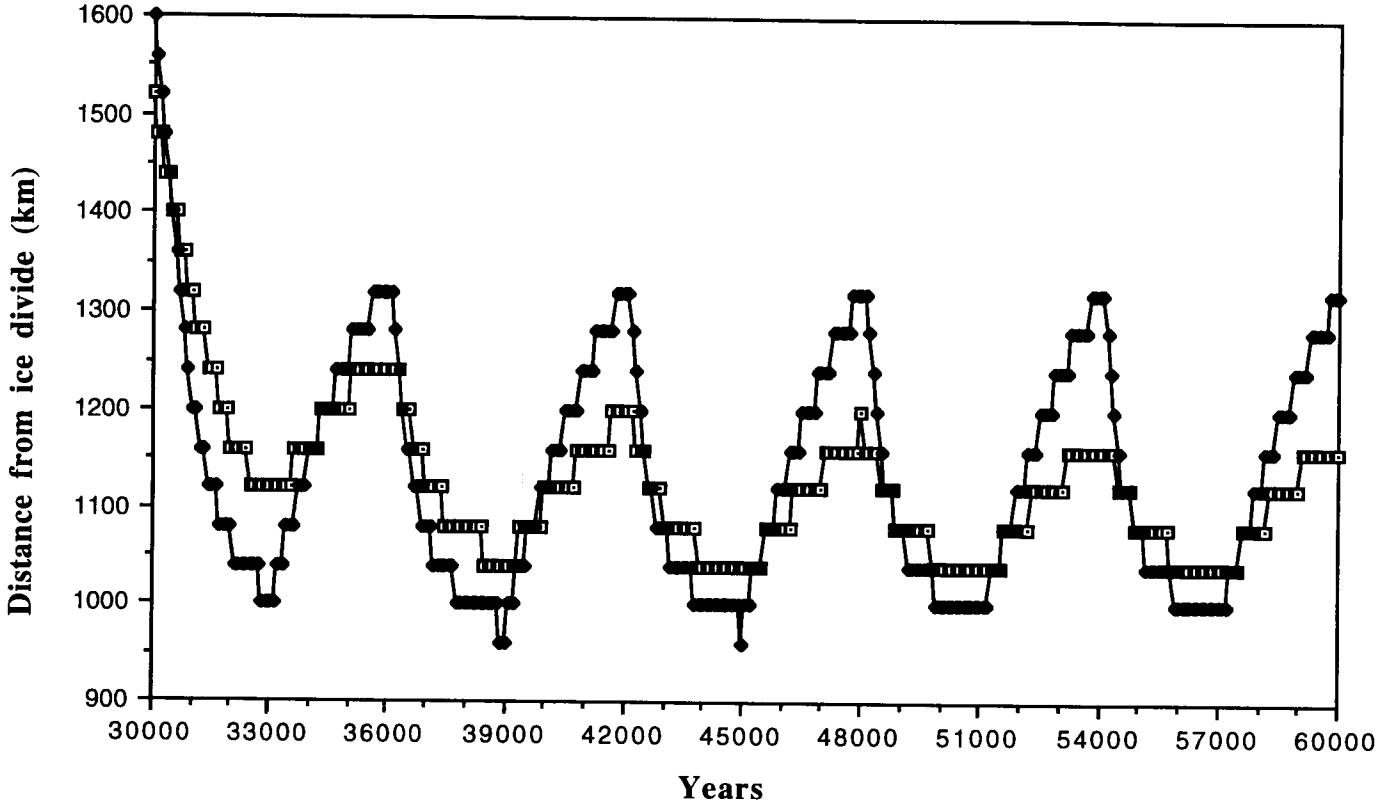

Fig. 5.37. Comparison of climate-induced oscillations for soft-bedded lobe and hard-bedded ice.

An important feature of the transient response to climate change is that for either of the two bed configurations the margin advance and retreat appears to be a purely monotonic response to the climate change. When the "wet-warm" climate is initiated, the lobe advances and continues to advance until the climate parameters are reversed. Then it recedes and continues to recede until the control climate is reinitiated. The response to the climate change thus appears to be a synchronous, "orderly march" with a characteristic time scale of much less than 3,000 years.

Fig. 5.38 shows the response of the steady-state margin to an abrupt order-of-magnitude oscillation in sediment viscosity from 5.2×10^9 to 5.2×10^8 Pa-sec, representing a hypothetical shift from fully-saturated to an oversaturated, presumably less viscous, condition beginning at 30,000 years. An interesting aspect of the transient response to sediment viscosity change is that even though the *steady state* margins associated with different sediment viscosities showed no variation (Fig. 5.21), the transient response to the *same* difference in viscosity is an immediate and rapid advance of about 250 km magnitude. In its new configuration, however, the lobe is out of equilibrium with the extant "climate" (which does not change). The margin therefore halts within about 500 years, then begins a rapid retreat (albeit somewhat slower than the advance). The forced return to the higher viscosity is imposed at 33,000 years of simulated time, while the margin is already in retreat. The margin continues to retreat, then appears to stabilize until 36,000 years, when the viscosity is changed from high to low. Again, there is a an immediate and rapid advance followed by an asynchronous, "autonomous" retreat of the margin before the higher viscosity is imposed again at 39,000 years. Following the second oscillation the system appears to equilibrating to the rhythm of the arbitrary forcing. For the parameters employed in this experiment it appears to have a characteristic time scale of much less than 3,000 years.

Fig. 5.39 shows the response of the margin to changes in sediment viscosity from 5.2×10^{10} to 5.2×10^9 Pa-sec superimposed upon the graph from previous viscosity sensitivity experiment (Fig. 5.38). In both cases the margin

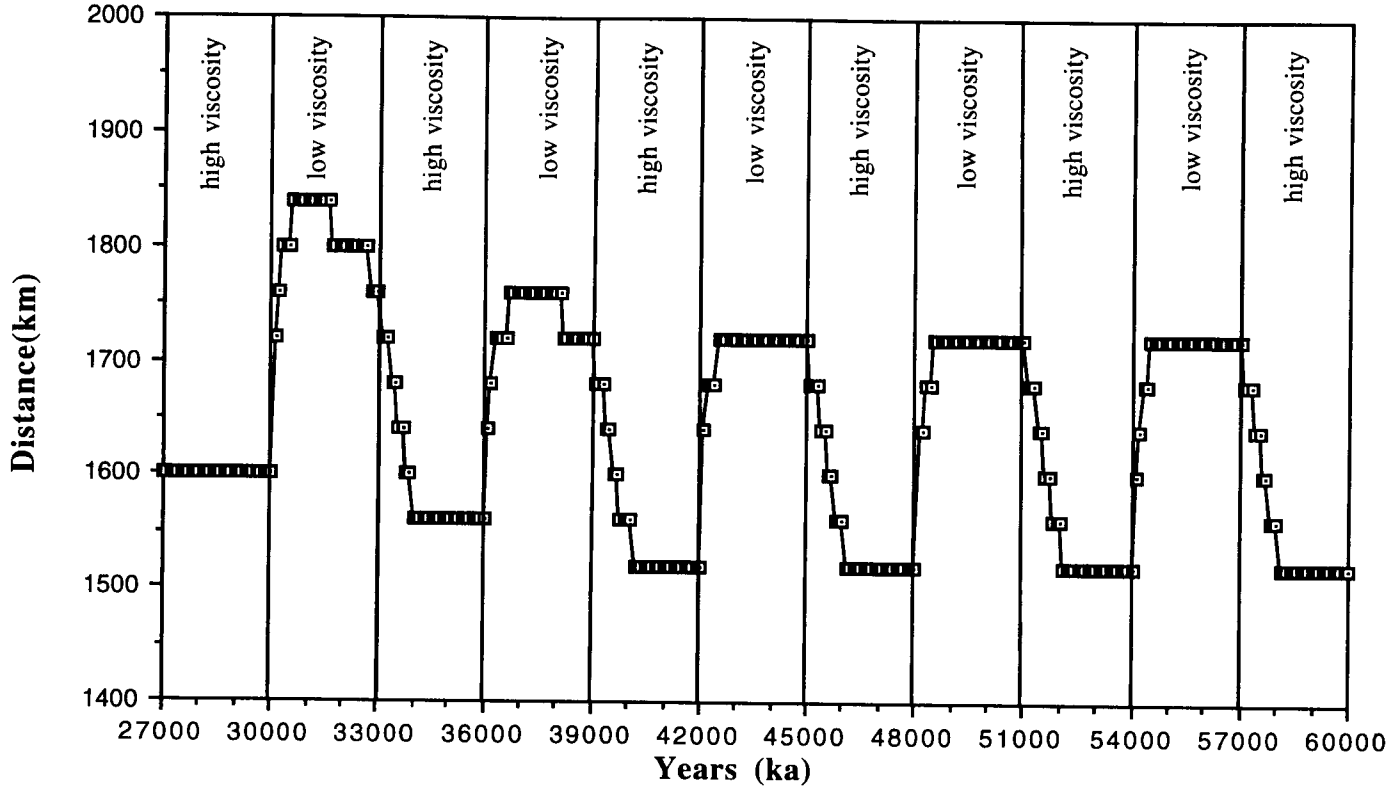

Fig. 5.38. Oscillations from steady-state terminus induced by 3000-year fluctuations in sediment viscosity from 5.2e9 to 5.2e8 Pa-sec. Data points are 100 years apart.

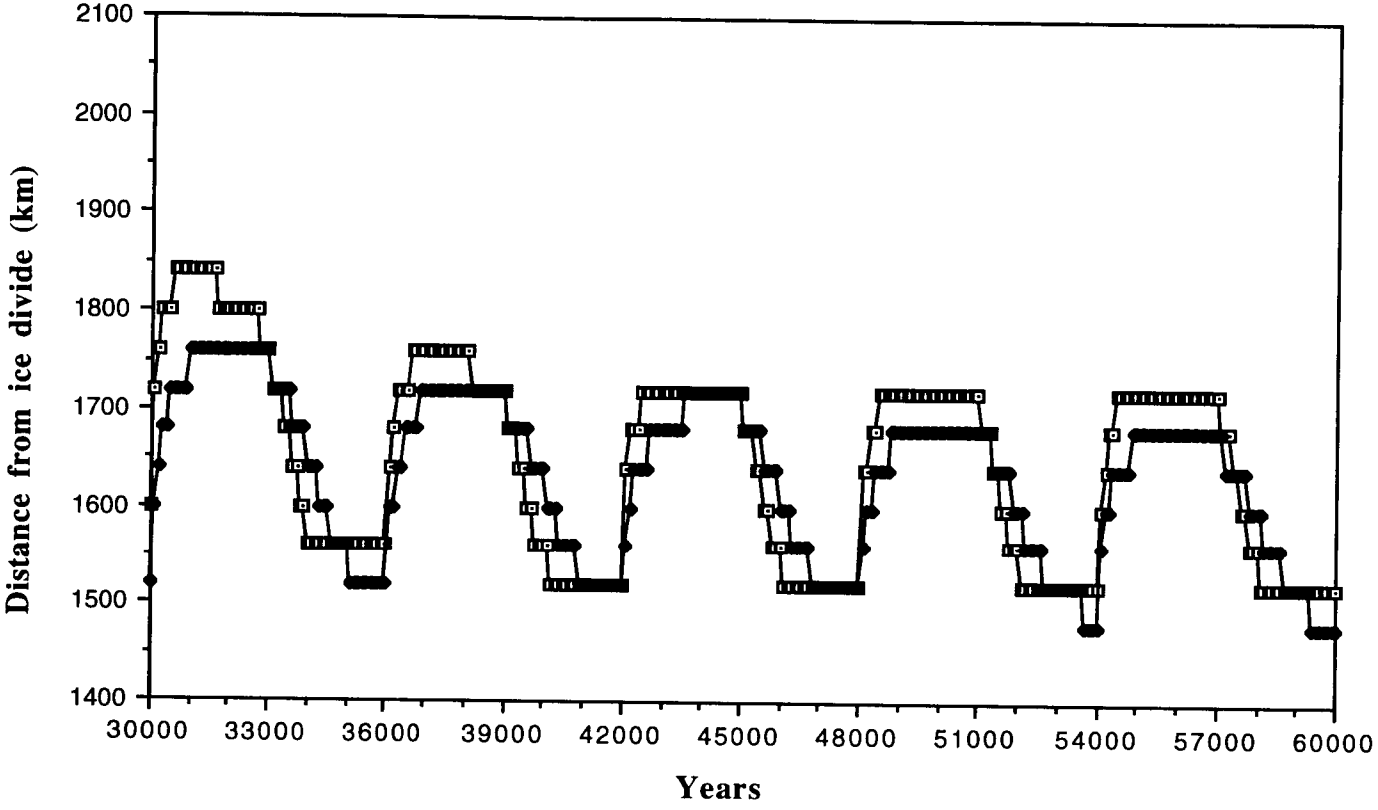

Fig. 5.39. Comparison of viscosity-induced oscillations for soft-bedded lobe.

reaches a maximum before the viscosity change is reversed. In the second experiment, however, the margin does not withdraw until the higher viscosity is imposed, suggesting that the characteristic time scale is longer than 3,000 years. Eventually, the system appears to be equilibrating to the imposed frequency, as in the lower-viscosity experiment (Fig. 5.38), but it takes longer to do so. The $5.2x10^{10}$-to-$5.2x10^{9}$ Pa-sec system thus appears to posses, not unexpectedly, more "inertia" than the $5.2x10^{9}$-to-$5.2x10^{8}$ Pa-sec system.

The two experiments with sediment viscosity change were designed to investigate potential implications of deviations in sediment viscosity form the measured value of $5.2x10^{9}$ Pa-sec. Both are only hypothetical--there is as yet no empirical basis for determining the extent to which either type of shift might explain the behavior of the LML. Nevertheless, both seem plausible. It is important to note that the measured viscosity of the sediment ($5.2x10^{9}$ Pa-sec) is its viscosity at 100% saturation, and in an unfrozen state. Lower water contents or frozen sediment conditions imply higher viscosity. The shift from $5.2x10^{10}$ to $5.2x10^{9}$ Pa-sec could thus reflect a hypothetical scenario in which unsaturated or partially frozen sediment is overridden by the lobe, then becomes saturated or fully thawed once covered by an insulating layer of ice melting at the base (as is assumed to be the case for this model). The shift from the $5.2x10^{9}$ to $5.2x10^{8}$ Pa-sec is somewhat more problematical since it implies that the sediment must achieve an oversaturated or slightly "slurrified" state. While such a mechanism is only hypothetical, the possibility seems worthy of investigation, especially given the evidence for high water volume and basal water pressure in modern ice streams (Englehardt and others, 1990).

Forced oscillations in sediment viscosity and climate forcing result in large-magnitude fluctuations in the margin if the ice is soft-bedded. Both appear capable of generating the magnitude of the lobe oscillations observed in the geologic record (Clark, in press). There are, however, some significant differences between the lobe responses to the two types of forcing. In the two viscosity-change experiments conducted for this study, the advance of the margin following the imposition of the lower viscosity was extremely rapid--about 250 km in 500-600 years. In contrast, the simulated climate-change

experiments caused the margin to advance only about 80 km in 500-600 years. About 2000 years were required for the margin to advance beyond 250 km. Also, the response to climate forcing, as previously noted, bore a strictly monotonic relationship to the direction of the forcing. A reversal in the movement of the margin associated with a change in climate probably implies a corresponding reversal in climate conditions. The retreat of the margin following a sediment-viscosity-induced advance, on the other hand, does not necessarily imply a reversal in sediment viscosity.

The results of the transient experiments reported for this study are highly dependent on the selected forcings, and there is, moreover, no basis for direct comparison between changes in climate and changes in sediment conditions. The values of the parameters employed in both sets of experiments, however, were selected to reflect realistic forcings based on historical and experimental evidence. The results should therefore provide a meaningful first approximation for lobe behavior that can serve at least as a basis for designing more definitive experiments and suggesting further productive lines for future model development. Before numerical experiments can be designed to make reliable inferences about the actual timing and magnitude of responses to actual changes in paleo-climate and sediment conditions, it will be necessary to conduct a more comprehensive investigation of the responses associated with different parameter values and transient time scales. It will also be necessary to incorporate more sophisticated paleoclimate models as well as precise and accurate data on actual changes in paleo-climate and sediment conditions affecting the LML.

Summary and conclusion

Ice surface profiles and sediment flux calculated from the measured sediment parameters are consistent with independent reconstructions and estimates from geological data. Both changes in climate forcing and changes in sediment-viscosity appear to be capable of generating the magnitude of fluctuations in the lobe margin observed in the geologic record. Oscillations of the magnitude and timing seen in the geologic record can be induced by *plausible* deviations in sediment viscosity from the *measured* value of 5.2×10^9 Pa-s.

Climate-induced fluctuations in the ice margin appear to be generally slower than the transient sediment-viscosity-induced fluctuations, especially if the climate-induced fluctuations are applied to hard-bedded ice. More comprehensive experimentation with the climate and sediment parameters is needed in order to identify and quantify definitive differences between ice lobe behavior induced by climate change and that induced by changes in sediment conditions.

Given the evidence from the Greenland ice cores (e.g., Johnsen and others, 1992) for climate shifts within only a few decades or less, the numerical experiments in this study, though obviously preliminary, suggest that immediate, rapid, and large-magnitude fluctuations of the lobe--if induced by climate shifts of the magnitude imposed in the experiments--can probably be more readily accounted for by a soft-bedded system than by a hard-bedded one. The outcome of the numerical experiments in this study also suggest that ice lobe response to changes in sediment viscosity are likely to have been much more rapid than responses to extant climate changes.

The results of the numerical experiments suggest that while both climate and sediment viscosity changes induce profound responses in terms of the magnitude, the character and rates of the responses--at least within the ranges of the parametric changes in these experiments--are probably fundamentally different. While either of the two processes could produce responses consistent with various observations in the geologic record, the differences in behavior suggest that it may be possible to find empirical clues in the geologic record that could distinguish between oscillations induced by changes in climate forcing and those induced by changes in subglacial conditions.

Finally, it should be noted that there is still much more that can be done with the model constructed for this study to investigate the roles of other variables as well as to probe more intensively the parameters investigated in this study. The implications of abrupt changes in basal water pressure over time and space (hence effective stress in the sediment), for example, were not addressed in this study, nor were the implications of changes in basal melting/freezing changes. Improvements and additions to the model that would enhance its utility

over the long run include the incorporation of a climate model that can account for time-, space-, and temperature-dependent changes in net accumulation, and incorporation of a mass-conservative model for till flux that includes all of the likely sediment production, transport, and erosion processes, as well as geologic limitations on source material and the relative contributions of the various processes that might have governed sediment production and removal over time and space.

BIBLIOGRAPHY

Alley, R.B., 1993, Abrupt increase in Greenland snow accumulation at the end of the Younger Dryas event: Nature, v.362, p. 527-29.

Alley, R.B., 1991, Deforming bed origin for the southern Laurentide till sheets?: Journal of Glaciology, v. 37, p. 67-76.

Alley, R.B., 1989, Water pressure coupling of sliding and bed deformation: II Velocity-depth profiles: Journal of Glaciology, v. 35, p. 119-129.

Alley, R.B., Blankenship, D.D., Rooney, S.T., and Bentley, C.R., 1987, Till beneath Ice Stream B 4. A coupled ice-till flow model: Journal of Geophysical Research, v. 92, p. 8931-8940.

Ambrose, 1964, J.W., 1964, Exhumed paleoplains of the Precambrian Shield of North America: American Journal of Sciences, v. 262., p. 817-857.

Andrews, J.T., Shilts, W.W., and Miller, G.H., 1983, Multiple deglaciations of the Hudson Bay Lowlands, Canada, since deposition of the Missinaibi (last interglacial) Formation: Quaternary Research, 19,p. 18-37.

Barnes, P. Tabor, D., and Walker, J.F.C., 1971, Friction and creep of polycrystalline ice: Proceedings of the Royal Society of London, Series A., v. 324 (1557), p. 127-155.

Binschadler, R.A., 1983, The importance of pressurized subglacial water in separation and sliding at the glacier bed: Journal of Glaciology, v. 29, p. 3-19.

Birchfield, G.E., Weertman, H., and Lunde, A.T., 1981, A paleoclimate model of the Northern Hemisphere ice sheets: Quaternary Research, v. 15, p. 126-142.

Boulton, 1987, A theory of drumlin formation by subglacial sediment deformation: in: Menzies, J., and Rose, J., eds., Drumlin Symposium: A.A. Balkema, Rotterdam, p. 25-80.

Boulton, G.S, and Dobbie, K.E, 1993, Consolidation of sediments by glaciers: relations between sediment geotechnics, soft-bed glacier dynamics and subglacial ground-water flow: Journal of Glaciology, v. 39, p. 26-44.

Boulton, G.S, and Hindmarsh, R.C.A., 1987, Sediment deformation beneath glaciers: Rheology and geological consequences: Journal of Geophysical Research, v. 92, p. 9050-9082.

Boulton, G.S., Smith, G.D., and Morland, L.W., 1984, The reconstruction of former ice sheets and their mass balance characteristics using a non-linearly viscous flow model: Journal of Glaciology, v. 30, p. 140-152.

Boulton, G.S, Smith, G.D., Jones, A.S., and Newsome, J., 1985. Glacial geology and glaciology of the last mid-latitude ice sheets. Journal of the Geological Society of London, 142: 447-474.

Broecker, W., Bond, G., Klas, M., Clark, E., and McManus, J., 1992, Origin of the northern Atlantic's Heinrich events: Climate Dynamics, v.6, 265-73.

Broecker, W.S., and Denton, G.H., 1989, The role of ocean-atmosphere reorganizations in glacial cycles: Geochimica et Cosmochimica Acta, v. 53, p. 2465-2501.

Brown, N.E., Hallet, B. and Booth, D.B., 1987, Rapid soft-bed sliding of the Puget glacial lobe: Journal of Geophysical Research, v. 92, p 8985-8998.

Budd, W.F., Keage, P.L., and Blundy, N.A., 1979, Empirical studies of ice sliding. Journal of Glaciology, 23: 157-170.

Budd, W.F., and Smith. I.A., 1981, The growth and retreat of ice sheets in response to orbital radiation changes, in Allison, ed., Sea Level, Ice, and Climate Change, International Association of Hydrological Sciences, Pub. No. 131, p. 369-409.

Budd, W.F., and Smith, I.A., 1987, Conditions for growth and retreat of the Laurentide Ice Sheet: Geographie Physique et Quaternaire, 41, no. 2, p. 279-290.

Christiansen, E.A., 1987, Verendrye valley and Glidden esker, Saskatchewan: subglacial and ice-walled features in southwestern Saskatchewan, Canada: Canadian Journal of the Earth Sciences, v. 24, p. 170-176.

Clark, J.A. and Bruxvoort, J.B., 1989, Reconstruction of the Laurentide Ice Sheet from tilted glacial lake shorelines and sea-level data: An inverse calculation: Geological Society of America Abstracts with Program, v. 21, p.7.

Clark, P.U., 1991, Striated clast pavements: Products of deforming subglacial sediment? Geology, v. 19, p. 530-533.

Clark, P.U., 1992, Surface form of the southern Laurentide Ice Sheet and its implications to ice-sheet dynamics: Geological Society of America Bulletin, v. 104, p. 595-605.

Clark, P.U. and Hansel, A.K., 1989, Till lodgments, clast ploughing, and glacier sliding over a deformable glacier bed: Boreas, v. 18, p. 201-207.

Clark, P.U. and Rudloff. G.A., 1990, Sedimentology and stratigraphy of late Wisconsin deposits, Lake Michigan Bluffs, northern Illinois: Geological Society of America Special Paper 251, p. 29-41.

Clark, P.U., Clague, J.J., Curry, B.B., Dreimanis, A., Hicock, S.R., Miller, G.H., Berger, G.W., Eyles, N., Lamonthe, M., Miller, B.B., Mott, R.J., Oldale, R.N., Stea, R.R, Szabo, J.P., Thorleifson, L.H., and Vincent, J.-S., 1993, Initiation and development of the Laurentide and Coordilleran Ice Sheets following the a last interglaciation: Quaternary Science Reviews, v. 12, p. 79-114.

Clayton, L., Teller, J.T., and Attig, J.W., 1985, Surging of the southwestern part of the Laurentide ice sheet: Boreas, v. 14, p. 235-242.

Clayton, L., Mickelson, D.M., and Attig, J.W., 1989, Evidence against pervasively deformed bed material beneath rapidly moving lobes of the southern Laurentide Ice Sheet: Sedimentary Geology, v. 62, p. 203-208.

Denton and Hughes, 1983, Milankovitch theory of the ice ages: hypothesis of ice-sheet linkage between regional insolation and global climate, Quaternary Research, 20, p. 125-144.

Dredge, L.A. and Cowan, C.R., 1989, Quaternary geology of the southwestern Canadian Shield, in R.J. Fulton, J.A. Heginbottom and S. Funder, eds., Quaternary Geology of Canada and Greenland, Geological Survey of Canda, Geology of Canada, No. 1.

Dreimanis, A. and Goldthwaite, R.P., 1973, Wisconsin glaciation in the Huron, Erie, and Ontario lobes, in Black, R.F., Goldthwaite, R.P., and Wilman, H.B., eds., The Wisconsinan Stage: Geological Society of America Memoir 136, p.71-106.

Dyke, A.S. and Prest, V.K., 1987, Late Wisconsinan and Holocene history of the Laurentide Ice Sheet: Geographie Physique et Quaternaire, 41, no. 2, p. 237-263.

Englehardt, H.F., Humphrey, N., and Kamb. B., 1990, Borehole geophysical observations on Ice Stream B, Antarctica: EOS, v. 71, p. 1302.

Farrand, W.R., Mickelson, D.M., Cowan, W.R., and Goebel, J.E., edited and integrated by Richmond, G.M., and Fullerton, D.S., 1984, Quaternary Geological Map of the Lake Superior 4° x 6° Quadrangle, United States and Canada: U.S. Geological Survey Miscellaneous Investigations Series Map I-1420 (NL-16).

Fischer, D.A., Reeh, N. and Langley, K., 1985. Objective reconstructions of the Late Wisconsinan Ice Sheet, and the significance of deformable beds. Geographie Physique et Quaternaire., 39: 229-238.

Hansel, A.K, and Johnson, W.H., 1992, Fluctuations of the Lake Michigan Lobe during the late Wisconsin subepisode: Sveriges Geologiska Undersökning, Ser. Ca 81, p. 133-144.

Hansel, A.K., and Johnson, W.H., and Socha, B.J., 1987, Sedimentological characteristics and genesis of basal tills at Wedron, Illinois: Geoogical Survey of Finland, Special Paper 3, p. 11-21.

Harrison, W., 1958, Marginal zones of vanished glaciers reconstructed from preconsolidation pressure values of overridden silts: Journal of Geology, v. 66., p. 72-95.

Hays, J.D., Imbrie, J., and Shackelton, N.J., 1976, Variations in the Earth's orbit: Pacemaker of the ice ages: Science, v. 194, p. 1121-1132.

Heinrich, H., 1988, Origin and consequences of cyclic ice rafting in the northeast Atlantic Ocean during the past 130,000 years: Quaternary Research, v. 29, p. 142-152.

Hicock, S.R., Kristjansson F.J. and Sharpe, D.R., 1989, Carbonate till as a soft bed for Pleistocene ice streams on the Canadian Shield north of Lake Superior: Canadian Journal of the Earth Sciences, 26, p. 2249-2254.

Holtz, R.D. and Kovacs, W.D., 1981, An Introduction to Geotechnical Engineering: Prentice-Hall, Englewood Cliffs, N.J.

Hooke, R.B., 1977, Basal temperatures in polar ice sheets: a qualitative review: Quaternary Research, v. 7, p. 1-13.

Hovind, C.L., 1990, Determination of time-dependent soil parameters by triaxial tests: MS thesis, Washington State University, 109 p.

Huybrechts, P., 1991, The Antarctic Ice Sheet and environmental change: a three-dimensional modelling study: Berichte zur Polarforsshung, 99, 241 p.

Hyde and Peltier, 1985, Sensitivity experiments with a model of the ice age cycle: The response to harmonic forcing: Journal of Atmospheric Science, v. 44, p. 1351-1374.

Imbrie, J., 1985, A theoretical framework for the ice ages: Geological Society of London Journal, v. 142, p 417-432.

Imbrie, J. and Imbrie, J.Z., 1980, Modeling of the climatic response to orbital variations: Science, v.207, p. 943-953.

Iverson, R.M., 1984, Unsteady, non-uniform landslide motion: theory and measurement: PhD thesis, Stanford University, p. 303.

Iverson, R.M., 1985, A constitutive equation for mass movement behavior: Journal of Geology, 93, 143-160.

Iverson, R.M., 1986, Unsteady, nonuniform landslide motion: 1. Theoretical dynamics and the steady datum state: Journal of Geology, 94, 1-15.

Johnson, R.G., and Andrews, J.T., 1979, Rapid ice-sheet growth and initiation of the last glaciation: Quaternary Research, v. 12, p. 119-134.

Johnson, W.H., 1990, Ice-wedge casts and relict patterned ground in central Illinios and their environmental significance: Quaternary Research, v. 33, p. 51-72.

Johnson, W.H., Hansel, A.K., Socha, B.J., and Follmer, L.R., 1985, The Wedron Section *in* Johnson. W.H., Hansel, A.K. and others, eds., Depositional environments and correlation problems of the Wedron Formation (Wisconsinan) in northeastern Illinois: Geological Society of America Bulletin, v. 97, p. 1098-1105.

Johnson, W.H., Hansel, A.K., 1987, Fluctuations of the Late Wisconsinan (Woodfordian) Lake Michigan lobe in Illinois, U.S.A.: International Union for Quaternary Research, XII International Congress, Program with Abstracts, p. 195.

Johnson, W.H. and Hansel A.K., 1990, Multiple Wisconsinan glacigenic sequences as Wedron, Illinois: Journal of Sedimentary Petrology, 60, p. 26-41.

Johnson, W.H., Hansel, A.K., and Stiff, B.J., 1991, Glacial transport rates, late Wisconsinan Lake Michigan Lobe in Central Illinois: Implication for transport mechanisms and ice dynamics: Geological Society of America Abstracts with Program, v. 23, p. A61.

Korzoun, I., 1977, ed., Atlas of Word Water Balance: Gidrometeosdat, Leningrad.

Lamb and Woodruffe, 1970, Atmospheric circulation during the last Ice Age: Quaternary Research, v.1, p. 29-58.

Lindstrom, 1989, A study of the Eurasian Ice Sheet using a grounded ice flow-ice shelf numerical model: PhD thesis, University of Chicago.

Lindstrom, D.R., and MacAyeal, D.R., 1989, Scandinavian, Siberian, and Arctic Ocean Glaciation: Effect of Holocene Atmospheric CO2 Variations: Science, v. 245, p. 628-631.

Lineback, J.A., Bleur, N.K., Mickelson, D.M., Farrand, W.R., and Goldthwaite, R.P., 1983, Quaternary geologic map of the Chicago 4° x 6° quadrangle, United State: U.S. Geological Survey Miscellaneous Investigations Series Map I-1420 (NK-16).

Lupinini, J.F., Skinner, A.E., and Vaughan, P.A., 1981, The drained residual strength of cohesive soils: Geotechnique, v.31, 181-213.

MacAyeal, D.R, in press, Growth/Purge oscillations of the Laurentide ice sheet as a cause of the North Altantic's Heinrich events: Paleoceanography.

Manabe, S. and Broccoli, A.J., 1985, The influence of continental ice sheets on the climate of an ice age: Journal of Geophysical Research, v. 90, p. 2167-2190.

Manabe, S. and Hahn, D.J., 1977, Simulation of the tropical climate of an ice age: Journal of Geophysical Research, v. 82, p. 3889-3911.

Maron, M.J., 1987, Numerical Analysis: A Practical Approach: Macmillan Publishing Co., New York, NY.

Mathews, W.H., 1974, Surface profiles of the Laurentide Ice Sheet in its marginal areas: Journal of Glaciology, 13, 37-43.

Mickelson D.M., Acomb L.J., and Adil, T.B., 1979, The origin of preconsolidated and normally consolidated tills in Eastern Wisconsin, U.S.A.: in Schlüchter, Ch. (ed.), Moraines and Varves: Origin/Geneis/classification. Proceedings of an INQUA Symposium on Genesis and Lithology of Quaternary Deposits, Zürich, 10-20 September 1978. Rotterdam: Balkema, p. 179-197.

Oerlemans, J., 1980, Model experiments of the 100,000-year glacial cycle: Nature, v. 287, p. 430-432.

Oerlemans, J., 1982, A model of the Antarctic Ice Sheet: Nature, v. 297, p. 550-553.

Oerlemans, J., 1991, The role of ice sheets in Pleistocene climate: Norsk Geologisk Tidsskrift, v. 71, p. 155-161.

Paterson, 1981, The Physics of Glaciers: Pergamon Press, London.

Peteet, D., Rind, D., and Kukla, G., 1992, Wisconsinan ice-sheet initiation: Milankovitch forcing, paleoclimatic data, and global climate modeling: in: Clark, P.U., and Lea, P.D., eds., The Last Iterglacial-Glacial Transition in North America: Boulder, Colorado, Geological Society of America Special Paper 270, p. 53-69.

Pollard, D. Ingersoll, A.P., and Lockwood, J.G., 1980, Response of a zonal climate-ice sheet model to the orbital perturbations during the Quaternary ice ages: Tellus, v. 32, p. 301-319.

Rind, D., Peteet, D., and Kukla, G., 1989, Can Milankovitch orbital variations initiate the growth of ice sheets in a general circulation model?: Journal of Geophysical Research, v. 94, p. 12,851-12,871.

Rudiman, W.F., and MacIntyre, A., 1979, Warmth of teh subpolar North Atlantic ocean during Northern Hemisphere ice-sheet growth: Science, v. 204, p. 173-175.

Sauer, E. Karl, 1974, Geotechnical Implications of Pleistocene Deposits on Southern Saskatchewan, Canadian Journal of the Earth Sciences, v. 11, p. 359-373.

Sauer, E.K., and Christiansen, E.A., 1991, Preconsolidation pressures in the Battleford Formation, southern Saskatchewan, Canada: Canadian Journal of the Earth Sciences, v. 28, p. 1613-1623.

Skempton, A.W., 1964, Fourth Rankine Lecture: Long term stability of clay slopes: Geotechnique,v. 14, 77-102.

Skempton, A.W., 1985, Residual strength of clays in landslides, folded strata, and the laboratory: Geotechnique, v. 35, 3-18.

Skempton, A.W. and Petley, D.J., 1967, The strength along structural discontinuities in stiff clays: in Proceedings of the Geotechnical Conference on shear strength properties of natural soils and rocks, Oslo, Norwegian Geotechnical Institute.

Smith, W.C., 1961, The Geology of Some Pleistocene Deposits and their Engineering Properties: PhD thesis, University of Illinois.

Thomas, R.H., MacAyeal, D.R., Bentley, C.R., and Clapp, J.L., 1980, The creep of ice, geothermal heat flow, and Roosevelt Island, Antarctica: Journal of Glaciology, v. 25 (91), p. 47-60.

Thorleifson, L.H., Wyatt, P.H., and W.W. Shilts, 1992, Hudson Bay Lowland and Quaternary stratigraphy: Evidence for early Wisconsinan glaciation centered in Quebec, *in* Clark, P.U., and Lea, PD., eds., The Last Interglacial-Glacial Transition if North America: Boulder, CO, Geological Society of America Special Paper 270.

van Gelder, G., de Graff, L.W.S., and Schurink, 1990, Subglacial consolidation of fine-grained stratified sediments: a neglected tool in reconstructing ice-thickness in Pleistocene valley glaciers: Arctic and Alpine Research, v. 22, p. 329-340.

Vela, J.,C., in prep., Viscoplastic soil parameters for a fine-grained glacial till.

Vincent, J.S., and Prest, V.K., 1987, The Early Wisconsinan history of the Laurentide Ice Sheet, Geographie Physique et Quaternaire, 41, no. 2, p. 199-213.

Vyalov, S.S., 1986, Rheological Fundamentals of Soil Mechanics: Elsevier, Amsterdam, 564 p.

Walter, H. and Leith, H., eds., 1967, Klimadigramn Weltatlas: Fischer Verlag, Jena, German Democratic Republic.

Wang, H., 1993, The Thermodynamics of Ice Sheets: A Flowline Modelling Study: MS thesis, University of Chicago.

Washburn, A.L., 1980, Geocryology: A Survey of Periglacial Processes and Environments: Halsted Press, John Wiley and Sons, New York.

Willman, H.B., and Frye, J.C., 1970, Pleistocene stratigraphy of Illinois: Illinois State Geological Survey Bulletin 94, 204 p.

Wong, W.W.H., Ho, C.L., Iverson, R.L., and Hovind, C.L., in review, Viscoplastic soil parameters from triaxial tests: GSA Reviews in Engineering Geology.

Wright, H.E., 1973, Tunnel valleys, glacial surges and subglacial hydrology of the Superior Lobe, Minnesota: in The Wisconsinan Stage, Black. R.F., Goldthwaite, R.P., and Willman, H.B. (eds.), Geological Society of America, Memoir 136, p. 251-276.

APPENDICES

Appendix A

Numerical implementation of the governing equations

The equations of the main algorithm (Fig. 2.6) are discretized using cell-centered differencing (Fig. A.1) in order to ensure continuity of quantities across physical boundaries. The relevant boundary in this case is the contact between soft- and hard-bed lithologies at the base of the ice sheet. The fundamental quantities, z_S, surface elevation; h, ice thickness; and z_b, basal elevation; reside on the grid nodes. The gradients of these quantities, as well as other quantities that are dependent on the gradients, reside at the centers of the grid cells. Cell-centering of the numerical calculations ensures that mass is conserved across physical boundaries, but restricts time-stepping to fairly small increments (0.5-3.0 years).

Numerical implementation of the governing equations is described below, following the order computational sequence in the algorithm (See Fig. 2.6 and Appendix B).

Isostatic adjustment

Basal elevation is recomputed at the beginning of each timestep by eqn. (2.1a), discretized as follows:

$$z_{b(i)}^{n+1} = z_{b(i)}^{n} + \frac{\Delta t}{t^*}\left(z_{b_{mual}} - \frac{\rho_{ice}}{\rho_{mantle}} \cdot h_{(i)} - z_{b(i)}^{n} \right) \quad \text{(A.1)}$$

where i is the index for the horizontal dimension, superscript n indicates the value of z_b from the previous timestep, and superscript n+1 indicates the unknown value of z_b at the current timestep.

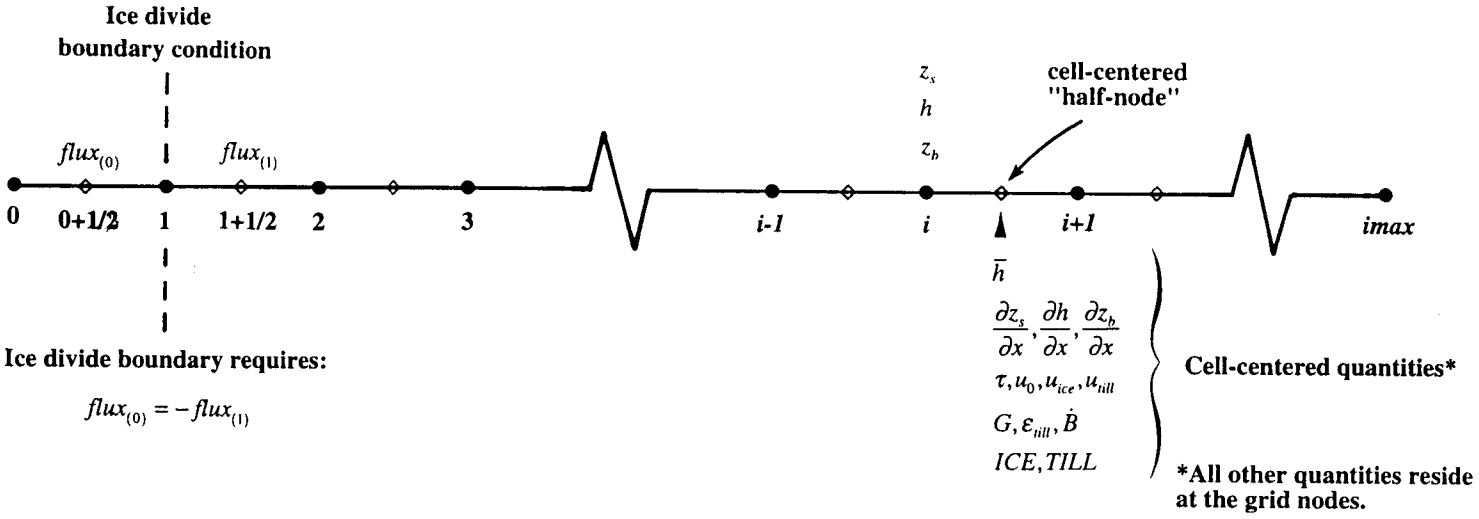

Fig. A.1. Grid positioning of numerical calculations and boundary conditions.

Net accumulation/ablation

Net accumulation is recomputed at the beginning of each timestep, as determined by eqn. (2.3), which is implemented as

$$x_{(i)} < x_{\dot{A}_{\max}} \Rightarrow \dot{A}_{(i)} = \dot{A}_{present(i)} - \frac{\partial \dot{A}}{\partial z_s} \cdot z_{s(i)}$$

$$x_{(i)} \geq x_{\dot{A}_{\max}} \Rightarrow \dot{A}_{(i)} = \left[\dot{A}_{\max} - \frac{\partial \dot{A}}{\partial x} \cdot \left(x_{(i)} - x_{\dot{A}_{\max}} \right) \right] - \frac{\partial \dot{A}}{\partial z_s} \cdot z_{s(i)} \qquad \text{(A.2)}$$

Explicit quantities employed throughout the algorithm

Gradient quantities: To calculate diagnostic output, the algorithm requires explicit values (i.e., values computed from quantities calculated at the previous timestep) for the gradients of z_S, h, and z_b. The mass continuity equation also must use explicit values for certain terms which cannot be discretized and calculated implicitly. (The vertical bar notation by the derivatives (A.3a,b,c) indicates that they have been explicitly computed from values of z_S, h, and z_b, respectively, that were calculated at the previous timestep. Derivative terms carrying the vertical bar thus cannot be discretized in the numerical equations that employ them. Derivatives not accompanied by the vertical bar can be rendered into finite difference form.)

$$\left. \frac{\partial z_s}{\partial x} \right|_{(i)} = \left(z_{s(i+1)} - z_{s(i)} \right) / \Delta x \qquad \text{(A.3a)}$$

$$\left. \frac{\partial h}{\partial x} \right|_{(i)} = \left(h_{(i+1)} - h_{(i)} \right) / \Delta x \qquad \text{(A.3b)}$$

$$\left. \frac{\partial z_b}{\partial x} \right|_{(i)} = \left(z_{b(i+1)} - z_{b(i)} \right) / \Delta x \qquad \text{(A.3c)}$$

Cell-centered ice thickness: Cell-centered ice thickness values are also computed at the beginning of the algorithm, as these are required for the subsequently computed cell-centered quantities (Fig. A.1): shear stress, effective

stress, till and ice velocities, viscous dissipation and basal melting, and mass flux.

$$\bar{h}_{(i)} = \frac{1}{2}\left(h_{(i+1)} + h_{(i)}\right) \qquad \text{(A.3d)}$$

Shear stress equation

Shear stress is computed directly from

$$\tau_{(i)} = -\rho_{ice} g \bar{h}_{(i)} \left.\frac{\partial z_s}{\partial x}\right|_{(i)} \qquad \text{(A.4)}$$

Shear zone thickness

The time-relaxed depth to the dilatant horizon is calculated from the instantaneous value, z_{dinst}, as determined by eqn (3.13), which is implemented as

$$z_{dinst(i)} = \left\{\left[\left(\left|\tau_{basal(i)}\right| - c\right)/\tan\phi\right] - P_{basal(i)}\right\}/(\rho' g) \qquad \text{(A.5)}$$

The relaxation condition, eqn. (3.14) is then imposed. In discretized form eqn. (3.14) is

$$z_d{}^{n+1}{}_{(i)} = \left(1 + \frac{\Delta t}{t^*}\right)^{-1}\left(z_d{}^{n}{}_{(i)} + \frac{\Delta t}{t^*} z_{dinst(i)}{}^{n+1}\right) \qquad \text{(A.6)}$$

where n is the timestep index for the previous step and n+1 is the index for the current step.

Sediment velocity field

The diagnostic sediment velocity field at each node is then computed from eqn. (2.6), the analytical solution to Iverson's constitutive equation,

$$u_{(i,j)} = \left|\left(\frac{2D_0^{1-n}}{\mu_0^n (n+1) A_1}\right)\left[\left(A_{2(i)} + A_1 (j \cdot \Delta z)\right)^{n+1} - \left(A_{2(i)} + A_1 z_{d(i)}\right)^{n+1}\right]\right| \qquad \text{(A.7a)}$$

$$A_1 = -\rho' g \tan\phi \qquad \text{(A.7b)}$$

$$A_{2(i)} = \left|\tau_{basal(i)}\right| - \left(c + P'_{basal(i)} \tan\phi\right) \qquad \text{(A.7c)}$$

where j is the index for the vertical dimension, z is the distance below the ice-sediment interface, Δz is the selected increment at which velocity vectors are to be computed, and n is the visco-plastic power law exponent.

Ice internal velocity, depth-averaged ice velocity, and depth-averaged total velocity

To compute the diagnostic ice velocity profiles and depth-averaged velocities for each grid cell, the algorithm computes the single integral expression in eqn. (2.8),

$$\int_{z_b}^{z} A_{(x,z)}\left(z_s - z\right)^3 dz \qquad \text{(A.8)}$$

and the double integral in (2.9),

$$\int_{z_b}^{z_s}\int_{z_b}^{z} A_{(T(x,z))}(z_s - z)dzdz \qquad \text{(A.9)}$$

as separate entities, then inserts them into the numerical renderings of eqn.s (2.8) and (2.9). The quantity computed for eqn. (A.9) is also passed to the mass continuity equation, in which it contributes to the calculation of the mass flux due to ice flow (see eqn.s (A.14) and (A.19b) below).

Because neither the ice surface nor the basal elevation is fixed over the x-direction, however, a normalized vertical coordinate system is required to keep the ice velocity (and temperature field) calculations manageable. The ice velocity (and thermal calculations) thus are based on a "flexible-grid" approach, defining a unit-normal vertical dimension, ζ, where

$$\zeta \equiv \frac{z_s - z}{z_s - z_b} = \frac{z_s - z}{h} \qquad \text{(A.10a)}$$

Note that ζ is zero at the ice surface and unity at the base.

Derivatives of eqn. (A.10a) used in the implementation of the normalized coordinate system are

$$\frac{\partial \zeta}{\partial z} = -\frac{1}{h} \qquad \text{(A.10b)}$$

and

$$\frac{\partial z}{\partial \zeta} = -h \qquad \text{(A.10c)}$$

In terms of the normalized coordinate system, eqn. (A.8) is

$$-\int_1^{\zeta} A_{(x,\zeta)} \zeta^3 h^4 d\zeta \qquad \text{(A.11)}$$

and eqn. (A.9) is

$$-h \int_1^0 \int_1^{\zeta} A_{(x,\zeta)} \zeta'^3 h^4 d\zeta' d\zeta \qquad \text{(A.12)}$$

The numerical rendering of eqn. (A.11) is

$$\frac{\bar{h}_{(i)}^4}{(k_{\max} - 1)^4} \cdot AZZ_{(i,k)} \qquad \text{(A.13a)}$$

where

$$AZZ_{(i,k)} \equiv \sum_{k=k_{\max}}^{k} A_{(i,k)}(k-1)^3 \qquad \text{(A.13b)}$$

The numerical rendering of (A.12) is

$$\left(\frac{\bar{h}_{(i)}}{k_{\max}-1}\right)^5 \cdot AZ_{(i)} \qquad \text{(A.14a)}$$

where

$$AZ_{(i)} = \sum_{k=k_{\max}}^{1} \sum_{k=k_{\max}}^{k} A_{(i,k)}(k-1)^3 \qquad \text{(A.14b)}$$

k is the index for the vertical dimension, and $k_{\max}$ is the index for the base of the ice sheet.

The diagnostic ice velocity profile is calculated by inserting the quantity eqn. (A.13a) into the numerical implementation of eqn (2.8):

$$u_{(i,k)} = -2(\rho_{ice}g)^3\left(\left.\frac{\partial z_s}{\partial x}\right|_{(i)}\right)^3 \frac{\bar{h}_{(i)}^4}{(k_{\max}-1)^4} \cdot AZZ_{(i,k)} \qquad \text{(A.15)}$$

Similarly, inserting eqn. (A.14a) into the numerical implementation of eqn. (2.9) gives

$$u_{ice(i)} = \frac{-2(\rho_{ice}g)^3\left(\left.\frac{\partial z_s}{\partial x}\right|_{(i)}\right)^3}{\bar{h}_{(i)}}\left(\frac{\bar{h}_{(i)}}{k_{\max}-1}\right)^5 \cdot AZ_{(i)} \qquad \text{(A.16)}$$

To compute the diagnostic depth-averaged total velocity, u_O, the basal velocity, u_{zb}, from eqn. (A.7a) is added to the depth-averaged ice velocity, u_{ice}, from eqn. (A.16) at each node:

$$u_{0(i)} = u_{ice(i)} + u_{z_b(i)} \qquad \text{(A.17)}$$

Mass continuity equation

Inserting equations (2.9) and (3.9) into eqn (2.10c) gives

$$\frac{dh}{dt} = \dot{A} + \dot{B} + \frac{\partial}{\partial x}\left(2(\rho_{ice} g)^3 \left(\frac{\partial z_s}{\partial x}\right)^3 \int_{z_b}^{z_s} \int_{z_b}^{z} A_{(T(x,z))}(z_s - z) dz dz \right) - \frac{\partial}{\partial x}\left(Q_{(x)} \left(\frac{\partial h}{\partial x} + \frac{\partial z_b}{\partial x} \right) \cdot h \right) \qquad \text{(A.18)}$$

Discretizing eqn. (A.18) gives

$$\frac{h_{(i)}^{n+1}}{\Delta t} - \frac{h_{(i)}^{n}}{\Delta t} = \dot{A}_{(i)} + \dot{B}_{(i)} + \frac{ICE_{(i)}}{\Delta x}(h_{(i+1)}^{n+1} - h_{(i)}^{n+1}) - \frac{ICE_{(i-1)}}{\Delta x}(h_{(i)}^{n+1} - h_{(i-1)}^{n+1}) + ICE_{(i)} \left.\frac{\partial z_b^n}{\partial x}\right|_{(i)} - ICE_{(i-1)} \left.\frac{\partial z_b^n}{\partial x}\right|_{(i-1)} - \frac{TILL_{(i)}}{\Delta x}(h_{(i+1)}^{n+1} - h_{(i)}^{n+1}) + \frac{TILL_{(i-1)}}{\Delta x}(h_{(i)}^{n+1} - h_{(i-1)}^{n+1}) - TILL_{(i)} \left.\frac{\partial z_b^n}{\partial x}\right|_{(i)} + TILL_{(i-1)} \left.\frac{\partial z_b^n}{\partial x}\right|_{(i-1)} \qquad \text{(A.19a)}$$

where

$$ICE_{(i)} = \frac{2(\rho_{ice} g)^3}{\Delta x \cdot \bar{h}_{(i)}} \left.\frac{\partial z_s}{dx}\right|_{(i)}^2 \left(\frac{\bar{h}_{(i)}}{k_{\max} - 1} \right)^5 \cdot AZ_{(i)} \qquad \text{(A.19b)}$$

and

$$TILL_{(i)} = \frac{Q_{(i)} \cdot \bar{h}_{(i)}}{\Delta x} \qquad \text{(A.19c)}$$

The superscript, n, indicates the value of h from the previous timestep, and $n+1$ indicates the at the unknown value at the current timestep, for which the matrix equation is being solved. At nodes where there is no soft sediment, $TILL_{(i)} = 0$.

After the collecting terms associated with each of the unknowns, a tridiagonal matrix equation is obtained:

$$\begin{bmatrix} B_{(1)} & C_{(1)} & 0 & 0 & 0 & 0 & 0 & 0 & 0 \\ A_{(2)} & B_{(2)} & C_{(2)} & 0 & 0 & 0 & 0 & 0 & 0 \\ 0 & . & . & . & 0 & 0 & 0 & 0 & 0 \\ 0 & 0 & A_{(i-1)} & B_{(i-1)} & C_{(i-1)} & 0 & 0 & 0 & 0 \\ 0 & 0 & 0 & A_{(i)} & B_{(i)} & C_{(i)} & 0 & 0 & 0 \\ 0 & 0 & 0 & 0 & A_{(i+1)} & B_{(i+1)} & C_{(i+1)} & 0 & 0 \\ 0 & 0 & 0 & 0 & 0 & . & . & . & 0 \\ 0 & 0 & 0 & 0 & 0 & 0 & A_{(i_{max}-1)} & B_{(i_{max}-1)} & C_{(i_{max}-1)} \\ 0 & 0 & 0 & 0 & 0 & 0 & 0 & A_{(i_{max})} & B_{(i_{max})} \end{bmatrix} \times \begin{bmatrix} h_{(1)}^{n+1} \\ h_{(2)}^{n+1} \\ . \\ h_{(i-1)}^{n+1} \\ h_{(i)}^{n+1} \\ h_{(i+1)}^{n+1} \\ . \\ h_{(i_{max}-1)}^{n+1} \\ h_{(i_{max})}^{n+1} \end{bmatrix} = \begin{bmatrix} RHS_{(1)} \\ RHS_{(2)} \\ . \\ RHS_{(i-1)} \\ RHS_{(i)} \\ RHS_{(i+1)} \\ . \\ RHS_{(i_{max}-1)} \\ RHS_{(i_{max})} \end{bmatrix} \qquad \text{(A.20a)}$$

where

$$A_{(i)} = \left(-ICE_{(i-1)} + TILL_{(i-1)}\right)/\Delta x \qquad \text{(A.20b)}$$

$$B_{(i)} = 1/\Delta t + \left(ICE_{(i-1)} + ICE_{(i)} - TILL_{(i-1)} - TILL_{(i)}\right)/\Delta x \qquad \text{(A.20c)}$$

$$C_{(i)} = \left(-ICE_{(i)} + TILL_{(i)}\right)/\Delta x \qquad \text{(A.20d)}$$

and

$$RHS_{(i)} = \dot{A}_{(i)} + \dot{B}_{(i)} + \frac{h^n_{(i)}}{\Delta t} + ICE_{(i)} \cdot \left.\frac{\partial z_b}{\partial x}\right|_{(i)} - ICE_{(i-1)} \cdot \left.\frac{\partial z_b}{\partial x}\right|_{(i-1)} \quad \text{(A.20e)}$$
$$-TILL_{(i)} \cdot \left.\frac{\partial z_b}{\partial x}\right|_{(i)} + TILL_{(i-1)} \cdot \left.\frac{\partial z_b}{\partial x}\right|_{(i-1)}$$

where the superscript, n, on h indicates the ice thickness from the previous timestep. Note that the square of the ice surface gradient and the topographic surface gradient in eqns. (A.19b) and (A.20d), respectively, cannot be discretized, and therefore make use of the explicitly computed values from conditions at the previous timestep.

The boundary condition at node 1 imposes equal and opposite flux, as must occur at an ice divide. The boundary condition is implemented by assuming a "zeroth" node to the left of node 1, along with a corresponding "zeroth half-node" at the center of the cell (Fig. A.1). Since flux is calculated at the center of the cells, the flux assumed for the zeroth half-node must be equal in magnitude but opposite in sign to the flux at the first half node, in the center of the first cell. This condition is met numerically by replacing all the flux terms that would be calculated in the zeroth cell (i.e., to the left of node 1 in Fig. A.1) eqn. (A.19a) with their counterparts in the first cell (i.e., to the right of node 1 in Fig. A.1) and reversing the algebraic sign on the counterpart term. Thus eqn. (A.19a) at node 1 becomes:

$$\frac{h^{n+1}_{(i)}}{\Delta t} - \frac{h^n_{(i)}}{\Delta t} = \dot{A}_{(i)} + \dot{B}_{(i)} + \frac{ICE_{(i)}}{\Delta x}(h^{n+1}_{(i+1)} - h^{n+1}_{(i)}) - \left[-\frac{ICE_{(i)}}{\Delta x}(h^{n+1}_{(i+1)} - h^{n+1}_{(i)})\right]$$
$$+ICE_{(i)} \left.\frac{\partial z^n_b}{\partial x}\right|_{(i)} - \left[-ICE_{(i)} \left.\frac{\partial z^n_b}{\partial x}\right|_{(i)}\right] - \frac{TILL_{(i)}}{\Delta x}(h^{n+1}_{(i+1)} - h^{n+1}_{(i)}) \quad \text{(A.21)}$$
$$+\left[-\frac{TILL_{(i)}}{\Delta x}(h^{n+1}_{(i+1)} - h^{n+1}_{(i)})\right] - TILL_{(i)} \left.\frac{\partial z^n_b}{\partial x}\right|_{(i)} + \left[-TILL_{(i)} \left.\frac{\partial z^n_b}{\partial x}\right|_{(i)}\right]$$

After separating terms, and setting i=1, we obtain the coffecients for the boundary condition:

$$A_{(1)} = 0 \tag{A.21a}$$

$$B_{(1)} = \frac{1}{\Delta t} + \frac{2}{\Delta x}\left(ICE_{(1)} - TILL_{(1)}\right) \tag{A.21b}$$

$$C_{(1)} = \frac{2}{\Delta x}\left(-ICE_{(1)} + TILL_{(1)}\right) \tag{A.21c}$$

and

$$RHS_{(1)} = \dot{A}_{(1)} + \dot{B}_{(1)} + \frac{h^n_{(1)}}{\Delta t} + 2 \cdot \left.\frac{\partial z_b}{\partial x}\right|_{(1)} \left(ICE_{(1)} - TILL_{(1)}\right) \tag{A.21d}$$

The ice thickness at the end of the timestep, h^{n+1}, is then obtained by solving eqn. (A.20).

Appendix B

Source code for model

This appendix contains the source code for the model. The programming language is Language Systems FORTRAN, which is written for Macintosh computers by Language Systems Corporation, 441 Carlisle Drive, Herndon, VA 22070.

The code was compiled and run a Macintosh Quadra 950. I have minimized the use of non-standard FORTRAN and Language System FORTRAN extensions so the code should be portable to other platforms with minimum modification. A dictionary of identifiers is provided with the code, and I have thoroughly documented the code to parallel the description of the governing equations in Chapter 2 and the description of the numerical implementation in Appendix A, both of which follow the order of implementation in the code.

9/10/93 16:11Ymir:Desktop Folder:Results:Baseline runs:...:declaration

```
C Declarations:
C
c      IMPLICIT NONE
C
C Variables for switching on programming management options:
       LOGICAL ISOTHM,Bug
C
C Function names:
*      REAL MEAN
C
C Variables for node and timestep control:
       REAL MINTHK
       INTEGER i,imax,j,jmax,k,kmax,l,Xnode,
     .         Xmax,Znode,Zmax,Zeta,ZTAmax,
     .        INCRMT,Count,Xvel,Length,m,mmax,kmtot
       REAL deltaT,TimSpn
       INTEGER TimStp,TotStp
C
c Note: If X-grid is redimesioned (1) Make sure that N in TRIDAG is
c sufficiently large, (2) Redimension Snapshot data files in OUTPUT
c
C Grid dimensioning parameters and variables:
      PARAMETER(imax=51,jmax=11,kmax=30,mmax=20,
     .          INCRMT=5)
      PARAMETER(kmtot=kmax+mmax)
      PARAMETER(Xmax=imax,Zmax=jmax,ZTAmax=kmax)
      REAL deltaX,deltaZ(Xmax),Zdilat(Xmax),dZeta,dZrok
C
C Grid parameters and time; Units: distance (meters), time (seconds).
C
      PARAMETER(deltaX = 40 * 1.0E3)
C
      PARAMETER(deltaT = 3.0 * 3.1559E7) ! Timestep years*sec/yr
      PARAMETER(TotStp = 20000)
C
      PARAMETER(dZrok=1500.0/mmax)
C
C Variables for output control:
      INTEGER IRANK,IROWS,ICOLS
      INTEGER IRET,DFSDputdata,INTRVL,TimCnt,NCOL
C
C Parameters and variables for Spyglass output:
C
C *** NOTE *** If INTRVL is is such as to create NCOL > 10, unit no.s for
C Cricket Graph output files will exceed 99. (See OUTPUT subroutine).
C
      PARAMETER(INTRVL=2000,IROWS=imax,
     ,          ICOLS=TotStp/INTRVL,IRANK=2)
c     PARAMETER(INTRVL=1,IROWS=imax,ICOLS=1,IRANK=2)
C        IROWS is equal to IMAX (no. nodes = no. rows)
C        ICOLS is the total number of timesteps at which you want to
C              sample the time domain (Not every timestep goes into
C              output file.)
C        IRANK is always equal to 2 (the rank of the matrix).
C
      REAL Tau(IROWS,ICOLS)
      REAL PrsBas(IROWS,ICOLS)
      REAL Thknss(IROWS,ICOLS)
      REAL Elevn(IROWS,ICOLS)
      REAL TilThk(IROWS,ICOLS)
      REAL Velcty(IROWS,ICOLS)
      REAL Base(IROWS,ICOLS)
      REAL VelBas(IROWS,ICOLS)
```

9/10/93 16:11Ymir:Desktop Folder:Results:Baseline runs:...:declaration

```
      INTEGER IDIMS(IRANK)
      data idims/irows,icols/
C
C Climate variables:
      REAL THETA(imax),THETAs(imax)
C
C Isostacy constants and variables:
      REAL TAUiso,RHOmtl,Zinitl(imax)
C
C Ice profile and continuity equation:
      REAL IceThk(Xmax),ElvBas(Xmax),ElvSrf(Xmax)
     .     ,ZsN(Xmax),TAUbas(Xmax)
      REAL Unot(Xmax),Umax,Aice(Xmax),Bice(Xmax),
     .     Cice(Xmax),FrcIce(Xmax),RHSice(Xmax)
C
C Climate and ice forcing parameters and variables:
      INTEGER EqlLin,Margin,TERMNS
      REAL LAPSwt,LAPSdr,AblGrd
      REAL Clgm,Cpres,LAPS,THRSHD,LAPShi,MINSMR,Adotz
      REAL Cglac,deltaC,TemCO2(Xmax),TemElv(Xmax)
      REAL SenCO2(Xmax),THETAp(Xmax),THETsp(Xmax),
     .     CHI(Xmax),Adotp(Xmax)
      REAL CO2Efc(Xmax),ElDsrt(Xmax),SrfAbl(Xmax)
      REAL Adot(Xmax),Bdot(Xmax)
      REAL HetFlx(Xmax),GeoFlx(Xmax),Epsiln(Xmax)
      REAL IceHet(Xmax),GeoHet(Xmax)      ! 20 July
C
C Ice physical constants:
      REAL RHOice,LHFice
C
C Bedrock condition indicator:
      CHARACTER*6 BedTyp(Xmax)
C
C Effective stress field variables:
      REAL RHOs,RHOw,RHOprm,g,Pbasal(Xmax)
C
C Till constitutive parameters:
      REAL Cohesn,PHIprm,tanPHI,MUnot,Dnot,n,b
C
C Till constitutive equation variables:
      REAL TAUtil(Xmax),Pprime(Xmax,Zmax)
C
C Temporarily fixed stress values:
      REAL Pfix
C
C Till deformation velocity field variables:
C
      REAL ALPHA(Xmax),BETA,GAMMA,Ztill(Zmax)
      REAL Utill(Xmax,Zmax),Uzb(Xmax),dUzbdx(Xmax),Ubase(Xmax) ! 10 Mar
      REAL A1(Xmax),A2(Xmax),dA1dx(Xmax),A3(Xmax)              ! 21 Mar
      REAL COEFF(Xmax),dhdx(Xmax),Atill(Xmax),Btill(Xmax),Ctill(Xmax)  ! 22 Mar
      REAL F,RHStil(Xmax),Q(Xmax),TERM1(Xmax),TERM2(Xmax),dQdx(Xmax) ! 27 Mar
      REAL Snot(Xmax),TERMc                                    ! 1 Apr
      INTEGER CONTAC
      REAL SUMtil,Utillo(Xmax)    ! 16 Aug
C
C For therml code:
      LOGICAL MELTED(Xmax)
      REAL Wzeta(xmax,kmax)
C Ice velocity field variables:
      REAL A(Xmax,ZTAmax),Ag,Qg,e,Uice(ZTAmax),
     .HorVel(Xmax,ZTAmax),IceTmp(Xmax,ZTAmax),
     .RokTmp(Xmax,mmax),CONDrk,CONDic,KAPice,KAProk
```

9/10/93 16:11Ymir:Desktop Folder:Results:Baseline runs:...:declaration

```
      REAL HN(Xmax) ! 10 June
C
C Variables for Cricket Graph velocity field output:
      PARAMETER(Xvel=(Xmax/INCRMT)+1)
      REAL TilFld(Xvel,Zmax),Depth(Xvel,Zmax)
      REAL IceFld(Xvel,ZTAmax),Height(Xvel,ZTAmax)
C
C Predictor-correcter variables:        PC 13 Oct
      LOGICAL Cnvrgd
      INTEGER kPC
      REAL hPRVIS(Xmax),hTNTk(Xmax),ZsTNT(Xmax),hTNTk1(Xmax)
      REAL UoPRVS(Xmax),UoTNTk(Xmax),UTNTk1(Xmax)
      REAL TauTNT(Xmax),PbTNT(Xmax),HVtnt(Xmax,ZTAmax),
     .     ZdTNT(Xmax),dZtnt(Xmax)
      REAL EpsTNT(Xmax),BdtTNT(Xmax)
      REAL MaxDh,MaxDu,PrvDfH,PrvDfU,UmxTNT,CnvCrt
      PARAMETER(CnvCrt = 1.0e-3)
      COMMON /PCcode/Cnvrgd

C THINGS TO CHECK--STILL NEEDED:
      REAL SPAN

C
      PARAMETER(e = 2.71828)
      PARAMETER(Ag = 1.3)  ! Thermal const for A
      PARAMETER(Qg = 1.2e5)  ! Thermal const for A
      PARAMETER(TAUiso = 4700.0*3.1559e7)  ! Iso decay, years*sec/yr
      PARAMETER(RHOmtl = 3300.0)  ! Mantle density, Kg/m3
      PARAMETER(RHOice = 917.0)  ! Ice density, Kg/m3
      PARAMETER(LHFice = 3.315e5)  ! Latent heat of fusion, ice, J/Kg
      PARAMETER(CONDrk = 3.0)  ! Thermal conductivity of rock, W/C/m
      PARAMETER(CONDic = 2.0)  ! Thermal conductivity of ice, W/C/m
      PARAMETER(KAProk = 1.4e-6)  ! Ther diffu rock, m2/s
      PARAMETER(KAPice = 1.4e-6)  ! Ther diff ice, m2/s
C
C     Minimum significant ice thickness
            PARAMETER(MINTHK=1.0e-2)
C
C Till parameters: Units are: c (Pa), PHIprm (degrees), MUnot (Pa-s),
C Dnot (1/s), n (dimensionless), TAUfix (Pa), Pfix (Pa), deltaZ (m).
C
C Effective stress field parameters:
      PARAMETER (RHOs=2650.0)
      PARAMETER (RHOw=1000.0)
      PARAMETER (g=9.80655)
C
C Velocity field integrals:
C
      REAL dZsdX(Xmax),AZ(Xmax),AZZ
      INTEGER kk
      REAL ZbN(Xmax)  ! 10 June for vervel
C
C Mass Balance terms:
C
      REAL dZbdX(Xmax),dZb2dx(Xmax),dAZdx(Xmax)
      REAL Flux(Xmax),FlxUH(Xmax),FlxTil(Xmax),FlxIce(Xmax)
      REAL Hbar(Xmax),TILL(Xmax),ICE(Xmax)

C debugging
      REAL Q1(Xmax),Q2(Xmax),Q3(Xmax),Q4(Xmax)
```

```
9/10/93 16:34 Ymir:Desktop Folder:Thesis:Dictionaryfor code:Dictiona

C ID DICTIONARY: (Separate dictionaries are provided in subroutines for IDs
C peculiar to the subroutine.  IDs below are common to entire
C program.)  In all dictionaries upper case is used for names of parameters,
C constants, subroutines, and file names.  For variable names initial letter
C is upper case, with subscripts (when used) in lower case.
C
C  A: Thermal coefficient for the ice flow law, CONSTANT FOR NOW, real.
C  Adot:   'A-dot', acculmulation rate, variable, real.
C  Adotp:  'A-dot, subscript Present', present-day acculmulation rate, data, real.
C  Adotz:  'A-dot, subscript z', constant for elevation deset effect, real
C  Aice: 'A sub ICE'--Subdiagonal element, coefficient matrix, real
C  ALPHA: Local (to each X-node) parameter for analytical solution
C         to sediment rheological equation, real.
C  AZ: Double integral used in ice velocity calculations, real
C  AZZ: Single integral used in ice velocity calculations, real
C  Bdot: 'B-DOT'--net Accumulation, real
C  BedTyp:
C  Bice: 'B sub ICE'--Diagonal element, coefficient matrix, real
C  BETA:  Parameter for analytical solution to sediment rheological
C         equation, real.
C  BnkCnt: 'Bonk count', counter variable for number of times the
C           margin reached the end of the grid, integer
C  Bonked: 'Bonked', logical variable indicating that ice margin reached
C           the end of the grid
C  CHI:   'CHI', Proportionality factor for CO2 dependence on CO2 concentration
C           and latitude, data, real
C  Cice: 'C sub ICE'--Superdiagonal element, coefficiant matrix, real
C  Cohesn: 'COHESioN', rheological parmeter for till, real
C  CONTAC: 'CONTACt', node marking the first occurance of the soft bed,
C           i.e., the contact between the hard and soft beds, integer
C  Count: Counter for incrementing data to the output files
C  Cpres:  'CO2present', present day atmospheric CO2 content, real
C  deltaC: 'Delta C'--difference between glacial and present atmospheric
C           CO2 concentrations, real
C  deltaT: 'Delta T'--Time increment, parameter, real
C  deltaX: 'Delta X'--Distance increment, parameter, real
C  deltaZ: 'Delta Z'--Variable distance increment for till velocity field, real
C  Depth: Depth of Z-node below the ice-till interface, variable, real
C  DFSDputdata: Command for creating Spyglass data files.
C  Dnot: 'D-nought', reference deformation rate, rheological parameter for till,
C         real
C  dAzdx: 'derivative of AZ wrt x', spacial derivative of the double
C           integral in ice velocity calculations, real
C  dQdx: 'derivative of Q wrt x', spacial derivative of the quantity used
C         in solution of the nonlinear sediment flow equation, real
C  dUzbdx: 'derivative of Uzb wrt x', spacial derivative of the basal ice
C           velocity, real
C  dZbdx: 'derivative of Zb wrt x', spacial derivative of the basal elevation
C           (ground surface), real
C  dZb2dx: 'second derivative of Zb wrt x', second spacial derivative of
C           the basal elevation (ground surface), real
C  dZsdx: 'derivative of Zs wrt x', spacial derivative of the ice surface, real
C
C  dZeta: 'delta zeta',Vertical interval on the zeta grid for the ice velocity
C          field, real.
C  Elevn: Output array, collects ElvSrf for Spyglass, 2-D array, real.
C  Elevn.hdf: Hierachical Data File for Spyglass.  Contains ElvSrf at selected tim
C  ElvBas: 'ELeVation of Base'--basal (topography) elevation along transect,
C           variable, real
C  ElvSrf: 'ELeVation of ice SuRFace'--Surface elevation of ice along
C           transect, variable, real
C  F: 'Flow law parameter', Iverson flow law parameter, (derived from b
C      or Do and MUo), real
```

9/10/93 16:34 Ymir:Desktop Folder:Thesis:Dictionaryfor code:Dictiona

```
C  Epsiln: 'EPSILoN', heat of viscous dissipation from deforming till, variable, r
C  FrcIce: 'FoRCing for ICE',--aggregate of all forcings for ice, variable, real
C  g: gravitational constant, real
C  GAMMA: Parameter for analytical solution to sediment rheological
C         equation, real.
C  GENRAT: 'GENeRATe' subroutine.  Generates initial ice profile
C  GEODAT: 'GEOlogical and GEOtechnical DATa' subroutine, reads input data files
C          containing topography, till parameter data, etc.
C  GeoFlx: 'GEOthermal heat FLuX', data, real.
C  HetFlx: 'HEat FLuX', vertical heat flux away from base of ice, variable, real.
C  Height: 'Height to vertical nodes in the ice profile at selected x-nodes,
C           2-d array, real
C  HORVEL:  'HORizontal VELocity', horizontal velocity vector inside the ice,
C           real
C  HRDBED: 'HaRD BED', subroutine, calculates ice velocity profile for
C           hard bed dynamics.
C  ICOLS: Number of columns in array, for Spyglass output data.
C  IceThk: 'Ice THicKness', variable, real
C  ICEBND: 'ICE BouNDary' accumulation, constant, real
C  IceFld: 'Ice velocity FieLD', velocity field values at selected x-nodes,
C           2-d array, real.
C  ICEFLX: 'ICE FLuX' subroutine.  Calculates ice thickness at each x-node.
C  ICESRF: 'ICE SuRFace' subroutine.  Calculates ice surface elevation, real
C  ISOSTY: 'ISOSTacY' subroutine.  Adjusts base of ice sheet for isostatic
C          loading.
C  Idims: DIMensions for Spyglass output data files, integer.
C  imax: 'I subscript MAXimum', maximum number of X-nodes, parameter, integer
C  INITL: 'INITiaL condition' subroutine.  Generates initail ice profile
C         before program enters time loop
C  INRACT: 'INtRACTive mode' subroutine.  Allows interactive input of parameters
C          from keyboard.
C  INTRVL: 'INTeRVaL' of time for selectively writing output to the
C      Spyglass output files, integer.
C  IRANK: Rank of matrix (variable array), for Spyglass output data.
C  iret: Command for opening Spyglass output files.
C  IROWS: Number of rows in array, for Spyglass output data.
C  k: Counter for the vertical ice dimension, Zeta, (k=1 at surface)
C    variable, integer.
C  kmax: 'k-maximum', endpoint value for the zeta-grid, parameter, integer.
C  LAPS: 'LAPSe rate', atmospheric lapse rate, real
C  Length: 'LENGTH, in terms of X-nodes up to which ice is significantly thick
C          (i.e., >MINTHK), variable, integer.
C  LHFice: 'Latent Heat of Fusion, ice', parameter, real.
C  Mdot: Basal melting rate of the ice, variable, real.
C  MEAN: 'MEAN of data' function.  Computes mean of one-dimensional arrays.
C         Returns real value.
C  MELTED: 'MELTED at the base', logical variable indicating that ice is
C           melted at the base
C  MINSMR: 'MINimum SuMmeR temperature', lowest summer temerature at which
C           ablation is permitted, real
C  MINTHK: 'MINimum significant THicKness of ice', parameter for ensuring positive
C           definite ice thickness, real
C  MUnot: 'MU-nought', reference viscosity, rheological parameter for till, real
C  n: 'n', power law exponent, rheological parameter for till, real
C  NCOL:  'Number of COLumns'--index for Spyglass output file columns, integer.
C  Pbasal: 'Pressure sub BASAL', effective pressure at the base of the
C          ice (i.e., ice overburden pressure minus basal water
C          pressure, real
C  Pfix: 'effective Pressure-fixed'.  Specified effective pressure, constant, real
C  PHIprm: 'PHI-PRiMe,' angle of internal friction
C  Pprime: effective pressure, P-prime, in subglacial sediments
C  PrsBas: Output array, collects Pbasal for Spyglass, 2-D array, real.
C  PrsBas.hdf: Hierachical Data File for Spyglass.  Contains Pbasal at selected ti
```

```
9/10/93 16:34 Ymir:Desktop Folder:Thesis:Dictionaryfor code:Dictiona

C  VFIELD: 'Velocity FIELD' subroutine, collects and exports final output to exter
C          files.
C  Q,Q1,Q2,Q3,Q4: 'Quantities', explicitly computed quantities used to
C                  solve the non-linear sediment flow equation, real
C  RanPas: 'Ran Past', logical varible indicating the ice marign ran past
C          the historical margin
C  RHOice: 'RHO, subsript ICE'--density of ice, parameter, real
C  RHOprm: 'RHO-prime', bouyant density of till, constant, real
C  RHOmtl: 'RHO subscript ManTLe', density of the mantle, parameter, real.
C  RHSice: 'Right-hand-side terms for constant vector, ice equation, variable,
C          real
C  RokTmp:  'ROcK TeMPerature', temperature of the bedrock, real
C  SenCO2: 'SENsitivity of temperature to CO2' concentration, varies with
C          latitude, real, data.
C  SETFIL: 'SET up FILes' subroutine.  Sets up format and headers for time-
C          dependent-output files.
C  SHEAR: 'SHEAR stress' subroutine.  Computes basal shear stress at
C         each X-node, based on ice surface profile.
C  SLOPE: 'initial SLOPE of ice surface'--constant, real
C  SFTBED: 'SoFT BED' subroutine.  Invokes deforming till rheology for coupled
C          ice movement over deforming bed.
C  Snot:  'Strength-sub nought',portion of strength term in sediment rheology
C         equation that is not depth-dependent, real
C  Span: 'Span of the ice' from first to last node
C  tanPHI: Coefficient of effective stress computed from PHIprm, the
C          angle of internal friction
C  TAUtil: 'Tau subscript till' shear stress in the till layer
C  TAUbas: 'TAU sub BASe', shear stress at base of ice sheet, as determined by the
C          ice profile, real
C  Tau.hdf: Hierachical Data File for Spyglass.  Contains TAUbas at selected times
C  TAUiso: 'TAU, subscript ISOstacy', decay constant for isostatic,
C         adjustment, parameter, real.
C  TERMS:  'TERMiNus', node marking historic terminus of ice sheet, integer variab
C  THERML: 'THERMaL system' subroutine.  Computes ice themodynamic parameters
C          based on atmospheric and geothermal forcing.
C  THETA:  'THETA', paleo mean annual surface temperature, variable, real
C  THETAp: 'THETA, subscript Present', Present-day value of mean annual surface
C          temperature, data, real.
C  THETAs: 'THETA, subscript Summer', paleo mean summer temperature, variable, rea
C  THETsp: 'THETa, subscript Summer, Present', Present-day mean summer temperature
C          data, real.
C  Thknss: Output array, collects IceThk for Spyglass, 2-D array, real.
C  Thknss.hdf: Hierachical Data File for Spyglass.  Contains IceThk at selected ti
C  TilFld: 'VELocity FieLD' in the till, over both x and z, two-dimensional array,
C          real
C  TilThk: Output array, collects Zdilat for Spyglass, 2-D array, real.
C  TilThk.hdf: Hierachical Data File for Spyglass.  Contains Zdilat at selected ti
C  TimCnt: TIMe CouNTer for incrementing data to the output files
C     over the time domain, integer.
C  OUTPUT: 'OUTPUT', subroutine.  Computes data at end of
C          each time-step and writes to external file.
C  TimSpn: 'TIMe SPaN', span of time covered by run of model, variable, real
C  TimStp: 'TIMe STeP', counter for time steps, parameter, integer
C  TOPOGRAPHY: File name for topographic data
C  TotStp: 'Total time STePs', total times steps selected for run of
C          model, integer
C  Tstar: 'Time-star', relaxation term for depth to dilatant
C          horizon, variable, real
C  TstarC: 'Time-star constant', relaxation constant for depth to dilatant
C          horizon (as decimal fraction of the timestep), constant, real
C  Ubase:
C  Uice: 'U, subsrcript ICE', ice velocity in the x direction, variable, real.
C  Umax: 'U-MAXimum', maximum velocity of Unot at any given time-step during
```

9/10/93 16:34 Ymir:Desktop Folder:Thesis:Dictionaryfor code:Dictiona

```
C         computations.  Used to set value of Pekle' number, variable, real
C  Unot: 'U sub NOughT', ice-till velocity at interface, variable, real
C  Utill: 'U-till', horizontal velocity of till, varaible, real
C  HorVel: 'HORizontal VELocity' of the ice, contains ice velocity
C           field values across all X-nodes.  Two-dim. array.
C          Store values of the ice velocity field used for calculating the tempera
C  Velcty: Output array, collects Unot for Spyglass, 2-D array, real.
C  Velcty.hdf: Hierachical Data File for Spyglass.  Contains Unot at selected time
C  Wzeta: 'W sub zeta', verical velocity vector inside the ice, real
C  Zeta: Vertical (positive upward) nodes within the ice sheet, index, integer.
C  Zdilat: 'Z-DILATant horizon', depth of dilatant horizon beneath the base
C          (ice-till interface) of the glacier, real
C  Zdinst: 'Zd sub instantaneous', depth to dilatatn horizon befor being
C           adjusted by relaxation condition, real
C  Zinitl: 'Z, subscript INITiaL', initial elevation of the base of the
C          ice sheet/ground surface (present-day values are used).
C  ZsN: Elevation of the surface at the nth (previous) timestep.  Used to compute
C       time derivative in for the temperature field calculations, variable, real.
C  Ztill: Depth in meters below ice-till interface of selected points
C         in till, variable, real.
C ***************************************************************************
C Predictor-corrector variables:
C CnvCrt: 'CoNVergence CRiTerion', maximum allowable difference between current
C          and previous ice thickness values for predictor-corrector algorithm,
C          parameter, real.
C Cnvrgd: 'CoNVeRGeD', Indicates whether convergence criterion for predictor-
C          corrector algorithm has been met, variable, logical.
C dZtnt:  'deltaZ TeNTative', distance increment for expanding grid, Z, in till,
C          variable, real.
C EpsTNT: 'Epsiln TeNTative at k', temporary value of Epsiln calculated within
C          PC loop at step k, variable, real.
C hPRVIS: 'h PReVIouS', Ice thickness at previous timestep; input to SHEAR,
C          DYNAMC, and ICEFLX inside PC loop, variable, real.
C hTNTk:  'h TeNTative at k', temporary value of ice thickness calculated within
C          PC loop at step k, variable, real.
C hTNTk1:  'h TENtative at k+1', ice thickness calculated by ICEFLX
C           (returned from TRIDAG) at the end of each PC loop (k+1th step),
C           variable, real.
C HVtnt:  'HorVel TeNTative at k', temporary value of HorVel calculated within
C          PC loop at step k, variable, real.
C kPC:     Counter for PC iterations, variable, integer
C MaxDh:  'MAXimum Difference, h', maximum difference between tentative values
C          of ice thickness at PC steps k and k+1, variable, real.
C MaxDu:  'MAXimum Difference, Uo', maximum difference between tentative values
C          of ice velocity at PC steps k and k+1, variable, real.
C MdtTNT:  'Mdot TeNTative', variable, real.
C PbTNT:  'Pbasal TeNTative at k', temporary value of Pbasal calculated within
C          PC loop at step k, variable, real.
C PrvDif: 'PReVious DIFference', Value of MaxDif at during previous iteration
C          within P-C loop, variable, real.
C PrvDfH: 'PReVious Difference, h', previous maximum difference between
C           tentative values of ice thickness at PC steps k and k+1, variable, rea
C PrvDfU: 'PReVious Difference, Uo', previous maximum difference between
C           tentative values of ice velocity at PC steps k and k+1, variable, real
C TauTNT: 'TAU TeNTative at k', temporary value of TAUbas calculated within
C          PC loop at step k, variable, real.
C UmxTNT: 'Umax TeNTative at k', temporary value of Umax calculated within
C          PC loop at step k, variable, real.
C UoPRVS: 'Uo PReViouS', Ice velocity at  previous timestep, variable, real.
C UoTNTk: 'Uo TeNTative at k', ice velocity calculated by DYNAMC within each PC
C          loop (k+1th step), variable, real.
C UTNTk1: 'Uo TeNTative at k+1', temporary value of Unot calculated within
C          PC loop at step k, variable, real.
```

```
9/10/93 16:34 Ymir:Desktop Folder:Thesis:Dictionaryfor code:Dictiona

C Uzb:  'U at Zb', ice velocity at the base (Zb), real
C ZdTNT:  'Zdilat TeNTative at k', temporary value of Zdilat calculated within
C          PC loop at step k, variable, real.
C ZsTNT:  'Zs TeNTative at k', surface elevation calculated from current value
C          of hTNTk, used as input to SHEAR, DYNAMC, and ICEFLX inside PC loop,
C          variable, real.
C  CLIMATE ID DICTIONARY:
C  Adotz:  'Partial derivative of Adot wrt Zs (elevation), constant, real.
C  Cglac:  'C, subscript GLACial', paleo-CO2 concentration , variable, real.
C  Clgm:  'C, subscript Late Glacial Maximum (LGM)', CO2 concentration at LGM,
C          constant, real.
C  CO2Efc: 'CO2 EFfeCt', variable, real.
C  Cpres:  'Cpresent' present-day CO2 concentration, constant, real.
C  deltaC: 'DELta CO2', difference between present and past glabal average
C           levels of CO2, varies over time, data, real.
C  ElDsrt: 'ELevation DeSeRT effect', variable, real.
C  LAPShi: 'Increase in LAPSe rate at HIgh elevations (i.e., above THRSHD)',
C           parameter, real.
C  LAPS:   'LAPSe rate ', parameter, real.
C  LwrLmt: 'LoWeR LiMiT of melting rate, variable, real.
C  MINSMR: 'MINimum SuMmeR temperature required to induce net melting,
C           parameter, real
C  SrfAbl:  'SURface ABLation', variable, real.
C  t:       Counter for initializing time-dependent variables, integer.
C  TemCO2: 'TEMperature adjustment for differences in CO2 levels' between LGM
C           present, variable, real.
C  TemElv: 'TEMperature adjustment for ELeVation' as ice surface evolves,
C           variable, real.
C  THRSHD: 'THReSHholD for increased lapse rate', parameter, real
C  tnot:   't, subscript NOughT', index number of data point for start of
C           model run, integer. (Used to select start point in Vostok core
C           data.)
```

```
10/1/93 10:22 PM       Ymir:Desktop Folder:Model:tildef.f

      PROGRAM TILDEF
C
C *********************************
C DECLARATIONS:
C
      INCLUDE 'declarations.f'
      REAL Tstar,Zdinst(Xmax),Zdn(Xmax)    ! 29 Apr Zdilat
      REAL TERM3(Xmax),TERM4(Xmax),TERMct        ! 10 May/20may Zb terms
      LOGICAL Bonked,RanPas
      INTEGER BnkCnt

      INTEGER ACCmax
      REAL grdABL,WETDRY
C
C   Variables for climate ocsillation option:

      LOGICAL CLMOSC
      INTEGER ClmPrd,StrtCl,OscCnt
      REAL NewAcc,NewAbl

C   Variables for viscosity ocsillation option:

      LOGICAL VISOSC
      INTEGER VisPrd,StrtVi
      REAL OrigMu,NewMu

      OPEN (20, FILE='PARAMETERS.DAT', FORM='FORMATTED',STATUS='OLD')

C CONSTANTS:
C
C  Climate control constants:
C
       TERMNS = 41          ! Terminus of ice margin
       Clgm   = 100         ! ppm CO2
       Cpres  = 295         ! ppm CO2
       LAPS   = -6.1e-3     ! Lapse rate (degrees C per m)
       MINSMR =273.0
       Adotz  = -2.452e-5/3.1559e7
C                                    (m/a per m elv., conv. to m/s).
C                                    (Bromwich, 1988)
       Cglac  = Clgm                ! CO2 concentration
       deltaC =  Cglac - Cpres  ! deltaC is held constant thru run
C
C Ice velocity field interval (Zeta-space is an expanding grid):

        dZeta =-1.0/(REAL(kmax-1))

C Read logical switch for isothermal/thermal conditions:

       READ(20,*) ISOTHM     ! ISOTHM=true ==> isothermal run
        IF (ISOTHM) THEN
         write(6,*)'This run is isothermal.'
        ELSE
         write(6,*)'This run includes thermodynamics.'
        END IF

C Read accumlation/ablation parameters:

       READ(20,*) WETDRY  ! Coefficient for relative wet/dry adjustment
        write(6,*)'Accum is ',WETDRY*100.0,' percent of modern value.'
       READ(20,*) ACCmax       ! Location of max accumulation
        write(6,*)'Max accum is at node ',ACCmax
       READ(20,*) grdABL       ! Net abl grad (m/yr/dX)
```

```
        write(6,*)'Net abl grad in m/yr/dX is ',grdABL
        write(6,*)

C Read sediment rheologic paramters:

       READ(20,*) Cohesn        ! Sediment cohesion, KPa
        write(6,*)'Cohesn =',Cohesn,'kPa'
        Cohesn = Cohesn*1000.0  ! Convert kPa to Pa
       READ(20,*) PHIprm        ! Sediment angle of int. friction, degrees
        write(6,*)'PHIprm = ',PHIprm,'degrees'
        PHIprm = PHIprm/57.29577951  ! Convert degrees to radians
        tanPHI = tan(PHIprm)
       READ(20,*) n        ! Exponent for power law
        write(6,*)'n =',n
       READ(20,*) b        ! triaxial-derived visc param
        write(6,*)'b =',b
       READ(20,*) Dnot        ! Ref. deformation rate
        write(6,*)'Dnot =',Dnot
        write(6,*)

C Read dilatant horizon relaxation constant:

       READ(20,*) TstarC        ! Zdilatant relaxation constant
        write(6,*)'TstarC =',TstarC
       Tstar = TstarC*deltaT    ! Dilation relaxation paramter
        write(6,*)'Tstar=',Tstar
        write(6,*)'dT/Tstar=',deltaT/Tstar
        write(6,*)

C Read basal pressure coefficient:
       READ(20,*) Pfix
        write(6,*)'Pfix=',Pfix     ! 16 Aug
       RHOprm=RHOs-RHOw            ! Buoyant density of till
        write(6,*)

C Compute parameters for sed. const. eqn.:

      MUnot = b/( 2.0 * ( Dnot**((n-1)/n) ) )
      write(6,*)'MUnot= ',MUnot

      BETA = -RHOprm*g*tanPHI
      GAMMA = ((2.0*Dnot)**(1.0-n))/((MUnot**n)*(n+1.0)*BETA )
      write(6,*)'GAMMA= ',GAMMA

      F     = ((2.0*Dnot)**(1.0-n))/( MUnot**n )
       write(6,*)'F(Do,MUo)= ',F
      F = 2.0*(b**(-n))
       write(6,*)'F(b)= ',F
       write(6,*)
C
      READ(20,*) CLMOSC

      IF (CLMOSC) THEN

        write(6,*)'Climate will oscillate in this run.'

        READ(20,*) StrtCl
        OrgAcc = WETDRY  ! Original accumulation coefficient
        OrgAbl = grdABL  ! Original ablation gradient
        READ(20,*) NewAcc
        READ(20,*) NewAbl
        READ(20,*) ClmPrd
```

10/1/93 10:22 PM Ymir:Desktop Folder:Model:tildef.f

```
        write(6,*)'Starting at',StrtCl,' timetsteps,'
        write(6,*)'WETDRY will alternate from ',OrgAcc,' to ',NewAcc
        write(6,*)'grdABL will alternate from ',OrgAbl,' to ',NewAbl
        write(6,*)'and back again at periods of ',ClmPrd,' timesteps.'

      ELSE ! Reads climate change parmeters, but does not use them

        write(6,*)'No climate oscillations in this run'
        READ(20,*) StrtCl
        OrgAcc = WETDRY  ! Original accumulation coefficient
        OrgAbl = grdABL  ! Original ablation gradient
        READ(20,*) NewAcc
        READ(20,*) NewAbl
        READ(20,*) ClmPrd

      END IF  ! Climate change option

C Viscosity oscillation option:

      READ(20,*) VISOSC

      IF (VISOSC) THEN

        write(6,*)'Viscosity will oscillate in this run.'

        READ(20,*) StrtVi
        OrigMu = MUnot  ! Original visc. from exp. data (b,m)
        READ(20,*) NewMu
        READ(20,*) ClmPrd

        write(6,*)'Starting at',StrtVi,' timetsteps,'
        write(6,*)'Viscosity will alternate from ',OrigMu,' to ',NewMu
        write(6,*)'and back again at periods of ',ClmPrd,' timesteps.'

      ELSE

        write(6,*)'No viscosity oscillations in this run'

      END IF


C ***********************************************************************
C Open remaining input files:
      OPEN (21, FILE='TOPOGRAPHY', FORM='FORMATTED',STATUS='OLD')
      OPEN (22, FILE='GEOTHERMAL', FORM='FORMATTED',STATUS='OLD')
      OPEN (23, FILE='BEDROCK', FORM='FORMATTED', STATUS='OLD')
      OPEN (24, FILE='CO2SENSITIVITY', FORM='FORMATTED',
     &                STATUS='OLD')
      OPEN (25, FILE='PRESENTSURFACETEMP', FORM='FORMATTED',
     &                STATUS='OLD')
      OPEN (26, FILE='PRESENTSUMMERTEMP', FORM='FORMATTED',
     &                STATUS='OLD')
      OPEN (27, FILE='CHI', FORM='FORMATTED', STATUS='OLD')
      OPEN (28, FILE='PRESENTACCUM',FORM='FORMATTED',STATUS='OLD')
C
C Open Cricket Graph output files:
      OPEN (30, FORM='FORMATTED', STATUS='NEW', FILE='MARGIN.OUT')
      OPEN (34, FORM='FORMATTED', STATUS='NEW', FILE='CLIMATEDATA.OUT')
C Write 'Cricket Graph' format instructions:
C
      WRITE(30,'(A1)') '*'
C
C Write column headings to MARGIN.OUT:
```

```
      WRITE( 30,'(A12,3(A1,A16))' )
     & 'Timestep',char(9)
     & ,'Node',char(9)
     & ,'Years (ka)',char(9)
     & ,'Distance(km)'

C ***************************************************************************
C
C ***************** BEGIN MAIN PROGRAM EXECUTION ************************
C
C *** Read data files, set parameters, initialize variables and output files ***
C
C (1) Load geological/geophysical data from input files and
C (2) initialize the basal elevation:
C     (Input: File data; Output:Zinitl, ElvBas(initial), GeoFlx, SenCO2,
C      THETAp, THETsp, CHI, Adotp):
C
      CALL GEODAT(Zinitl,ElvBas,GeoFlx,BedTyp,SenCO2,THETAp,
     &           THETsp,CHI,Adotp)
C
C Read parameters from keyboard.
C
          CALL INRACT
C
C Initialize remaining variables:

      RanPas = .FALSE.
      Bonked = .FALSE.
      BnkCnt = 0

      DO i=1,imax
           IF (ISOTHM) THEN
            MELTED(i) = .true. ! Isothermal case only
           ELSE
            MELTED(i) = .false.
           END IF
           ElvSrf(i) = 0.0                        ! 24 July test
*          ElvSrf(i) = 1500.0
           IceThk(i) = MINTHK   !THERML requires
*          IceThk(i) = ElvSrf(i) - Zinitl(i)     ! 24 July test
           ZsN(i)    = 0.0
           TAUbas(i) = 0.0
           TauTNT(i) = 0.0
           Pbasal(i) = 0.0
           PbTNT(i)  = 0.0
           Zdilat(i) = 0.0
           ZdTNT(i)  = 0.0
           Unot(i)   = 0.0
           Uzb(i)    = 0.0     ! 10 March
           Utillo(i) = 0.0
           dUzbdx(i) = 0.0
           Ubase(i)  = 0.0     ! 12 March
           Epsiln(i) = 0.0
           EpsTNT(i) = 0.0
           THETA(i)  = 273.0
           THETAs(i) = 273.0
           TemCO2(i) = 0.0
           TEmElv(i) = 0.0
           CO2Efc(i) = 0.0
           ElDsrt(i) = 0.0
           SrfAbl(i) = 0.0
           Bdot(i)   = 0.0
```

```
            Adot(i)    = 0.0
            HetFlx(i)  = 0.0
            A1(i)      = 0.0     ! 21 Mar
            A2(i)      = 0.0
            A3(i)      = 0.0
            dA1dx(i)   = 0.0
      Q(i)   = 0.0                ! 27 Mar Non lin till MB
      Q1(i)  = 0.0                ! 27 Mar Non lin till MB
      Q2(i)  = 0.0                ! 27 Mar Non lin till MB
      Q3(i)  = 0.0                ! 27 Mar Non lin till MB
      Q4(i)  = 0.0                ! 27 Mar Non lin till MB
      dQdx(i)   = 0.0
      TERM1(i) =0.0
      TERM2(i) = 0.0
      RHStil(i) = 0.0
      Atill(i) = 0.0
      Btill(i) = 0.0
      Ctill(i) = 0.0
      Snot(i)   = 0.0
      END DO
      Umax    = 0.0
      Length = 0.0
      Span    = 0.0
C
C Till dynamics variables:
C
      DO i=1,imax
           TAUtil(i) = 0.0
           deltaZ(i) = 0.0
           Zdinst(i) = 0.0
           Zdn(i)    = 0.0
      END DO
C
      DO j=1,jmax
           DO i=1,imax
                Utill(i,j)  = 0.0
                Pprime(i,j) = 0.0
           END DO
      END DO
C
C Ice velocity variables:
      DO k=1,kmax
           DO i=1,imax
            IceTmp(i,k) =272.0    ! 10 Mar changed from 268.0
            HorVel(i,k) = 0.0
            Wzeta(i,k)=0.0
            A(i,k) = 6.2e-20  ! TEMPORARY (Units Pa-3 s-1)
            END DO
      END DO
C
C  INITIALIZE RokTmp :

        DO k=1,mmax
         DO i=1,imax
         RokTmp(i,k)=271.15+GeoFlx(i)/CONDrk*FLOAT(k)*dZrok
         END DO
        END DO
C
C Ice mass balance variables:
      DO i=1,imax
           RHSice(i)=0.0
           Aice(i)=0.0
           Bice(i)=0.0
```

```
            Cice(i)=0.0
            FrcIce(i)=0.0
        END DO
C
C       Velocity field output control and output variables:
C
        Count = 0
        kPC = 0  ! 29 Apr
C
        DO j=1,jmax
            DO i=1,Xvel
                TilFld(i,j) = 0.0
                Depth(i,j) = 0.0
            END DO
        END DO

        DO k=1,kmax
            DO i=1,Xvel
                IceFld(i,k) = 0.0
                Height(i,k) = 0.0
            END DO
        END DO
C
C ***************************************************************************
C
        TimStp = 1              ! Initialize time loop
        TimCnt = 0
        NCOL = 0
        OscCnt = 0

C ********************
C * ENTER TIME LOOP *
C ********************

        DO 10 WHILE (TimStp.LE.TotStp)     ! Enter time loop


C  Oscillations in CLIMATE *********************

        IF (TimStp.GE.StrtCl) THEN

          IF ( Mod((TimStp-StrtCl),ClmPrd).EQ.0 ) THEN

            write(6,*)'OscCnt',OscCnt

            IF (Mod(OscCnt,2).EQ.0) THEN

              write(6,*)'At timestep ',TimStp,' WETDRY was ',WETDRY
              WETDRY = NewAcc
              write(6,*)'but has changed to ',WETDRY
              write(6,*)' grdABL was ',grdABL
              grdABL = NewAbl
              write(6,*)'but has changed to ',grdABL

            ELSE

              write(6,*)'At timestep ',TimStp,' WETDRY was ',WETDRY
              WETDRY = OrgAcc
              write(6,*)'but has changed to ',WETDRY
              write(6,*)' grdABL was ',grdABL
              grdABL = OrgAbl
              write(6,*)'but has changed to ',grdABL
```

```
          END IF

          OscCnt = OscCnt+1

        END IF

      END IF

C Vicosity oscillation *************************:

      IF (VISOSC.AND.(TimStp.GE.StrtVi)) THEN

        IF ( Mod(TimStp,ClmPrd).EQ.0 ) THEN

          IF (MUnot.EQ.OrigMu) THEN

            write(6,*)'At timestep ',TimStp,' MUnot was ',MUnot
            MUnot = NewMu
            write(6,*)'but has changed to ',MUnot
            F     = ((2.0*Dnot)**(1.0-n))/( MUnot**n )
            write(6,*)'F(Do,MUo,n)= ',F

          ELSE

            write(6,*)'At timestep ',TimStp,' MUnot was ',MUnot
            MUnot = OrigMu
            write(6,*)'but has changed to ',MUnot
            F     = ((2.0*Dnot)**(1.0-n))/( MUnot**n )
            write(6,*)'F(Do,MUo,n)= ',F

          END IF

        END IF

      END IF

C ***********************************************
*     write(6,*)'TimStp=',TimStp  ! 29 Apr

      Umax=0.0 ! Reset Umax for each time-step
C
C ************************
C * ISOSTATIC ADJUSTMENT *
C ************************
C
      DO i=1,imax
        ZbN(i) = ElvBas(i)    ! 10 June--save prev. value for VERVEL
        ElvBas(i) = ElvBas(i) + (deltaT/TAUiso)*(Zinitl(i)
     &           - ((RHOice/RHOmtl)*IceThk(i)) - ElvBas(i))
      END DO
C
C Where there is significant ice, compute ice surface elevation at each
C node (= base elevation + ice thickness):
C
      DO i=1,imax
        ZsN(i) = ElvSrf(i) ! Save from previous ts (for THERML)
C
        IF (IceThk(i).GT.MINTHK) THEN ! 13 Dec
          ElvSrf(i) = ElvBas(i) + IceThk(i)
        ELSE
          ElvSrf(i) = ElvBas(i)
        END IF
      END DO
```

10/1/93 10:22 PM Ymir:Desktop Folder:Model:tildef.f

```
C
C ****************************
C * PALEOCLIMATE CALCULATIONS *
C ****************************
C
C     (Input: SenCO2,THETAp,THETsp,CHI,Adotp,ElvSrf,IceThk)
C     (Output: THETA,THETAs,Adot)
C
C
C Compute required adjustments to paleotemperatures, due to CO2 and elevation effe
C
C     (1) CO2 effect: Temperature difference at each x-node due to difference betw
C     past and present CO2 levels at each latitude.  (Note: CO2 concentration is
C     held constant; but sensitivity may vary with latitude (Lindstrom & MacAyeal,
C     1989, Table 1).  Elevation effect: Temperature difference at each x-node due
C     to elevation changes as ice sheet grows:
C
          DO i=1,imax
               TemCO2(i) = deltaC*SenCO2(i)
               TemElv(i) = LAPS*ElvSrf(i) ! Dec 15 New lapse rate, Run 20
          END DO
C
C Compute paleo- mean annual surface and mean summer temperatures:
C
          DO i=1,imax
             THETA(i)  = THETAp(i) + TemCO2(i) + TemElv(i)
             THETAs(i) = THETsp(i) + TemCO2(i) + TemElv(i)
          END DO
C
C Compute paleo-accumulation-rates at each x-node based on present
C accumulation (Lindstrom & MacAyeal, 1989, Table 1):
C
      DO i=1,imax
        CO2Efc(i) = (1.0 - CHI(i)*deltaC)*Adotp(i) ! CO2 effect
        ElDsrt(i) = Adotz*ElvSrf(i)  ! Elev. desert effect
        Adot(i) = (CO2Efc(i) + ElDsrt(i))
        Adot(i) = Adot(i)*WETDRY    ! Selected proportion of modern value 18 Aug
      END DO
C
C Compute Surface Ablation starting at node 20:
C
C   Surface ablation rate:
      DO i=1,imax          ! OEERLEMAANS-STYLE ABLATION
        SrfAbl(i) = 0.0
      END DO
      DO i=ACCmax,imax
        SrfAbl(i) = Adot(ACCmax-1)-( ( grdABL*REAL(i-ACCmax)
     &              )/3.1559e7 )
        Adot(i) = SrfAbl(i)
C        Restrict ablation rate to range between maximum of zero
C        and physical mimimum imposed by thickness of the ice:
        Adot(i) = MAX((-IceThk(i)/deltaT),Adot(i))
      END DO
C
C    Thermal coefficient, A, for ice flow law:
C
      DO i= 1,imax
        DO k=1,kmax
           A(i,k) = 5.0/((Ag*(EXP(Qg/(3.0*
     &     8.3*IceTmp(i,k)))))**3)
        END DO
      END DO
C
```

```
10/1/93 10:22 PM       Ymir:Desktop Folder:Model:tildef.f

C ******************************
C * Predictor-corrector segment *
C ******************************
C Reset PC loop-control variables:
C
      kPC = 0                    ! Counter for PC loop
      MaxDh = 0.0                ! Convergence test for ice thickness
      MaxDu = 0.0                ! Convergence test for ice velocity
      Cnvrgd = .false.           ! Convergence indicator
C
C Retain ice thickness and velocity from previous time step:
C
      DO i=1,imax
           hPRVIS(i) = IceThk(i)
           UoPRVS(i) = Unot(i)
      END DO
C
C Initialize tentative PC variables with values from previous timestep:
C
      DO i=1,imax
           hTNTk1(i) = hPRVIS(i)     ! Ice thickness
           UTNTk1(i) = UoPRVS(i)     ! Ice velocity
      END DO
C
C ENTER PC LOOP UNTIL CONVERGENCE ACHIEVED ************************************
C
      DO 11 WHILE (.NOT.Cnvrgd )
C
           UmxTNT = 0.0      ! Reset UmxTNT
*     write(6,*)'kPC=',kPC  ! 29 Apr
C
C     Retain values from previous PC iteration, (become kth values):
C
      DO i=1,imax
        hTNTk(i) = hTNTk1(i)                          ! Retain ice thickness
        IF (hTNTk(i).GT.MINTHK) THEN                  ! 13 Dec
          ZsTNT(i) = hTNTk(i) + ElvBas(i)             ! Surface elevation
        ELSE
           ZsTNT(i) = ElvBas(i)
        END IF
        UoTNTk(i) = UTNTk1(i)            ! Ice velocity
      END DO
      PrvDfH = MaxDh     ! Previous maximum difference for ice thick.
      PrvDfU = MaxDu     ! Previous maximum difference for ice vcty.
C
C ************************************************
C *     CELL-CENTERED GRANDIENT QUANTITIES       *
C *     for till dynamics AND diagnostics        *
C ************************************************
C
C Gradients of ice surface, ice thickness, and
C basal topography:
C
      DO i=1,xmax-1
       dZsdX(i) = ( ZsTNT(i+1) -  ZsTNT(i))/(deltaX)
       dhdx(i)  = ( hTNTk(i+1) -  hTNTk(i))/(deltaX)
       dZbdX(i) = (ElvBas(i+1) - ElvBas(i))/(deltaX)
      END DO
      dZsdx(imax) =( ZsTNT(imax) -  ZsTNT(imax-1))/deltaX
      dhdx(imax)  =( hTNTk(imax) -  hTNTk(imax-1))/deltaX
      dZbdX(Xmax) =(ElvBas(Xmax) - ElvBas(Xmax-1))/deltaX
C
C ***********************************
```

```
10/1/93 10:22 PM       Ymir:Desktop Folder:Model:tildef.f

C *   CELL-CENTERED ICE THICKNESS    *
C ************************************

      DO i=1,imax-1
       Hbar(i) = 0.5*( hTNTk(i) + hTNTk(i+1) )
      END DO
      Hbar(imax) = Hbar(imax-1)
C
      DO i=1,imax
       IF (Hbar(i).LE.MINTHK) THEN
       dZsdX(i) = 0.0
       dhdx(i)  = 0.0
       dZbdX(i) = 0.0
       END IF
      END DO
C
C *********************************
C *   CELL-CENTERED SHEAR STRESS  *
C *********************************

*     TauTNT(1) = 0.0 ! old Ice divide b.c.
      DO i=1,imax
       TauTNT(i) = -RHOice*g*Hbar(i)*dZsdX(i)

       IF (Hbar(i).LE.MINTHK) THEN
         TauTNT(i) = 0.0
       END IF
      END DO
C
C ************************************
C * TILL/ICE DIAGNOSTICS CALCULATIONS *
C ************************************
C Calculate cell- centered velocity for step k+1 of PC loop
C
      DO 12 Xnode=1,Xmax-1              !  Walk thru Xnodes
C
      PbTNT(Xnode) = RHOice*g*Hbar(Xnode)*Pfix  ! Basal pressure

C ******************
C *    SOFT BEDS   *
C ******************
C

C DEPTH TO DILATANT HORIZON:
C *************************

*     IF (Xnode.GE.CONTAC) then
      IF (BedTyp(Xnode).EQ.'SOFT') THEN

        Zdinst(Xnode) = MAX(0.0,
     & (((ABS(TauTNT(Xnode))-Cohesn)/tanPHI)-PbTNT(Xnode))
     & /(RHOprm*g) )

C    Adjust Zdilatant for time relaxation:

       ZdTNT(Xnode) = ( 1.0/( 1.0+(deltaT/Tstar) ) )
     &   * ( Zdn(Xnode) + (deltaT/Tstar)*Zdinst(Xnode) ) ! Implicit

       Zdn(Xnode) = ZdTNT(Xnode)     ! Save value for next timestep
C
C  Depth intervals for till velocity measurement:
C
            dZtnt(Xnode) = ZdTNT(Xnode)/REAL(Zmax-1)
```

```
10/1/93 10:22 PM       Ymir:Desktop Folder:Model:tildef.f

C
C  DIAGNOSTIC TILL VELOCITY CALCULATIONS:
C  ************************************
C
C  Confining stress and sediment velocity at depth intervals:
C
       ALPHA(Xnode) =
     & ABS(TauTNT(Xnode)) - ( Cohesn + PbTNT(Xnode)*tanPHI )
C
       SUMtil = 0.0      ! 16 Aug. Initialize till flux integral
       DO Znode=1,Zmax
C
       Ztill(Znode) = dZtnt(Xnode)*REAL(Znode-1)
C
       Pprime(Xnode,Znode) = PbTNT(Xnode) + ( RHOprm*g*Ztill(Znode) )
C
        Utill(Xnode,Znode) = GAMMA*
     & (((MAX(0.0,(ALPHA(Xnode)+(BETA*Ztill(Znode)))))**(n+1.0) )
     & -((MAX(0.0,(ALPHA(Xnode)+(BETA*ZdTNT(Xnode)))))**(n+1.0) ) )
C
         Utill(Xnode,Znode) = SIGN(Utill(Xnode,Znode),
     &                                TauTNT(Xnode))

        SUMtil = SUMtil + Utill(Xnode,Znode)*dZtnt(Xnode)  ! Till flux integral
C
       END DO

C   DEPTH-AVERAGED TILL VELOCITY:

       IF ((Hbar(Xnode).GT.MINTHK)
     &    .AND.(Zdilat(Xnode).GT.0.0)) THEN
          Utillo(Xnode) = SUMtil/ZdTNT(Xnode)  ! 16 Aug
       ELSE
         Utillo(Xnode) = 0.0
       END IF

C   BASAL ICE VELOCITY:
C
       Uzb(1)=0.0
       Uzb(Xnode) = Utill(Xnode,1)    ! Full coupling of nonlin ice-till
       Uzb(Xmax)=Uzb(Xmax-1)
C
C   ************************************
C   * HEAT PRODUCTION IN THE TILL LAYER *
C   ************************************
C
       EpsTNT(Xnode) = ABS(TauTNT(Xnode)*Uzb(Xnode))    ! 14 May
C
       ELSE

C ******************
C *   HARD  BEDS   *
C ******************
C
         ZdTNT(Xnode) = 0.0      ! No dilatant horizon
         Uzb(Xnode)=0.0
         Utillo(Xnode) = 0.0
         EpsTNT(Xnode) = 0.0 ! Set till viscous dissipation to zero

         DO Znode=1,Zmax
            Utill(Xnode,Znode) = 0.0 ! Zero till velocity
         END DO
```

```
      END IF ! Soft vs. hard bed
C
C ************************************
C * CELL-CENTERED ICE DEFORM. INTEGRAL *
C ************************************
C
C (1) Ice deformation integral AZ(xmax) for mb equation

C  NOTE: VALUES OF A(TEMP) MUST BE CELL CENTERED HERE:
C
      AZ(Xnode)=0.0
      AZ(Xmax)=0.0

      DO kk=1,kmax

        AZZ=0.0
        DO k=kk,kmax
        AZZ =AZZ + A(Xnode,k) * (k-1)**3
        END DO

      AZ(Xnode)=AZ(Xnode) +  AZZ

C ***************************************
C * DIAGNOSTIC ICE VELOCITY CALCULATIONS *
C ***************************************

      Uice(kk) = - (( Hbar(Xnode)/(kmax-1) )**4)*
     &    2.0*(RHOice*g*dZsdx(Xnode))**3 * AZZ

      Uice(kmax)=0.0

C (3) Fill tentative v-field array, HVtnt with values for Uice:

      HVtnt(Xnode,kk) = Uice(kk)
      HVtnt(xmax,kk) = HVtnt(xmax-1,kk)

      END DO       !  END DOLOOP FOR kk

      AZ(Xnode)=AZ(Xnode)*(( Hbar(Xnode)/(kmax-1) )**5)
      AZ(Xmax)=Az(Xmax-1)

C
C (4) Compute tentative MEAN ICE VELOCITY for Unot: UTNTk1(Xmax)
C     (Uo = Uice + Uzb)
C

      IF (Hbar(Xnode).GT.MINTHK) THEN

        UTNTk1(Xnode)=-2.0*(RHOice*g*dZsdx(Xnode))**3
     &                * AZ(Xnode)/Hbar(Xnode)
     &                + Uzb(Xnode)              ! ADD BASAL VELOCITY
      ELSE

        UTNTk1(Xnode)=0.0

      END IF

        UTNTk1(Xmax)=UTNTk1(Xmax-1)
C
C
12    CONTINUE    ! LOOP THROUGH X-NODES
C
```

```
10/1/93 10:22 PM        Ymir:Desktop Folder:Model:tildef.f

C ****************************************
C       Track maximum Unot in each PC loop:
        DO i=1,imax-1
             UmxTNT = MAX(UmxTNT,UTNTk1(i))
        END DO
C  ****************************************
C
C ************************
C *   BASAL HEAT BUDGET   *
C ************************
C Compute basal melting rate (Note: Basal freezing prohibited):
C
       DO i=1,imax-1
        IF (Hbar(i).GT.MINTHK) THEN
         BdtTNT(i) = MIN(0.0,
     &    ( 0.5*( HetFlx(i) + HetFlx(i+1) ) - EpsTNT(i))
     &    /(RHOice*LHFice) )
        ELSE
         BdtTNT(i) = 0.0
        END IF
       END DO
         BdtTNT(imax) = BdtTNT(imax-1)
C
C ************************
C * MASS BALANCE EQUATION *
C ************************
C New tentative Ice thickness (step k+1) for PC loop.
C
C Compute terms for ice flux:

       DO i=1,imax-1
         ICE(i)  =  (1.0/deltaX) * 2.0*((RHOice*g)**3)
     &             * AZ(i) * (dZsdx(i)**2)
       END DO
       ICE(imax)  = ICE(imax-1)
C
C Compute mass balance quantities for till:
C NOTE: THE CONFIGURATION FOR THE TRIDIAGONAL COEFFICIENTS
C AT THE CONTACT IS EMBEDDED IN THE DO-LOOP CONSTRUCTION
C BELOW:

       DO i=1,imax-1

*       IF (i.LT.CONTAC) THEN  ! Hard-bedded
        IF (BedTyp(i).EQ.'SHIELD') THEN  ! Hard-bedded
         ZdTNT(i)  = 0.0
         Snot(i)   = 0.0
         Q(i)      = 0.0
         TILL(i) = 0.0
        ELSE
         Snot(i) = (Cohesn + PbTNT(i)*tanPHI)
         if (TauTNT(i).EQ.0.0) then        ! Don't divide by 0
          Q1(i) = 0.0
         else
          Q1(i) = ( ZdTNT(i)/ ( (n+1.0)*Abs(TauTNT(i)) ) )
         end if
         Q2(i) = Max( 0.0, (Abs(TauTNT(i)) - Snot(i)) )**n
         Q(i) = - F * Q1(i) * Q2(i) * RHOice*g*Hbar(i)
         TILL(i) = ( Q(i) * Hbar(i) )/deltaX
        END IF
       END DO
         Q(imax)=Q(imax-1)
         TILL(imax) = TILL(imax-1)
```

10/1/93 10:22 PM Ymir:Desktop Folder:Model:tildef.f

```
C Compute tridiagonal coefficients for the till equation:

      DO i=2,imax-1
       RHStil(i) = - TILL(i)*dZbdx(i) + TILL(i-1)*dZbdx(i-1)
       Atill(i) = TILL(i-1)/deltaX
       Btill(i) = -( TILL(i-1) + TILL(i) )/deltaX
       Ctill(i) = TILL(i)/deltaX
      END DO
       RHStil(imax) = RHStil(imax-1)
       Atill(imax)  =  Atill(imax-1)
       Btill(imax)  =  Btill(imax-1)
       Ctill(imax)  =  Ctill(imax-1)

C Constant flux boundary condition at ice divide:

        Aice(1)=0.0

        Bice(1) =  1/deltat
     &          + ( 2.0 * ICE(1) )/deltaX
     &          + - 2.0*TILL(1)/deltaX

      Cice(1) = -2.0*ICE(1)/deltaX
     &          + 2.0*TILL(1)/deltaX

      RHSice(1) =  Adot(1) + BdtTNT(1) + hPRVIS(1)/deltaT      ! h at ts=n
     &            + 2.0*ICE(1)*dZbdx(1)
     &            - 2.0*TILL(1)*dZbdx(1)

C  IMPLICIT ICE DEFORMATION VELOCITY plus BASAL VELOCITY:

      DO i=2,xmax-1

      Aice(i) = - ICE(i-1)/deltaX
     &          + Atill(i)

      Bice(i) =  1/deltat
     &          + ( ICE(i-1) + ICE(i) )/deltaX
     &          + Btill(i)

      Cice(i) = -ICE(i)/deltaX
     &          + Ctill(i)

      RHSice(i) =  Adot(i) + BdtTNT(i) + hPRVIS(i)/deltaT      ! h at ts=n
     &            + ICE(i)*dZbdx(i) - ICE(i-1)*dZbdx(i-1)
     &            + RHStil(i)
      END DO
C *** Constant thickness boundary *** h(imax) = MINTHK
      Aice(imax) = 0.0
      Bice(imax) = 1.0
      Cice(imax) = 0.0
      RHSice(imax) = MINTHK                ! RH BC: Set RHS to minimum thickness
C
C
C ******************************
C * COMPUTE DIAGNOSTIC ICE FLUX *  7 Aug
C ******************************

      DO i=1,imax-1
       FlxIce(i) = - 2.0*((RHOice*g)**3) * Az(i) * (dZsdx(i)**3)
      END DO
      FlxIce(imax) = FlxIce(imax-1)
```

```
10/1/93 10:22 PM       Ymir:Desktop Folder:Model:tildef.f

      DO i=1,imax-1
*      IF (i.LT.CONTAC) THEN
       IF (BedTyp(i).EQ.'SHIELD') THEN  ! Hard-bedded
        FlxTil(i) = 0.0       ! Hard bedded ice here
       ELSE
        FlxTil(i) = Q(i) * Hbar(i) * dZsdx(i)
       END IF
      END DO
      FlxTil(imax) = FlxTil(imax-1)

      DO i=1,imax
       FlxUH(i)  = ( FlxTil(i) + FlxIce(i) )  ! units m2/sec
      END DO
      FlxIce(imax) = 0.0
      FlxUH(imax)  = 0.0

*******************************************************************************

C Solve the matrix equation for tentative ice thickness (step n+1):
C
      CALL TRIDAG(Aice,Bice,Cice,RHSice,hTNTk1,imax)        ! Mac version
C
C Enforce positive definite condition to ice thickness:
C
      DO i=1,imax
           hTNTk1(i)=MAX(hTNTk1(i),MINTHK)          ! PC 13 Oct
      END DO
C
C ****************************************************************************
C Find maximum difference between current and previous values of ice thickness
C     and velocity within PC loop:
C
      DO i=1,imax
      MaxDh = MAX( MaxDh, ABS(hTNTk(i) - hTNTk1(i)))
      END DO
C
C Check for convergence (defined as MaxDifs changing by specified small %):
C
      IF ( ABS(PrvDfH-MaxDh) .LE. (PrvDfH*CnvCrt) ) THEN
C
           Cnvrgd = .true.          ! Convergence achieved
C
C          Update variables for TS n+1 and exit PC loop:
C
           Umax = UmxTNT
           DO i=1,Xmax
             HN(i) = IceThk(i)  ! 10 June, save previous value for THERML
             IceThk(i) = hTNTk1(i)
             IF (IceThk(i).GT.MINTHK) THEN        ! Indentify bare surface
                ElvSrf(i) = ElvBas(i) + IceThk(i)
             ELSE
                ElvSrf(i) = ElvBas(i)
             END IF

             IF (IceThk(imax-1).GT.MINTHK) THEN    ! Ice bonking end of grid?
               IF (Bonked.EQ..FALSE.) THEN
                 Bonked = .TRUE.
                 BnkCnt = BnkCnt+1
                 write(6,*)'Bonked end of grid at:'
                 write(6,*)'Timstep =',TimStp
                 write(6,*)'IceThk(',imax-1,')=',IceThk(imax-1)
                 write(6,*)'Total bonks so far:',BnkCnt
               END IF
```

```
            ELSE
              Bonked = .FALSE.
            END IF ! Bonked

            IF (RanPas.EQ..FALSE.) THEN
             IF (IceThk(TERMNS).GT.MINTHK) THEN   ! Ice past the terminus?
               WRITE(6,*)'Lobe ran past terminus at:'
               WRITE(6,*)'Timstep =',TimStp
               WRITE(6,*)'IceThk(',TERMNS,')=',IceThk(TERMNS)
               RanPas = .TRUE.
             END IF
            END IF ! RanPas

               Flux(i)   = FlxUH(i)   ! 29 July
               Unot(i)   = UTNTk1(i)
               Ubase(i)  = Uzb(i)
               TAUbas(i) = TauTNT(i)
               Pbasal(i) = PbTNT(i)
               Zdilat(i) = ZdTNT(i)
               deltaZ(i) = dZtnt(i)
               Epsiln(i) = EpsTNT(i)
               Bdot(i)   = BdtTNT(i)
                IF ( Bdot(i).LT.0.0 ) THEN ! 5 Jan: Checks for melting
                 MELTED(i) = .TRUE.
                ELSE
                 MELTED(i) = .FALSE.
                END IF
          END DO

          DO k=1,ZTAmax
                DO i=1,Xmax
                    HorVel(i,k) = HVtnt(i,k)
               END DO
          END DO
C
C     Collect velocity-field data at selected timesteps and selected nodes:
C
       IF ( MOD(TimStp,INTRVL).EQ.0 ) THEN      ! 30 Oct added
         Count = 0
         DO Xnode=1,Xmax
          IF ( MOD(Xnode,INCRMT).EQ.1 ) THEN
           Count = Count +1
           DO Znode = 1,Zmax
            TilFld(Count,Znode) = Utill(Xnode,Znode)
            Depth(Count,Znode) = - deltaZ(Xnode)*REAL(Znode-1)
           END DO
           DO Zeta = 1,ZTAmax
            IceFld(Count,Zeta) = HorVel(Xnode,Zeta)
            Height(Count,Zeta) =- dZeta*REAL(ZTAmax-Zeta)
           END DO
          END IF
         END DO
       END IF
C
      ELSE
           Cnvrgd = .false.          ! Not converged yet--reiterate
           kPC = kPC + 1             ! Increment PC loop counter
      END IF
C
C
11    CONTINUE                       ! RE-EXECUTE PC LOOP
C *****************************************************************
C
```

```
10/1/93 10:22 PM       Ymir:Desktop Folder:Model:tildef.f

C Thermodynamic segment ****************************************

      IF (.NOT.ISOTHM) THEN

C Compute Vertical Advection rates in ice:
C
       CALL VERVEL(IceThk,ElvSrf,ElvBas,ZbN,Bdot,HorVel,Wzeta) ! 10 June
C
C (NOTE: It may prove necessary to restrict the accumulation so that
C the elevation desert effect cannot drive it negative.)
C Compute the temperature field in the ice.
C     (Input:IceThk ,ElvSrf, ZsN, GeoFlx, THETA, Bdot, Unot, HorVel:
C     Output: IceTmp,RokTmp)
C
      CALL THERML (MELTED,IceThk,ElvSrf,ZsN,HN,GeoFlx,THETA,
     &               IceTmp,RokTmp,Wzeta,Epsiln,HetFlx)

      END IF
C
C ***************************************************************
C
C WRITE TO OUTPUT FILES at selected timesteps:
C
C
      TimCnt=TimCnt+1
      IF (TimCnt.EQ.INTRVL) THEN
           NCOL=NCOL+1
           TimCnt=0
C
      CALL OUTPUT(TimStp,TimCnt,NCOL,TAUbas,Pbasal,Pprime,
     &IceThk,ElvSrf,ElvBas,Zdilat,Unot,Umax,Length,Span,Tau,
     &  PrsBas,Thknss,Elevn,Base,TilThk,Velcty,THETA,THETAs,
     &  SrfAbl,Epsiln,Bdot,Adot,IceTmp,RokTmp,Depth,TilFld,
     &  Height,IceFld,Wzeta,Ubase,VelBas,Flux,FlxIce,FlxTil,Q,
     &  dZsdx,dhdx,dZbdx,dZb2dx,dQdx,dAZdx,Zinitl,BedTyp,
     &  MELTED,Utillo,ISOTHM)
C
       WRITE(6,*)'Output written at time step ',TimStp  ! Write to screen
C
***       END IF ! TEMPORARY OUTPUT 17 MAY ****************************
      END IF        ! Finish filling files at selected time steps

      TimStp=TimStp+1       ! Increment timestep counter
C
C     Write progress of run to screen:          ! Write to screen
       IF ( MOD(TimStp,100).EQ.0 ) THEN         ! For intervals > 100
*      IF ( MOD(TimStp,INTRVL).EQ.0 ) THEN      ! For intervals <= 100
            WRITE(6,*) 'Timestep =', TimStp     ! Write to screen
            WRITE(6,*)'Maximum Uo is ',Umax     ! Write to screen

C     Determine the length of the lobe, in terms of the number elements associated
C     with significantly thick (i.e., >MINTHK) ice:
C
           Length = 0
           DO i=1,imax
                IF (IceThk(i).GT.MINTHK) THEN
                     Length = Length+1
                END IF
           END DO
C
           Margin = REAL(Length-1)*deltaX
           write(6,*)'Margin is at node',Length
*          write(6,*)'which is',Margin/1000.0,'km from ice divide'
```

```
10/1/93 10:22 PM       Ymir:Desktop Folder:Model:tildef.f

C
C    Track ice margin over time:

      WRITE( 30,'(I6,A1,I3,2(A1,E12.5))' )
     & TimStp,char(9)
     & ,Length,char(9)
     & ,(Real(TimStp)*deltaT)/3.1559E7,Char(9)
     & ,Margin/1000.0

       END IF ! Progress to screen
C
10    CONTINUE  ! RE-EXECUTE TIME LOOP
C
C *** EXIT TIME LOOP ************************************************************

C     Write key data to screen:
C
       WRITE(6,*)                              ! Write to screen
       WRITE(6,*) 'Computations complete:'  ! Write to screen
       TimSpn=(TimStp-1)*deltaT
       WRITE(6,*)'Time elapsed in years=',TimSpn/3.1559E7   ! Write to screen
       WRITE(6,*)                              ! Write to screen
       DO i=1,imax
            WRITE(6,*)'Unot(',i,')',Unot(i) ! Write to screen
       END DO
C
C Open and fill Spyglass data files:                ! 20 Oct debug
       iret = DFSDputdata( 'Tau.hdf', irank, idims, Tau )
       iret = DFSDputdata( 'PrsBas.hdf', irank,idims, PrsBas)
       iret = DFSDputdata( 'Thknss.hdf', irank,idims, Thknss)
       iret = DFSDputdata( 'Elevn.hdf', irank, idims, Elevn )
       iret = DFSDputdata( 'TilThk.hdf', irank,idims, TilThk)
       iret = DFSDputdata( 'Velcty.hdf', irank,idims, Velcty)
       iret = DFSDputdata( 'Base.hdf', irank, idims, Base )
       iret = DFSDputdata( 'VelBas.hdf', irank, idims, VelBas )
C
C ******************
C Close input files:
      CLOSE (20)
      CLOSE (21)
      CLOSE (22)
      CLOSE (23)
      CLOSE (24)
      CLOSE (25)
      CLOSE (26)
      CLOSE (27)
      CLOSE (28)
C
C Close Cricket Graph output files:
       CLOSE (34)
C ******************
C
C End MAIN PROGRAM execution:
C
      WRITE(6,*)'END TILDEF EXECUTION'      ! Write to screen
C
      STOP
      END
C
C ************************************************************
C
      SUBROUTINE GEODAT(Zinitl,ElvBas,GeoFlx,BedTyp,SenCO2,
     &      THETAp,THETsp,CHI,Adotp)        ! Dec 16 Run 23
```

```
10/1/93 10:22 PM       Ymir:Desktop Folder:Model:tildef.f

C
C ABSTRACT: Reads geological and geotechnical data from pre-existing files.
C
C INPUT:  Topographic data from external file TOPOGRAPHY; geothermal heat flux
C         from GEOTHERMAL.
C
C OUTPUT: Elevation at base of ice, geothermal flux at each X-node.
C
C *********************************
C DECLARATIONS AND CONSTANT VALUES:
      INCLUDE 'declarations.f'
      INCLUDE 'constants.f'
C
C *****************
C Begin subroutine:
C
C Read topographic and geophysical data from files:
C
      DO i=1,imax
           READ(21,*) Zinitl(i)              ! Topography (data in feet)
            Zinitl(i) = Zinitl(i)/3.28       ! Convert to meters
*           write(6,*)'Zinitl(',i,')',Zinitl(i)
           READ(22,*) GeoFlx(i)              ! Geothermal heat flux distribution
           READ(23,*) BedTyp(i)              ! Bedrock lithology
      END DO
C
C Initialize the basal elevation:
C
      DO i=1,imax
           ElvBas(i) = Zinitl(i)
      END DO
C
C
C Read the climatic and geotechnical data from files:
C
      DO i=1,imax
           READ(24,*)SenCO2(i)
           READ(25,*)THETAp(i)       ! Data in Celcius
           READ(26,*)THETsp(i)       ! Data in Celcius
           READ(27,*)CHI(i)
           READ(28,*)Adotp(i)        ! Data in m/yr
      END DO
C
C Write climate input data column headings to output file:
C
       WRITE(34,'(A1)') '*' ! 'Cricket Graph' format instructions
       WRITE(34,'(5(A10,A1),A10)') 'Xnode',char(9),'SenCO2',char(9),
     &        'THETAp(C)',char(9),'THETsp(C)',char(9),'CHI'
     &        ,char(9),'Adotp(m/a)'
C
C (1) Write input data to file for each X-node and
C (2) Convert data to kgs units for use by program:
C
       DO i=1,imax
       WRITE(34,'(I4,A1,4(E12.5,A1),E12.5)') i,char(9),SenCO2(i),char(9)
     & ,THETAp(i),char(9),THETsp(i),char(9),CHI(i),char(9),Adotp(i)
C
      THETAp(i) = THETAp(i)+273.0        ! Convert to Kelvin
      THETsp(i) = THETsp(i)+273.0        ! Convert to Kelvin
      Adotp(i)  = Adotp(i)/3.1559e7      ! Convert to m/s
      END DO
C
C ****************
```

```
10/1/93 10:22 PM        Ymir:Desktop Folder:Model:tildef.f

C Exit subroutine:
C
      RETURN
C
      END
C
C ***************************************************************************
C
      SUBROUTINE INRACT
C
C ABSTRACT: Prompts for and reads parameters from the keyboard.
C
C INPUT: Selected parameters.
C
C OUTPUT: Same as input.
C
C *********************************
C DECLARATIONS AND CONSTANT VALUES:
      INCLUDE 'declarations.f'
      INCLUDE 'constants.f'
C
C *****************
C Begin subroutine:
C
C Display or prompt for and read parameters:
C
      WRITE(6,*) 'TILDEF computes steady state conditions'  ! Write to screen
      WRITE(6,*) 'for a soft-bedded ice lobe.'              ! Write to screen
C
C Time control parameters:
C
       WRITE(6,*) 'Time control parameters:'                ! Write to screen
       WRITE(6,*)                                           ! Write to screen
       WRITE(6,*) 'Delta-T is ',deltaT/3.1559E7,' years.'   ! Write to screen
       WRITE(6,*)                                           ! Write to screen
       WRITE(6,*) 'TotStp= ',TotStp                         ! Write to screen
       WRITE(6,*) 'THIS RUN IS FOR',TotStp*deltaT/3.1559e7,'YEARS.'
       WRITE(6,*)                                           ! Write to screen
C
      WRITE(6,*) 'Parameters have been entered,press RETURN to execute'
      READ*
C
       WRITE(6,*) '*** PROGRAM IS RUNNING ***'              ! Write to screen
C
C Exit subroutine:
C
      RETURN
C
      END
C
*******************************************************************************
C
       SUBROUTINE VERVEL(IceThk,ElvSrf,ElvBas,ZbN,Bdot,HorVel,Wzeta)
C
C ABSTRACT: Calculates the vertical velocity of the ice.
C
C INPUT: Current X-node, ice thickness, surface elevation,base elevation
C  melting rate, averaged ice velocity,
C ice horizontal velocities over the Zeta-grid
C
C OUTPUT: VERTICAL VELOCITY Wzeta(imax,Kmax)
C
C *********************************
```

```
10/1/93 10:22 PM        Ymir:Desktop Folder:Model:tildef.f

C DECLARATIONS AND CONSTANT VALUES:
C
      INCLUDE 'declarations.f'

      REAL ZETAt(kmax),dUbar(imax,kmax),
     &     dZzeta(imax,kmax),SIGMA,dUzeta(imax,kmax),COMTEM(imax)

      INCLUDE 'constants.f'
C
C**********************
C Begin subroutine:
C
C Compute ZETAt(k) for the no. of k-nodes on the zeta-grid:
C

      DO k=1,kmax
         ZETAt(k) = (REAL(k-1))/(REAL(kmax-1))
      END DO

C
C Calculate veritcal velocities at he k-nodes above each x-node:
C


      DO k=2,kmax-1
           dUbar(imax,k)  = (HorVel(imax,k+1) + HorVel(imax,k-1)
     &           - HorVel(imax-1,k+1) - HorVel(imax-1,k-1))/2.0
           dZzeta(imax,k) = (ElvSrf(imax) - ElvSrf(imax-1)) -
     &          (ZETAt(k)*(IceThk(imax) - IceThk(imax-1))) !Nov.6
           dUzeta(imax,k) = (HorVel(imax,k-1) - HorVel(imax,k+1))/2.0
      END DO

           dUbar(imax,1)  = (HorVel(imax,2) + HorVel(imax,1)
     &           - HorVel(imax-1,2) - HorVel(imax-1,1))/2.0
           dZzeta(imax,1) = (ElvSrf(imax) - ElvSrf(imax-1)) -
     &          (ZETAt(1)*(IceThk(imax) - IceThk(imax-1))) !Nov.6
           dUzeta(imax,1) = (HorVel(imax,1) - HorVel(imax,2))

           dUbar(imax,kmax)  = (HorVel(imax,kmax) + HorVel(imax,kmax-1)
     &           - HorVel(imax-1,kmax) - HorVel(imax-1,kmax-1))/2.0
           dZzeta(imax,kmax) = (ElvSrf(imax) - ElvSrf(imax-1)) -
     &          (ZETAt(kmax)*(IceThk(imax) - IceThk(imax-1))) !Nov.6
           dUzeta(imax,kmax) = (HorVel(imax,kmax-1) - HorVel(imax,kmax))


C
* Compute the commom term at imax (shelf)
C

      COMTEM(imax)= Bdot(imax)+ horVel(imax,kmax)
     &              *( ElvBas(imax) - ElvBas(imax-1)) /deltaX
     &               +(ElvBas(imax)-ZBn(imax))/deltaT

        DO k=2,kmax-1
           dUbar(1,k)  = (HorVel(2,k+1) + HorVel(2,k-1)
     &           - HorVel(1,k+1) - HorVel(1,k-1))/2.0
           dZzeta(1,k) = (ElvSrf(2) - ElvSrf(1)) -
     &          (ZETAt(k)*(IceThk(2) - IceThk(1))) !Nov.6
           dUzeta(1,k) = (HorVel(1,k-1) - HorVel(1,k+1))/2
      END DO

           dUbar(1,1)  = (HorVel(2,2) + HorVel(2,1)
     &           - HorVel(1,2) - HorVel(1,1))/2.0
```

```
10/1/93 10:22 PM        Ymir:Desktop Folder:Model:tildef.f

            dZzeta(1,1) = (ElvSrf(2) - ElvSrf(1)) -
     &          (ZETAt(1)*(IceThk(2) - IceThk(1))) !Nov.6
            dUzeta(1,1) = (HorVel(1,1) - HorVel(1,2))

            dUbar(1,kmax)  = (HorVel(2,kmax) + HorVel(2,kmax-1)
     &           - HorVel(1,kmax) - HorVel(1,kmax-1))/2.0
            dZzeta(1,kmax) = (ElvSrf(2) - ElvSrf(1)) -
     &          (ZETAt(kmax)*(IceThk(2) - IceThk(1))) !Nov.6
            dUzeta(1,kmax) = (HorVel(1,kmax-1) - HorVel(1,kmax))
C
* Compute the commom term at devide:
C
       COMTEM(1)= Bdot(1)+ horVel(1,kmax)
     &              *( ElvBas(2) - ElvBas(1)) /deltaX
     &               +(ElvBas(1)-ZBn(1))/deltaT

       DO   i=2,imax-1          ! Do-loop across x-nodes

       DO k=2,kmax-1
            dUbar(i,k)  = (HorVel(i+1,k+1) + HorVel(i+1,k)
     &           - HorVel(i-1,k+1) - HorVel(i-1,k))/4.0
            dZzeta(i,k) = (ElvSrf(i+1) - ElvSrf(i-1))/2 -
     &          (ZETAt(k)*(IceThk(i+1) - IceThk(i-1)))/2 !Nov.6
            dUzeta(i,k) = (HorVel(i,k-1) - HorVel(i,k+1))/2
       END DO

            dUbar(i,1)  = (HorVel(i+1,2) + HorVel(i+1,1)
     &           - HorVel(i-1,2) - HorVel(i-1,1))/4.0
            dZzeta(i,1) = (ElvSrf(i+1) - ElvSrf(i-1))/2 -
     &          (ZETAt(1)*(IceThk(i+1) - IceThk(i-1)))/2 !Nov.6
            dUzeta(i,1) = HorVel(i,1) - HorVel(i,2)

            dUbar(i,kmax)  = (HorVel(i+1,kmax) + HorVel(i+1,kmax-1)
     &           - HorVel(i-1,kmax) - HorVel(i-1,kmax-1))/4.0
            dZzeta(i,kmax) = (ElvSrf(i+1) - ElvSrf(i-1))/2 -
     &          (ZETAt(kmax)*(IceThk(i+1) - IceThk(i-1)))/2 !Nov.6
            dUzeta(i,kmax) = HorVel(i,kmax-1) - HorVel(i,kmax)
C
* Compute the commom term for both soft and hard bed and shelf:
C


       COMTEM(i)= Bdot(i)+ horVel(i,kmax)
     &              *( ElvBas(i+1) - ElvBas(i-1)) /(2*deltaX)
     &               +(ElvBas(i)-ZBn(i))/deltaT


       END DO
C
* Compute Wzeta at each k-level in ZETAt-space:
C
       DO 20 i=1,imax


       DO L=1,kmax-1
       SIGMA = 0.0
          DO k=kmax-1,L,-1
          SIGMA = SIGMA+dZeta*IceThk(i) *dUbar(i,k)/deltaX
     &          + dUzeta(i,k)*dZZETA(i,k)/deltaX
          END DO
       Wzeta(i,L) = SIGMA +COMTEM(i)

       END DO
```

```
10/1/93 10:22 PM       Ymir:Desktop Folder:Model:tildef.f


C
      Wzeta(i,kmax) =COMTEM(i)
C

20    CONTINUE            ! end loop thru x-nodes

      RETURN
      END

C
*******************************************************************************
C
      SUBROUTINE THERML(MELTED,IceThk,ElvSrf,ZsN,HN,GeoFlx,THETA,
     &      IceTmp,RokTmp,Wzeta,Epsiln,HetFlx)
C
C ABSTRACT: Computes thermal field in ice, based on atmospheric and
C geothermal forcing.  Thermal field at each X-node is computed on
C an expanding, normalized grid, called ZETAt, which has value 0 at
C the ice surface and 1 at the base.  The index for ZETAt, k, varies
C 1 at the surface to kmax at the base.
C
C INPUT: Current X-node, ice thickness, surface elevation, surface
C elevation at prevoius timestep, melting rate, averaged ice velocity,
C ice horizontal velocities over the Zeta-grid.
C
C OUTPUT: Ice and bed rock temperature field.
C
C ID DICTIONARY:
C
C  AtempK: 'A' along the k-nodes for ice sheet.
C  BtempK: 'B' along the k-nodes for ice sheet.
C  CtempK: 'C' along the k-nodes for ice sheet.
C  RHStpK: RHS along the X-nodes for ice sheet.
c  AtempX(imax-2): 'A' along the x-nodes for ice sheet.(i=2,imax-1)
c  BtempX(imax-2):'B' along the x-nodes for ice sheet.
C  CtempX(imax-2):'C' along the x-nodes for ice sheet.
c  RHStpX(imax-2): RHS along the X-nodes for ice sheet
C ************************************************
C DECLARATIONS AND CONSTANT VALUES:
C
       INCLUDE 'declarations.f'
       REAL ZETAt(kmax),C1(kmax),C2,
     &   AtempK(kmtot),BtempK(kmtot),CtempK(kmtot),
     &   RHStpK(kmtot),NewTpK(kmtot),PrsMlt(imax)

       INCLUDE 'constants.f'
*************************************************

C
C DEFINE LOCAL VARIABLES AND CONSTANTS:
C
       DO k=1,kmax
       ZETAt(k) = (REAL(k-1))/(REAL(kmax-1))
       END DO

*********************************

      DO 30 i=1,imax                        ! Do-loop for entire subroutine

       PrsMlt(i) = -0.36-0.00759e-5*(IceThk(i)*g*Rhoice)+273.0

      IF ((IceThk(i).GE.10.)) THEN      ! if 2
```

```
10/1/93 10:22 PM       Ymir:Desktop Folder:Model:tildef.f

************************************

C (1) Set boundary conditions at ice surface:

      AtempK(1) = 0.0
      BtempK(1) = 1.0
      CtempK(1) = 0.0
      RHStpK(1) = THETA(i)
C
C (2) Compute coefficients for implicit solution of ice temp over vertical grids:
C


      C2 = - (KAPice*deltaT) / ((IceThk(i)*dzeta)**2)

      DO k=2,kmax-1

      C1(k) =-deltaT*( (ElvSrf(i) - ZsN(i))/deltaT -
     &              Zetat(k)*(IceThk(i)-HN(i))/deltaT-Wzeta(i,k))
     &               / (2*IceThk(i)*dZeta)

      AtempK(k) =  C2-C1(k)
      BtempK(k) = 1.0 - 2.0*C2
      CtempK(k) =  C2 +C1(k)
      RHStpk(k) = IceTmp(i,k)

       END DO
C
C (3) Set boundary conditionss at ice base:
C
      IF (MELTED(i))THEN

       AtempK(kmax) = 0.0
       BtempK(kmax) = 1.0
       CtempK(kmax) = 0.0
       RHStpK(kmax) = PrsMlt(i)
C
      ELSE
       AtempK(kmax) = -CONDic/(IceThk(i)*dZeta)
       BtempK(kmax) = CONDic/(IceThk(i)*dZeta)
     &                            - CONDrk/dZrok
       CtempK(kmax) =CONDrk/dZrok
       RHStpK(kmax) = 0.0

      END IF
C
C (4) Compute coefficients for implicit solution of rock temp over vertical grids:
C
      DO k=Kmax+1,Kmtot-1
      AtempK(k) = - KAProk*deltaT/(dZrok**2)
      BtempK(k) = 1.0+2.0*KAProk*deltaT/(dZrok**2)
      CtempK(k) = - KAProk*deltaT/(dZrok**2)
      RHStpK(k) = RokTmp(i,k-kmax)
      END DO
C
C (5) Set boundary conditions at depth in bedrock:
C
      AtempK(kmtot) = -1.
      BtempK(kmtot) =1.
      CtempK(kmtot) =0.0
      RHStpK(kmtot) = GeoFlx(i)*dZrok/CONDrk
C
```

```
10/1/93 10:22 PM       Ymir:Desktop Folder:Model:tildef.f

C (6) Solve the tridiagnal system:
C
      CALL TRIDAG(AtempK,BtempK,CtempK,RHStpK,NewTpK,kmtot) ! Mac version
C
C Assign newly computed temperatures to main program variables:
C

      DO k=1,kmax
      IceTmp(i,k) = NewTpk(k)

      END DO

      DO k=kmax+1,kmtot
      RokTmp(i,k-kmax) = NewTpk(k)
      END DO

C Compute the ice heat flux and geothermal (rock) heat flux at current node :
C
         IceHet(i) = - Kapice*(IceTmp(i,kmax-1)-IceTmp(i,kmax))
     &                 / (IceThk(i)*dZeta)

         GeoHet(i) = - KAProk*(RokTmp(i,1)-IceTmp(i,kmax))
     &                 / dZrok

         HetFlx(i) = IceHet(i) + GeoHet(i)


       ELSE      ! Icethk<1.0m or floating

       DO k=1,kmax
       IceTmp(i,k)= (Float(k)-1)*(PrsMlt(i)-THETA(i))/(kmax-1)+THETA(i)
       END DO

         IceHet(i) = - Kapice*(IceTmp(i,kmax-1)-IceTmp(i,kmax))
     &                 / (IceThk(i)*dZeta)

        DO k=1,mmax
        RokTmp(i,k) = 273.16+GeoFlx(i)/CONDrk*FLOAT(k)*dZrok
        END DO

         GeoHet(i) = - KAProk*(RokTmp(i,1)-IceTmp(i,kmax))
     &                 / dZrok


         HetFlx(i) = IceHet(i) + GeoHet(i)


       END IF          ! END IF2

30     CONTINUE       ! Do-loop for entire subroutine

          RETURN
          END
C
*******************************************************************************

C
      SUBROUTINE TRIDAG(A,B,C,R,U,N)
C
C ABSTRACT: Solves tridiagonal matrix equations
C
C INPUT: Coefficients of unknowns, solution vector, number of unknowns
C
```

```
10/1/93 10:22 PM       Ymir:Desktop Folder:Model:tildef.f

C OUTPUT: Computed values for the unknowns
C
C REFERENCE: Press, William H., Flannery, Brian P., Teukolsky, Saul A.,
C Vetterling, William T., Numerical Recipes: The Art of Scientific
C Computing, Cambridge University Press, 1989.
C
C ID DICTIONARY:
C
C   A: Subdiagonal coefficients, real
C   B: Main diagonal coefficients, real
C   C: Superdiagonal coefficients,real
C   R: 'Right-hand side', (solution vector), real
C   U: 'Unknowns' (output), real
C   N: 'Number' of nodes (equations), integer
C   J: Counter
C   BET: 'Beta'--holds Beta values for manipulation
C   GAM: 'Gamma'--holds Gamma values for manipulation
C
C *************
C Declarations and constants:
C
      INTEGER NMAX,J,N
      PARAMETER(NMAX=101)
      REAL GAM(NMAX),A(N),B(N),C(N),R(N),U(N),BET
C
C *****************
C Begin subroutine:
C
C Perform matrix operations:
      IF(B(1).EQ.0.)PAUSE
      BET=B(1)
      U(1)=R(1)/BET
C
      DO J=2,N
           GAM(J)=C(J-1)/BET
           BET=B(J)-A(J)*GAM(J)
           IF(BET.EQ.0.)PAUSE
           U(J)=(R(J)-A(J)*U(J-1))/BET
      END DO
C
      DO J=N-1,1,-1
           U(J)=U(J)-GAM(J+1)*U(J+1)
      END DO
C
C ****************
C Exit subroutine:
C
      RETURN
C
      END
C
C ***************************************************************************
C
      SUBROUTINE OUTPUT(TimStp,TimCnt,NCOL,TAUbas,Pbasal,Pprime,
     &    IceThk,ElvSrf,ElvBas,Zdilat,Unot,Umax,Length,Span,Tau,
     &    PrsBas,Thknss,Elevn,Base,TilThk,Velcty,THETA,THETAs,
     &    SrfAbl,Epsiln,Bdot,Adot,IceTmp,RokTmp,Depth,TilFld,
     &    Height,IceFld,Wzeta,Ubase,VelBas,Flux,FlxIce,FlxTil,Q,
     &    dZsdx,dhdx,dZbdx,dZb2dx,dQdx,dAZdx,Zinitl,BedTyp,
     &    MELTED,Utillo,ISOTHM)
C
C
C ABSTRACT:
```

```
10/1/93 10:22 PM       Ymir:Desktop Folder:Model:tildef.f

C Collects values of variable at end of selected time intervals and enters
C them into arrays that (a) will be written, at end of run, to output files used b
C Spyglass, (b) can be used by Cricket Graph to display time evolution at a
C given point on the horizontal grid, and (c) can be used by Cricket Graph to
C display snapshots of the variable values across the entire grid at the selected
C time intervals .
C
C INPUT: Time step, basal shear stress, basal confining pressure, ice
C thickness, elevation of the surface, depth to the dilatant till
C horizon, basal ice velocity.
C
C OUTPUT: (1) Elapsed time and values of each variable. (2) Values of each
C variable at end of selected time intervals.
C
C LOCAL ID DICTIONARY:
C
C Time: Time step identifier for snapshot output data files, variable, character.
C FilNam: 'FILe NAMe' identifier for snapshot output data files, variable, charact
C
C *********************************
C DECLARATIONS AND CONSTANT VALUES:
      CHARACTER*8 Time
      CHARACTER*100 FilNam,TmpFil,VerFil,TilFil,IceFil
      INCLUDE 'declarations.f'
      REAL dTFdx(Xmax),VablGD(Xmax),Fxpred(Xmax) ! Local variables 19 Aug
      INCLUDE 'constants.f'
C
C *****************
C Begin subroutine:
C
C (1) Fill Spyglass files for data at each X-node:      ! 20 Oct debug
      DO i=1,imax
       Tau(i,NCOL)=TAUbas(i)/1000.0
       PrsBas(i,NCOL)=Pbasal(i)/1000.0
       Thknss(i,NCOL)=IceThk(i)
       Elevn(i,NCOL)=Elvsrf(i)
       TilThk(i,NCOL)=Zdilat(i)
       Velcty(i,NCOL)=Unot(i)*3.1559e7
       Base(i,NCOL)=ElvBas(i)
       VelBas(i,NCOL)=Ubase(i)*3.1559e7
      END DO
C
C (2) Open and fill Cricket Graph files with SNAPSHOT data.
C (These files show values of variables over all/selected X-nodes at
C  a selected point in time):
C
      WRITE (Time,'(F8.0)')  TimStp*deltaT/3.1559E7
C
      FilNam = 'RESULTS YRS ='//Time
      OPEN(UNIT=49+NCOL, FORM='FORMATTED',STATUS='NEW',
     &     FILE=FilNam)
C
      IF (.NOT.ISOTHM) THEN
       TmpFil = 'TEMP FIELD'//Time
       OPEN(UNIT=59+NCOL, FORM='FORMATTED',STATUS='NEW',
     &     FILE=TmpFil)
      END IF
C
      TilFil = 'TILL VELOCITY'//Time
      OPEN(UNIT=69+NCOL, FORM='FORMATTED',STATUS='NEW',
     &     FILE=TilFil)
C
      IceFil = 'ICE VELOCITY'//Time
```

10/1/93 10:22 PM Ymir:Desktop Folder:Model:tildef.f

```
      OPEN(UNIT=79+NCOL, FORM='FORMATTED',STATUS='NEW',
     &     FILE=IceFil)
C
*     IF (.NOT.ISOTHM) THEN
*      VerFil = 'VER VELOCITY'//Time
*     OPEN(UNIT=89+NCOL, FORM='FORMATTED',STATUS='NEW',
*    &     FILE=VerFil)
*     END IF
C
C RESULTS files:
C
C    Write 'Cricket Graph' format instructions:
C
           WRITE(49+NCOL,'(A1)') '*'
C
C     Write column headings to RESULTS:

C Diagnostic till flux derivative and vertical ablation gradient:

      do i=1,imax-1
       IF (IceThk(i).GT.MINTHK) THEN
        dTFdx(i) =
     &   ((Utillo(i)*Zdilat(i)-Utillo(i+1)*Zdilat(i+1))
     &    /deltaX)*3.1559e7
       VablGD(i) =
     &   ( Adot(i+1)-Adot(i) )
     &    /( ElvSrf(i+1)-ElvSrf(i) )*3.1559e7
      ELSE
       dTFdx(i)  = 0.0
       VablGD(i) = 0.0
      END IF
      end do

C    Compute ice flux for diagnostics:  29 July

      Fxpred(1)=0.0
      DO i=2,imax
      Fxpred(i)=0.0
       DO j=1,i-1
        Fxpred(i) = Fxpred(i)
     &            + (0.5*( Adot(j)+Adot(j+1) + Bdot(j)+Bdot(j+1) )
     &            *deltaX)
      END DO
      END DO

C Column headers for RESULTS files:

      WRITE(49+NCOL,'(33(A16,A1),A16)')
     & 'X-node',char(9)
     & 'Distance(km)',char(9)
     & ,'TAU (kPa)',char(9)
     & ,'Pbas (kPa)',char(9)
     & ,'H (m)',char(9)
     & ,'Elev. (m)',char(9)
     & ,'Base (m)',char(9)
     & ,'Topog (m)',char(9)
     & ,'Bedrock',char(9)
     & ,'Hbar (m)',char(9)
     & ,'Zsbar (m)',char(9)
     & ,'hb (m)',char(9)
     & ,'Uo (m/y)',char(9)
     & ,'THETA (C)',char(9)
     & ,'THETAs (C)',char(9)
```

```
     & ,'Epsiln',char(9)
     & ,'Bdot(m/y)',char(9)
     & ,'Adot(m/y)',char(9)
     & ,'Ablation(m/y)',char(9)
     & ,'VablGD(m/y/m)',char(9)  ! Vertical ablation gradient
     & ,'SrfAbl(m/y)',char(9)
     & ,'Ubase(m/y)',char(9)
     & ,'Hbar*U(m2/y)',char(9)  ! cell-centered
     & ,'FLUX(m2/y)',char(9)
     & ,'FLUXi(m2/y)',char(9)
     & ,'FLUXt(m2/y)',char(9)
     & ,'Q',char(9)
     & ,'FLXp(m2/y)',char(9)
     & ,'Utillo(m/y)',char(9)        ! 16 Aug
     & ,'Till Flux(m2/y)',char(9)    ! 16 Aug
     & ,'dTlFx/dx(m2/y/m)',char(9)    ! 17 Aug
     & ,'dZsdx',char(9)
     & ,'dhdx',char(9)
     & ,'dZbdx'
C
C     Write final data to RESULTS:
C
      DO i=1,imax-1
      WRITE(49+NCOL,'(I3,A1,32(E12.5,A1),E12.5)')
     & i,char(9)
     & ,REAL(i-1)*40.0,char(9)
     & ,TAUbas(i)/1000.0,Char(9)
     & ,Pbasal(i)/1000.0,char(9)
     & ,IceThk(i),char(9)
     & ,ElvSrf(i),char(9)
     & ,ElvBas(i),char(9)
     & ,Zinitl(i),char(9)
     & ,BedTyp(i),char(9)
     & ,0.5*( IceThk(i)+IceThk(i+1) ),char(9)
     & ,0.5*( ElvSrf(i)+ElvSrf(i+1) ),char(9)
     & ,Zdilat(i),char(9)
     & ,Unot(i)*3.1559e7,char(9)
     & ,THETA(i)-273.0,char(9)
     & ,THETAs(i)-273.0,char(9)
     & ,Epsiln(i),char(9)
     & ,Bdot(i)*3.1559e7,char(9)
     & ,Adot(i)*3.1559e7,char(9)
     & ,(Adot(i)+Bdot(i))*3.1559e7,char(9)
     & ,VablGD(i),char(9)
     & ,SrfAbl(i)*3.1559e7,char(9)
     & ,Ubase(i)*3.1559e7,char(9)
     & ,Unot(i)*3.1559e7*0.5*(IceThk(i)+IceThk(i+1)),char(9)
     & ,flux(i)*3.1559e7,char(9)
     & ,FlxIce(i)*3.1559e7,char(9)
     & ,FlxTil(i)*3.1559e7,char(9)
     & ,Q(i),char(9)
     & ,Fxpred(i)*3.1559e7,char(9)
     & ,Utillo(i)*3.1559e7,char(9)   ! 16 Aug
     & ,Utillo(i)*3.1559e7*Zdilat(i),char(9)
     & ,dTFdx(i),char(9)
     & ,dZsdx(i),char(9)
     & ,dhdx(i),char(9)
     & ,dZbdx(i)
          END DO
C
               CLOSE(49+NCOL)
C
C TEMP FIELD files:
```

10/1/93 10:22 PM Ymir:Desktop Folder:Model:tildef.f

```
C
      IF (.NOT.ISOTHM) THEN

C     Write 'Cricket Graph' format instructions:
C
           WRITE(59+NCOL,'(A1)') '*'
C
C     Write column headings to output file:
C
         WRITE(59+NCOL,'(A10,A1,<(Xmax-1)/INCRMT>(A6,I3,A1,A1),A3,I3,A1)')
     &        'Zeta',char(9),(('T(x= ',i,')',char(9)),
     &         i=1,imax-INCRMT,INCRMT),'T(x= ',i,')'
C
C     Write temperature data to output file :
C
         DO k=1,kmax
         WRITE(59+NCOL,'(I3,A1,<(Xmax-1)/INCRMT>(E12.5,A1),E12.5)') k,char(9),
     & ((IceTmp(i,k),char(9)),i=1,imax-INCRMT,INCRMT),   !Nov 12
     &      IceTmp(imax,k)                                    !Nov 12
            END DO
C
         DO k=kmax+1,Kmtot
         WRITE(59+NCOL,'(I3,A1,<(Xmax-1)/INCRMT>(E12.5,A1),E12.5)') k,char(9),
     &   ((RokTmp(i,k-kmax),char(9)),i=1,imax-INCRMT,INCRMT),
     &            RokTmp(imax,k-kmax)
         END DO

C     Write column headings to output file:
C
*         WRITE(59+NCOL,'(A10,A1,<Xmax-1>(A6,I3,A1,A1),A3,I3,A1)')
*    &        'Zeta',char(9),(('T(x= ',i,')',char(9)),
*    &         i=1,imax-1),'T(x= ',i,')'
C
C     Write temperature data to output file :
C
*        DO k=1,kmax
*        WRITE(59+NCOL,'(I3,A1,<Xmax-1>(E12.5,A1),E12.5)') k,char(9),
*    & ((IceTmp(i,k),char(9)),i=1,imax-1),
*    &      IceTmp(imax,k)
*           END DO
C
*        DO k=kmax+1,Kmtot
*        WRITE(59+NCOL,'(I3,A1,<Xmax-1>(E12.5,A1),E12.5)') k,char(9),
*    &   ((RokTmp(i,k-kmax),char(9)),i=1,imax-1),
*    &            RokTmp(imax,k-kmax)
*        END DO

      END IF
C
C TILL VELOCITY files:
C
C     Write 'Cricket Graph' format instructions:
C
      WRITE(69+NCOL,'(A1)') '*'
C
C     Write column headings to output file:
C
      WRITE(69+NCOL,'(<(Xvel-1)*2>(A10,I2,A1,A1,A10,I2,A1,A1),
     & A10,I2,A1,A1,A10,I2,A1)')
     & (('Depth (x= ',i*INCRMT+1,')',char(9),
     & 'U (x= ',i*INCRMT+1,')',  char(9)),i=0,xvel-1)
C
```

```
10/1/93 10:22 PM       Ymir:Desktop Folder:Model:tildef.f

C     Write velocity field data to output file (U in m/y):
C
      DO j=1,jmax
       WRITE(69+NCOL,'(<(Xvel-1)*2>(E12.5,A1,E12.5,A1),E12.5,A1,E12.5)')
     &((Depth(i,j),char(9),TilFld(i,j)*3.1559e7,char(9)),
     &i=1,xvel-1),Depth(xvel,j),char(9),TilFld(xvel,j)*3.1559e7
      END DO
C
C
C ICE VELOCITY files:
C
C     Write 'Cricket Graph' format instructions:
C
      WRITE(79+NCOL,'(A1)') '*'
C
C     Write column headings to output file:
C
      WRITE(79+NCOL,'(<(Xvel-1)*2>(A10,I2,A1,A1,A10,I2,A1,A1),A10,
     & I2,A1,A1,A10,I2,A1)') (('Height(x= ',i*INCRMT+1,')'
     & ,char(9),'U(x= ',i*INCRMT+1,')',char(9)),i=0,Xvel-1)
C
C     Write velocity field data to output file (U in m/y):
C
      DO k=1,kmax
      WRITE(79+NCOL,'(<(Xvel-1)*2>(E12.5,A1,E12.5,A1),E12.5,A1,E12.5)')
     &((Height(i,k),char(9),IceFld(i,k)*3.1559e7,char(9)),i=1,
     &Xvel-1), Height(Xvel,k),char(9),IceFld(Xvel,k)*3.1559e7
      END DO
C
C VERTICAL ADVECTION files:
C

*     IF (.NOT.ISOTHM) THEN

C     Write 'Cricket Graph' format instructions:
C
*      WRITE(89+NCOL,'(A1)') '*'
C
C     Write column headings to output file:
C
*     WRITE(89+NCOL,'(A10,A1,<(Xmax-1)/INCRMT>(A6,I3,A1,A1),A6,I3,A1)')
*    &        'k',char(9),(('Wzeta(x= ',i,')',char(9)),
*    &         i=1,imax-INCRMT,INCRMT),'Wzeta(x= ',i,')'
C
C    Write vertical velocity data to output file:
C
*     DO K=Kmax,1,-1
*     WRITE(89+NCOL,'(I3,A1,<(Xmax-1)/INCRMT>(E12.5,A1),E12.5)') k,char(9),
*    &((Wzeta(i,k),char(9)),i=1,imax-INCRMT,INCRMT),Wzeta(imax,k)
*     END DO

*     END IF
C
C ****************
C Exit subroutine:
C
      RETURN
C
      END
C
```

Appendix C

Preconsolidation test data

Preconsolidation tests (Tables C.1 and C.2) were conducted on each of three test specimens taken from a single 6-inch-cube field sample collected from the upper portion of a 0.5-meter-thick lens of glaciolacustrine clay in the proglacial deposit underlying the second glacial sequence (see description of stratigraphy in Chapter 4). The lens was exposed in the access road-cut at the northeast end of Pit #6 of the Wedron Silica Company mine, Wedron, IL. Tests were conducted at the Civil Engineering Laboratory, Washington State University.

The curve obtained from the first specimen lacked a distinct break, suggesting that the specimen had been disturbed during test preparation. The second and third specimens (Fig.s C.1 and C.2) produced curves with distinct breaks and gave consistent results, both reflecting about 1500 kPa preconsolidation. The preconsolidation value for the field sample was therefore based the results of the second and third tests. The precision of the estimate is limited primarily by the precision of the graphical analysis (about ± 100 kPa).

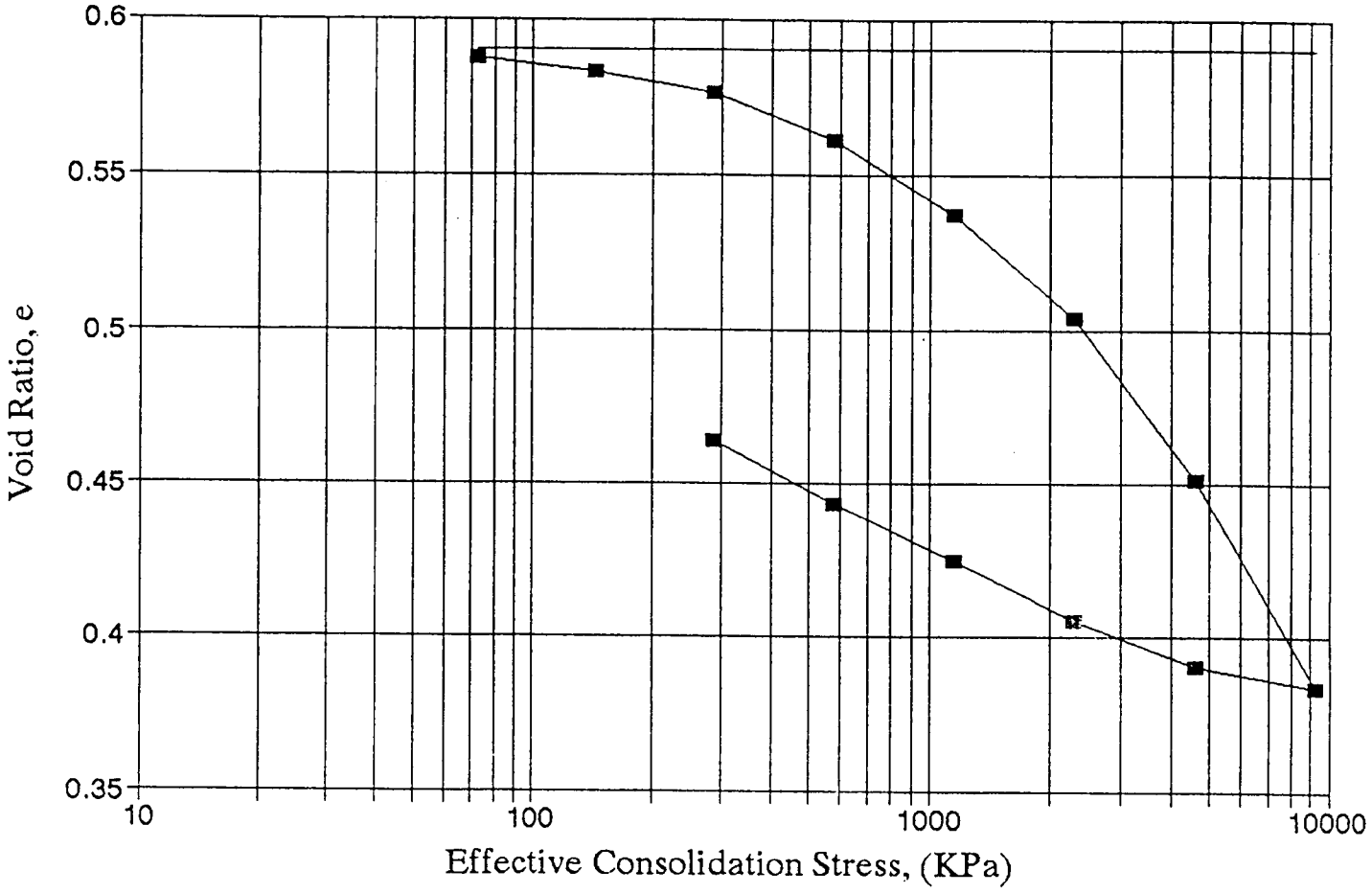

Fig. C.1. Consolidation curve (in terms of void ratio vs. effective consolidation stress) for the second test specimen from the block sample of glaciolacustrine clay beneath glacial sequence II, exposed at Pit #6, Wedron Silica Company mine, Wedron, IL.

Test was run from 10-12-92 to 10-23-92.

Calibration Data

Load	Deflected Dial Reading
72	7.75
144	13.25
288	20.6
576	30.35
1152	38.85
2304	51.75
4608	72.85
9217	110.4

Initial Void Ratio, eo = 0.59
Height of Solids, Hs = 12.26 mm
Initial Dial Reading = 0
Initial height of soil, Hi = 19.5 mm

Effective Consol. Stress (KPa)	Initial Dial Rdg.	Final Dial Rdg.	Total Delta Dial Rdg.	Calbrtd. Dial Rdg.	Adjusted (x.002) (mm)	Change in Void Ratio	Inst. Void Ratio	Drainage Path (cm)	Time** For 50% Consol. (min)	Coeff. o Consol. Cv cm^2/sec	Coeff. o Compre av m^2/N	Coeff. of Permeab k cm/s	Compren. Index Cc	Secondary Compren. Index C	Secondary Compren. Ratio C /Cc
72	0	25.5	25.5	17.75	0.0355	0.0029	0.587				5.89E-05	2.35E-06			
144	0	57	57	43.75	0.0875	0.0071	0.583	0.972813	4.8	6.47E-04	4.61E-05	1.50E-06			
288	57	105	105	84.4	0.1688	0.0136	0.576	0.966405	5.8	5.29E-04	5.34E-05	4.96E-06	1.12	0.0082	0.0073
576	105	209	209	178.65	0.3573	0.0291	0.561	0.957628	2	1.51E-03	4.12E-05	3.70E-06	3.05	0.0125	0.0041
1152	209	363	363	324.15	0.6483	0.0529	0.537	0.940928	2	1.45E-03	2.92E-05	2.16E-06	5.22	0.011	0.0021
2304	363	582	582	530.25	1.0605	0.0865	0.503	0.916073	2.3	1.20E-03	2.27E-05	1.42E-06	5.95	0.023	0.0039
4609	582	923.5	923.5	850.65	1.7013	0.1388	0.451	0.879443	2.5	1.02E-03	1.47E-05	8.47E-07	11.64	0.073	0.0063
9217	923.5	1376	1376	1265.8	2.5312	0.2065	0.384	0.826655	2.4	9.35E-04			13.43	0.183	0.0136
4609			1296	1223.15	2.4463	0.1995	0.390								
2304			1185	1133.25	2.2665	0.1849	0.405								
1152			1052	1013.15	2.0263	0.1653	0.425								
576			930	899.65	1.7993	0.1468	0.443								
288			794	773.4	1.5468	0.1262	0.464								
144			663	649.75	1.2995	0.1060	0.484								
72			393	385.25	0.7705	0.0628	0.527								

Avg. Cv50% = 1.22E-03 k avg. = 2.02E-06 cm/s

Avg. Compression Index Cc = 5.735
Avg. Secondary Comp. Index = 0.0518
Avg. Secondary Comp. Ratio = 0.0062

Table C.1. Consolidation data for the second test specimen from the block sample of glaciolacustrine clay beneath glacial sequence II, exposed at Pit #6, Wedron Silica Company mine, Wedron, IL. See Fig. C.1.

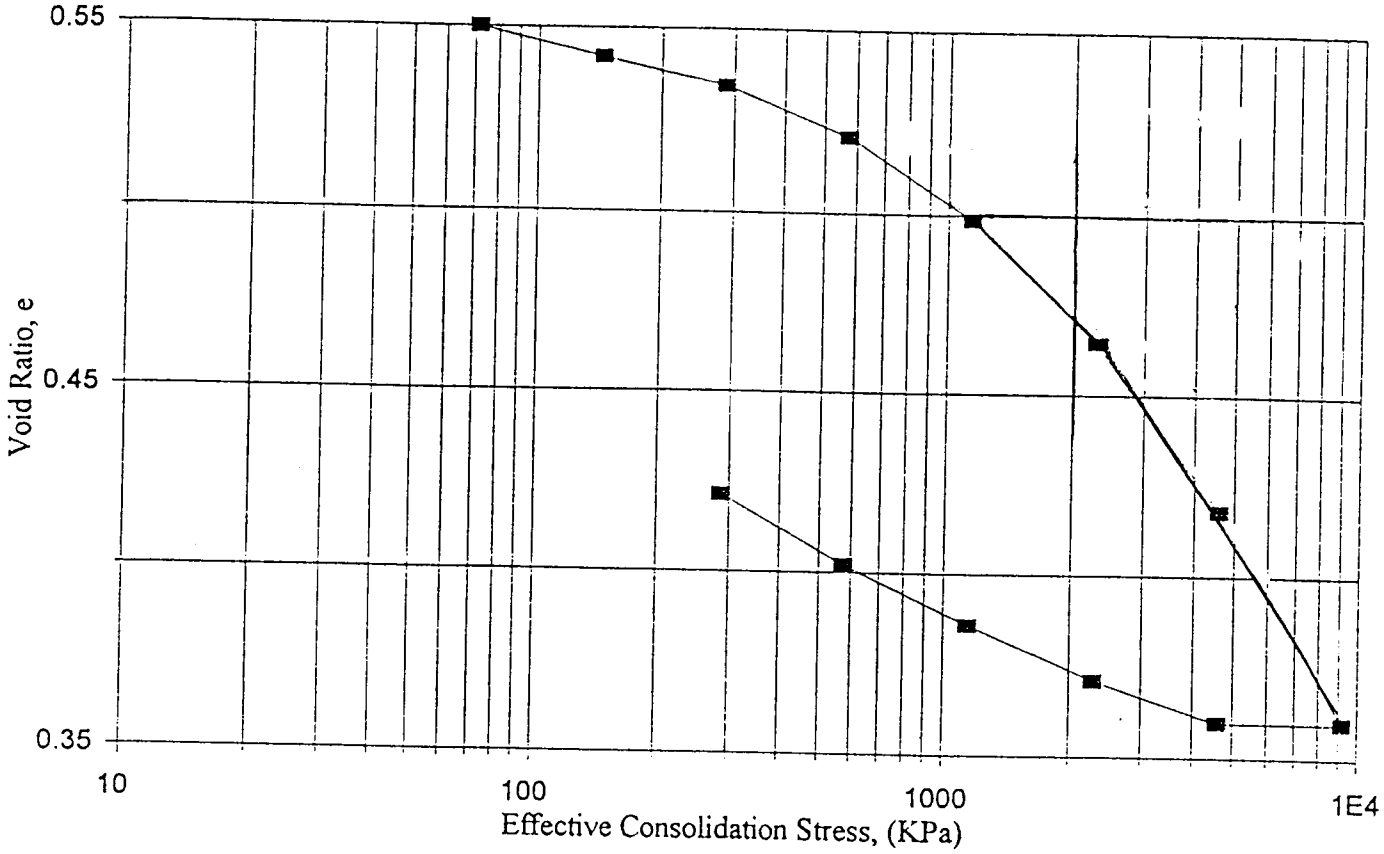

Fig. C.2. Consolidation curve (in terms of void ratio vs. effective consolidation stress) for the third test specimen from the block sample of glaciolacustrine clay beneath glacial sequence II, exposed at Pit #6, Wedron Silica Company mine, Wedron, IL.

Test was run from 11-5-92 to 11-12-92

Calibration Data

Load	Deflected Dial Reading
72	7 75
144	13 25
288	20 6
576	30 35
1152	38 85
2304	51 75
4608	72 85
9217	110 4

Initial Void Ratio, eo	0 55	
Height of Solids, Hs=	12.51	mm
Initial Dial Reading	0	
Initial height of soil, Hi	19 5	mm

Effective Consol Stress (KPa)	Initial Dial Rdg	Final Dial Rdg	Total Delta Dial Rdg	Calibrtd. Dial Rdg	Adjusted (x 002) (mm)	Change in Void Ratio	Inst. Void Ratio	Drainage Path (cm)	Time** For 50% Consol (min)	Coeff o Consol Cv cm^2/sec	Coeff o Compres av m^2/N	Coeff of Permeab k cm/s	Compren Index Cc	Secondary Compren Index C	Secondary Compren Ratio C /Cc
72	0	7 75	7 75	0	0	0 0000	0 550				0 00011	1 44E-05			
144	0	63	63	49 75	0 0995	0 0079	0 542	0 972513	1 5	2 07E-03	5 19E-05	3 59E-06			
288	63	117 5	117 5	96 9	0 1938	0 0154	0 535	0 96518	2 8	1 09E-03	4 72E-05	4 49E-06	0 335	0 0023	0 0069
576	117 5	213	213	182 65	0 3653	0 0290	0 521	0 956178	2	1 50E-03	3 9E-05	3 58E-06	0 55	0 003	0 0055
1152	213	363	363	324 15	0 6483	0 0514	0 499	0 940528	2	1 45E-03	2 94E-05	2 56E-06	3 02	0 0143	0 0047
2304	363	589 5	589 5	537 75	1 0755	0 0853	0 465	0 915698	2	1 38E-03	2 02E-05	1 16E-06	6 56	0 03	0 0046
4609	589 5	904	904	831 15	1 6623	0 1318	0 418	0 879668	2 8	9 07E-04	1 27E-05	2 28E-07	11 93	0 0506	0 0042
9217	904	1310	1310	1199 6	2 3992	0 1903	0 360	0 831905	8	2 84E-04			4 921	0 029	0 0059
4609			1272 5	1199 65	2 3993	0 1903	0 360								
2304			1181	1129 25	2 2585	0 1791	0 371								
1152			1074	1035 15	2 0703	0 1642	0 386								
576			963	932 65	1 8653	0 1479	0 402								
288			831	810 4	1 6208	0 1285	0 421								
144			730	716 75	1 4335	0 1137	0 436								

Avg Cv50% 1 10E-03 k avg 2 4E-06 cm/s

Avg Compression Index Cc = 4 552667
Avg Secondary Comp Index= 0 0215
Avg Secondary Comp. Ratio= 0 0053

Table C.2. Consolidation data for the third test specimen from the block sample of glaciolacustrine clay beneath glacial sequence II, exposed at Pit #6, Wedron Silica Company mine, Wedron, IL. See Fig. C.2.

Appendix D

Triaxial test data

To determine sediment strength and viscoplastic parameters, triaxial tests were conducted on samples of till taken from the second (Batestown) glacial sequence exposed at the Wedron Silica Co. mine at Wedron, IL. The sample from which the specimens were taken was collected in the bottom meter of the sequence, exposed in the access road-cut on the northeast end of Pit #6. The triaxial tests were conducted at the Civil Engineering Laboratory, Washington State University from November 1993 through July 1993. Test instrument precision was ± 1 kPa for shear stress, ± .1% strain, and ± .02% for pore water pressure. Full details regarding the execution of the tests and the methodologies employed are reported in Vela (in prep.).

Sediment strength

To determine the yield and failure strengths of the sediment, consolidated drained triaxial (CDTX) tests were conducted for both overconsolidated and normally consolidated conditions on separate 5-specimen sets of till. Tables D.1 and D.2 summarize the test data and statistics regarding the precision of the tests.

Sediment viscoplastic parameters

To determine the viscoplastic parameters, a consolidated drained controlled strain rate test (CDSR) test was conducted on a single specimen of Batestown till at 5 different stress levels Fig.s D.1 and 2 show the results in terms of deviatoric stress and principal stress ratios, respectively. Table D.3 contains the data associated with the curves in Fig.s D.1 and 2. See Chapter 4 for synoptic description of the test methodology. Detailed description of test execution and methodology is contained in Vela (in prep.).

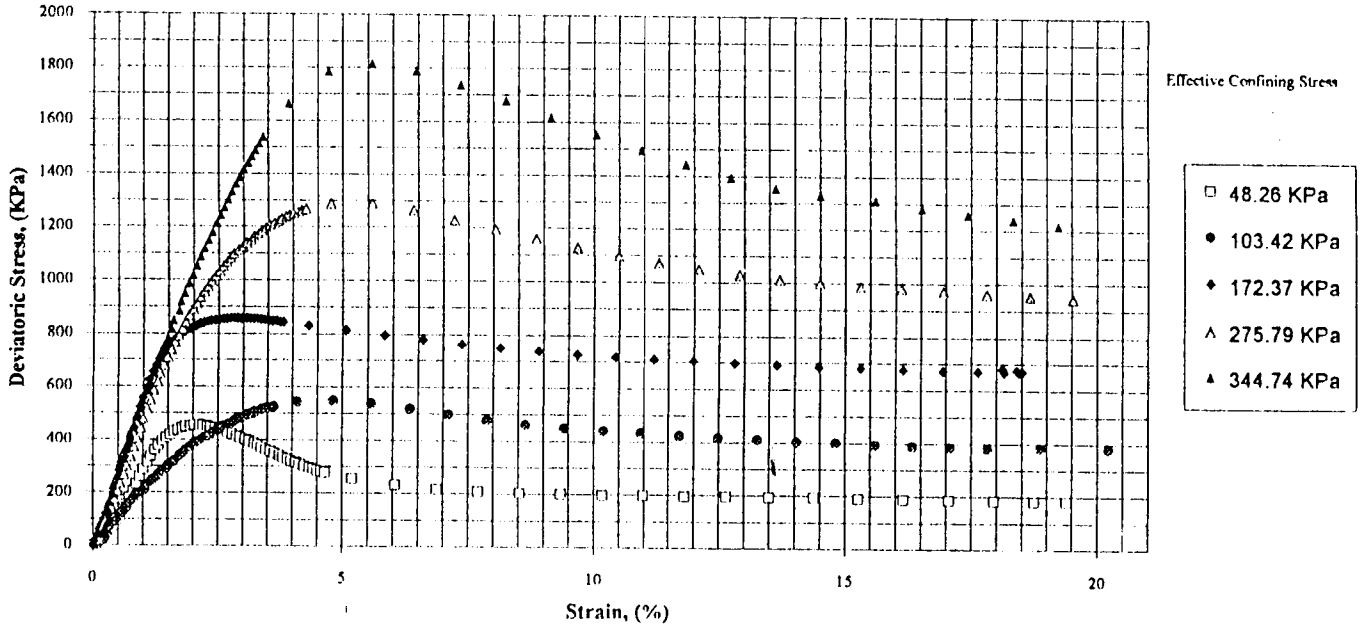

Fig. D.1 Deviatoric stress $(\sigma_1 - \sigma_3)$ vs. strain curves for CDSR test at various confining stresses. See Table D.3 for data and Chapter 4 for discussion.

Summary of in-situ concolidated drained triaxial tests (CDTX)
Using Duncan-Chang evaluation of hyperbolic parameters.

Confining Stress (σ3)	Deviator Stress at Failure (σ1−σ3)	70% Stress Level			95% Stress Level			at failure	
		Deviator Stress (σ1−σ3)	Axial Strain (ε)	ε /(σ1−σ3)	Deviator Stress	Axial Strain	ε /(σ1−σ3)	p	q
48.30	454.34	318.04	0.012	3.71E-05	431.62	0.018	4.05E-05	299.6	227.2
103.42	546.26	382.38	0.022	5.75E-05	518.95	0.035	6.74E-05	428.3	273.1
172.37	856.49	599.54	0.012	1.92E-05	813.67	0.018	2.24E-05	686.8	428.2
275.80	1287.99	901.59	0.020	2.23E-05	1223.59	0.037	3.02E-05	1057.7	644.0
344.74	1813.28	1269.30	0.027	2.13E-05	1722.62	0.043	2.50E-05	1423.8	906.6

σ3 Pa	1 (σ1−σ3)	Rf	Ei/Pa	Ei	A	Yield Strength σ	(σ1−σ3)	(σ1)	at yield p	at yield q
0.483	6.04E-04	0.274	333.59	33359.34	0.6936	276.8	1655.9	325.1	186.7	138.4
1.034	7.62E-04	0.416	245.32	24532.04	0.7021	212.6	1311.8	316.0	209.7	106.3
1.724	4.76E-04	0.407	729.31	72930.55	0.6265	438.3	2102.5	610.7	391.5	219.2
2.758	4.70E-04	0.606	778.54	77854.38	0.6195	453.0	2127.1	728.8	502.3	226.5
3.447	2.31E-04	0.418	664.71	66471.32	0.7242	646.1	4335.6	990.8	667.8	323.0

Regression Output of p and q:

Constant	43.31228	Constant	22.39751
Std Err of Y Est	23.47264	Std Err of Y Est	22.71816
R Squared	0.942497	R Squared	0.995117
No. of Observations	5	No. of Observations	5
Degrees of Freedom	3	Degrees of Freedom	3
X Coefficient(s)	0.406954	X Coefficient(s)	0.607576
Std Err of Coef.	0.058035	Std Err of Coef.	0.024573
Friction Angle at Yield=	24.0	*Friction Angle at Fail.=*	37.4

A = Factorial coefficient dependent on limiting strain (Wong and others, in review)

Ei = Initial tangent modulus

Ei/Pa = Normalization of initial atmospheric pressure

$p = (\sigma_1 + \sigma_3)/2$

$q = (\sigma_1 - \sigma_3)/2$

Rf = Failure ratio relating failure stress to ultimate stress

Table D.1. Data from consolidated drained triaxial tests (CDTX) to determine yield and failure strengths for overconsolidated Batestown till. Duncan-Chang method employed to evaluate strength parameters (Vela, in prep).

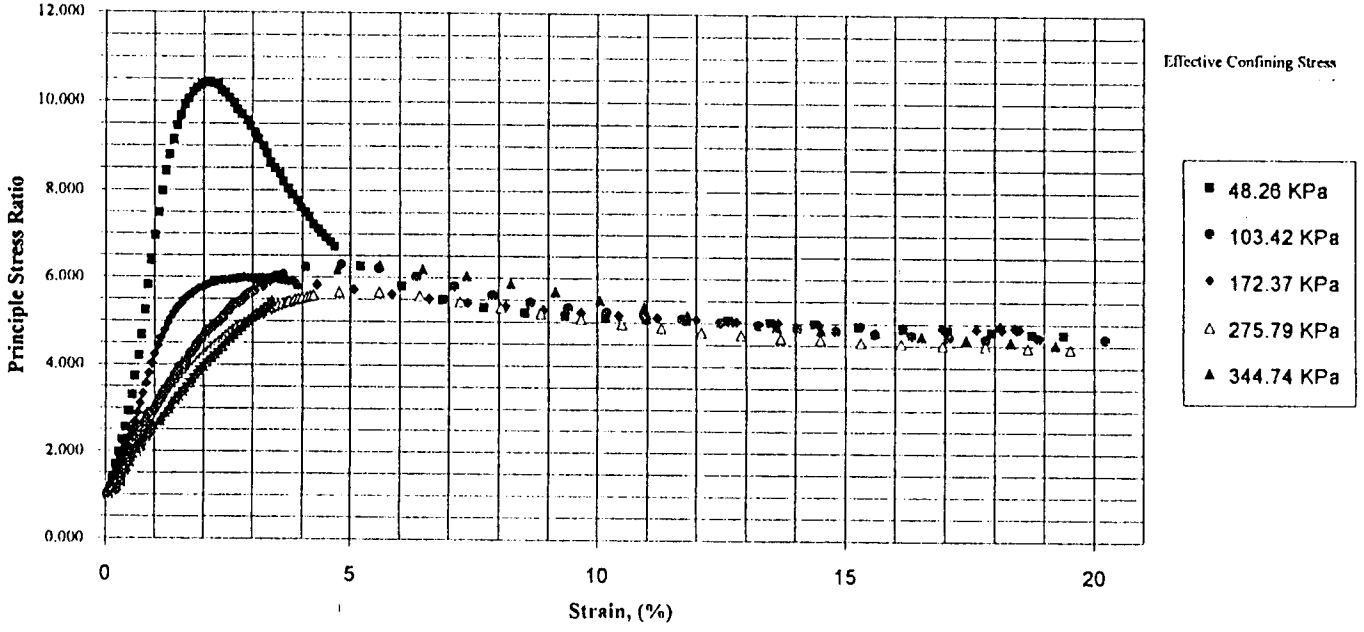

Fig. D.2 Principal stress ratio (σ_1/σ_3) vs. strain curves for CDSR test at various confining stresses. See Table D.3 for data and Chapter 4 for discussion.

Summary of normally concolidated triaxial tests (NCTX)

Failure					*Yield*						
Confining Stress (σ3) (KPa)	Deviator Stress at Failure (σ1-σ3) (KPa)	(σ1) at Failure	p	q	Ei*	Ultimate Deviator Stress* (σ1-σ3) (KPa)	A**	Deviator Stress at Yield (σ1-σ3) (KPa)	(σ1) at Yield	p	q
48.30	124	172.3	110.3	62.0	6655	139	0.583	57.9	106.2	77.3	29.0
103.42	251	354.4	228.9	125.5	9136	304	0.645	107.9	211.3	157.4	54.0
172.37	423	595.4	383.9	211.5	22300	474	0.586	196.4	368.8	270.6	98.2
275.80	692	967.8	621.8	346.0	34378	794	0.597	320.0	595.8	435.8	160.0
344.74	891	1235.7	790.2	445.5	50950	986	0.573	421.4	766.1	555.4	210.7

Regression Output for Failure:

Constant	0
Std Err of Y Est	2.840282
R Squared	0.999674
No. of Observations	5
Degrees of Freedom	4
X Coefficient(s)	0.559222
Std Err of Coef.	0.002568

Friction Angle at Failure= 34.0

Regression Output for Yield:

Constant	0
Std Err of Y Est	3.466975
R Squared	0.997862
No. of Observations	5
Degrees of Freedom	4
X Coefficient(s)	0.371954
Std Err of Coef.	0.004467

Friction Angle at Yield= 21.8

*Calculated from NCTX tests.
**Secant Modulus Method.

Table D.2. Data from consolidated drained triaxial tests (CDTX) to determine yield and failure strengths for normally consolidated Batestown till. Duncan-Chang method employed to evaluate strength parameters (Vela, in prep).

Date of Test..... November 20, 1992
Project..... CDTX Research
Location of Lab..... Sloan B20
Tested by..... JCV
Sample from..... Bagged Batestown
Sample Number..... Test 1
Soil Type..... Batestown Till
Test Type..... Drained

Confining Stress

7 psi
48.3 KPa

Sample Dimensions

Diameter	7.18 cm	Water %	8.79 %
Height	18.1 cm	Sample Wt	1713.8 g
Volume	732.9 ml	Density	2.34 g/cm^3

Time (min)	Measured Volume Change (ml)	Strain (%)	Area Change (cm^2)	Deviatoric Stress (KPa)	Total Volume Change (ml)	Volumetric Strain (%)	Principal Stress Ratio (1/ 3)
0	4.9331	0.0382	40.51	0	0	0	1.000
1	5.1647	0.0759	40.52	1.74	0.2316	-0.032	1.036
2	5.3962	0.1512	40.55	17.35	0.4631	-0.063	1.359
3	5.5947	0.2077	40.57	32.94	0.6616	-0.090	1.683
4	5.7601	0.2829	40.61	45.91	0.8270	-0.113	1.951
5	5.9255	0.3394	40.63	60.16	0.9924	-0.135	2.246
6	6.0578	0.4147	40.66	74.39	1.1247	-0.153	2.541
7	6.1571	0.4712	40.68	92.50	1.2240	-0.167	2.917
8	6.2563	0.5465	40.71	110.57	1.3232	-0.181	3.291
9	6.3556	0.6029	40.73	131.22	1.4225	-0.194	3.719
10	6.3887	0.6782	40.77	154.41	1.4556	-0.199	4.199
11	6.3887	0.7347	40.79	177.60	1.4556	-0.199	4.680
12	6.3887	0.81	40.82	204.60	1.4556	-0.199	5.239
13	6.3556	0.8665	40.84	231.61	1.4225	-0.194	5.799
14	6.2894	0.9417	40.87	258.53	1.3563	-0.185	6.357
15	6.2563	1.017	40.91	286.70	1.3232	-0.181	6.940
16	6.1571	1.0923	40.94	312.26	1.2240	-0.167	7.470
17	6.0248	1.1676	40.96	336.48	1.0917	-0.149	7.972
18	5.8594	1.2429	40.99	358.10	0.9263	-0.126	8.420
19	5.6609	1.3182	41.03	375.82	0.7278	-0.099	8.787
20	5.4624	1.3935	41.06	392.23	0.5293	-0.072	9.127
21	5.2308	1.4688	41.09	407.34	0.2977	-0.041	9.440
22	4.9993	1.5441	41.12	418.57	0.0662	-0.009	9.673
23	4.7015	1.6194	41.16	429.78	-0.2316	0.032	9.905
24	4.4369	1.6947	41.19	435.86	-0.4962	0.068	10.031
25	4.1722	1.7888	41.23	443.12	-0.7609	0.104	10.181

Table D.3. Data from CDSR test on consolidated Batestown till. Details of test execution and methodology are contained in Vela (in prep.).

Table D.3, continued

26	3.8745	1.8641	41.26	447.89	-1.0586	0.144	10.280
27	3.6098	1.9582	41.29	451.29	-1.3233	0.181	10.351
28	3.3121	2.0335	41.33	453.50	-1.6210	0.221	10.396
29	3.0144	2.1276	41.37	454.34	-1.9187	0.262	10.414
30	2.6836	2.2029	41.41	452.72	-2.2495	0.307	10.380
31	2.3858	2.297	41.44	451.01	-2.5473	0.348	10.345
32	2.0881	2.3535	41.47	445.66	-2.8450	0.388	10.234
33	1.7904	2.4476	41.51	442.69	-3.1427	0.429	10.172
34	1.4927	2.5229	41.54	437.27	-3.4404	0.469	10.060
35	1.1949	2.617	41.58	431.77	-3.7382	0.510	9.946
36	0.9303	2.6923	41.61	425.10	-4.0028	0.546	9.808
37	0.6326	2.7864	41.65	419.62	-4.3005	0.587	9.694
38	0.3349	2.8805	41.69	412.89	-4.5982	0.627	9.555
39	0.1033	2.9558	41.72	406.25	-4.8298	0.659	9.417
40	-0.1614	3.0499	41.76	399.54	-5.0945	0.695	9.278
41	-0.426	3.1252	41.79	392.92	-5.3591	0.731	9.141
42	-0.6907	3.2193	41.84	384.97	-5.6238	0.767	8.976
43	-0.95553	3.2946	41.87	377.11	-5.8886	0.804	8.814
44	-1.9809	3.3699	41.91	368.01	-6.9140	0.943	8.625
45	-1.9809	3.464	41.94	361.36	-6.9140	0.943	8.487
46	-1.9809	3.5581	41.98	354.73	-6.9140	0.943	8.350
47	-1.9809	3.6334	42.02	346.92	-6.9140	0.943	8.188
48	-1.9809	3.7275	42.06	339.05	-6.9140	0.943	8.025
49	-1.9809	3.8028	42.09	332.52	-6.9140	0.943	7.890
50	-1.9809	3.8968	42.13	325.94	-6.9140	0.943	7.753
51	-1.9809	3.9722	42.16	318.17	-6.9140	0.943	7.592
52	-1.9809	4.0663	42.21	312.86	-6.9140	0.943	7.482
53	-1.9809	4.1416	42.24	307.62	-6.9140	0.943	7.374
54	-1.9809	4.2357	42.28	299.84	-6.9140	0.943	7.213
55	-1.9809	4.3298	42.32	294.56	-6.9140	0.943	7.103
56	-1.9478	4.4051	42.36	289.34	-6.8809	0.939	6.995
57	-1.9478	4.4804	42.39	284.14	-6.8809	0.939	6.887
58	-1.9478	4.5745	42.43	280.13	-6.8809	0.939	6.804
59	-1.9478	4.6687	42.47	274.88	-6.8809	0.939	6.695
60	-1.9478	4.6687	42.47	274.88	-6.8809	0.939	6.695
70	-1.9011	5.2051	42.71	253.21	-6.8342	0.933	6.246
80	-1.8879	6.0446	43.09	231.38	-6.8210	0.931	5.794
90	-1.8747	6.8766	43.48	216.47	-6.8078	0.929	5.485
100	-1.8747	7.701	43.87	208.30	-6.8078	0.929	5.316
110	-1.878	8.5311	44.27	202.86	-6.8111	0.929	5.203
120	-1.8912	9.3499	44.67	199.98	-6.8243	0.931	5.144
130	-1.8978	10.1743	45.08	197.11	-6.8309	0.932	5.084
140	-1.8978	10.9969	45.49	196.11	-6.8309	0.932	5.063
150	-1.8945	11.8175	45.92	194.76	-6.8276	0.932	5.035
160	-1.9011	12.6495	46.35	195.54	-6.8342	0.933	5.052
170	-1.9044	13.4965	46.81	193.42	-6.8375	0.933	5.008
180	-1.9111	14.3831	47.29	192.44	-6.8442	0.934	4.987
190	-1.9111	15.264	47.78	189.47	-6.8442	0.934	4.926
200	-1.9276	16.1618	48.29	187.35	-6.8607	0.936	4.882
210	-1.9309	17.0616	48.82	185.45	-6.8640	0.937	4.842
220	-1.9309	17.9462	49.34	183.69	-6.8640	0.937	4.806
230	-1.9342	18.7462	49.83	181.79	-6.8673	0.937	4.767
240	-1.9375	19.3862	50.23	181.20	-6.8706	0.938	4.754

Table D.3, continued

Date of Test..... March 12, 1993
Project..... CDTX Research
Location of Lab..... Sloan B20
Tested by..... JCV
Sample from..... Bagged Batestown
Sample Number..... Test 4
Soil Type..... Batestown Till
Test Type..... Drained

Confining Stress

15 psi
103.42 KPa

Sample Dimensions

Diameter	3.56 cm	Water %	8.79 %
Height	8.76 cm	Sample Wt	208.37 g
Volume	87.2 ml	Density	2.39 g/cm^3

Time (min)	Measured Volume Change (ml)	Strain (%)	Area Change (cm^2)	Deviatoric Stress (KPa)	Total Volume Change (ml)	Volumetric Strain (%)	Principal Stress Ratio (1/ 3)
0	-23.4540	0.0451	9.96	0	0	0	1.000
1	-23.4871	0.1617	9.95	10.63	-0.0331	0.038	1.103
2	-23.4871	0.2395	9.97	21.25	-0.0331	0.038	1.205
3	-23.4540	0.2783	9.97	42.40	0.0000	0.000	1.410
4	-23.4210	0.2783	9.97	58.26	0.0330	-0.038	1.563
5	-23.3879	0.3172	9.98	68.82	0.0661	-0.076	1.665
6	-23.3548	0.3950	9.99	84.63	0.0992	-0.114	1.818
7	-23.3217	0.4339	9.99	89.89	0.1323	-0.152	1.869
8	-23.3217	0.4727	9.99	105.70	0.1323	-0.152	2.022
9	-23.3217	0.5505	10.00	116.18	0.1323	-0.152	2.123
10	-23.2886	0.5894	10.01	126.69	0.1654	-0.190	2.225
11	-23.2556	0.6671	10.01	137.14	0.1984	-0.228	2.326
12	-23.2556	0.7060	10.02	147.63	0.1984	-0.228	2.427
13	-23.2225	0.7449	10.02	158.11	0.2315	-0.265	2.529
14	-23.2225	0.8226	10.03	173.78	0.2315	-0.265	2.680
15	-23.2225	0.8615	10.03	189.50	0.2315	-0.265	2.832
16	-23.1894	0.9393	10.04	194.62	0.2646	-0.303	2.882
17	-23.1894	1.0170	10.05	204.98	0.2646	-0.303	2.982
18	-23.1894	1.0559	10.05	215.41	0.2646	-0.303	3.083
19	-23.1894	1.0948	10.06	225.82	0.2646	-0.303	3.183
20	-23.1563	1.1726	10.07	241.38	0.2977	-0.341	3.334
21	-23.1563	1.2114	10.07	246.54	0.2977	-0.341	3.384
22	-23.1563	1.2892	10.08	256.83	0.2977	-0.341	3.483
23	-23.1563	1.3281	10.08	267.20	0.2977	-0.341	3.584
24	-23.1563	1.4058	10.09	282.70	0.2977	-0.341	3.733
25	-23.1232	1.4836	10.10	292.94	0.3308	-0.379	3.832

Table D.3, continued

26	-23.1232	1.5225	10.10	303.28	0.3308	-0.379	3.932
27	-23.1332	1.6002	10.11	308.28	0.3208	-0.368	3.981
28	-23.1563	1.6391	10.11	318.60	0.2977	-0.341	4.081
29	-23.1563	1.7169	10.12	334.00	0.2977	-0.341	4.229
30	-23.1563	1.7557	10.13	339.08	0.2977	-0.341	4.279
31	-23.1563	1.8335	10.13	349.25	0.2977	-0.341	4.377
32	-23.1563	1.8724	10.14	359.52	0.2977	-0.341	4.476
33	-23.1563	1.9501	10.15	369.66	0.2977	-0.341	4.574
34	-23.1894	2.0279	10.15	379.77	0.2646	-0.303	4.672
35	-23.1894	2.0668	10.16	390.02	0.2646	-0.303	4.771
36	-23.1894	2.1445	10.17	394.92	0.2646	-0.303	4.819
37	-23.1894	2.2223	10.17	404.99	0.2646	-0.303	4.916
38	-23.2225	2.3000	10.18	409.87	0.2315	-0.265	4.963
39	-23.2225	2.3389	10.19	414.89	0.2315	-0.265	5.012
40	-23.2556	2.4167	10.19	424.93	0.1984	-0.228	5.109
41	-23.2556	2.4944	10.20	434.95	0.1984	-0.228	5.206
42	-23.2556	2.5333	10.21	439.96	0.1984	-0.228	5.254
43	-23.2886	2.6111	10.21	449.95	0.1654	-0.190	5.351
44	-23.2886	2.6888	10.22	454.77	0.1654	-0.190	5.397
45	-23.2886	2.7666	10.23	459.59	0.1654	-0.190	5.444
46	-23.3217	2.8444	10.24	469.54	0.1323	-0.152	5.540
47	-23.3217	2.8832	10.24	474.51	0.1323	-0.152	5.588
48	-23.3548	2.9610	10.25	479.30	0.0992	-0.114	5.634
49	-23.3548	3.0387	10.26	484.07	0.0992	-0.114	5.681
50	-23.3879	3.1165	10.27	493.98	0.0661	-0.076	5.776
51	-23.3879	3.1942	10.28	493.60	0.0661	-0.076	5.773
52	-23.3879	3.2331	10.28	503.68	0.0661	-0.076	5.870
53	-23.4210	3.3109	10.29	503.29	0.0330	-0.038	5.866
54	-23.4210	3.3886	10.30	513.15	0.0330	-0.038	5.962
55	-23.4210	3.4664	10.30	517.88	0.0330	-0.038	6.007
56	-23.4540	3.5441	10.31	517.48	0.0000	0.000	6.004
57	-23.4871	3.6219	10.32	522.19	-0.0331	0.038	6.049
58	-23.4871	3.6219	10.32	522.19	-0.0331	0.038	6.049
70	-23.5761	4.0768	10.37	539.68	-0.1221	0.140	6.218
80	-23.7548	4.8232	10.45	546.26	-0.3008	0.345	6.282
90	-23.9253	5.5697	10.53	537.16	-0.4713	0.541	6.194
100	-24.0823	6.3395	10.62	518.07	-0.6283	0.721	6.009
110	-24.2411	7.1093	10.71	495.79	-0.7871	0.903	5.794
120	-24.3800	7.8752	10.80	475.29	-0.9260	1.062	5.596
130	-24.4958	8.6411	10.89	458.46	-1.0418	1.195	5.433
140	-24.6083	9.4148	10.98	446.14	-1.1543	1.324	5.314
150	-24.7009	10.1924	11.08	437.28	-1.2469	1.430	5.228
160	-24.8001	10.9427	11.17	430.52	-1.3461	1.544	5.163
170	-24.8928	11.7242	11.27	422.27	-1.4388	1.650	5.083
180	-24.9821	12.4901	11.37	414.18	-1.5281	1.752	5.005
190	-25.0615	13.2638	11.47	408.43	-1.6075	1.844	4.949
200	-25.1309	14.0413	11.57	401.34	-1.6769	1.923	4.881
210	-25.1971	14.8189	11.68	396.57	-1.7431	1.999	4.834
220	-25.2434	15.5926	11.79	388.71	-1.7894	2.052	4.759
230	-25.2930	16.3391	11.89	385.49	-1.8390	2.109	4.727
240	-25.3526	17.0816	12.00	382.28	-1.8986	2.177	4.696
250	-25.3956	17.8242	12.11	377.33	-1.9416	2.227	4.648
260	-25.4518	18.8778	12.27	380.97	-1.9978	2.291	4.684
270	-25.5213	20.2308	12.47	377.98	-2.0673	2.371	4.655

Table D.3, continued

Date of Test..... March 2, 1993
Project..... CDTX Research
Location of Lab..... Sloan B20
Tested by..... JCV
Sample from..... Bagged Batestown
Sample Number..... Test 3
Soil Type..... Batestown Till
Test Type..... Drained

Confining Stress

25 psi
172.37 KPa

Sample Dimensions

Diameter	7.18 cm	Water %	8.79 %
Height	18.5 cm	Sample Wt	1737.8 g
Volume	749.0 ml	Density	2.32 g/cm^3

Time (min)	Measured Volume Change (ml)	Strain (%)	Area Change (cm^2)	Deviatoric Stress (KPa)	Total Volume Change (ml)	Volumetric Strain (%)	Principal Stress Ratio (1/ 3)
0	-17.6729	0.0249	39.74	0	0	0	1.000
1	-17.5737	0.0616	39.75	3.99	0.0992	-0.013	1.023
2	-17.5075	0.0616	39.75	10.62	0.1654	-0.022	1.062
3	-17.4744	0.0984	39.77	26.54	0.1985	-0.027	1.154
4	-17.3421	0.1167	39.77	39.80	0.3308	-0.044	1.231
5	-17.2759	0.1351	39.78	58.36	0.3970	-0.053	1.339
6	-17.1436	0.1719	39.79	76.90	0.5293	-0.071	1.446
7	-17.0113	0.2270	39.82	96.74	0.6616	-0.088	1.561
8	-16.9121	0.2638	39.83	119.22	0.7608	-0.102	1.692
9	-16.7797	0.3189	39.85	141.67	0.8932	-0.119	1.822
10	-16.6474	0.3740	39.88	165.41	1.0255	-0.137	1.960
11	-16.4820	0.4108	39.89	191.80	1.1909	-0.159	2.113
12	-16.3828	0.4659	39.91	222.10	1.2901	-0.172	2.289
13	-16.2835	0.5394	39.94	253.64	1.3894	-0.185	2.472
14	-16.1512	0.5945	39.96	287.83	1.5217	-0.203	2.670
15	-16.0189	0.6497	39.99	324.61	1.6540	-0.221	2.883
16	-15.9527	0.7048	40.01	362.68	1.7202	-0.230	3.104
17	-15.8535	0.7599	40.03	400.70	1.8194	-0.243	3.325
18	-15.7873	0.8334	40.06	441.23	1.8856	-0.252	3.560
19	-15.6881	0.8885	40.08	480.48	1.9848	-0.265	3.787
20	-15.6550	0.9437	40.10	519.67	2.0179	-0.269	4.015
21	-15.5888	0.9988	40.13	556.20	2.0841	-0.278	4.227
22	-15.5557	1.0723	40.16	589.95	2.1172	-0.283	4.423
23	-15.5557	1.1274	40.18	622.45	2.1172	-0.283	4.611
24	-15.5557	1.2009	40.21	652.17	2.1172	-0.283	4.784
25	-15.5557	1.2744	40.24	677.92	2.1172	-0.283	4.933

Table D.3, continued

26	-15.5888	1.3296	40.26	701.13	2.0841	-0.278	5.068
27	-15.6219	1.4031	40.29	722.88	2.0510	-0.274	5.194
28	-15.6881	1.4582	40.31	740.80	1.9848	-0.265	5.298
29	-15.7873	1.5501	40.35	757.12	1.8856	-0.252	5.392
30	-15.8204	1.6052	40.37	772.38	1.8525	-0.247	5.481
31	-15.8865	1.6787	40.40	784.87	1.7864	-0.238	5.553
32	-15.9196	1.7522	40.43	796.04	1.7533	-0.234	5.618
33	-15.9858	1.8441	40.47	805.74	1.6871	-0.225	5.674
34	-16.0519	1.8992	40.50	814.41	1.6210	-0.216	5.725
35	-16.1181	1.9911	40.53	822.77	1.5548	-0.208	5.773
36	-16.1843	2.0646	40.56	828.67	1.4886	-0.199	5.808
37	-16.2504	2.1381	40.59	835.86	1.4225	-0.190	5.849
38	-16.3166	2.2116	40.62	840.44	1.3563	-0.181	5.876
39	-16.3828	2.2851	40.66	843.71	1.2901	-0.172	5.895
40	-16.4489	2.3586	40.69	846.98	1.2240	-0.163	5.914
41	-16.5151	2.4321	40.72	848.94	1.1578	-0.155	5.925
42	-16.6143	2.5240	40.75	850.75	1.0586	-0.141	5.936
43	-16.6805	2.5975	40.79	852.71	0.9924	-0.132	5.947
44	-16.7466	2.6710	40.82	854.66	0.9263	-0.124	5.958
45	-16.8128	2.7445	40.85	856.61	0.8601	-0.115	5.970
46	-16.9121	2.8180	40.88	857.26	0.7608	-0.102	5.973
47	-16.9782	2.8915	40.91	856.63	0.6947	-0.093	5.970
48	-17.0444	2.9650	40.94	855.99	0.6285	-0.084	5.966
49	-17.1436	3.0569	40.98	856.49	0.5293	-0.071	5.969
50	-17.2098	3.1304	41.01	855.85	0.4631	-0.062	5.965
51	-17.2759	3.2039	41.04	855.21	0.3970	-0.053	5.962
52	-17.3421	3.2774	41.07	854.58	0.3308	-0.044	5.958
53	-17.4083	3.3509	41.10	852.66	0.2646	-0.035	5.947
54	-17.4744	3.4244	41.13	852.02	0.1985	-0.027	5.943
55	-17.5406	3.5163	41.17	849.94	0.1323	-0.018	5.931
56	-17.6068	3.5898	41.21	848.03	0.0661	-0.009	5.920
57	-17.7060	3.6633	41.24	847.40	-0.0331	0.004	5.916
58	-17.7722	3.7368	41.27	844.21	-0.0993	0.013	5.898
59	-17.8383	3.8103	41.30	843.57	-0.1654	0.022	5.894
60	-17.8383	3.8103	41.30	843.57	-0.1654	0.022	5.894
70	-18.2581	4.3065	41.51	831.18	-0.5852	0.078	5.822
80	-18.9098	5.0691	41.85	812.46	-1.2369	0.165	5.714
90	-19.4921	5.8354	42.19	794.79	-1.8192	0.243	5.611
100	-20.0412	6.5980	42.53	778.19	-2.3683	0.316	5.515
110	-20.5507	7.3716	42.89	762.17	-2.8778	0.384	5.422
120	-21.0204	8.1416	43.25	748.66	-3.3475	0.447	5.343
130	-21.4405	8.9060	43.61	735.91	-3.7676	0.503	5.269
140	-21.8540	9.6705	43.98	725.68	-4.1811	0.558	5.210
150	-22.2312	10.4312	44.35	716.38	-4.5583	0.609	5.156
160	-22.5951	11.2049	44.74	708.57	-4.9222	0.657	5.111
170	-22.9424	11.9969	45.14	701.58	-5.2695	0.703	5.070
180	-23.2732	12.8109	45.56	694.67	-5.6003	0.748	5.030

Table D.3, continued

190	-23.5974	13.6452	46.00	689.44	-5.9245	0.791	5.000
200	-23.9018	14.4721	46.45	683.91	-6.2289	0.832	4.968
210	-24.1962	15.3138	46.91	678.81	-6.5233	0.871	4.938
220	-24.4641	16.1517	47.38	674.37	-6.7912	0.907	4.912
230	-24.7255	16.9400	47.83	670.51	-7.0526	0.942	4.890
240	-24.9901	17.6347	48.23	667.34	-7.3172	0.977	4.872
250	-25.2614	18.1529	48.54	665.53	-7.5885	1.013	4.861
260	-25.5426	18.4414	48.71	665.95	-7.8697	1.051	4.863
270	-25.8039	18.5112	48.75	668.85	-8.1310	1.086	4.880
280	-26.0719	18.4009	48.68	673.85	-8.3990	1.121	4.909
290	-26.3200	18.1198	48.52	680.36	-8.6471	1.154	4.947

Table D.3, continued

Date of Test..... December 5, 1992
Project..... CDTX Research
Location of Lab..... Sloan B20
Tested by..... JCV
Sample from..... Bagged Batestown
Sample Number..... Test 2
Soil Type..... Batestown Till
Test Type..... Drained

Confining Stress

40 psi
275.8 KPa

Sample Dimensions

Diameter	7.18 cm	Water %	8.79 %
Height	18.4 cm	Sample Wt	1737.8 g
Volume	745.0 ml	Density	2.33 g/cm^3

Time (min)	Measured Volume Change (ml)	Strain (%)	Area Change (cm^2)	Deviatoric Stress (KPa)	Total Volume Change (ml)	Volumetric Strain (%)	Principal Stress Ratio (1/ 3)
0	4.8614	0.0724	40.52	0	0	0	1.000
1	5.0268	0.1279	40.54	19.53	0.1654	-0.022	1.071
2	5.1591	0.1649	40.56	44.24	0.2977	-0.040	1.160
3	5.3245	0.2020	40.57	68.93	0.4631	-0.062	1.250
4	5.4569	0.2575	40.59	93.59	0.5955	-0.080	1.339
5	5.6223	0.3131	40.62	119.52	0.7609	-0.102	1.433
6	5.7877	0.3686	40.64	146.72	0.9263	-0.124	1.532
7	5.9200	0.4242	40.66	175.18	1.0586	-0.142	1.635
8	6.0854	0.4982	40.69	203.58	1.2240	-0.164	1.738
9	6.2508	0.5538	40.71	234.57	1.3894	-0.186	1.851
10	6.4162	0.6278	40.75	266.77	1.5548	-0.209	1.967
11	6.5155	0.6834	40.77	300.27	1.6541	-0.222	2.089
12	6.6478	0.7575	40.80	333.67	1.7864	-0.240	2.210
13	6.7801	0.8315	40.83	369.61	1.9187	-0.258	2.340
14	6.9124	0.8871	40.85	405.57	2.0510	-0.275	2.471
15	7.0117	0.9611	40.88	442.69	2.1503	-0.289	2.605
16	7.1109	1.0167	40.91	477.27	2.2495	-0.302	2.731
17	7.2102	1.0907	40.94	513.00	2.3488	-0.315	2.860
18	7.2763	1.1648	40.97	547.40	2.4149	-0.324	2.985
19	7.3756	1.2204	40.99	583.13	2.5142	-0.337	3.114
20	7.4417	1.2944	41.02	616.14	2.5803	-0.346	3.234
21	7.5079	1.3500	41.04	647.93	2.6465	-0.355	3.349
22	7.5410	1.4240	41.07	678.27	2.6796	-0.360	3.459
23	7.6071	1.4981	41.11	708.57	2.7457	-0.369	3.569
24	7.6402	1.5722	41.14	737.55	2.7788	-0.373	3.674
25	7.6733	1.6462	41.17	765.19	2.8119	-0.377	3.775

Table D.3, continued

26	7.7064	1.7203	41.20	792.80	2.8450	-0.382	3.875
27	7.7395	1.7758	41.22	819.23	2.8781	-0.386	3.970
28	7.7395	1.8499	41.25	844.20	2.8781	-0.386	4.061
29	7.7395	1.9240	41.28	867.85	2.8781	-0.386	4.147
30	7.7395	1.9980	41.31	891.46	2.8781	-0.386	4.232
31	7.7395	2.0721	41.35	912.49	2.8781	-0.386	4.309
32	7.7395	2.1461	41.38	936.03	2.8781	-0.386	4.394
33	7.7064	2.2202	41.41	956.99	2.8450	-0.382	4.470
34	7.6733	2.2943	41.44	975.37	2.8119	-0.377	4.537
35	7.6402	2.3683	41.47	994.99	2.7788	-0.373	4.608
36	7.6402	2.4424	41.50	1014.59	2.7788	-0.373	4.679
37	7.6071	2.5165	41.53	1032.88	2.7457	-0.369	4.745
38	7.5741	2.5905	41.57	1049.87	2.7127	-0.364	4.807
39	7.5410	2.6646	41.60	1066.84	2.6796	-0.360	4.868
40	7.5079	2.7387	41.63	1081.24	2.6465	-0.355	4.921
41	7.4748	2.8127	41.66	1095.63	2.6134	-0.351	4.973
42	7.4087	2.9053	41.70	1111.04	2.5473	-0.342	5.029
43	7.3756	2.9794	41.73	1124.11	2.5142	-0.337	5.076
44	7.3094	3.0534	41.76	1138.42	2.4480	-0.329	5.128
45	7.2763	3.1460	41.80	1149.97	2.4149	-0.324	5.170
46	7.2432	3.2016	41.83	1161.93	2.3818	-0.320	5.213
47	7.1771	3.2941	41.87	1172.17	2.3157	-0.311	5.250
48	7.1109	3.3682	41.90	1183.87	2.2495	-0.302	5.293
49	7.0778	3.4423	41.93	1194.30	2.2164	-0.298	5.330
50	7.0117	3.5163	41.96	1204.71	2.1503	-0.289	5.368
51	6.9455	3.6089	42.01	1212.36	2.0841	-0.280	5.396
52	6.8794	3.7015	42.05	1221.25	2.0180	-0.271	5.428
53	6.8132	3.7570	42.07	1229.33	1.9518	-0.262	5.457
54	6.7470	3.8496	42.11	1236.93	1.8856	-0.253	5.485
55	6.6809	3.9237	42.14	1243.50	1.8195	-0.244	5.509
56	6.6147	3.9977	42.18	1250.06	1.7533	-0.235	5.533
57	6.5485	4.0903	42.22	1255.11	1.6871	-0.226	5.551
58	6.4824	4.1644	42.25	1261.65	1.6210	-0.218	5.575
59	6.4162	4.2384	42.28	1266.92	1.5548	-0.209	5.594
60	6.4162	4.2384	42.28	1266.92	1.5548	-0.209	5.594
70	5.9799	4.7698	42.52	1286.66	1.1185	-0.150	5.665
80	5.2752	5.5827	42.88	1287.99	0.4138	-0.056	5.670
90	4.5772	6.3974	43.26	1264.58	-0.2842	0.038	5.585
100	3.9553	7.2232	43.64	1228.43	-0.9061	0.122	5.454
110	3.3962	8.0379	44.03	1192.75	-1.4652	0.197	5.325
120	2.8934	8.8563	44.42	1158.30	-1.9680	0.264	5.200
130	2.4270	9.6729	44.83	1126.18	-2.4344	0.327	5.083
140	2.0101	10.4913	45.24	1095.95	-2.8513	0.383	4.974
150	1.6363	11.2948	45.64	1071.13	-3.2251	0.433	4.884
160	1.2857	12.0984	46.06	1048.17	-3.5757	0.480	4.801
170	0.9582	12.9057	46.49	1029.51	-3.9032	0.524	4.733
180	0.6604	13.7019	46.92	1011.82	-4.2010	0.564	4.669
190	0.3726	14.4981	47.35	1000.74	-4.4888	0.603	4.629
200	0.1245	15.3054	47.81	986.81	-4.7369	0.636	4.578
210	-0.1236	16.1164	48.27	980.80	-4.9850	0.669	4.556
220	-0.3585	16.9514	48.75	970.87	-5.2199	0.701	4.520
230	-0.5867	17.8087	49.26	963.06	-5.4481	0.731	4.492
240	-0.7951	18.6586	49.78	955.18	-5.6565	0.759	4.463
250	-1.0135	19.5196	50.31	947.13	-5.8749	0.789	4.434

Table D.3, continued

Date of Test..... March 22, 1993
Project..... CDTX Research
Location of Lab..... Sloan B20
Tested by..... JCV
Sample from..... Bagged Batestown
Sample Number..... Test 5
Soil Type..... Batestown Till
Test Type..... Drained

Confining Stress

50 psi
344.74 KPa

Sample Dimensions

Diameter	3.56 cm	Water %	8.79 %
Height	8.76 cm	Sample Wt	208.37 g
Volume	87.2 ml	Density	2.39 g/cm^3

Time (min)	Measured Volume Change (ml)	Strain (%)	Area Change (cm^2)	Deviatoric Stress (KPa)	Total Volume Change (ml)	Volumetric Strain (%)	Principal Stress Ratio ($\sigma 1/\sigma 3$)
0	-23.5702	0.046	9.9584	0	0	0	1.000
1	-23.5702	0.046	9.9584	26.48	0.0000	0.000	1.077
2	-23.5702	0.1237	9.9662	42.37	0.0000	0.000	1.123
3	-23.5702	0.2015	9.9739	47.65	0.0000	0.000	1.138
4	-23.5702	0.2404	9.9878	63.31	0.0000	0.000	1.184
5	-23.5702	0.3182	9.9957	94.76	0.0000	0.000	1.275
6	-23.5371	0.3182	9.9957	126.23	0.0331	-0.038	1.366
7	-23.5371	0.3182	9.9957	162.94	0.0331	-0.038	1.473
8	-23.504	0.3959	10.0037	194.29	0.0662	-0.076	1.564
9	-23.5371	0.3959	10.0037	225.74	0.0331	-0.038	1.655
10	-23.504	0.4737	10.0116	262.25	0.0662	-0.076	1.761
11	-23.471	0.5126	10.0155	293.57	0.0992	-0.114	1.852
12	-23.471	0.5515	10.0195	324.86	0.0992	-0.114	1.942
13	-23.4379	0.6293	10.0275	361.23	0.1323	-0.152	2.048
14	-23.4379	0.7071	10.0354	392.32	0.1323	-0.152	2.138
15	-23.4048	0.746	10.0394	423.52	0.1654	-0.190	2.229
16	-23.4048	0.8237	10.0474	454.52	0.1654	-0.190	2.318
17	-23.3717	0.8626	10.0514	485.66	0.1985	-0.228	2.409
18	-23.3386	0.9404	10.0594	516.57	0.2316	-0.266	2.498
19	-23.3386	0.9793	10.0634	547.64	0.2316	-0.266	2.589
20	-23.3056	1.096	10.0754	583.46	0.2646	-0.303	2.692
21	-23.2725	1.1349	10.0794	614.46	0.2977	-0.341	2.782
22	-23.2725	1.2127	10.0875	650.38	0.2977	-0.341	2.887
23	-23.2394	1.2905	10.0955	681.06	0.3308	-0.379	2.976
24	-23.2394	1.3293	10.0995	717.14	0.3308	-0.379	3.080
25	-23.2394	1.4071	10.1076	752.91	0.3308	-0.379	3.184

Table D.3, continued

26	-23.2063	1.4849	10.1157	783.44	0.3639	-0.417	3.273
27	-23.2063	1.5627	10.1238	819.10	0.3639	-0.417	3.376
28	-23.2063	1.6016	10.1278	849.85	0.3639	-0.417	3.465
29	-23.1732	1.7183	10.14	885.08	0.3970	-0.455	3.567
30	-23.1732	1.7572	10.1441	920.92	0.3970	-0.455	3.671
31	-23.1732	1.8349	10.1522	951.21	0.3970	-0.455	3.759
32	-23.1732	1.9127	10.1604	986.60	0.3970	-0.455	3.862
33	-23.1732	1.9905	10.1686	1016.78	0.3970	-0.455	3.949
34	-23.1402	2.0683	10.1768	1052.06	0.4300	-0.493	4.052
35	-23.1732	2.1461	10.1849	1087.29	0.3970	-0.455	4.154
36	-23.1732	2.2239	10.1932	1117.31	0.3970	-0.455	4.241
37	-23.1732	2.3016	10.2014	1147.28	0.3970	-0.455	4.328
38	-23.1732	2.3794	10.2096	1177.21	0.3970	-0.455	4.415
39	-23.1732	2.4572	10.2179	1212.21	0.3970	-0.455	4.516
40	-23.2063	2.535	10.2261	1242.03	0.3639	-0.417	4.603
41	-23.2063	2.6128	10.2344	1271.81	0.3639	-0.417	4.689
42	-23.2063	2.6906	10.2427	1301.53	0.3639	-0.417	4.775
43	-23.2063	2.7683	10.251	1331.20	0.3639	-0.417	4.861
44	-23.2063	2.8461	10.2593	1360.82	0.3639	-0.417	4.947
45	-23.2063	2.9239	10.2676	1385.29	0.3639	-0.417	5.018
46	-23.2394	3.0017	10.276	1414.82	0.3308	-0.379	5.104
47	-23.2394	3.0795	10.2843	1439.20	0.3308	-0.379	5.175
48	-23.2725	3.1573	10.2927	1463.54	0.2977	-0.341	5.245
49	-23.2725	3.235	10.3011	1487.84	0.2977	-0.341	5.316
50	-23.3056	3.3128	10.3095	1512.09	0.2646	-0.303	5.386
51	-23.3056	3.3906	10.3179	1536.31	0.2646	-0.303	5.456
60	-23.3056	3.3906	10.3179	1536.31	0.2646	-0.303	5.456
70	-23.3946	3.904	10.3737	1662.74	0.1756	-0.201	5.823
80	-23.56	4.7285	10.4647	1783.98	0.0102	-0.012	6.175
90	-23.7386	5.588	10.5613	1813.28	-0.1684	0.193	6.260
100	-23.904	6.4631	10.6614	1786.84	-0.3338	0.383	6.183
110	-24.0496	7.3498	10.7648	1736.00	-0.4794	0.550	6.036
120	-24.1918	8.2482	10.8716	1677.41	-0.6216	0.713	5.866
130	-24.3175	9.1505	10.981	1615.75	-0.7473	0.857	5.687
140	-24.4201	10.0489	11.0921	1552.71	-0.8499	0.975	5.504
150	-24.5259	10.9395	11.2046	1494.95	-0.9557	1.096	5.336
160	-24.6119	11.8262	11.3187	1441.37	-1.0417	1.195	5.181
170	-24.6814	12.7246	11.4368	1393.44	-1.1112	1.274	5.042
180	-24.7575	13.6153	11.5563	1353.58	-1.1873	1.362	4.926
190	-24.8171	14.5098	11.6789	1327.69	-1.2469	1.430	4.851
200	-24.87	15.6065	11.8327	1308.76	-1.2998	1.491	4.796
210	-24.9262	16.5283	11.9652	1280.26	-1.3560	1.555	4.714
220	-24.9692	17.4344	12.0983	1257.95	-1.3990	1.604	4.649
230	-25.0222	18.3251	12.232	1238.21	-1.4520	1.665	4.592
240	-25.0552	19.2274	12.3705	1218.87	-1.4850	1.703	4.536

Appendix E

Determination of sediment viscoplastic parameters from experimental data

Value of n

The value of n is readily obtained from m, by eqn. (4.3b):

$$n = 1/m \qquad (4.3b)$$

For the values of m determined in this study (0.57-0.80) n thus ranges from 1.25 to 1.75.

Newtonian reference parameters

To determine the value of D_0 the model is run with the sediment rheology parmeterized using only b and n as the viscoplastic parameters to calculate the sediment velocity profiles. (See discussion in Chapter 4.) A representative velocity profile can then be selected. (In this study I used the velocity profile at node 31, which for the LML simulation experiment, was about midway between the origin and terminus of the soft-bedded lobe, and presumably less likely to be affected by possible "end effects." Analyses of velocity at other nodes, however, verified that the results were independent of the node selected for sampling.) D_0 can then be determined by graphical construction (Fig. E.1).

The first step is to determine the Newtonian reference depth, i.e., the depth at which the strain rates are identical for the observed nonlinear material and a hypothetical linear material that would produce the same maximum velocity. This is done by drawing a line connecting the topmost (maximum velocity) and bottommost (minimum velocity) points of the profile (Fig. E.1). This line represents the velocity profile that an analogous Newtonian material would produce under the same shear stress. Next, one constructs a parallel line tangent to the velocity profile. The point of tangency, at which the strain rate (slope of the velocity profile) is identical to the strain rate (slope) of the analogous Newtonian profile, determines the Newtonian reference depth.

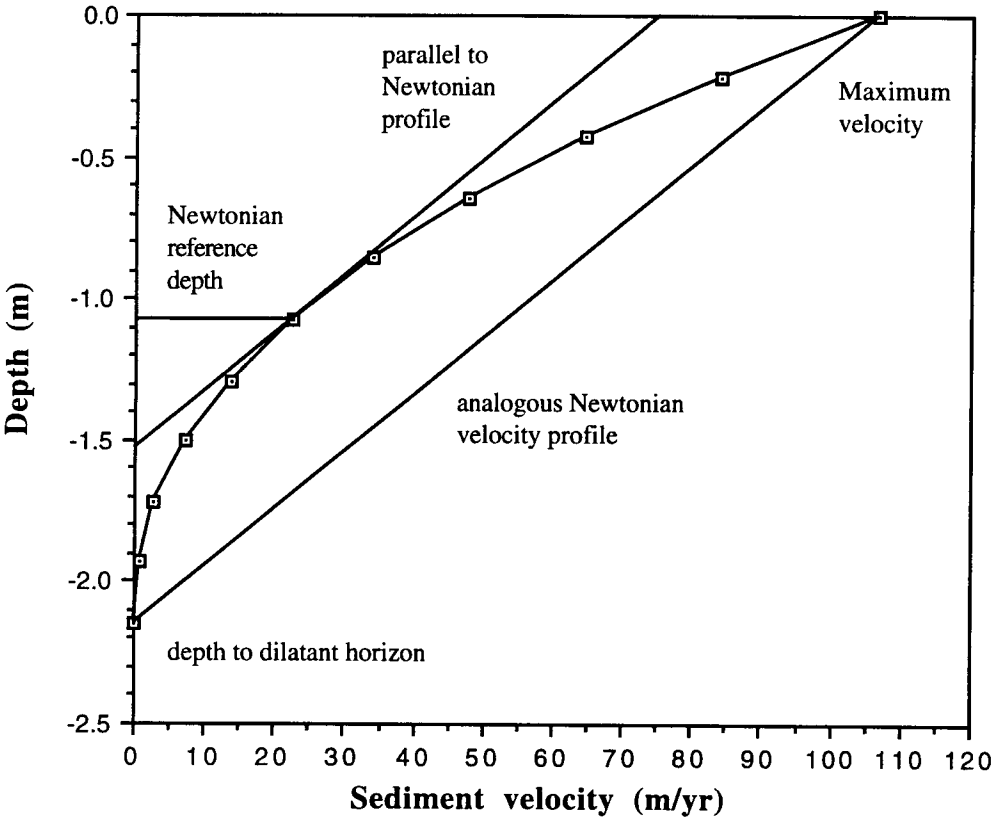

Fig. E.1. Determination of the Newtonian reference parameters and their interpretation in terms of velocity profile geometry.

D_0 can then be computed by substituting eqn (29) from Wong and others (in review):

$$y_{ref} = z_d\left(\frac{2}{n+1}\right)^{\left(\frac{1}{n-1}\right)} \quad \text{(eqn. 29, Wong and others)}$$

into equation (30):

$$D_0 = \frac{2^{\left(\frac{1}{n-1}\right)} v_{max}}{z_d (n+1)^{\left(\frac{1}{n-1}\right)}} \quad \text{(eqn. 30, Wong and others)}$$

to obtain:

$$D_0 = \frac{y_{ref} \cdot v_{max}}{z_d^2} \text{ sec}^{-1} \quad \text{(E.1)}$$

where y_{ref} is the Newtonian reference depth, z_d is the depth to the dilatant horizon, and v_{max} is the maximum (topmost) velocity in the velocity profile. From the profile in Fig. E.1, a value of 7.9×10^{-7} sec^{-1} was obtained for the present study.

Once the value of D_0 is known, one can substitute it , along with b and n, into eqn. (4.3a), which in rearranged form is:

$$\mu_0 = \frac{b}{2D_0^{[(n-1)/n]}} \text{ Pa-sec} \quad \text{(E.2)}$$

to obtain the reference viscosity, μ_0.

Using the values of b and n obtained from the test data (6.21×10^9 Pa for b, and 1.25 to 1.75 for n), along with the calculated value of D_0 above, gives values of μ_0 ranging from 5.2×10^9 to 1.3×10^{11} Pa-sec.

Appendix F:

Algebraic equivalence of equations (3.1) and (3.2)

First transform eqn. (3.2)

$$\frac{du}{dz} = F\left[\left(\frac{z_d - z}{z_d}\right)(|\tau| - S_0)\right]^n \qquad \text{(F.1)}$$

$$\frac{du}{dz} = F\left[\frac{z_d}{z_d}(|\tau| - S_0) - \frac{z}{z_d}(|\tau| - S_0)\right]^n \qquad \text{(F.1a)}$$

$$\frac{du}{dz} = F\left[(|\tau| - S_0) - \frac{z}{z_d}(|\tau| - S_0)\right]^n \qquad \text{(F.1b)}$$

Then transform eqn. (3.13):

$$z_d = \left\{\left[(|\tau| - c)/\tan\phi\right] - P_{basal}\right\}/(\rho' g) \qquad \text{(F.2a)}$$

$$z_d = \left(\frac{1}{\rho' g \tan\phi}\right)(|\tau| - c - P_{basal}\tan\phi) \qquad \text{(F.2b)}$$

Substitute (F.2b) into (3.1c) to obtain

$$z_d = \left(\frac{1}{\rho' g \tan\phi}\right)(|\tau| - S_0) \qquad \text{(F.2c)}$$

Then substitute (F.2c) for z_d into (F.1b) to obtain

$$\frac{du}{dz} = F\left[(|\tau| - S_0) - \frac{z \cdot \rho' g \tan\phi}{(|\tau| - S_0)}(|\tau| - S_0)\right]^n \qquad \text{(F.3)}$$

After canceling terms and substituting in (3.1d) for the numerator in the second term inside the brackets, the equation becomes identical to eqn. (3.1a):

$$\frac{du}{dz} = F \cdot \left(|\tau| - S_0 - S_{(z)} \right)^n \qquad \text{(F.4)}$$